Kimio Toda · Abraham Salazar
Kozo Saito *Editors*

Automotive Painting Technology

A Monozukuri-Hitozukuri Perspective

Springer

Automotive Painting Technology

Kimio Toda • Abraham Salazar • Kozo Saito
Editors

Automotive Painting Technology

A Monozukuri-Hitozukuri Perspective

Springer

Editors
Mr. Kimio Toda
Asahi Sunac Corporation
Owariasahi, Aichi
Japan

Dr. Abraham Salazar
Institute of Research for Technology Development
College of Engineering
University of Kentucky
Lexington, KY
USA

Prof. Kozo Saito
Institute of Research for Technology Development
College of Engineering
University of Kentucky
Lexington, KY
USA

ISBN 978-94-007-5094-4 ISBN 978-94-007-5095-1 (eBook)
DOI 10.1007/978-94-007-5095-1
Springer Dordrecht Heidelberg London New York

Library of Congress Control Number: 2012952151

Printed on acid-free paper

Springer is part of Springer Science+Business Media (www.springer.com)

Foreword: Monozukuri-based Automotive Painting Science and Technology

I would like to send my sincere congratulations to the 10th anniversary of the University of Kentucky's Painting Technology Workshop directed by Professor Kozo Saito and his hard working and talented IR4TD staff members. I very much welcome a special publication of an anniversary volume: Monozukuri-based automobile painting technology to celebrate this occasion.

My company, Asahi Sunac has been working on innovative solutions to global environmental and energy problems through spray paint equipment and technology development for the past 55 years. When looking back at the past 55 years, we have made technology developments mainly based on our experience, by accumulating a series of experiments and a large collection of data; largely through our own small continuous effort, known as Kaizen, since we could not find resources and help available in lectures or scientific research from academic institutions around the world. That unfortunate trend eventually came to end when we found that the University of Kentucky had initiated the first Painting Technology Workshop (PTW 2000) in the year 2000. I have been thrilled to find the new and exciting scientific research results that PTW has produced. I had the good fortune to invite Professor Saito for Asahi Sunac's 50th anniversary lecture, and followed with collaborative research on spray painting technology conducted at the Institute of Research for Technology Development (IR4TD) at the University of Kentucky.

I am also very pleased to see Mr. Toda, an internationally recognized expert in automobile painting technology who has played a key role in production engineering at Toyota and NUMMI, became a regular lecturer for PTW. In his introduction, Mr. Toda addresses automobile painting technology based on his extensive knowledge and experience. Then, in later sections, IR4TD researchers bring a scientific approach to the experience based technology, making this book very unique and valuable. Mr. Toda also played an important role as a facilitator in making IR4TD's scientific research available to solve industry problems in automobile painting processes, systems and equipment. I am confident that this unique book will help engineers, researchers and students interested in learning both basics and applications of automobile painting technology.

Masahiko Amari
President of Asahi Sunac Corp. Japan

Preface

The University of Kentucky's Institute of Research for Technology Development (IR4TD) operates through interdependent and sustainable partnership with industry. This unique institute is a good example of University of Kentucky's (UK) effort to seek a new and better way of doing research, education, and service.

At IR4TD, we began a series of scientific studies on automobile coating technology around 1993 in response to a request from Toyota which is interested in finding scientific reasoning for the largely experience-based automobile painting technology area, as explained by Kimio Toda in his chapter in this book. I was totally unfamiliar with automobile painting technology at that time, since my research background was scale modeling and combustion. Therefore, I needed to visit a newly opened Toyota Georgetown plant to ask questions: What are the scientific principles to support a rotary bell sprayer, why so much over-sprayed paint fumes are created? How to collect these over-sprayed fumes? Why they need such a large size spray paint booth? What is the paint film thickness and how many different layers of paint is required and why? These are all questions coming from a totally novice point of view but they helped us to create a baseline for our scientific research. Following the Genchi-Genbutsu principle, I made a frequent visit to the automobile plant to collect various data and obtain discussions with engineers and operators, then conducted simple scale model laboratory experiments at the University of Kentucky. During this initial three year phase, we formed a small research team consisting of a graduate student, an industrial extension engineer and myself as a faculty researcher and head of the team.

Around 1996, Abraham Salazar joined our team, accelerating this research with his expertise in CFD (Computational Fluid Dynamics) model calculations analyzing the airflow pattern containing paint particles and the capturing mechanism of typical conventional wet scrubbers used by automobile manufacturers to capture over-sprayed paint. It was our first breakthrough to quantitatively estimate energy usage, relative efficiency, and fluid dynamics of particle capturing of existing wet scrubbers.

Our next task was focused on how to improve the performance of wet scrubbers. This task required new ideas through thinking outside-the-box and a paradigm shift. We learned from nature that sand dune structure in a desert can be the most efficient

way to capture paint particles with minimum energy consumption. This approach led our team to invent Vortecone in collaboration with Toyota and Trinity engineers. Vortecone wet scrubber is 30–50 % energy efficient and has a higher capturing capability than other similar products available on the market. Our team's success lies in the combination of the following factors: basic research to understand the capturing mechanisms, thinking outside-the-box, paradigm shift, and Toyota' continuous and steady funding support. Without any of the above elements, I doubt this invention would have been possible. In this case, the box was technology, that is, the outcome if human thought combined with engineering principles. We shifted our focus to nature, another source for models of how to make things efficiently.

This initial success attracted other companies to pay attention to our automobile coating research, leading to the establishment of UK's Painting Technology Consortium (PTC) in 1999. In the following year, we initiated the annual Painting Technology Workshop with the following aims: (1) to provide a place where industry engineers, government agency regulatory personnel, and academic researchers meet and discuss coating research and technology development; (2) to share common problems in coating technology and seek win-win solutions; and (3) to provide educational and training opportunity. Around 2005, Kimio Toda, an internationally renowned automobile painting technology expert joined PTW as a special lecturer bringing his thirty two years experience at Toyota.

Based on this Toda-UK PTW collaboration, we created a two-day special short course on automobile painting technology which produced rich documentation on automobile painting technology. This course led to the idea to publish a more comprehensive book on automobile painting technology. As a result, this book was born.

Kozo Saito

Contents

Contributors

Nelson K. Akafuah Institute of Research for Technology Development, College of Engineering, University of Kentucky, KY 40506-0503, Lexington, USA
e-mail: nkakaf0@engr.uky.edu

Eric Grulke Institute of Research for Technology Development, College of Engineering, University of Kentucky, Lexington, KY 40506-0503, USA
e-mail: egrulke@engr.uky.edu

Ken Kreafle Institute of Research for Technology Development, College of Engineering, University of Kentucky, Lexington, KY 40506-0503, USA
e-mail: ken.kreafle@tema.toyota.com

Kozo Saito Institute of Research for Technology Development, College of Engineering, University of Kentucky, Room: RGAN 179, Lexington, KY 40506-0503, USA
e-mail: saito@engr.uky.edu

Abraham J. Salazar Institute of Research for Technology Development, College of Engineering, University of Kentucky, Lexington, KY 40506-0503, USA
e-mail: ajsala00@uky.edu

V. Srinivasan ANSYS FLUENT, 15915 Katy Freeway, Suite 550, Houston, TX 77094, USA
e-mail: Vedanth.Srinivasan@ansys.com

Kimio Toda Asahi Sunac Corporation, Asahimae-cho 5050, Owariasahi, 488-8688 Aichi, Japan
e-mail: kimio_toda@sunac.co.jp

Chapter 1
Introduction

Kozo Saito

Abstract It is sometimes claimed that industry and academia are two very different cultures, with the former concerned with how to deliver reasonably-priced high quality products to customers in a timely fashion, while the latter focus on education, research, and service. Yet this difference does not mean there is no common ground. A common mission does exist between companies that value *hitozukuri* (education and training) and *monozukuri* (roughly, manufacturing) and academic institutions that focus on education and research. A win-win relationship, therefore, is possible between academia and industry in research and technology development. This book was created as a successful example of this win-win relationship between a world class automobile maker and University of Kentucky to study surface coating and inspection technology.

Monozukuri, a Japanese term which appears in the title of this book, may require some explanation. *Monozukuri* consists of "mono" which means "products," and "zukuri" which means "process of making or creation." But the word means more than simply making something; it has overtones of excellence, skill, spirit, zest, and pride in the ability to make things, good things, very well. Monozukuri is not mindless repetition; it requires creative minds and is often related to craftsmanship which can be earned through lengthy apprenticeship rather than the structured curricula taught at traditional schools. Monozukuri represents the maker's philosophy of how to make things—the philosophy deeply rooted in Japanese and East Asian traditions, for example, in Zen and in the Analects of Confucius. Monozukuri is therefore a philosophy rather than technique or method but provides a clear and visible guiding principle for Japanese engineers.

On the other hand, the Scientific Method, based on the Western model of logical thinking, also guides engineers by providing theory, experiment, and numerical methods to solve engineering problems associated with automobile painting technology. One focus of this book is to show the combination of these two different

K. Saito (✉)
Institute of Research for Technology Development, College of Engineering,
University of Kentucky, Room: RGAN 179, Lexington, KY 40506-0503, USA
e-mail: saito@engr.uky.edu

K. Toda et al. (eds.), *Automotive Painting Technology,*
DOI 10.1007/978-94-007-5095-1_1,

methods—Monozukuri and Scientific Method—can make for a very beneficial result that would not be possible by one method alone.

Therefore, this book is structured to show Monozukuri at the beginning (Sect. 1) and in the end (Sect. 4), with Scientific Method addressed in the middle (Sects. 2 and 3).

More specifically, this book, the collection of our past work on automobile painting technology, consists of four different Sections, Sect. 1: The empirical approach; Sect. 2: Numerical simulation and scale modeling; Sect. 3: Visualization and characterization; and Sect. 4: An integrative approach—Hitozukuri and Monozukuri. Section 1 offers practical aspects of automobile painting technology and was written by Kimio Toda who worked at Toyota's surface coating division for 32 years as an engineer and later manager. This unique Section is written for general engineers and university engineering students to grasp the overall nature of this technology and helps to prepare for more technical Sects. 2 and 3 where computational fluid dynamic simulations and scale modeling, and infrared thermography application for paint spray characterization are presented. These Sects. 2 and 3, written by former and current members of the University of Kentucky's painting technology research team, may require knowledge of advanced numerical simulation, fluid dynamics, heat transfer, and experimental methods.

The final Sect. 4 offers the Monozukuri concept, a unique product of Japanese culture, which significantly influenced Japanese technology development including automobile painting technology. This Section offers a picture of this unique thinking process associated with technology development and improvement, known as *Kaizen* (a small incremental improvement) and the thinking associated with *Kaikau* (a quantum leap breakthrough). The author of this Section intends to show readers automobile painting technology as part of Monozukuri culture, so that they may be able to see by their own interpretation the trend and direction of the current and future technology.

I hope readers enjoy and benefit from reading this unique Monozukuri-based automobile painting technology book and use the method and the thinking addressed in this book to solve and improve their problems related in automobile painting technology.

Part I
Painting Technology—The Empirical Approach

Chapter 2
What Is Spray Coating?

Kimio Toda

Abstract The aim of this chapter is to give an overview of the development of spray painting technology in the automotive industry through this author's over 30 plus years' experience in the industry, both in automobile manufacturing and spray equipment manufacturing. The author's perspective reflects monozukuri, the Japanese term for manufacturing that refers not only to technical issues but to traditional Japanese values and philosophies centered around the art and craft of making things. The chapter touches on the history of current spray paint technology and offers the author's view on future directions and challenges for automobile painting technology. The author discusses the evolution of painting technology as an art rather than science and highlights the need for scientific study of the kind the rest of the volume offers.

Keywords Automobile painting process · Protection of substrates · Surface appearance · Paint spray booth · Energy efficiency and waste · Paint spray atomizer · Water borne and solvent-based paint · Paint transfer efficiency

2.1 Introduction

The automotive assembly plant consists of stamping, welding, painting and assembly shops, and the painting shop is located in the center of the plant (Fig. 2.1). Although painting occupies the important position, the painting has not been treated so important, compared to other engineering areas. There are few universities and laboratories that study painting technology, in the world. Painting technology had been left as it was for long time. Under such a circumstance, the painting workshop lead by Dr. Saito of UK, University of Kentucky started 10 years ago.

I have been in charge of painting for almost 40 years since I joined the Toyota Motor Corporation in 1971. For the first 13 years, I had studied and developed the painting system while making a lot of experiments with many different types of

K. Toda (✉)
Asahi Sunac Corporation, Asahimae-cho 5050, Owariasahi, 488-8688 Aichi, Japan
e-mail: kimio_toda@sunac.co.jp

K. Toda et al. (eds.), *Automotive Painting Technology,*
DOI 10.1007/978-94-007-5095-1_2, © Springer Science+Business Media Dordrecht 2013

Fig. 2.1 Automotive assembly plant

paint, such as solvent-borne, NAD: non aqueous dispersion, water-borne and powder coatings, as well as with many types of coating equipment, such as electrostatic and non electrostatic air spray guns and electrostatic bell applicators, and also while using and developing different types of painting machines, such as reciprocators and robots, at the paint laboratory in Toyota.

I had worked as a paint shop coordinator in NUMMI, New United Motor Manufacturing Inc. A joint venture between General Motors and Toyota for three years from 1984 to 1987, while utilizing the experience in Toyota. Since I returned to Toyota in 1987, as a manager or a general manager of surface finishing engineering division, I had been in charge of the development of the new painting system again, and also in charge of the construction of Toyota's paint shops worldwide including TMMK: Toyota Motor Manufacturing Kentucky, TMMC: Canada, TMMUK: United Kingdom and so on, as well as in charge of the introduction of new vehicles.

I have been in charge of painting up to now as a managing director or an advisor of Asahi Sunac Corporation, a manufacturer and a supplier of painting equipment and system, as well as a senior visiting scholar of UK, since I retired from Toyota in 2005.

I believe that I have and had two important roles in UK. One is to give a 2 days short course in painting technology held at the same timing of PTW, while summarizing my long experience. The other is to support UK researchers for making clear the unknown areas of painting technology.

Frankly speaking, I would have liked to introduce the whole content of the short course in the book, but it consists of almost 200 figures, pictures and films so that I and Dr. Saito decided to summarize only the essence.

I would like to give a special thanks to Toyota Motor Corporation, Asahi Sunac Corporation and UK, and also to paint suppliers, especially Kansai paint, Nippon paint, Dupont, PPG, BASF, as well as to automotive companies, members of painting conferences such as Surcar, Automotive Circle International held in Berlin, and facility and equipment suppliers.

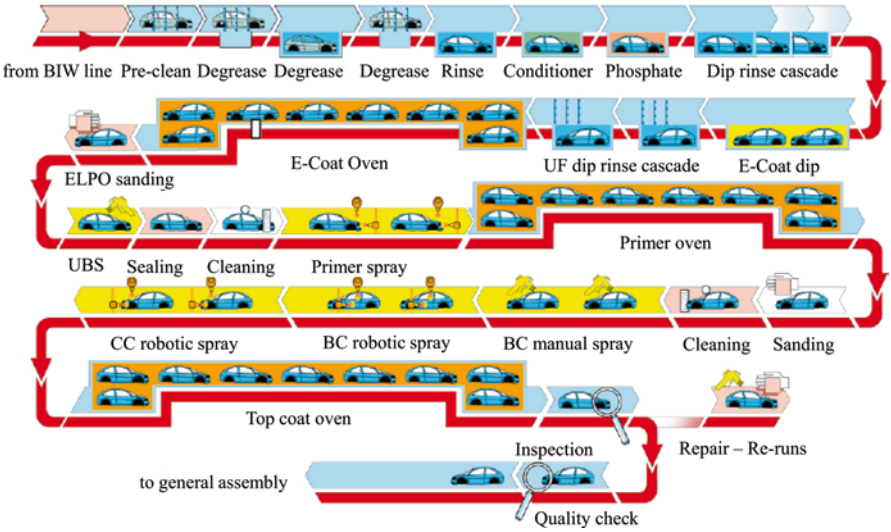

Fig. 2.2 Process in automotive paint shop

2.2 What Is Painting?

The painting has two important roles, one is to protect the substrate materials such as steal and plastics, and the other is to improve the appearance quality. The painting is a method or measures to achieve those roles with only an approx. 0.1 mm film, and it is very effective compared to others. Most customers have interest in the color and quality of painting. Therefore it is important for improving goods value. I believe that the definition of painting done by myself like this is probably welcome by most painting engineers.

Figure 2.2 shows the automotive painting process. First step consists of degreasing and phosphating, electro-coating: electro deposition coating and sealing. The main purpose of the first step is for protecting the substrate materials from corrosion. Second step consists of primer coating and top coating. The main purpose of the second step is for improving the appearance quality and for giving the color.

More than 50 years have passed since the E-coating was introduced into the automotive paint shop. I believe that painting itself has a long history, thousands years history, but only around 50 years ago, the current modern painting technology, such as electrostatic spraying, powder coating as well as E-coating, was developed and established. I have worked for painting for 40 years since I joined Toyota in 1971. Although I did not start my carrier 50 years ago, I have experienced almost all kinds of automotive coating, including study, development and introduction of water-borne painting, powder, hi-solid, cathodic e-coating, bell applicators and painting robots as well as construction of automotive paint shops worldwide. Therefore, I

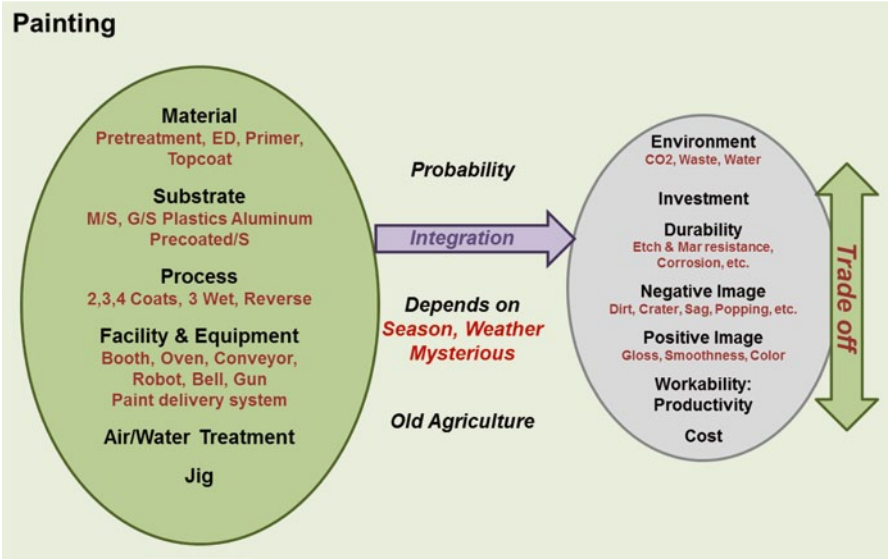

Fig. 2.3 Summary of painting

must be an expert of the painting. However, so often, I myself have still wondered what the painting is.

Eisenmann's Presentation Material in Berlin I have had more free time to summarize my experience, since I transferred from Toyota to Asahi Sunac in 2005. Still not clear, but I can imagine the answer to that question now. The following picture is a summary of my answer (Fig. 2.3).

Spray coating is a technology based on probabilistic model, for obtaining the best overall performance consisting of many outputs while integrating many inputs. There are two important key words, probabilistic model and integration.

(a) Probabilistic model Spray coating technology is typically based on the probabilistic model. Other technologies are usually based on the deterministic model. In other words, outputs have little or no variance. For the spray coating, even spray conditions cannot be set without variance. For instance, spray distance depends on shape of work piece. Even if spray conditions are controlled without variance, each particle among innumerable paint particles formed by atomization, has its own size, speed and direction. Therefore, to understand overall spray coating mechanism, we have to utilize statistical methods. In Sect. 2.3, I would like to show you the analysis of appearance quality with statistical methods.

(b) Integration According to Professor Takahiro Fujimoto, there are two types in product architecture, modular and integral. The typical example of modular architecture is personal computer. PC consists of modules, such as CPU, monitor, keyboard, power and so on. Once the interface between those modules is standardized,

we can combine any module without any integration. On the other hand, the typical example of integral architecture is automobile. It consists of many modules, such as engine, chassis, body, tire, and so on. In order to obtain the high performance, we have to integrate between those modules one by one.

I believe that there are also two types in technologies and engineering, modular and integral. Assembly, mechanics, welding basically belongs to modular type, but painting typically belongs to integral type. Even if paint suppliers develop the excellent paint, or equipment maker develops a good atomizer, we will not be able to obtain good result without continuous adjustment or integration between paint, equipment and other items. For painting, it is important not only to develop and improve each input module, but also how to integrate those inputs. I would like to show you development history of rotary bell atomizers, a key module for spray coating, in Sect. 2.4, and robotic painting system as an example of integration in Sect. 2.5.

2.3 Analysis of Appearance Quality with Statistical Methods

For painting, it is always a major issue to find the relationship between spray paint conditions and the painted surface quality, such as color, gloss, surface smoothness, etc [1]. My second assignment after I had joined Toyota was to conduct a series of paint spray experiments to establish a reliable quantitative database. In order to analyze this, there were two difficulties: (1) the lack of test paint booth which could provide well controlled temperature and relative humidity conditions, and (2) there are so many parameters involved in spray paint technology that the measurement itself can become extremely complex, as shown in Fig. 2.4.

In 1973, 2 years after I started working at Toyota, very fortunately those difficulties were removed. Toyota completed a large-scale paint test booth equipped with a large air conditioning unit. My colleague had just developed a new computer program for multi-parameter (multi-scale) analysis and was looking for his first customer.

I started the analysis. As shown in Fig. 2.5, I measured the painted surface quality by changing ten different parameters including the paint flow rate, the spraying distance, the spraying speed of the atomized paint particles, etc., one at the time. There were 30 other dependent variables influenced under these experimental conditions resulting in over 1,000 data points. I could analyze the relationship between parameters and painted surface quality.

I then expanded my spray paint characterization experiments to the paint manufactured by different paint companies and to different color paint. The additional data also supported the early correlation. Conducting a series of experiments, obtaining reliable data and establishing empirical correlations is one thing, but interpreting the correlations to find scientific reasoning behind them is different. I succeeded in the first step, but failed in the second process.

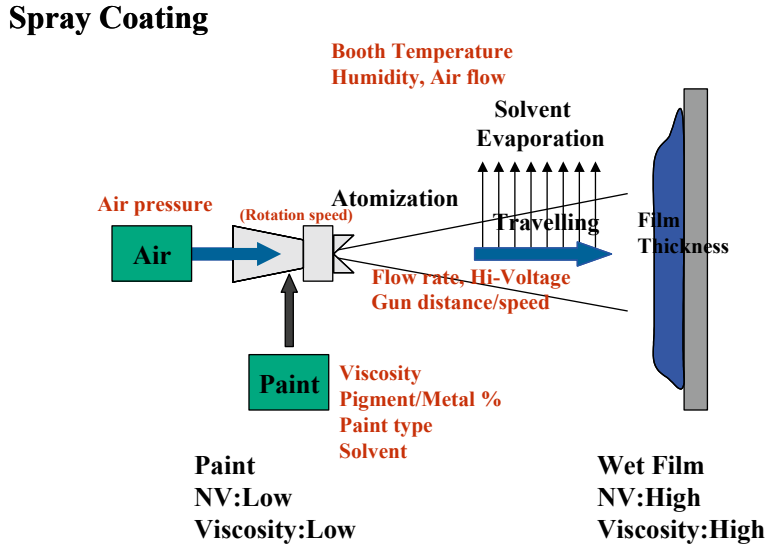

Fig. 2.4 Schematic of spray painting system

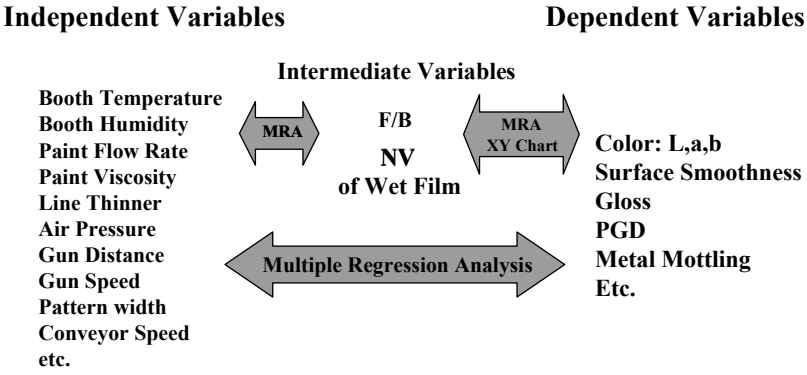

Fig. 2.5 Characteristics of the painted surface

To understand the essence of spray painting technology and its detailed mechanisms, I asked myself what the spray paint technology is. Imagining the spraying process and reviewing the experiment, the following emerged in my mind which is rather ordinal and common-sensed description of spray paint process: (1) Paint with low viscosity with high amount of solvent is ejected from a spray gun. (2) This low viscous paint will lose its solvent during travel from the spray gun to the target surface. (3) When atomized paint droplets reached the target surface, its viscosity is high due to the lost of solvent. (4) This forms a rather sticky thin film which prevents sagging.

Considering the spray painting process helped me to realize that the spray painting technology should be understood as a transient process, rather than the state relationships between input and output parameters. This transient process should include atomization of paint and change in viscosity of wet paint film at the target surface. This new approach, looking at the same problem differently, helped me to obtain a deeper understanding of the problem.

Characterization of the transient spray paint process, however, was not easy because there was no suitable equipment to measure the atomization process and the viscosity of wet paint film. Eventually I came up with an idea to measure the percent of solid content (Coated NV: which mainly consists of resin, pigment and metal flakes) in the wet paint. The idea is simple. First we measure the percent of solid content of the original paint (before spray) and then measure the percent of solid content of the wet paint film on the target surface. From the difference in the percent of the solid content, we should be able to calculate the amount of lost solvent during the atomization process. The higher loss of solvent usually translates into better atomization. Therefore, the degree of atomization can be measured by measuring the difference in the percent of solid content. Besides, coated NV has a one to one correspondence with the viscosity of wet paint film.

The above discussion can lead to an assumption that if we can measure the coated NV value and the film thickness, then we can determine brightness of color and several characteristics of the painted surface.

2.3.1 Color

The lightness of color: L value was found to be largely affected by the following three factors, spray rate of paint, air pressure of the spray gun, and the distance between the spray gun and the target. Specifically, L value increased with the following changes: a decrease in the amount of paint applied through a spray gun, an increase in the air pressure of the spray gun, and an increase in the spraying distance. At the same time, I found the relationship between NV of wet film and L value. This trend, as shown in Fig. 2.6, was sustained for a variety of paint manufactured by different companies and different colors.

When this correlation was presented at one of Toyota's group meetings, a paint engineer from Toyota Motomachi Plant asked a question on the accuracy of this correlation saying he had a completely different result. His claim was that during his spot repair process, the darkness of color increased with an increase of the spray distance (i.e., the lightness of color decreased with an increase of spray distance).

I could get the relationship between NV of wet film and L value as well as between spray parameters and *L* value, but I still could not find the mechanism or reason why the color changes when spray parameters change. At that time, I received a sample of the new type of metallic paint, NAD: Non Aqueous Dispersion and I tested. Surprisingly enough, I obtained the completely opposite trend to the previ-

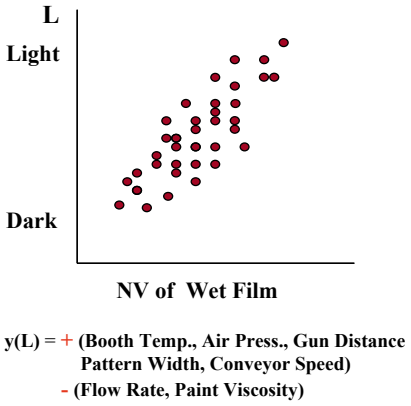

Fig. 2.6 Lightness of color trend

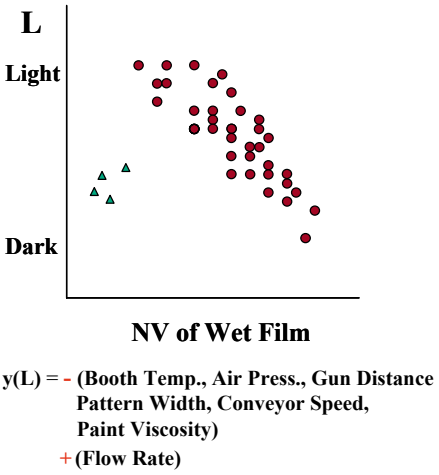

Fig. 2.7 The trend when using NDA metallic paint

ous Fig. 2.6. This new trend is shown with brown dots in Fig. 2.7. This discrepant trend is due to a difference in the type of paint. I did additional tests, and I got green triangle dots as well as brown dots.

Non-Aqueous Dispersion (NAD) Type Paint The major components of paint include resin: polymers, pigment, metallic flakes, solvent (organic solvent for solvent-based paint and water for water-based paint), and additives. For solvent-based paint, generally there is only one type of paint: soluble type which means that paint resin is dissolved in organic solvent. NAD was an epoch-making technology. It is almost impossible to disperse resin in organic solvent because resin is similar to solvent. Minimization of the particle size of resin, the effect of steric hindrance and use of aliphatic solvent having poor solubility, make resin disperse in solvent. In 1970s, NAD paint was expected to reduce VOC: volatile organic compounds, in other words organic solvent and to give better application workability for metallic

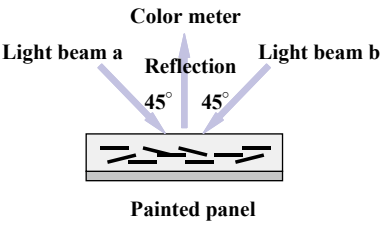

Fig. 2.8 Schematic of the measurement system

paint. However, as explained at the next section, NAD paint did not become popular because of its narrow workability window.

The story swings back and forth a little bit, but I have to show how a measurement system can determine brightness of color before we try to understand the discrepant results shown in Figs. 2.6 and 2.7.

Figure 2.8 shows a schematic of this measurement system in 1970s. There are two different beams shooting at the target surface, both with a 45° angle. Measurement was made right above the reflecting surface with a color meter while mixing both of reflecting beams. Three different typical cases are shown in Fig. 2.9a–c. Figure 2.9a is when all the metallic flakes inclined to a particular angle. Figure 2.9b is when the metal flakes are almost parallel to the paint surface. Figure 2.9c is when the metallic flakes are randomly oriented. The three arrows each also indicate brightness of color, (a) brown arrow: with mixed reflecting beams, (b) grey arrow: with only left side beam, (c) with only right side beam. L values in Figs. 2.6 and 2.7 were measured with mixed reflecting beams.

I tried to measure L value with only one side beam, and I obtained the following results shown in Fig. 2.10.

Figure 2.11 shows viscosity of two different types of paint: dispersion type and solution type, as a function of the paint NV value. This figure uses semi-logarithm graph. The linear relationship is obtained for solution type, but not for dispersion type. At the range of low density of dispersion particles, the interaction between particles is poor, and the increase rate of viscosity is slow. (Einstein's law) On the

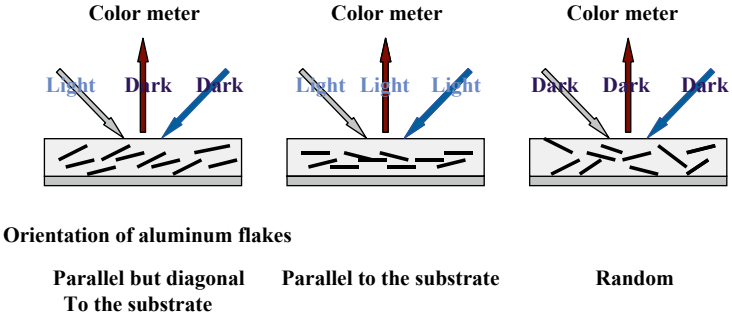

Fig. 2.9 a–c Orientation of aluminum flakes

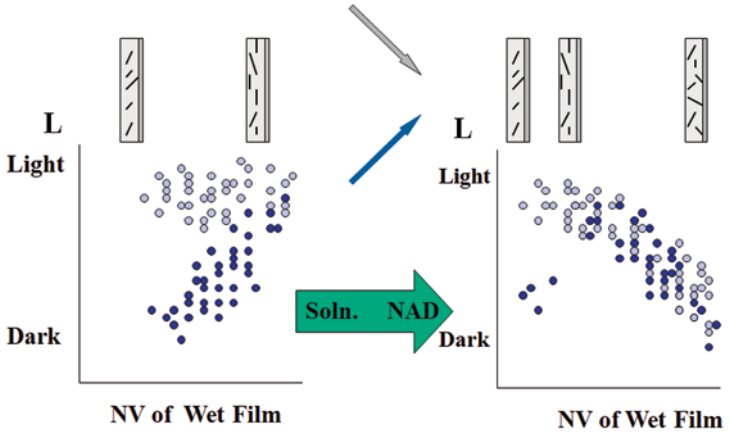

Fig. 2.10 **a–b** L value with a single beam. (**a**) Refers to Fig. 2.6. (**b**) Refers to Fig. 2.7

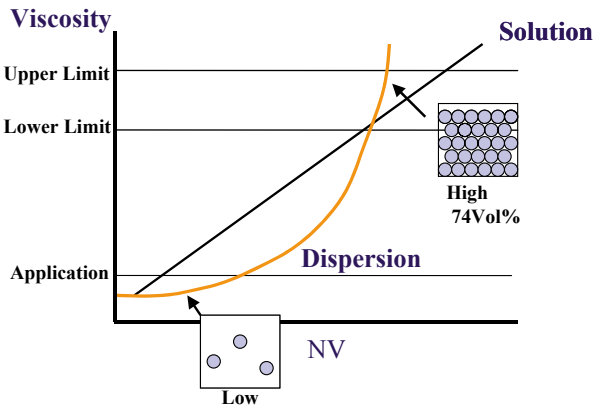

Fig. 2.11 Viscosity of dispersion type paint vs. solution type paint

other hand, at the high range, the interaction is strong, and the increase rate is fast. If particles have ideally same size and ball shape, the viscosity reaches infinite at 74 vol.%: the maximum density of particles.

Good coating surface quality including good color quality and requires a viscosity value between the upper and the lower limits as indicated in Fig. 2.11. At the general spray condition, the viscosity of wet film of soluble paint does not reaches the upper limit, but usually stays between upper and lower limits, or does not reach the lower limit. On the other hand, for the dispersion paint, the viscosity of wet film easily exceeds the upper limit and sometimes does not reach the lower limit. As you can see, the dispersion type paint has a much narrower range of the NV value to satisfy this limit than the solution type paint indicating that the dispersion type paint is more sensitive to NV value than the solution type.

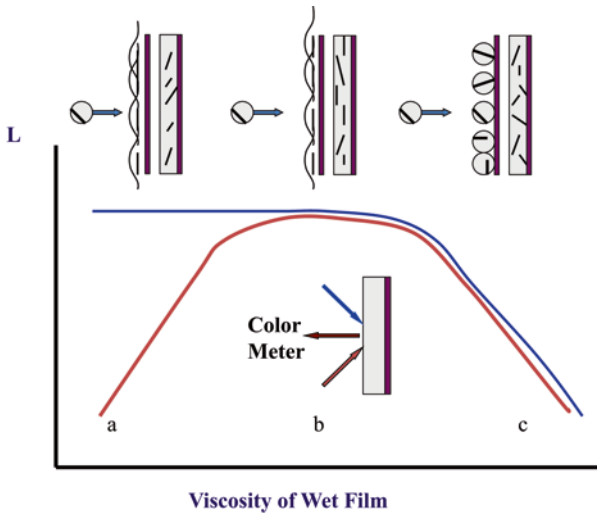

Fig. 2.12 Mechanism of the color of metallic paint

Back to Fig. 2.10. We can combine two figures and we get Fig. 2.12. At the range of the low NV of wet film, in other words low viscosity of that, aluminum flakes orientates parallel but diagonal to the substrate like Fig. 2.9a, and at the range of proper NV of wet film, proper viscosity of that, aluminum flakes orientates parallel to the substrate like Fig. 2.9b, and at the high NV of wet film, high viscosity of that, aluminum flakes orientates random like Fig. 2.9c.

Then we could estimate the mechanism of the color of metallic paint application as follow.

(a) Low viscosity of wet film means that the viscosity of each atomized particle is low. Just after such a particle hit the substrate, each particle's shape on the substrate becomes like flat and aluminum flake in the particle orientates parallel to the substrate. However, if the viscosity is too low, aluminum flakes tend to move freely in the film. The applied work piece: substrate was set perpendicular at the paint application. The gravity force gave restriction against the free movement of aluminum flakes in the film and caused the parallel but diagonal orientation of aluminum flakes.
(b) At the suitable range of viscosity of wet film, aluminum flakes cannot move freely, and this results parallel orientation.
(c) However, at the range of high viscosity, even if paint particle hit the substrate, each particle's shape remains round on the substrate, and aluminum flakes orientate at random.

Why the paint engineer from Toyota Motomachi Plant had the opposite opinion? His opinion was based on the experience at spot repairing. Paint flow rate is little and the atomization is extremely good at spot repairing. Solvent in paint particles evaporates so quickly so that the viscosity of spot repaired wet film becomes very high even with soluble paint. Therefore, at spot repairing, better atomization gives darker color.

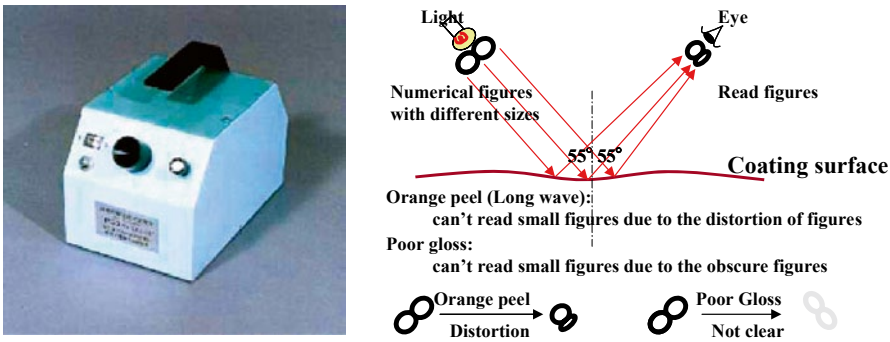

Fig. 2.13 PGD meter

Summary of the Color of Metallic Paint Application Atomized particles hit the substrate. When the viscosity of particles is low, aluminum flakes in wet film tend to orientate parallel to the substrate, and this gives bright color, but when the viscosity is too low, aluminum flakes in the wet film move freely and orientates parallel but diagonal to the substrate because of gravity. However, when the viscosity of particles is too high, aluminum flakes orientates random because paint particles shape on the substrate surface remains round [2].

Metallic bell is developed based on this theory as will be mentioned in Sect. 2.4.

2.3.2 Appearance Quality

The quality of appearance is an important aim for an engineer to achieve. In the 1980s the Japanese economy had a high rate of economic development, leading to the bubble burst in 1992. In the field of automobile engineering, around the end of the 1970s to the beginning of 1980s we accomplished a series of technology innovations such as full dip pretreatment system, cathodic electro-deposition coating, PVC under-coating. Those series of technological innovations were aimed at improving the quality of anti-corrosion. After the end of activities for anti-corrosion, new activities for improvement of appearance quality began. At this time, Japanese auto manufacturers launched high-end vehicles—for Nissan the Infinity and President—for Toyota the Lexus—for Honda the Legend—where the aim was to try to make the vehicles as luxurious as possible, with one element being surface appearance.

Measurement of Appearance Quality Surface appearance can be measured very precisely by a wave scan now. However, we did not have such an apparatus in 1970s. There are basically two measurements for evaluating appearance quality, one is surface smoothness and the other is gloss. The former is measured by comparing test panel with several standard panels. The latter is measured with a 60° angle gloss-meter. In Toyota, we also used to use our own PGD meter shown in Fig. 2.13.

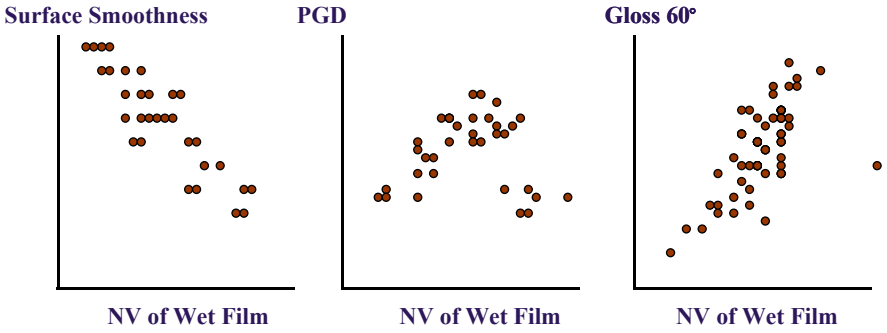

Fig. 2.14 The aspects of measurement

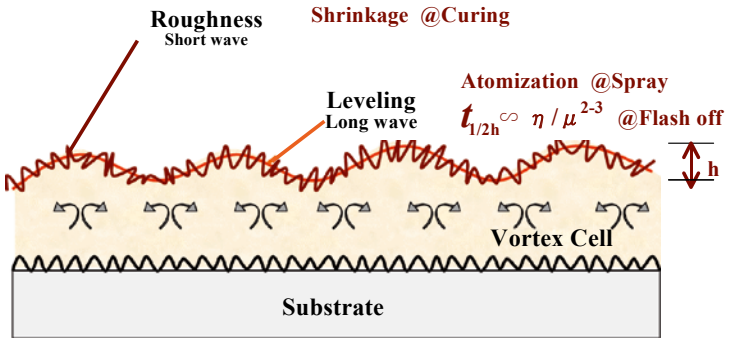

Fig. 2.15 Mechanism of surface appearance

From a 55° angle the light shines to the surface and at the other end the inspector can see the defects due to the reflection. This inspection system measures combination of surface smoothness and gloss.

Figure 2.14 shows a result. It is very interesting that higher NV = higher viscosity of wet film makes lower surface smoothness and makes higher gloss. PGD value is low at low and high range of NV of wet film. PGD is exactly combined measurements, surface smoothness and gloss. At low range of NV, PGD value is low because of poor gloss, and at hi range, it is also low because of poor surface smoothness.

It is easy to understand the reason why the smoothness is poor at high viscosity. Smoothness depends on the fluidity of the film. According to T.C. Patton, time required for leveling of the wet film depends on viscosity and film thickness as shown in Fig. 2.15.

How about gloss? Gloss has a close relationship with surface roughness. When I started the analysis, gloss was assumed to relate to vortex cell in the wet film during curing process. However, gloss or roughness of paint film depends on the surface roughness of the substrate. Then we noticed that roughness of dry paint film depends on the shrinkage rate of wet film during curing process. Usually, the wet film

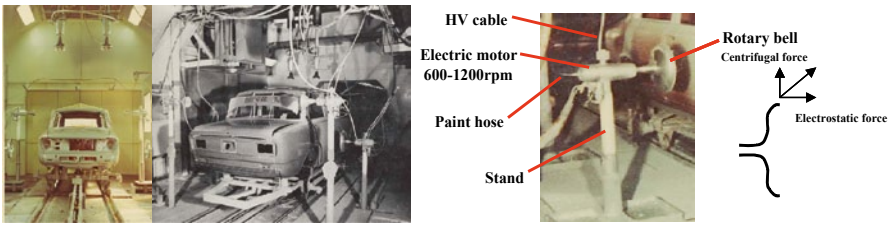

Fig. 2.16 Ransburg No. 2 bell

has shinny surface and we cannot see roughness on it. We see poor gloss after curing. If NV of wet film is 100 %, we will see the same shinny surface with wet film after curing, and if it is 0 %, we will see the same poor surface with the substrate. In other words, gloss depends on shrinkage rate during curing process.

Surface coating technology has been making progress during the past 30 years but still remains largely experience based. Therefore, now more than ever, the auto surface coating technology requires vigorous scientific research and prediction to make future progress. One reason for this section is to urge readers to share my long experience in this field to emphasize how important a scientific approach as well as statistical approach is to understanding experienced based technology. I am glad to be working with the UK research team on the CFD analysis and rigorous scientific method to understand this technology. Their chapters will follow, which will make this book valuable and unique in this area.

2.4 A Brief History of Spray Paint Technology

It is important to develop and improve each input module in order to integrate good input modules. The most important input module is a spray atomizer. It may be worthwhile to briefly explain how we came up with the current spray paint technology by looking back at the history of the technology development of the spray atomizer, especially electrostatic bell.

Number Two Bell When I entered Toyota in 1971, we used to use two types of spray equipment. One is an electrostatic or non-electrostatic air spray gun, the other is electrostatic rotary bell atomizer, so called just bell. The former has better atomization performance but shows poor transfer efficiency, and is used for topcoat application because good atomization is needed in order to get high quality, especially for metallic topcoat. The latter has poor atomization performance but shows high transfer efficiency, and is used for primer application because certain level of atomization is acceptable for the primer application. In the laboratory, the transfer efficiency of Ransburg's No. 2 bell is almost 100 %, and that of air spray gun is around 30 %. It was a dream for engineers to use bell for topcoat, especially for metallic paint.

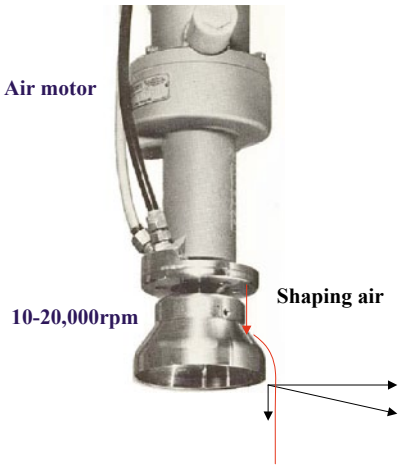

Fig. 2.17 Mini-bell

Mini Bell Painting Device Around 1975 Ransburg introduced mini-bell as shown in Fig. 2.17. No. 2 bell: large bell is rotated by the electric motor, and the rotation performance was maximum 1,800 rpm. On the other hand mini-bell is rotated by the air motor, and the rotation performance was around 15,000 rpm. The transfer efficiency of mini-bell is a little bit inferior to No. 2 bell, but atomization performance was much improved. Engineers expected to use mini-bell for topcoat. However there were a couple of problems as follows.

(a) Air popping or bubbles are created on the coated surface
(b) Maximum rotation speed was not enough for obtaining the atomization performance like air spray gun.

Grooved Mini-Bell Ransburg studied a lot for solving air popping problem. When they started their study, they thought that air bubbles were formed inside the bell cup. Paint is delivered to the back plate of bell cup rotating at high speed. Paint is splashed on the back plate and air bubbles are formed and trapped in the paint. For preventing paint from splashing, they tried to improve paint delivery method: (a) changed paint delivery nozzle angle against the back plate from perpendicular to diagonal (b) changed paint delivery method from side feed to center feed. However those could not work well (see Fig. 2.18).

While having continued their study, they became understanding gradually that air bubbles were formed due to poor atomization. Atomization is done at the edge of bell, but it fluctuates at portion by portion of the edge. In order to get an even atomization, they invented grooved mini-bell, shown in Fig. 2.19. Many fine grooves with the same pitch are engraved on the edge of the bell cup. The atomization starts at each groove, and then the atomization with the same pitch, even atomization is obtained. In order to evaluate atomization, general arithmetic mean diameter is not used but SMD: Sauter mean diameter is used. Even if arithmetic diameters of two groups of particles A and B are same, SMDs of two groups are different. SMD of group with higher variance of particle diameters is larger than that of group with

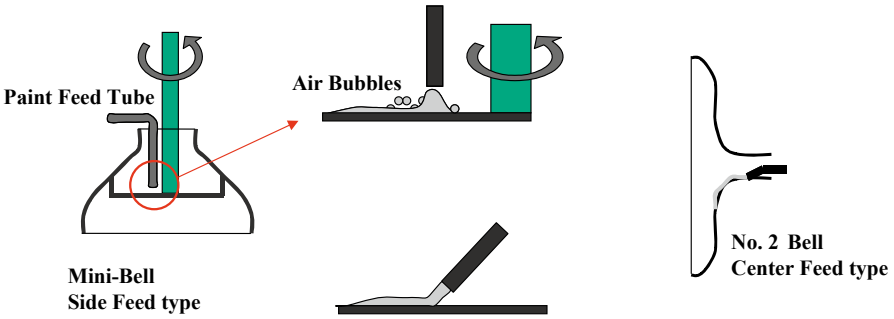

Fig. 2.18 Ransburg tried a lot to improve paint feeding method

Fig. 2.19 Grooved mini-bell

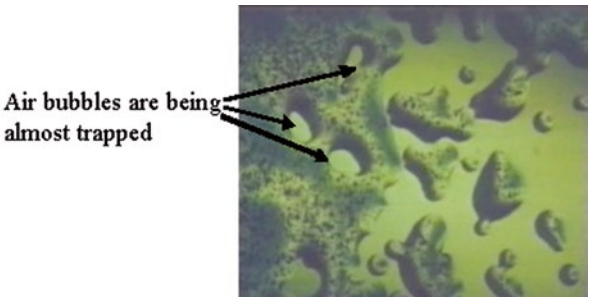

Fig. 2.20 Microscopic image of painted surface

lower variance. In other words, lower atomization performance with higher variance of particle diameters. The effect of grooves is excellent. Air popping problem had gone.

Figure 2.20 is one shot from the video of Daimler Benz. Paint particles are just hitting surface of the substrate and paint film is being formed. We can imagine that air bubbles are being trapped on the surface, and that poor atomization causes large air bubbles.

I assumed the mechanism of air popping like this 35 years ago. Now we come to 2008 when I attended a lecture by Professor Ito of Hachinohe Institute of Technology, I was amazed at one point when I heard him mention the mechanism of this bubble formation Prof. Ito explained the detailed mechanism of this formation, this was the first time I understood how complex this was and the need for scientific research which can help us to ultimately improve the surface quality. Without this scientific understanding it would take a long time to erase the bubble formation and improve the surface quality through trial and error/experience. According to him, air bubbles are formed by the shock wave caused by hard hitting of particles to the surface of substrate. Anyway, larger particles cause stronger shock wave and air bubbles.

Use of Air Bearing to Increase Rotational Speed of Bell Cup Around 1980 the rotary type bell sprayer had limitations in their speed due to mechanical friction caused by the ball bearings. Their max rotation speed was achieved at 1,500 rpm, however to further improve the painted surface quality the finer paint droplet size is required. To generate fine droplet size, higher rotation speed of the spray bell is required. When I was at Toyota's surface finishing division, several engineers worked to improve this limitation and came up with an idea to use air bearings which were used at that time at the gas turbine system. So this paradigm shift from the gas turbine tech to the paint spraying system brought new and improved rotation speeds of up to 60,000 rpm. Figure 2.21 shows a photograph of the first prototype of this air bearing type sprayer.

Metallic Bell Since mini-bell had been introduced in the middle of 1970s, a lot of developments and improvements had been done. As a result, mini-bell became popular for topcoat process as well as for primer process. However, we still could not use mini-bell for metallic application due to off-color problem. Table 2.1 shows that the color obtained with a rotary bell is very dark, whereas the air spray gun

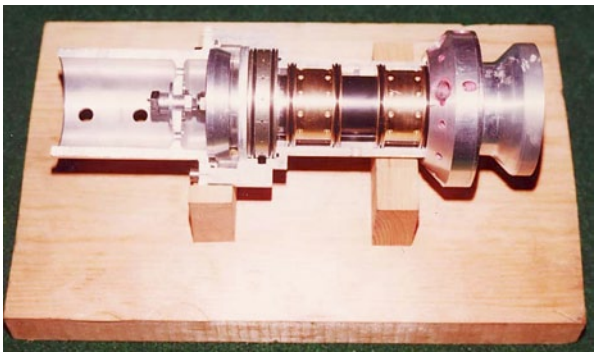

Fig. 2.21 Prototype air bearing sprayer

Table 2.1 Color comparison of silver metallic

	Electrostatic air spray gun	Conventional bell
HV (kV)	60	90
Air pressure (kPa)	450	150
Flow rate (ml/min)	300	150
Film thickness	15	15
Transfer efficiency (%)	40	80
Droplet sign (μm)	18	18
Al flakes size (μm)	14.5	7.9
Droplet speed (m/s)	12–15	2–5
Color	–	–
L	81.5	75.8
a	−0.5	−0.6
b	−1.2	−1.1

gave a much lighter (L value with bell is much lower than that with air spray gun, 75.8 vs. 81.5).

In the last section, I explained how we could obtain the light color. Atomized particles hit the substrate. When the viscosity of particles is low, aluminum flakes in wet film tend to orientate parallel to the substrate, and this gives bright color. Figure 2.22 shows the cross section of the paint film with a microscope. We found that using the rotary bell, aluminum flakes were bent and distorted, and randomly oriented, whereas using air gun, the flakes were flat are oriented mostly parallel to the substrate.

The distortion of aluminum flakes is considered to be due to the high shearing force created by the high circumference speed of the bell. It was hard to measure the degree of the distortion of each flake. We then decide to measure the size of aluminum flakes in the paint film instead of the degree of distortion. Figure 2.23 shows that the circumference speed must be less than 50 m/s to prevent the distortion of the aluminum flakes.

As already mentioned, the orientation of the aluminum flakes using air spray gun usually depends on the viscosity of the wet film. There is a suitable range of wet film viscosity to make the orientation of flakes parallel to the substrate. However,

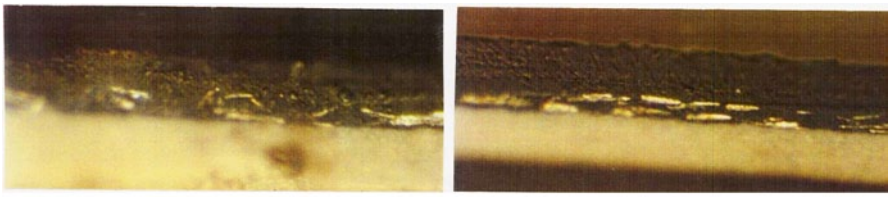

Fig. 2.22 Cross section of metallic basecoat

Fig. 2.23 Distortion of aluminum flakes

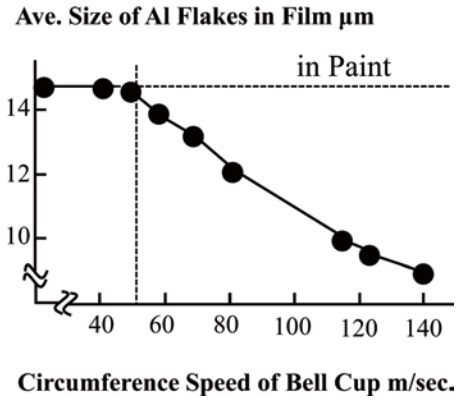

Fig. 2.24 Velocity of paint particles vs. L

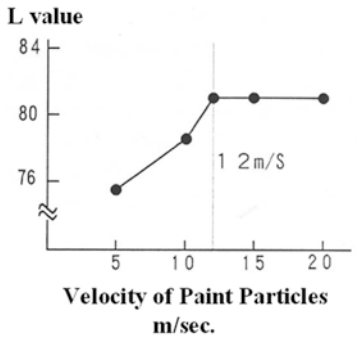

the orientation of aluminum flakes obtained with the bell application is always random at any viscosity of the wet film. We assumed that the collision between paint droplets and substrate determines the original flake orientation. If the paint droplets hit the substrate at a high speed, the droplet shapes are flat, and the resulting orientation of the aluminum flakes is parallel to the substrate. Figure 2.24 shows that the paint droplets at greater than 12 m/s result in light, bright metallic color.

The prototype of metallic bell was designed with the following items taken into consideration.

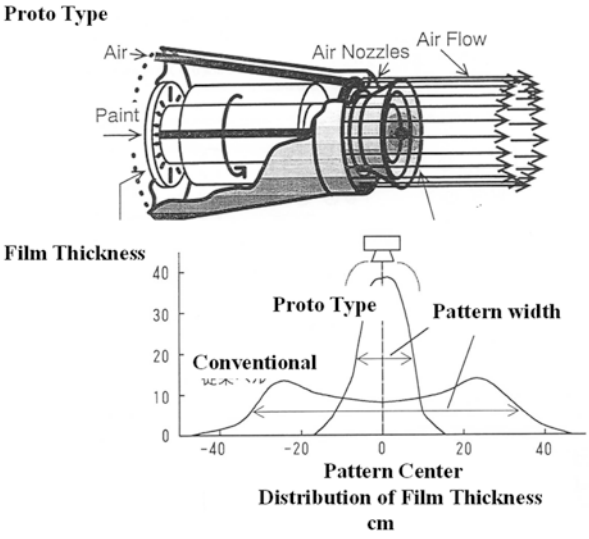

Fig. 2.25 Schematic of prototype metallic bell and film thickness distribution

(a) The rotation speed of the bell cup should be low enough to prevent the distortion of the aluminum flakes.
(b) The paint should be atomized not only by rotation but also by air because low rotation speed results in poor atomization and poor appearance quality.
(c) The velocity of the atomization air should be high enough to make the orientation of the aluminum flakes parallel to the substrate.

Figure 2.25 is a schematic of a prototype bell remodeled from the conventional bell. The biggest difference between two bells is the location of the air nozzles. Air from the conventional nozzles hits the back face of the bell cup and results in low air speed. On the other hand, air from the nozzles of the prototype bell hits the edge of the bell cup and results in improved atomization and high droplets speed.

When applying metallic paint, the prototype bell shows a light, bright metallic appearance; however it also shows a color-mottling defect like a zebra pattern because the spray pattern of the prototype bell is too narrow (Fig. 2.25).

In order to improve the spray pattern width, the airflow was investigated and analyzed with the spark trace method. From the spark photographs shown in Fig. 2.26, it was found that the conventional bell with a high circumference speed twisted the airflow. As a result, the twisted airflow induced other airflow into the center of the spray cloud (spark lines are drawn back toward the bell cup in Fig. 2.26 right). This may be one of the factors why the conventional bell has a large donut-like spray pattern. Left side of Fig. 2.26, the spark photographs of the prototype bell clearly show there is no twisted or induced airflow.

Based on the above analysis, the air nozzles of a new metallic bell were intentionally twisted, which created an induced air inlet path from the front. Figure 2.27 is a schematic of the new metallic bell and Fig. 2.28 is the spark photograph of its spray pattern. It can be seen that these spark photographs resemble those of the conventional bell shown in Fig. 2.26 right.

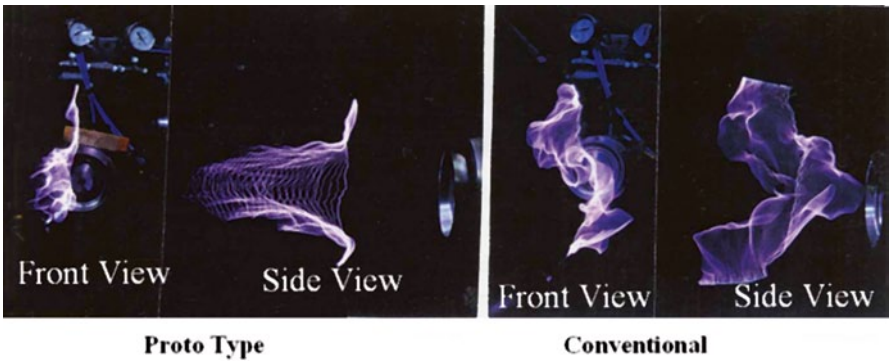

Fig. 2.26 Analysis of airflow with spark trace method

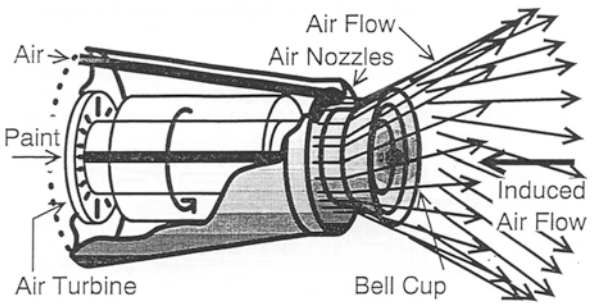

Fig. 2.27 Schematic of metallic bell

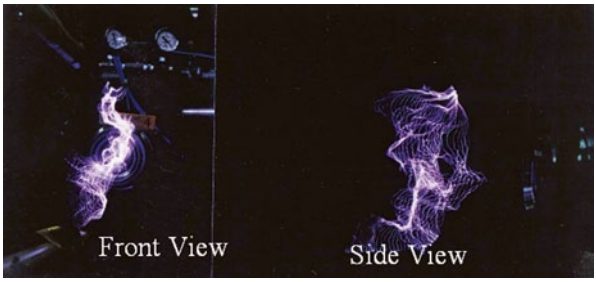

Fig. 2.28 Airflow of metallic bell

Table 2.2 shows a comparison of the colors applied with the air spray gun with the new metallic bell. The new metallic bell provides a metallic appearance with the same light and bright metallic colors as that of air spray equipment.

Bell with Multi-Feed Tubes Since the Toyota Production System does not allow us to apply block color painting, we must change colors frequently causing much paint loss.

Figure 2.29 shows a general color change system. At the automotive paint shop, topcoat color is changed car by car. If they manufacture 1,000 cars a day, they must

Table 2.2 Color comparison of metallic paints

Metallic color	New metallic bell			Electrostatic spray gun		
	L	a	b	L	a	b
Silver	64.2	–2.0	–0.6	64.3	–2.0	–0.6
Red	23.1	6.9	3.0	23.1	6.8	3.0
Beige	73.1	5.2	20.3	73.0	5.3	20.3
Green	40.2	–1.3	–3.0	40.4	–1.3	–3.0
Blue	16.6	–0.3	–21.9	16.7	–0.3	–21.9
Purple	36.5	2.9	–12.9	36.6	2.9	–12.9

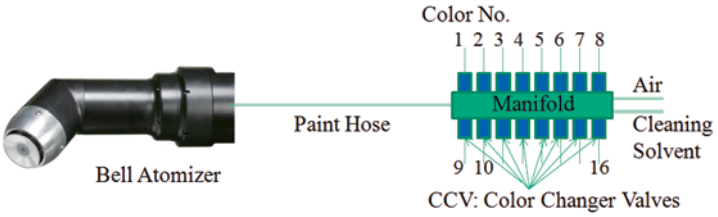

Fig. 2.29 Color change system for 16 colors

change color several hundred times. Color is changed at the color changer manifold with CCVs: color changer valves. When they change color from color 1 to 6, color 1 must be pushed out from CCV for color 1 to gun, then paint line from CCV to gun must be flushed and cleaned with cleaning solvent, and cleaning solvent is pushed out, and eventually color 6 is sent to the gun from CCV. Usually, there are almost 20 guns or bells in the topcoat line. A lot of topcoat paint and cleaning solvent is wasted during color change. It is important to reduce such losses for saving running cost as well as for reducing VOC.

In order to reduce the paint wasted during color change, we developed a bell with multi-feed tubes.

There are seven tubes in the bell so that six different colors remain in the tubes all the time and the seventh tube is used commonly for any additional colors. In other words, six colors do not have to be flushed out and cleaned during color change. When the multi-feed bell was installed to the clear and solid: non-metallic coating process, it shortened the cleaning time 40 % and reduced the solvent usage 50 % without paint loss.

For metallic paint, hi-voltage fault often occurred because aluminum flakes are settled in the feed tubes. So, multi-feed bell was replaced with the following cartridge bell.

Cartridge Bell Since 1960s, to reduce usage of VOC: volatile organic compounds, almost same as HC; hydrocarbon, is very important for the painting industry in order to prevent photochemical smog caused by the combination of HC and NOx. One of the most effective methods for painting is to use waterborne paint instead of solvent-borne paint. However, the electrostatic spray equipment such as bell cannot be used because waterborne paint is electrically conductive and causes the hi-

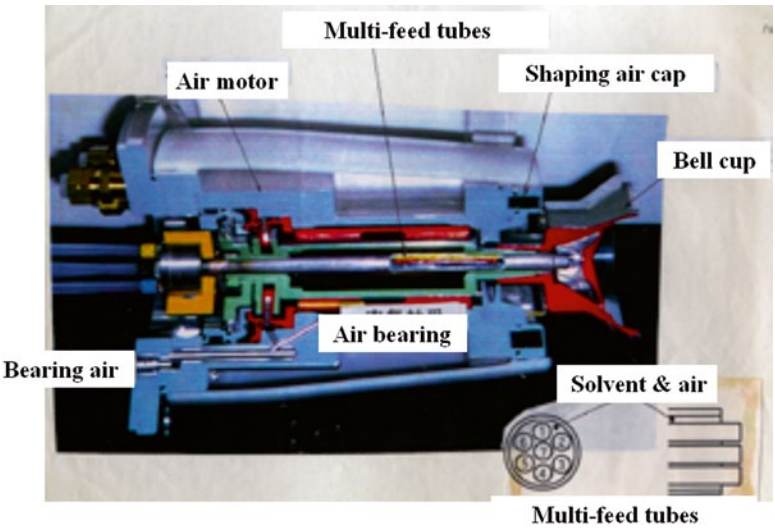

Fig. 2.30 Multi feed bell seven feed tubes are installed in the pipe inside of the bell

Fig. 2.31 Bell with external electrodes. (From Duerr's presentation at Surcar)

voltage leakage problem. One idea to prevent hi-voltage from leakage is to use bell with external electrodes. Hi-voltage is applied after paint spraying, in other words, hi-voltage does not directly contact with the conductive waterborne paint grounded. This method is still popular in Europe.

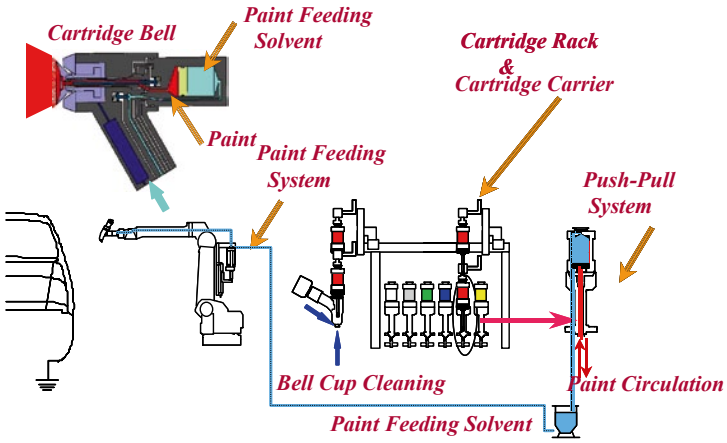

Fig. 2.32 Cartridge bell process schematic

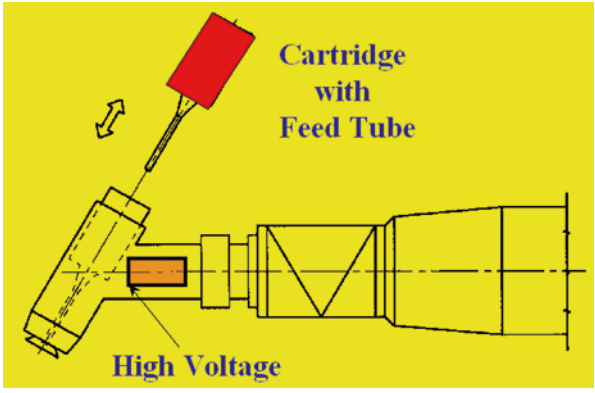

Fig. 2.33 Feed tube is installed just behind the bell cup

However, the transfer efficiency of bell with external electrodes is not so high as that of direct charge type bell. Toyota has been using a cartridge bell for the water-borne paint for more than 10 years. Originally, this system had been developed to improve color change. As shown in Fig. 2.29, the point is that paint in hose between CCV and gun must be flushed and cleaned.

Toyota's engineers provided good idea. If we don't have such a paint hose, we do not have to flush or clean it. They invented cartridge system based on this idea. Figure 2.32 shows an original cartridge system. In a cartridge rack, around 20 cartridges (each cartridge contains different topcoat color paint) are installed. The cartridge has a cylinder like an old fountain pen in it and feed tube is installed outside of it. The cartridge is inserted into the inside of the bell equipment by cartridge handling robot. The tip of feed tube is set just behind the bell cup as shown in Fig. 2.33. Paint is pushed out to the bell cup by the cylinder through feed tube. Color change, in other words cartridge change is done by a handling robot. Cleaning is done only around the bell cup, little waste of paint and solvent occurs.

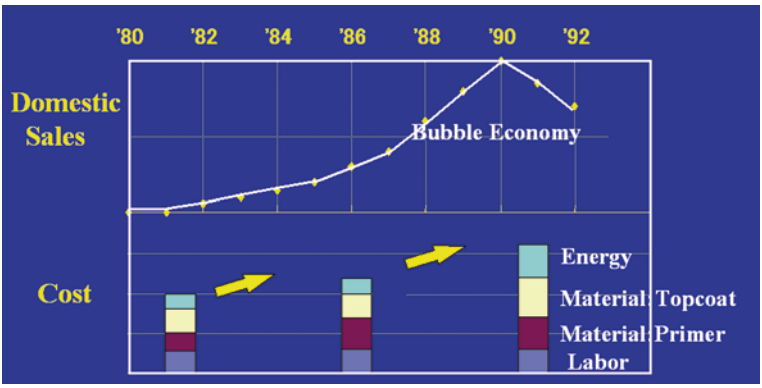

Fig. 2.34 Cost trend from 1980 to 1991 in the paint shop

At the paint application, cartridge is isolated and even if hi-voltage is applied on the bell cup, hi-voltage will not leak through water borne paint.

2.5 Painting Is Based on the Integral Technology

We were economically in the best era, so called bubble era from the end of 1980s to the beginning of 1990s in Japan, almost same as the period before Greek economy crisis in Europe or before Lehman's shock in US. Automotive makers concentrated on the luxurious cars with high quality. They forgot the importance of the cost and energy saving. Therefore at the end of bubble era, the plants and facilities which running cost was extremely high were just left. Almost all car manufacturers profit had gone.

Especially the paint shop was significant. Booth space became larger, from approximately 360 m^2 (60 m × 6 m) to 600 m^2 (100 m × 6 m), and number of paint machines as well as the number of bells increased. This causes a large amount of paint to be wasted during each color change and increases the energy consumption needed to control the air conditioning of the booth. Neither of these is beneficial to the environment or to the cost of the vehicle as shown in Fig. 2.34. I became one of general managers in Toyota at such timing. I decided to start a new project. The purpose was to improve everything at the same time. As I mentioned in first Sect. 2.1, painting is not based on the modular technology but integral technology. However, in bubble era, we forgot this. We concentrated on just one side, quality or luxury. We had to consider not only quality but also everything such as cost, environment, productivity and so on, while integrating all the input items, material, facilities, equipment and so on.

Eventually, we developed a new robot painting system. This was presented at ISATA: International Symposium on Automotive Technology and Automation held in Duesseldorf and we received the Nissan Award.

Figure 2.35 shows the topcoat layout in 1990. We introduced many robots in the topcoat booth which length became longer from 60–70 m to 100 m. You may not

1990's

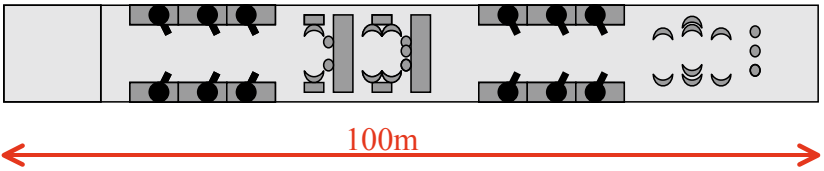

Fig. 2.35 Typical topcoat booth in 1990

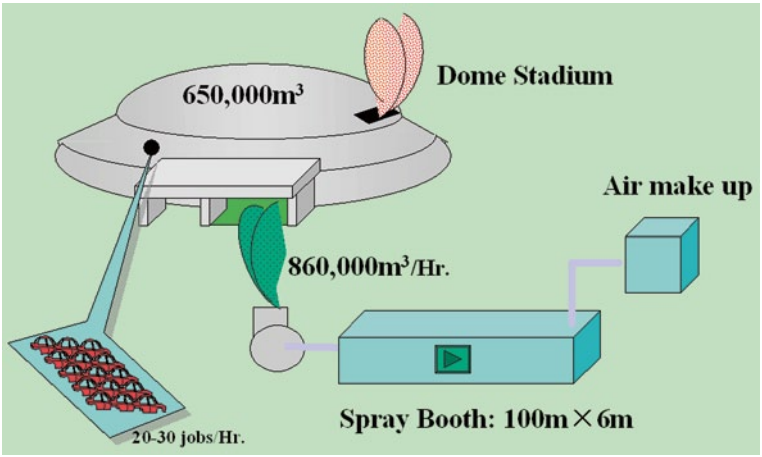

Fig. 2.36 Booth air volume with 1 h operation = size of domed stadium

understand the energy usage of the booth. Fresh air with controlled temperature and humidity must be introduced into the booth in order to get the constant quality and to eliminate over-sprayed painted particles at venturi scrubber. Normally air velocity is around 0.4 m/s and booth width is 6 m.

Those mean that we have to supply tremendous amount of the temperature and humidity controlled fresh air into the spray booth. 100 m × 6 m × 0.4 m/s × 60 s/min = 14,400 m^3/min. It is very hard to imagine the amount of 14,400 m^3, but it means 120 m × 120 m × 1 m. If we operate one hour, the amount of fresh air will be 120 m × 120 m × 60 m. This is exactly a size of a domed baseball stadium. In 1 h, we paint only 30 cars. Please imagine. There are 30 car bodies in the domed stadium. Outside temperature is below 0° in winter, and inside temperature and humidity is 20° and 70 % RH. After painting 30 cars, all the controlled air is exhausted to the outside of the plant and replaced with another controlled fresh air. Besides, tremendous amount of air is exhausted and replaced almost only through one door. Please imagine. We need a lot of energy in order to exhaust air from a floating ring or beach ball and to blow air into the ring or ball. In order to capture over-sprayed paint particles, venturi water scrubber with narrow slit is installed. All the exhausted air must pass this scrubber, it is almost like the state mentioned above.

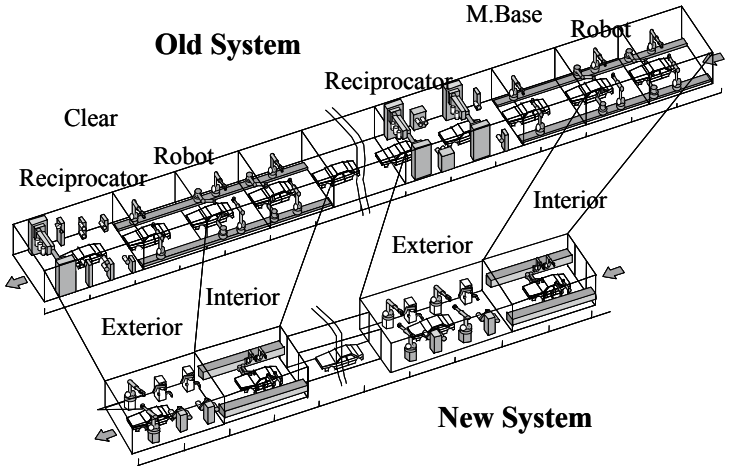

Fig. 2.37 Comparison between old system and new system

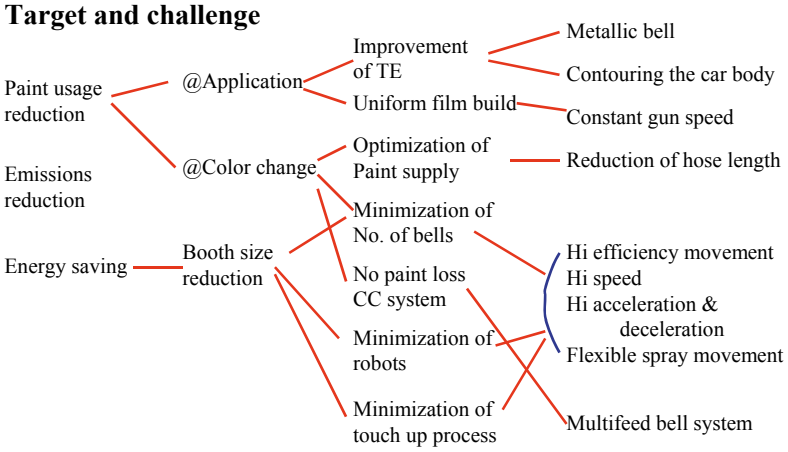

Fig. 2.38 What we did for developing new system

A summary of what we did is shown in Figs. 2.37 and 2.38 [3]. I would like to explain three points in this book.

1. Minimize paint usage
   To minimize paint usage, the entire amount of paint being delivered to the bells or spray guns, should be applied to the automobile body. Three approaches to reduce the amount of wasted paint were taken. The first is to improve transfer efficiency. The second is to minimize or eliminate the amount of paint used during color change. The third is to obtain a uniform coating on the car body.

1.1 Improve transfer efficiency

a. Electrostatic bells are used at all the stages in the topcoat process. For metallic paint, the air gun is commonly used throughout the world for the second stage of metallic basecoat. This is mainly due to the lack of brightness achieved by the use of bells during this stage. The disadvantage of using the air spray guns is poor transfer efficiency. Toyota developed its metallic bell as explained at the previous section.
b. The bells should follow the contour of the car body. For reducing the overspray, it is necessary to spray at a perpendicular direction to the car body while maintaining a constant gun distance.

1.2 Minimize paint loss during color change

a. A bell with multi-feed tubes was developed as described at the last section. Several years after its introduction, it was replaced with the cartridge bell.
b. To reduce number of bells leads to reduce paint loss during color change. The amount of wasted paint and cleaning solvent is related to the number of bells.

1.3 Obtain uniform coating

a. The bell speed must be constant.
b. In order to get enough time to paint the entire car body with a constant speed, a bell should move with high acceleration and deceleration.

2. Minimize total energy of topcoat process
As already mentioned, tremendous amount of energy is used for operating the booth. It is very important to reduce booth length to reduce cost and energy.

2.1 Minimize the number of painting machines
It is necessary to keep some distance between the bells and robots to prevent contamination of the bells and the interference between robots. In order to decrease the size of the booth, it is necessary to reduce the number of machines. It is important that the machine moves with a high efficiency in order to apply paint on the same application areas.

2.2 Eliminate the touch-up process
In the topcoat process with automatic reciprocators, a touch-up process is needed with operators or robots with air guns. This process causes the booth longer and poor transfer efficiency.

3. Maintain and keep improving high appearance quality
Even if we could reduce paint usage, energy, running cost, it could not be acceptable to decrease the level of quality. We have to improve all the output items at the same time.

3.1 Utilize the benefit of robot painting
The robotic paint machine has great advantages over the conventional reciprocator. When we design the topcoat system with conventional reciprocators, most spray parameters depend on the conveyor speed related to the produc-

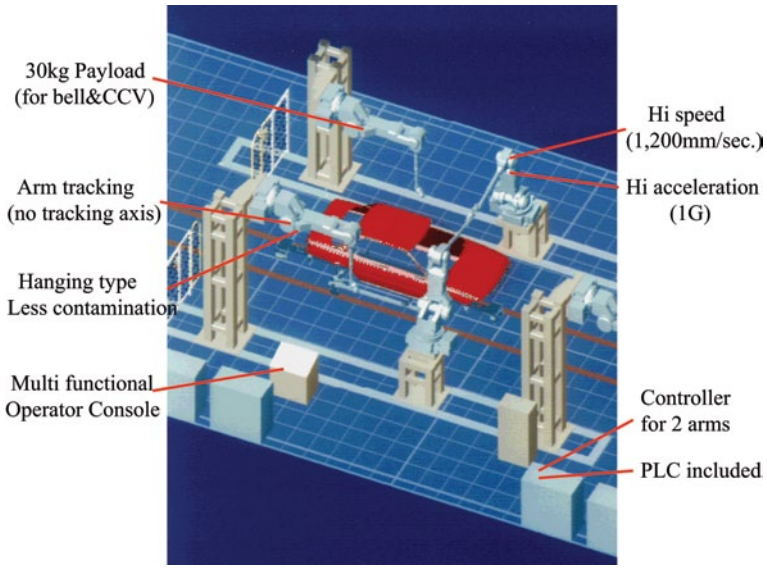

Fig. 2.39 New painting system

tion volume. For instance, we have to increase the paint flow rate at the high conveyor speed. When the line-tracking function of the robot is used, the speed of the robot varies, depending on whether the robot is moving in the same direction with, or against, the flow of the conveyor. The absolute speed will vary up and down with the conveyor speed, but the speed relative to the car body will remain constant. Therefore, with constant control of the paint parameters (i.e. paint flow rate, fan width, over wrapping, atomization), the robot is always able to give a consistent, uniform paint thickness and quality independently of the conveyor speed.
Besides, with the arm-type robot, the distance between strokes, the gun distance from the body, and its approach vector to the body is constant, because of its flexibility. The best conditions for painting, the most important factor, will be obtained for the entire body.

3.2 Set the best spray conditions while minimizing losses
Basically, it becomes easier to obtain the high appearance quality with lower paint flow rate, because of better atomization with lower flow rate. However, the low paint flow rate causes to increase number of bells and to increase all losses as already discussed above.
We worked hard together with material engineers and we found out the critical points of material parameters such as best NV of wet film, type of solvent, application viscosity and paint flow rate. It is very important for the integral type technology to work closely together with different areas.

Figure 2.39 shows the new system, and Fig. 2.40 shows a result.

The arm type robots carrying the metallic bells are applied to the topcoat process in order to eliminate the touch-up process, reduce the number of machines and

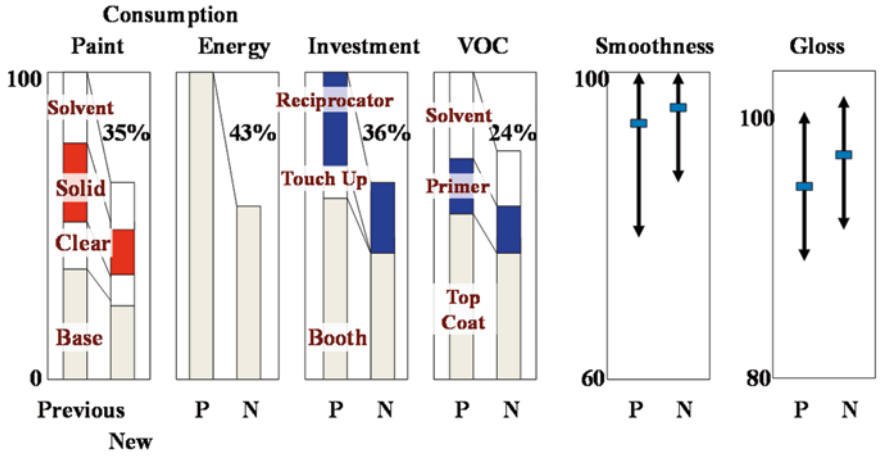

Fig. 2.40 Comparison between previous system and new system

bells, increase transfer efficiency and obtain a uniform coating. The highly intensive system is able to make the booth 40 % shorter in the exterior topcoat process. This leads to the energy consumption being reduced by the same ratio and paint consumption reduced by 32 % compared to the conventional system. VOC emission is also reduced by 24 %.

This system has been modified and improved. Currently, waterborne paint with cartridge bells instead of conventional paint with multi-feed tube bell. The new system has been introduced in Toyota, and the similar system has been used in other automotive companies, especially in Japan.

2.6 Future

2.6.1 Net Percentage

The year, 2012 is 100 anniversary of Mr. T. Ohno's birth. Mr. T. Ohno is a founder of TPS: Toyota Production System. He kept saying to eliminate "Muda, Mura, Muri," which means "Waste, Unevenness, Unreasonableness." One important measure for those items is net percentage. It is the best way to increase net percentage in order to eliminate Muda, Mura, Muri.

Example of Net Percentage: Transfer Efficiency
Transfer efficiency: TE can be defined as follows:

$$\mathrm{TE} = \frac{\text{paint coated}}{\text{paint sprayed}}$$

It is true, but is it the net percentage?

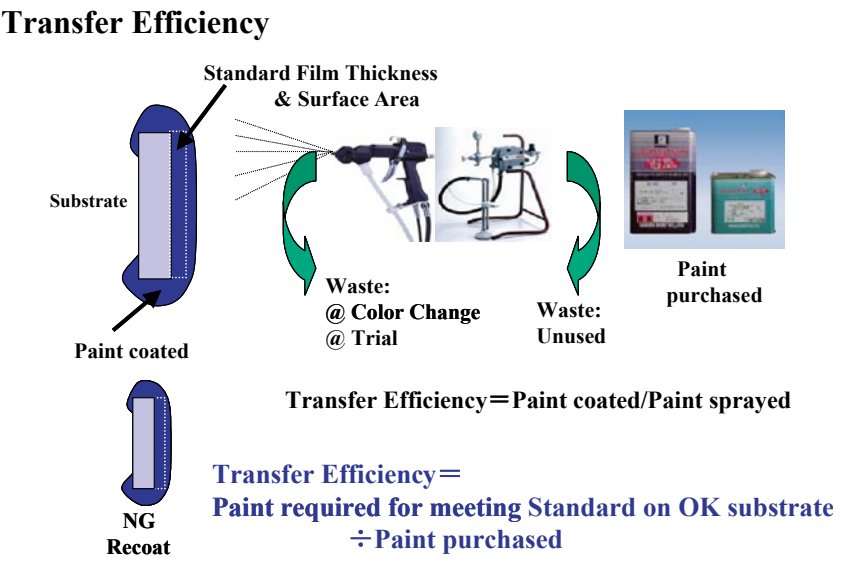

Fig. 2.41 Net transfer efficiency

Look at Fig. 2.41. Paint is sprayed from the spray gun and coat the work piece. The paint volume coated is shown with blue color. If the film thickness and coated area is provided as the dotted line by the standard, what should we call paint, coated on the back face of the piece or excessively coated? It must be the same as over sprayed paint. How about paint for recoat? It is also the same. During the painting operation, paint is wasted for changing color, for testing, trial and so on. At the paint kitchen, some amount of paint is left without use. Therefore, net percentage of transfer efficiency must be defined as follows:

$$\text{Net TE} = \frac{\text{Paint required for meeting standard on OK substrate}}{\text{Paint purchased}}$$

According to my experience, net TE used to be less than 40 % for car bodies, and less than 10 % for small parts. Once we realize that our net TE is such low value, we will try to increase net TE. However, most people believe that their net TE is higher than 30 or 50 % so that they do not make an effort to improve it.

Robotic painting with bells has contributed the improvement of net TE. Probably, net TE for car body topcoat painting is around 50 % at the best paint shop. We still have a room and we have to keep improving it. You may think that we still have big waste by 50 % and that it must be easy to increase net TE 10–20 %. However, it is very hard. It is not a matter of technology but a mater of integration, or daily Kaizen activity. The transfer efficiency of bell in the laboratory is around 90 %, but net TE is at highest 50 %. The difference between those consists of small wastes

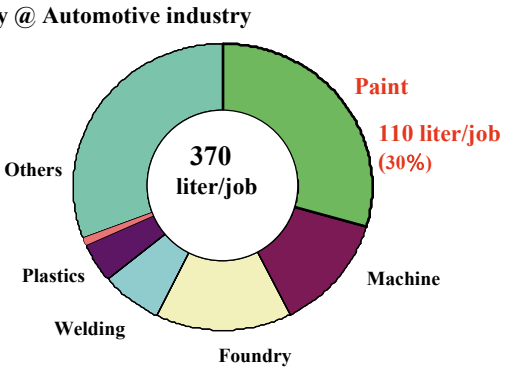

Fig. 2.42 Energy consumption for producing one car

almost innumerable. That's why Mr. T. Ohno emphasized the importance of Kaizen, continuous improvement.

Improvement of Net Percentage of Energy Consumption Is Most Important for Future The most important issue for environment is to reduce CO2 emission, in other words, to reduce energy usage. Unbelievably, tremendous amount of energy is consumed in the automotive paint shop, around100 l based on crude oil to paint one car. Figure 2.43 depicts the total energy usage for manufacturing one car and distribution of the painting process. Literally this means that the energy consumption in the automobile painting system is one of the highest, or least efficient (Fig. 2.42).

As I have already explained at the previous section, a lot of energy is consumed for the booths operation. The contribution rate of booths for primer and topcoat reaches almost 60 % of total energy consumption in the paint shop. Therefore, to reduce energy for booths is most important. What is present net percentage of energy consumption for booths? How can we calculate it?

Net Percentage of Booth Length For the automotive topcoat painting at 1 min takt (cycle) time, usually we need two 100 m booths. In other words, we need 100 m-booth length for the production of 30 cars an hour. In order to apply 30 cars an hour, minimum 12 robots are necessary. Robots are installed both side in the booth. If the occupied length of one robot is 2.5 m, 15 m-length booth is enough. It means that present net percentage of energy consumption is only 15 % from the viewpoint of booth length.

Net Percentage of Operation Hours For two shifts operation, usually we have to operate booths for 24 h. Huge fans are installed for booths, and cannot start or stop easily. Because good balance between supply fans and exhaust fans is important. Once the balance is lost, strong airflow occurs, and this causes dirt defects and problem in the paint shop. Accordingly, we cannot stop the operation of booths at lunch, break time, and between shifts.

It takes almost 30 min for car bodies to pass through 100 m-length booth. At the beginning or end of production, there are no car bodies at the exit side or entrance side of the booth, but whole booth is operated. Even during the production, we have

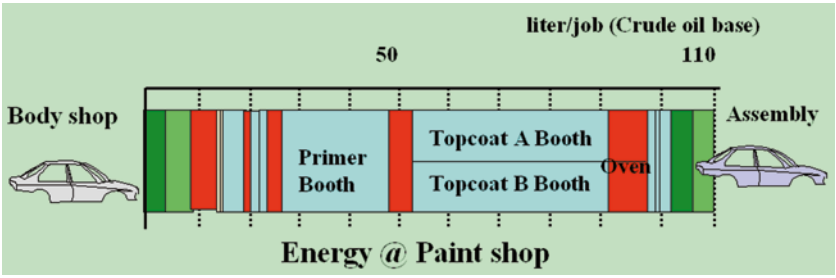

Fig. 2.43 Energy consumption in the paint shop

Fig. 2.44 Photo pictures of modular painting system in GM

a waste. Recoat jobs, ghost jobs, pass through the booth. Even from the viewpoint of operation hours, we waste energy by 40 %.

Net Percentage of Production Load At the bubble era, sales were excellent, and production load of each line was higher than 90 %. However, after the end of bubble era, or after the Lehman shock, sales ware down and production load became lower. If the production load is less than 50 %, we may be able to stop the operation of one booth, but if it is higher than 51 %, we have to keep operating two booths. Anyway, we waste energy by 20–30 %.

Now, you understand the true net percentage of the booth energy, 15 % × 60 % × 75 % = 7 %. Where has the rest, 85 % gone? How can we improve net percentage of booth energy consumption?

I believe that production with small booths is best.

Modular Painting System in GM In 1980s, GM developed a modular painting system with painting robots. Figure. 2.44 are not pictures of Hamtramck plant, but it is almost same as Hamtramck's system. When I was a NUMMI member, I had an opportunity to visit Hamtramck. Frankly speaking, I was much impressed with their system, modular painting system.

It consists of several small booths as shown in Fig. 2.45. Four painting robots on the conveying axis are installed in the small booth which length is approximately 15 m. Each line consists of two booths, one is for metallic basecoat application, and the other is for clear coat application. The total booth length is 30 m. They used to produce Cadillac, luxurious car, which size is a lot larger than compact cars.

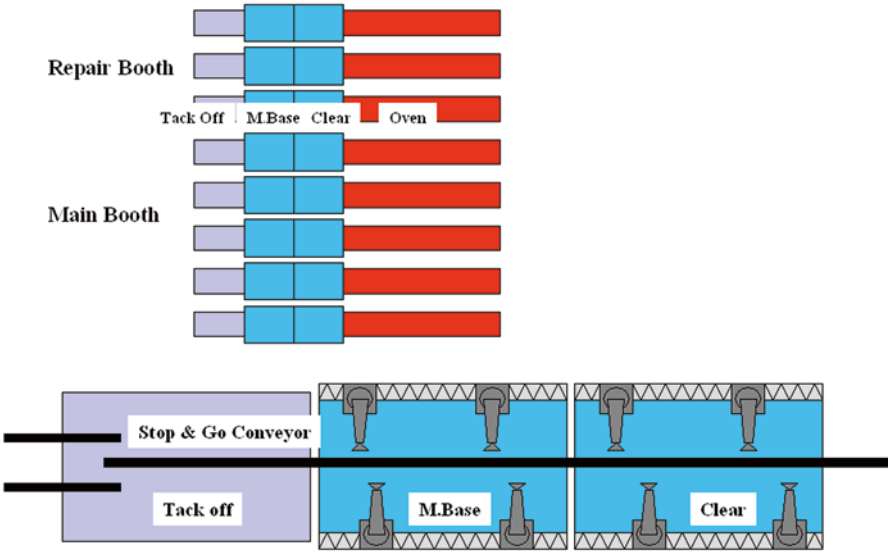

Fig. 2.45 Modular painting system in GM

According to my calculation, three lines are enough for painting compact cars at 1 min-takt time. In other words, total 90 m booth is enough. Please compare this system with the system shown in Fig. 2.43. The total length of booths is much shorter than Toyota's system explained in the previous section. Unfortunately, this system did not become so popular. I am not sure the reason, but I guess that it was too innovative to be accepted in 1980s.

Paint Box Concept of Duerr At the recent international conference, Duerr made a presentation regarding their paint box concept. I believe that this is a modification of GM's modular painting system. As Duerr explained, booth length can be reduced with paint box concept.

If we reduce the size of the booth, we can improve the net percentage of operation hours and production load as well as booth length. Because, we may be able to switch on/off the operation of small booths more easily with booth shutters. Anyway, the flexibility with combination system consisting of small booths is a lot higher than that with large or long booth system.

New Idea However, the net percentage of energy consumption is still far below 100 %.

One idea is moving work piece in front of the stationary bell installed on the ceiling of the booth. Conditioned air is supplied just around the bell. As long as the work piece is not big, this idea works well. The net percentage may reach higher than 50 %. Even if a robot with extra high payload is developed, it will be almost impossible to move car body in front of the stationary bell. Nobody can believe it, but actually, I tried it, but it was very hard to move the car body with constant relative speed to the bell and without shaking or oscillation of car body (Fig. 2.47).

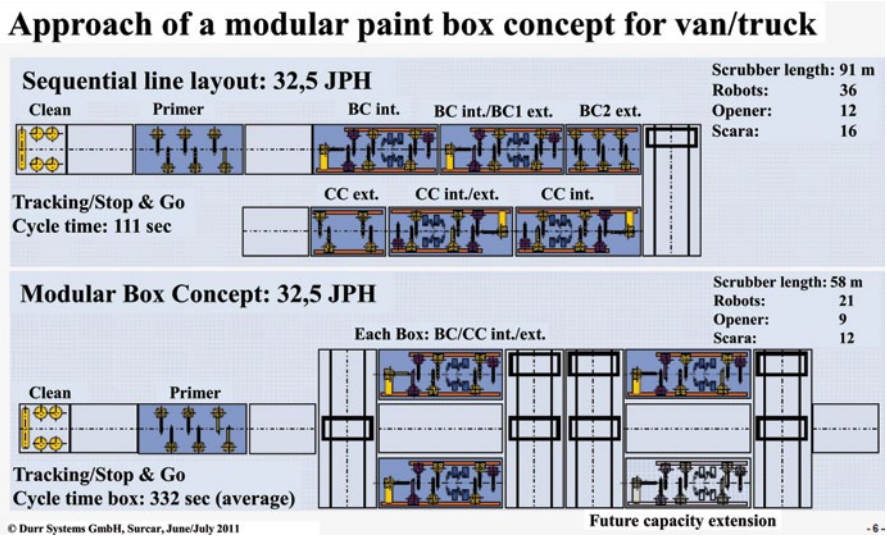

Fig. 2.46 Duerr's paint box concept

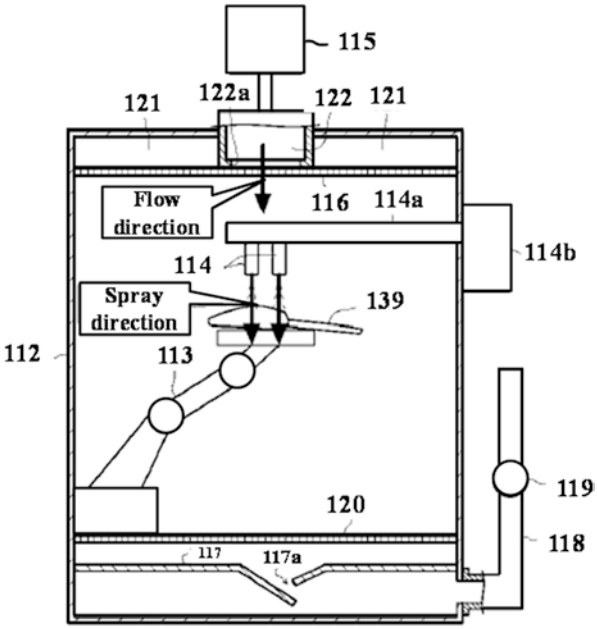

Fig. 2.47 New idea from Japanese Patent. 113: Robot, 114: Bells, 139: Door assembly part, 122: Booth air is supplied from this portion, not from 121

One trend of car manufacturing is modular production. "Smart" cars are manufactured with this method in MCC in France. Smart consists of modules, doors, engine compartment, luggage compartment and so on. Outer panels of each module are painted at the production site of each module. The parts with such size can be able to apply paint with this method.

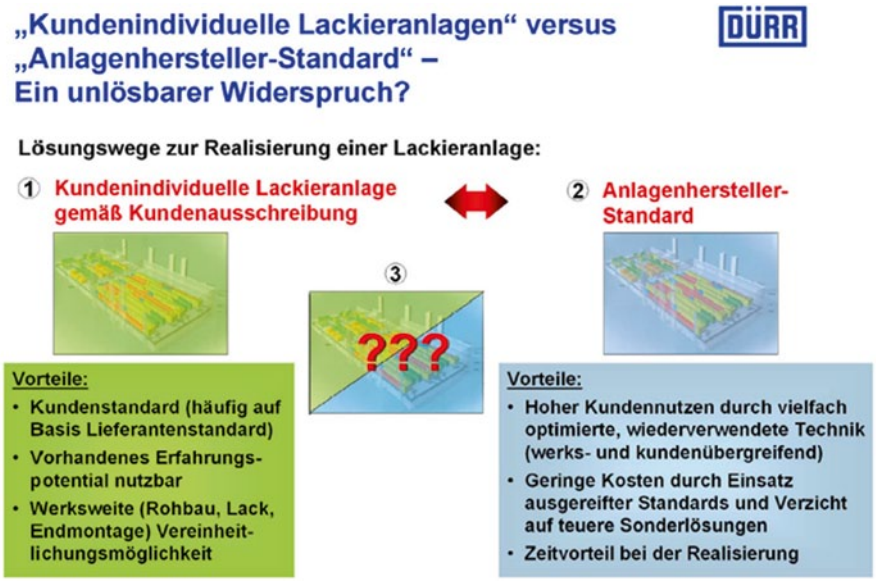

Fig. 2.48 Car maker's standard vs. facility supplier's standard. (From the presentation material at Berlin Conference)

2.6.2 Modular vs. Integral

Please look at Fig. 2.2 again. As I explained, painting is very tough because we have to keep making a lot of efforts to improve overall performances while integrating many inputs. It is almost impossible to keep doing this activity. There are two ways, I think. One is Japanese way, that is anyway to keep doing the continuous improvement. The other is the way in western countries, that is to reduce input items to be integrated by the standardization and modularization.

People in western countries are not good at integration, but at modularization according to Professor Fujimoto. They are trying to transfer from integral type to modular type, such as production of "Smart" mentioned above. I am not sure that their effort is working well or not, but it must be one answer. Figure 2.48 is a presentation material of Duerr for the international conference held in Berlin. At the construction of a new paint shop, which is better, to follow the facility suppliers (like Duerr) standard or to follow the individual car manufacturers standard? Duerr's answer is that to follow the facility suppliers' standard is better. I understand their opinion. I saw the system in western countries shown in Fig. 2.49. Duerr supplies the standard system to paint makers as well as car makers. Paint makers supply the standard material to car makers. Almost all car makers and paint makers use Duerr's standard system. Once they establish the standard spray condition in paint makers or car makers, all car makers can share and utilize it with small modification.

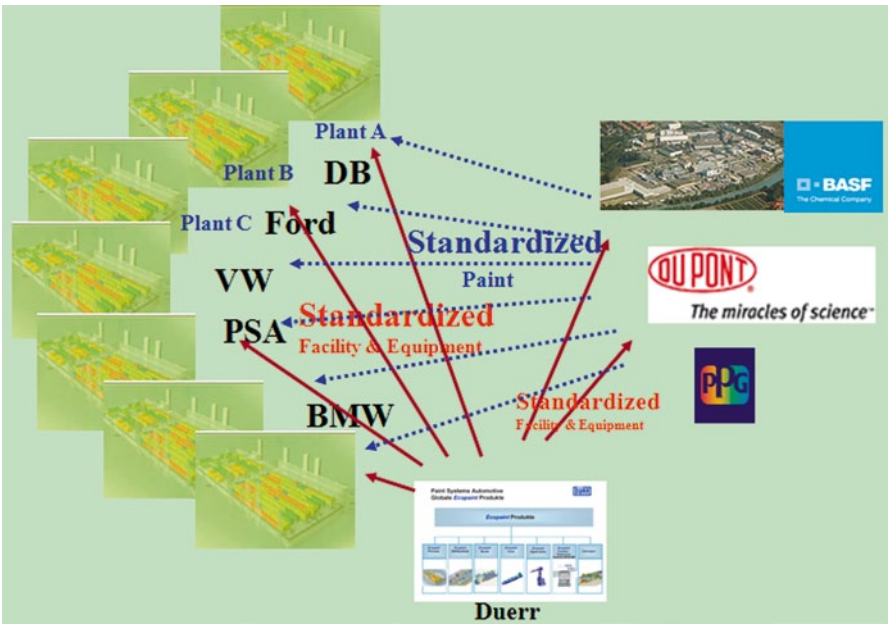

Fig. 2.49 Standard system in Europe

On the other hand, they use their own facilities and equipment in Japan. Even paint is modified by car makers. It is hard to share experiences between car makers.

I do not want to say which one is better. Each has its merits and demerits both. With western system, it may be hard to obtain better quality with lower investment and running cost compared to competitors, but they can reduce tough activities for integration. With Japanese system, it may be able to obtain better quality with lower cost, but they have to keep doing continuous integration by themselves. If their activities are not enough, their quality becomes lower and their cost becomes higher compared to their competitors not only in Japan but also in the world.

My opinion is that we should keep going ahead with standardization and modularization. But, who does it? The standards and modules established by facility suppliers or paint suppliers are best, is it true? In order to make the best standard and module, we have to integrate whole input and output items. Usually, facility suppliers are good at facility and equipment but not at material, and material suppliers are good at material but not at facility and equipment. I know there is cooperation or collaboration between paint suppliers and facility suppliers and car makers. I hope it is working well. What I want to emphasize is at this section, the leaders of users (managers or engineers in car makers) should study hard and gain a lot of experiences to integrate whole painting world. Otherwise, the standard will be biased to facility side and/or material side but not to user side. We cannot effectively reduce investment and running cost or energy with biased standards and modules. I hope that PTW and UK will be a good place to study, learn and gain experiences.

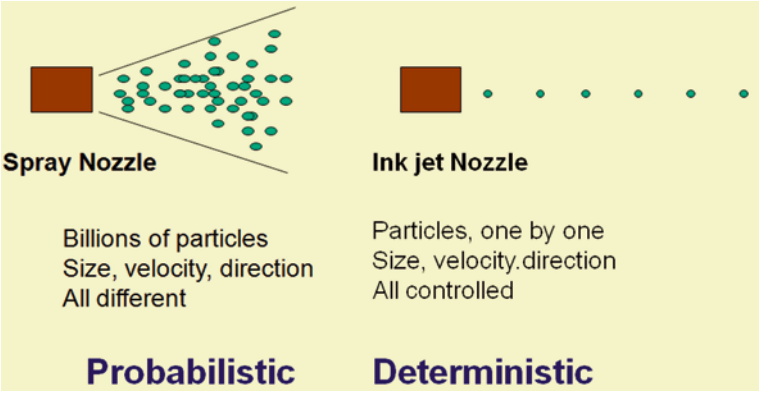

Fig. 2.50 Spray coating vs. ink jet printing

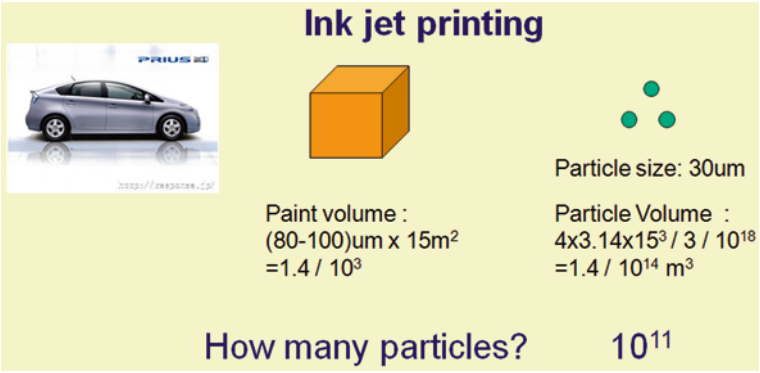

Fig. 2.51 How many paint particles do we need to apply a whole car?

2.6.3 Probabilistic to Deterministic

I said, spray coating technology is based on the probabilistic model. It is almost impossible to change from probabilistic to deterministic. Innumerable atomized particles have all different size, speed and direction. Gun distance to the substrate varies a lot. The shape of the substrates is usually not simple, and the gun or bell attached on the robot cannot follow the contour of the car body or other parts.

Inkjet printing is expected to control such parameters of particles. We may be able to introduce inkjet printing for applying small parts with nanometer film thickness. However, in order to paint car body, thousands or millions inkjet nozzles are necessary.

Then, what we have to do? Leave as it is? Absolutely not.

We have to realize that reducing the variance makes the probabilistic model change close to deterministic model. We can reduce efforts for integration by re-

ducing the variance, because number of experiments is reduced and accuracy of experiments is improved. The current atomizers, bells or spray guns atomize paint by force of high rotation or high air pressure. We still do not know the best 3D parameters and alignment of atomizers.

I expect that R&D in UK will bring the epoch-making improvement in developing new atomizers for reducing variance of atomization.

Acknowledgements I'd like to express my sincerest thanks to following companies and societies and people. Toyota Motor Corporation; Dr. Amari, a president of Asahi Sunac Corporation; Auto makers, especially Daimler Benz, BMW, GM; Paint suppliers, especially Kansai Paint, Nippon Paint, Dupont, PPG; Facility suppliers, especially Duerr, Eisenmann, ABB, Ransburg, Trinity; Surcar conference held in Cannes, France; International Strategy Conference on Car Body Painting held in Berlin, Germany; University of Kentucky. And special thanks to Dr. Saito and Dr. Salazar.

References

1. Patton T.C.: Paint Flow and Pigment Dispersion. Wiley, New York (1964)
2. Fukuta K., Ohashi Y., Murate M., Toda K.: New rotary bell for metallic paint application. Met. Finish. **1**, 39–42 (1993)
3. Ishiguro Y., Toda K., Tamura Y.: A new automotive body painting system. In: International Body Engineering Conference, 1995

Part II
Painting Technology: Numerical Simulation and Scale Modeling

Chapter 3
Computational Modeling of Relevant Automotive Rotary Spray Painting Process

Abraham J. Salazar

Abstract The intent of this chapter is to provide a non-exhaustive but useful guide to the capabilities of computational modeling to help understand the multiple phenomena coexisting in the automotive rotary spray painting process. This manufacturing process has been extensively used to coat automobile bodies in assembly plants. For the last three decades, auto makers as well as spray painting equipment manufacturers have dedicated substantial efforts to understand rotary atomization and to develop more efficient and versatile atomizers. Despite these efforts, it is accepted that the current level of understanding is not sufficient to accurately assess the operation of commercially available rotary bell spray painting systems. The reasons for this lack of understanding are two fold: the inherent complex nature of the rotary bell painting process and the traditional experience-based development of these types of systems. In addition, there is a limitation in what experimentation and theoretical studies alone can provide to enhance both the desired understanding and the efficiency of the paint application process. Based on this realization, efforts have been oriented toward using computational modeling as a new tool to develop this understanding. However, the use of computational modeling has proven to be not an easy task due to the high speed of translation and rotation of the atomizer in real scenarios, the different scales of the phenomena going from micrometer at the rotary cup paint film level to meter at the painted part and spray booth level, the complicated rheology of the paint material (especially for dispersed-type paints), etc.

The research efforts leading to the results presented herein were in its majority financially supported by Toyota, Honda and Nissan. We are very grateful to these companies for their contribution and vision. Without both their financial support and the advice of their plant site engineers, this work would not have been completed successfully.

Keywords Spray painting · Automotive painting · Computer modeling

A. J. Salazar (✉)
Institute of Research for Technology Development, College of Engineering,
University of Kentucky, Lexington, KY 40506-0503, USA
e-mail: ajsala00@uky.edu

K. Toda et al. (eds.), *Automotive Painting Technology,*
DOI 10.1007/978-94-007-5095-1_3,

3.1 Introduction

A flawless appearance and high quality paint finish are among the most important criteria for automotive customer satisfaction. In fact, customer perception of the overall quality of the product is positively influenced by the quality of its paint finish.

In addition to being a key sales factor, a high quality paint finish is fundamental to protect the metallic car shell against a variety of potentially corrosive weather conditions, which will directly influence the durability of the product. Aware of these facts, automobile manufacturers invest heavily in paint process equipment and materials to achieve the highest level of appearance and durability of painted surfaces on their products.

3.1.1 Current Status of the Automotive Spray Painting Technology

In a typical automobile-assembly plant, three different coats (primer, top and clear) are applied to the vehicle body using spray booth facilities. A spray booth is an enclosure that directs overspray, i.e. paint particles that do not coat the car shell and float in the air and solvent emissions from painting operations away from the operator and toward an entrainment or abatement section. Figure 3.1 presents a schematic of a typical automotive spray booth consisting of an upper (spraying) section—the portion above the floor grating, and an under (capturing) section—the portion below the floor grating.

The upper section of an automobile assembly plant spray booth has the form of an elongated corridor through which the automobiles are longitudinally conveyed over sliding rails and within which workers and/or spray robots spray paint the moving car bodies. In addition, to guarantee a repeatable high quality paint finish, the temperature and humidity of the booth are constantly monitored and controlled within a tight operational window.

For health and safety reasons, it is essential in the operation of a paint spray booth to maintain a proper supply of fresh air and to remove paint overspray by means of an air exhaust system. Supply air is blown through a supply plenum where dust and insect filters clean the air entering the upper section of the booth. This supply air also removes the paint overspray from the booth, drawing it down through hollow outlet structures dispersed along the sub-floor at regularly spaced intervals.

According to regulations of the Occupational Safety and Health Administration (OSHA) a minimum downward air speed of 0.5 m/s (100 fpm) is required in the upper section of the manual spray area of a booth [31]. A significant implication of this restriction is that, for each meter of length of the booth, an average of 3 m^3/s of fresh air should be supplied. Because a typical assembly-plant paintbooth may be 150 m long, 450 m^3/s (953,500 cfpm) of fresh air should be blown through, for

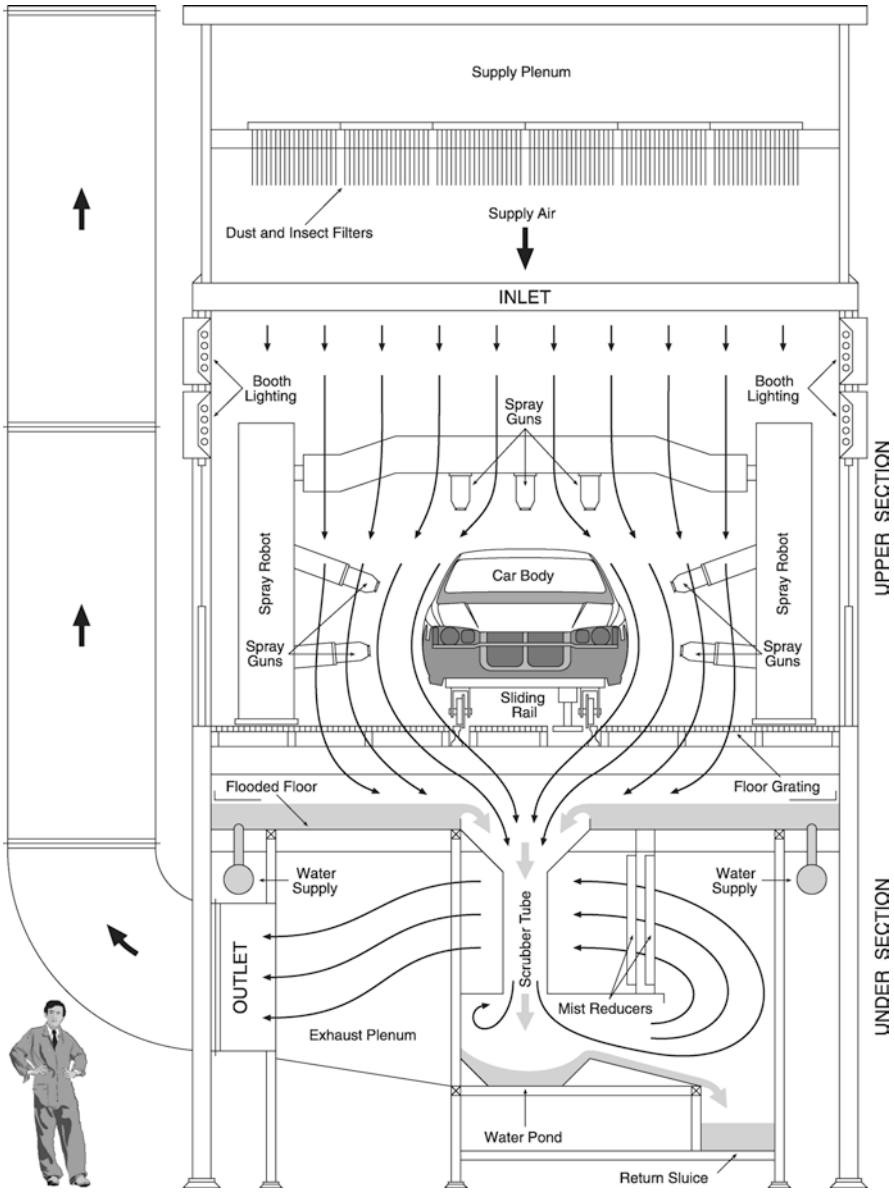

Fig. 3.1 Schematic view of a typical automobile assembly plant spray booth

example, the top coat spray booth. In addition, the need to control the temperature and humidity of the air implies the use of substantial air conditioning power. The equivalent electric power required to sustain this airflow increases proportionally with the pressure difference through the booth's exhaust, in particular, through the capturing system. Therefore, having an efficient overspray capturing system with a low pressure drop reduces booth operational costs.

As opposed to the upper section configuration, which is similar in all booths, the under section configuration depends on the manufacturer. In principle, each design is targeted toward trapping as much of the overspray as possible with minimal pressure drop.

In modern spray booths, the paint spraying process is commonly performed using high-volume-low-pressure (HVLP) spray guns and rotary spray guns. HVLP spray guns are employed mainly for manual spraying of the inside borders of the doors and trunk as well as some hard to reach places. HVLP spray guns are preferred to conventional spray guns due to their higher transfer efficiency [20, 25]. As is typical of other air-assisted atomizers, HVLP spray guns achieve paint atomization by colliding one or more high speed air jets with the incoming paint stream. However, its volumetric flow of air is relatively high (HV) and its pressure is relatively low (LP) when compared to that of conventional spray guns. The high shear generated by the colliding jets breaks the paint stream into very small droplets creating the spray mist. The pressure of the air jets and the amount of paint injected can be easily controlled. Additional air jets to shape the paint spray cone are often present.

Rotary spray guns, often called bell guns, are preferably employed during robot-assisted spraying. To increase the amount of sprayed paint that reaches and coats the automobile surface, paint drops exiting the rotary spray guns are purposely charged while the body of the vehicle remains grounded. Rotary spray guns atomize the paint by injecting it through a specially designed cup, rotating at speeds of up to 70,000 rpm. The centrifugal force exerted by the rotating cup on the injected paint and the action of small grooves at the edge of the cup break the paint film into small drops thereby generating the atomized spray mist. Additional airflow aimed at the edge of the cup is used to further control the shape of the paint spray cone.

Recently, powder coating has gained some ground due to the continual pressure to reduce volatile organic compounds (VOCs) emissions. However, its use is still restricted to some primer and clear coat applications [29]. The current powder coating technology cannot provide a complete coating system to replace conventional liquid paint systems because of its inability to achieve the high quality of finish demanded in automotive applications (Umeda H.: Coordinator, paint engineering, vehicle production engineering, Toyota Motor Manufacturing North America. Personal Communication (2000)).

3.1.2 Six Fundamental Problems in Automotive Spray Painting Systems

Six fundamental problems, illustrated in Fig. 3.2, are associated with automotive spray painting systems. Three of these problems have environmental implications and three have quality of finish implications. The paint cycle can be visualized to start from the paint guns spraying toward the car surface (see Fig. 3.3). After it is atomized by the spray guns, only part of the paint actually coats the vehicle surface. The ratio between the amount that coats the surface and the amount emitted by

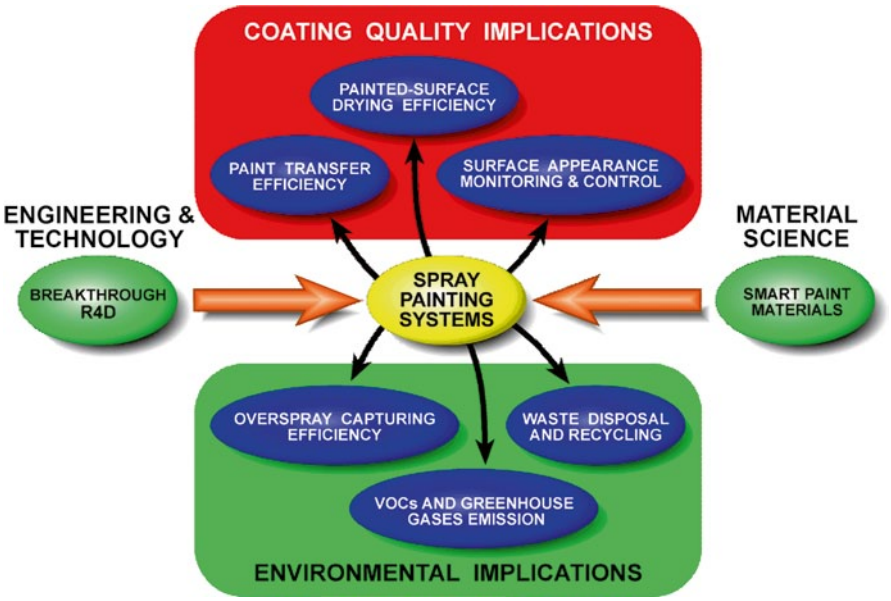

Fig. 3.2 Six fundamental problems in automotive spray painting systems

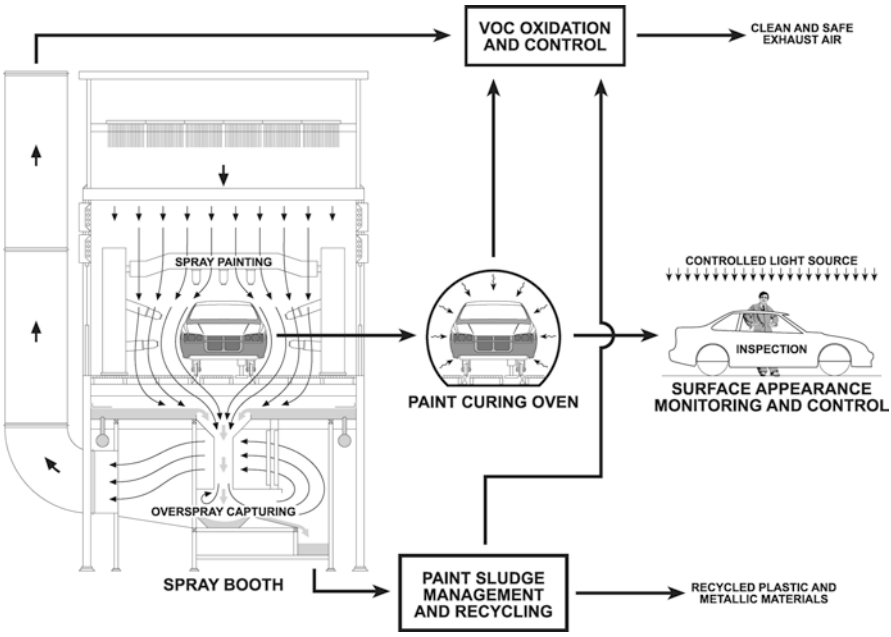

Fig. 3.3 Schematic view of a typical automotive painting cycle

the guns is defined as the *paint transfer efficiency*. The paint coating the surface affects the paint layer thickness, which has direct implications to the quality of finish. Although automotive spray painting is among the most sophisticated and controlled industrial painting operations currently performed, only 50–60 % of the spray emitted from the paint guns actually remains on the vehicle [9]. This relatively low transfer efficiency is a fundamental problem and is either the source of, or aggravates, the remaining five problems. Finding ways to increase paint transfer efficiency while maintaining a high quality of finish is a challenging task that has attracted the attention of researchers for many years.

A direct implication of this 50–60 % transfer efficiency is that the remaining 40–50 % oversprayed paint must be captured before it escapes into the environment. Due to the substantial amount of paint used, water washing or wet scrubbing has been the preferred capturing method. The ratio of the amount of overspray trapped to the amount entering the capturing system is defined as the *overspray capturing efficiency*. Capturing more with the less energy consumption is a fundamental issue that affects both the environment and the plant's operational cost. In recent years, capturing efficiency has become a significant concern because of the cost of filtering techniques needed to meet newly-enacted environmental regulations restricting the amount of particulate emissions.

Once the body of the car has been painted, the wet paint needs to be dried or cured. This process is normally performed inside radiation and/or convection ovens. Curing the paint to produce the highest quality finish with the least amount of energy expended is another fundamental issue that we have called the *painted-surface drying efficiency* problem. It has both coating quality implications and environmental implications. The best process to cure the paint depends among others factors on the type and composition of the paint and is typically recommended by the paint formulator.

The paint sludge generated by the overspray wet scrubbing operation is collected and processed. Some of the paint and scrubbing water components are recovered and recycled, while others are treated as waste and disposed. Recovering and/or recycling as many of the constituents of the paint as possible with the least expense and disposing of the remaining waste in an environmentally safe way is another fundamental issue that we have called the *waste disposal and recycling* problem. Recently, some automakers have found successful ways of using overspray paint components collected from the paint sludge to produce RSPP (Recycled Sound-Proofing Products), which when used correctly can enhance the driving experience by reducing the level of perceivable road noise inside the automobile's passenger cabin.

During the spray painting, wet scrubbing, curing, and paint sludge managing and recycling operations, VOCs and other gases originally dissolved in the paint and the scrubbing water are released. These gases, potentially harmful to the environment need to be collected and oxidized before they can be exhausted to the atmosphere. The danger of many VOCs present in paints to human health has been studied recently (cf. [43, 57]). Among these released gases, some could be categorized as greenhouse gases that may affect global warming [3, 32]. Controlling and minimizing the generation of greenhouse gases as well as efficiently oxidizing any re-

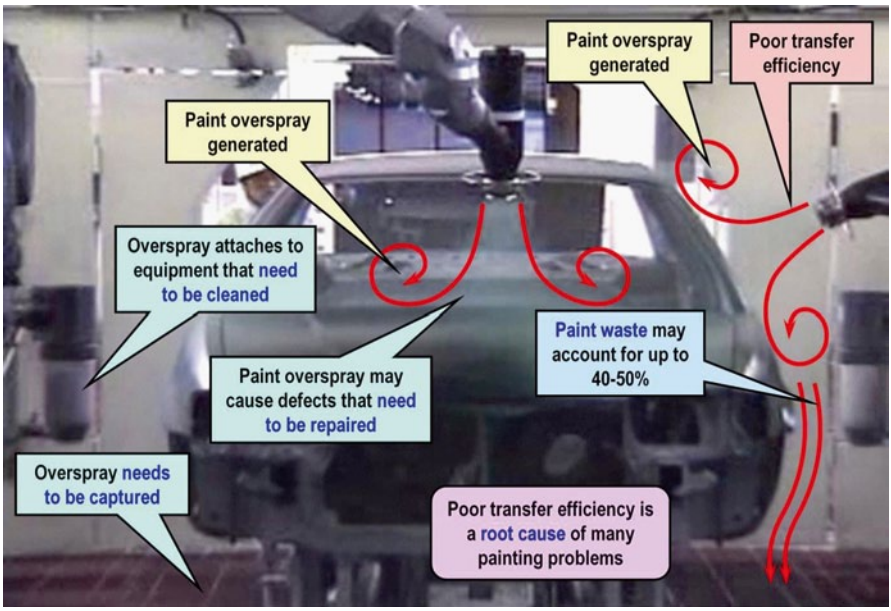

Fig. 3.4 Issues with current automotive spray painting process

maining VOCs constitutes another fundamental issue that we have called the *VOCs and greenhouse gases emission* problem. Lately, this issue has received worldwide attention with the Kyoto Protocol, in which leaders of developed countries signed binding agreements to decrease their emissions of greenhouse gases.

To guarantee that the final product—the painted car—meets or exceeds manufacturer specifications and satisfies customer's expectations, its quality of finish needs to be monitored and controlled constantly. Finding suitable means to accomplish these goals is the *surface appearance monitoring and control* problem.

3.1.3 Issues with the Current Automotive Spray Painting Technology

To concentrate on the application of the paint to the vehicle, Fig. 3.4 displays the upper section of a modern spray booth. Several efficient robots, to which are attached high speed rotary atomizers, simultaneously spray paint on the vehicle. The spray pattern, the atomizer orientation, the number of passes and their overlap, as well as the atomizer's distance from the vehicle surface are all computer-controlled. Paint droplets are purposely electrostatically charged to attract them to the grounded vehicle and increase transfer efficiency. What could be wrong with the most sophisticated mass production industrial painting operation available? Poor transfer efficiency generates excessive overspray and VOCs. The overspray typically ac-

counts for 40–50 % paint waste [9] which has a direct correlation with the amount of VOCs generated. This overspray also flies to other areas of the vehicle's surface, causing defects that need to be repaired. Part of this overspray attaches to booth walls and the spraying equipment, which have to be cleaned regularly. The remaining overspray and VOCs floating in the air need to be captured and/or abated before the air is released back into the environment. The overspray captured in the scrubbers generates a non-recyclable paint sludge, which is later separated from the water and collected for subsequent post-processing or disposal.

Painting cars in an assembly line is an expensive process [9]. In many cases, it can account for up to 40 % of a plant's total energy consumption (Umeda H.: Coordinator, paint engineering, vehicle production engineering, Toyota Motor Manufacturing North America. Personal Communication (2000)). A major portion of this energy, about 60 %, is required to blow fresh air into the booth and to capture the overspray in the wet scrubbers. Automobile manufacturers not only lose the cost of the oversprayed paint, they also have the costs of cleaning the booth regularly and of disposing the resulting paint sludge in an environmentally safe way.

For a typical automobile assembly plant, producing an average of 500,000 cars per year, the cost of the wasted overspray alone can amount to US$ 37.5 million[1] It is clear, then, that poor transfer efficiency could be envisioned as the root cause of many of the environmental problems usually associated with automotive spray painting processes and as a significant source of waste that increases booths' operational costs. For this reason, many attempts have been made to enhance paint transfer efficiency which have had limited success, mainly because of the complexity of the process.

Although computational analysis has been applied to study several of the six fundamental automotive spray system problems, for example: (a) booth airflow and volatile emissions control (cf. [53]); (b) overspray capturing (cf. [37, 38]); (c) curing oven (cf. [24, 41, 55, 58]); (d) evaporation and collision of droplets during transport (cf. [8, 10, 34, 35, 42]); (e) deposition onto the surface (cf. [36, 46, 56]); and (f) transfer efficiency (cf. [10, 11, 14–16, 50–52, 54]), only transfer efficiency studies (f) has the potential to contribute to the understanding of the root cause. However, since the droplet size distribution used in the simulations is either based on direct measurements at the given operating condition or on experimentally determined correlations, computational transfer efficiency studies cannot shed light onto how the rotary atomizer cup design plays a role in the achieved paint atomization characteristics because the phenomena that leads to atomization is missing from the model. Without this important link, the results of the simulation have limited usefulness to booth operators and automobile engineers that are seeking for those set of conditions or features in the cup design that would give them their desired performance.

Ideally, to achieve the task of linking the atomizer operating conditions to the achieved transfer efficiency, a simulation has to be able to predict both the micrometer scale, typical of the paint flow and atomization at the rotary cup, and the meter

[1] This amount does not include other costs that are consequences of the generated overspray such as overspray capturing, booth and equipment periodical cleaning, paint sludge collection, recycling and disposal, VOCs oxidation, etc., which easily exceed US$ 100 million per plant per year.

scale, typical of the spray booth and target surface, without losing accuracy. The ability of accurately handling this six order-of-magnitude change in scale is still beyond the current capabilities of available computers and solution algorithms.

In the meantime, there is a substantial amount of insight that can be realized by simulating the transient flow of paint on the face of the rotary cup. Salazar and Saito have studied extensively the unsteady flow of Newtonian and non-Newtonian fluids on rotary cups of different designs (cf. [39]). Their results have identified several new phenomena occurring on commercial cups that can help explain their performance and operational characteristics. In this chapter, research results regarding unsteady flow of paint on rotary cups of different geometries are summarized. A parametric study of several influencing design parameters of the atomizer is also presented.

The rest of this chapter is organized as follows. In Sect. 3.2 the physical processes occurring during the unsteady paint film flow and its subsequent atomization at a typical automotive rotary atomizer cup are presented. Based on this discussion, in Sect. 3.3 baseline assumptions required for suitable modeling are given. In addition, the limitations and possible extensions of these assumptions or simplifications are discussed along with formulation of the equations that describe the process. In Section 3.4 typical computational results are presented and discussed. Two distinct typical rotary sprayer configurations are simulated and compared for a variety of operational conditions. Finally, in Sect. 3.5 our concluding remarks are presented.

3.2 Overall Description of Rotary Electrostatic Spray Painting Process

This section presents the flow situation encountered in the analysis of automotive spray painting operations. The different mechanisms taking place during rotary electrostatic spray painting are discussed considering the range of properties associated with common automotive paints.

Figure 3.5 shows a simplified sketch of a typical automotive spray painting application. The airflow in the upper section of an automotive spray booth can be described as a three-dimensional (3-D) turbulent airflow with complex moving geometries. Typical Reynolds numbers (inertia forces/viscous forces) in the spraying section are in the range $5 \times 10^4 - 3 \times 10^5$ (moderately turbulent).

During the automotive spray painting process, metallic car shells are conveyed at a specified constant rectilinear speed through the booth. Robot-assisted rotary atomizers spray the car shell surface according to a computer-specified and complicated path particular to each shell geometry. Before painting a different color, rotary atomizers are flushed and cleaned to avoid color contamination.

The process can be envisioned to be composed of four distinguishable steps. The *atomization* of the paint is generated by the break of the paint film at the rotating cup edge (see Fig. 3.6). High speed air jets, namely shaping air jets, impinge onto the droplets providing additional momentum that directs them toward the target. To improve transfer efficiency, the atomized paint drops are purposely charged while

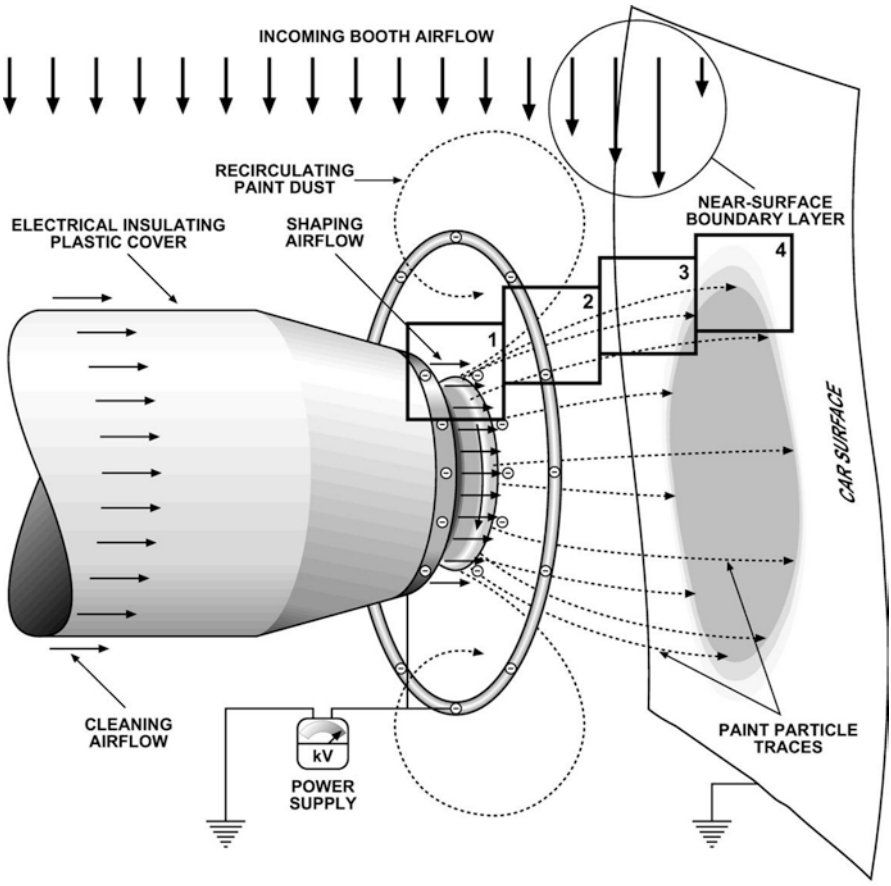

Fig. 3.5 Schematic view of a typical automotive spray painting process

the car shell is grounded. *Charging* is attained either by induction—by connecting the rotary cups to a electrostatic power supply (shown schematically in Fig. 3.6), or by corona—by placing a high potential electrode between the atomization region and the target (depicted in the sketch Fig. 3.7). *Evaporation* occurs as soon as the paint film is exposed to the booth air. A substantial surge occurs during the breakup of the film into droplets (atomization flashing) and, subsequently, during the travel of the charged paint droplets toward the target surface, which results in droplet mass loss and a change of its charge-to-mass ratio (see Fig. 3.8). Not all paint droplets reach the vicinity of the target surface, i.e. they become overspray. In addition, not all droplets that reach the target will attach to the surface, i.e. some of them may bounce back becoming overspray. *Deposition* onto the target surface is a process that depends on particle speed, incidence angle, surface tension, wettability and remaining particle charge; it is presented schematically in Fig. 3.9. Although the relation between paint transfer efficiency and finished surface quality is very important, it remains as an unknown to be studied in subsequent phases of the research.

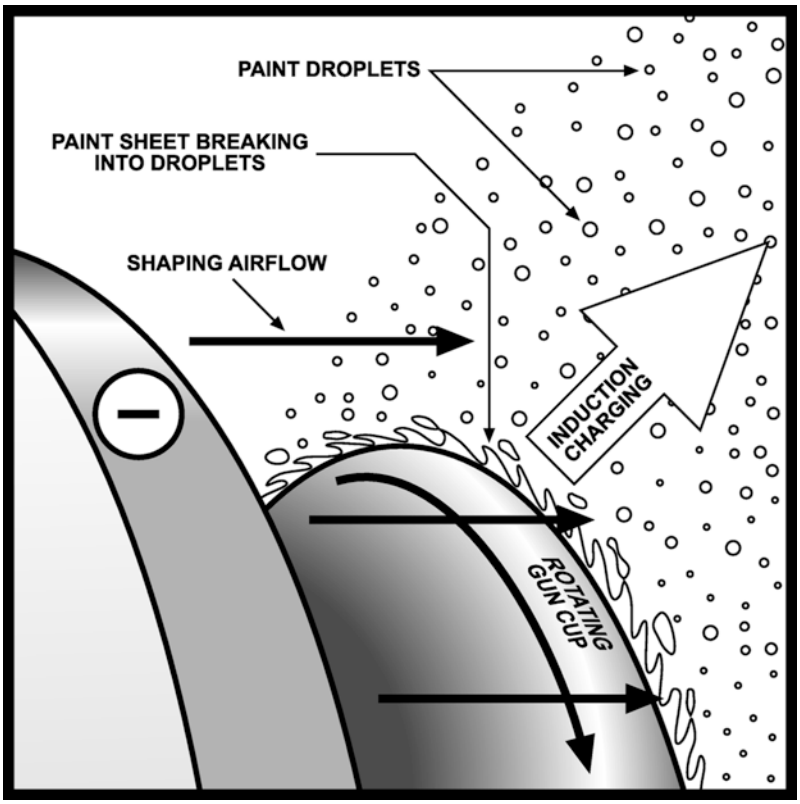

Fig. 3.6 Schematic view of paint atomization and induction charging processes

It is clear that the behavior of the generated droplets (atomized droplets) that leads to their response to the applied electrostatic charge (maximum attainable charge), their behavior (trajectory, speed, evaporation, etc.) during transport to the vicinity of the target surface, and their ultimate deposition onto the surface being painted (speed, angle, non-volatile content, viscosity, etc.), depend in great degree on the characteristics of the atomization (droplet size distribution) achieved. It is expected that increasing the degree of control on the atomization would have a positive impact on the achieved deposition characteristics. Therefore, atomization performance is a root cause of coating quality of finish. Within this frame of ideas, in the following subchapter, we examine in more detail each the different mechanisms of rotary paint atomization.

3.2.1 Rotary Paint Atomization

Figure 3.10 shows a cross-sectional view of a typical rotary sprayer cup. Atomization is achieved by introducing the paint onto the center of a cup-like sprayer

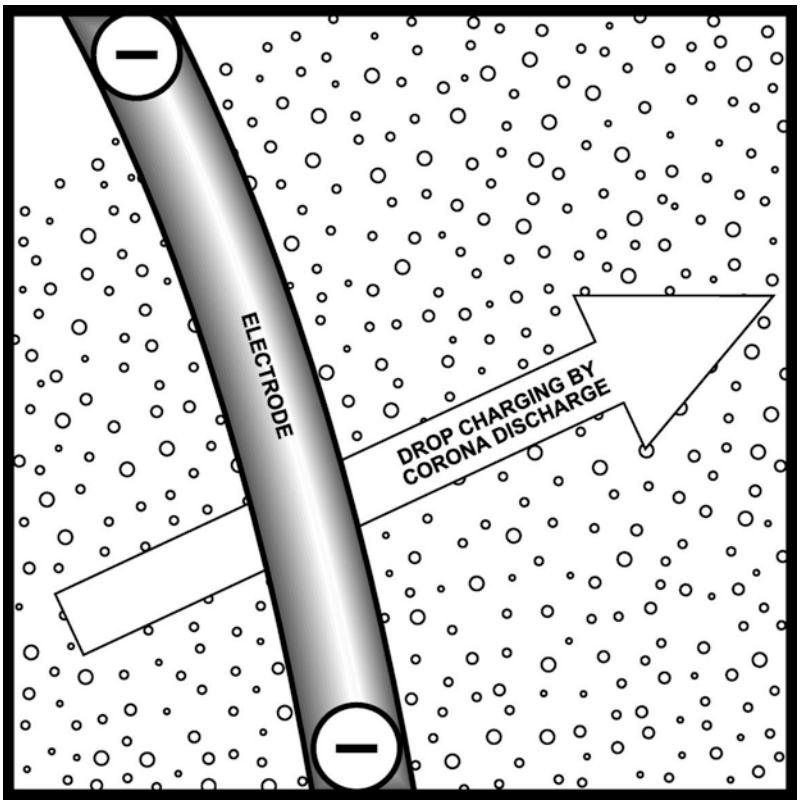

Fig. 3.7 Schematic view of corona charging process

rotating at a speed of several thousand revolutions per minute (typical values range from 10,000 to 70,000 rpm). Centrifugal force drives the liquid in the form of a thin film to the edge or lip of the cup where it is thrown off into a spray of drops. For optimal performance the thin film should be free of flow disturbances. Earlier researchers assumed that the spinning cup was, in itself, capable of smoothing out any thin film flow disturbances under the action of a sufficiently strong centrifugal force alone. However, this statement is true only for the case of cups of infinite extent or when the liquid flow rate is sufficiently small to ensure an adequate residence time within the cup [19].

Early investigations revealed that the diameter distribution of droplets was highly influenced by their formation process [12, 13]. Many slightly different cup designs were fabricated to experimentally find a design that performs optimally under a wide range of conditions while producing a controllable and very narrow range of droplet sizes (cf. [47, 48]). However, this trial-and-error approach is very time consuming and requires substantial resources.

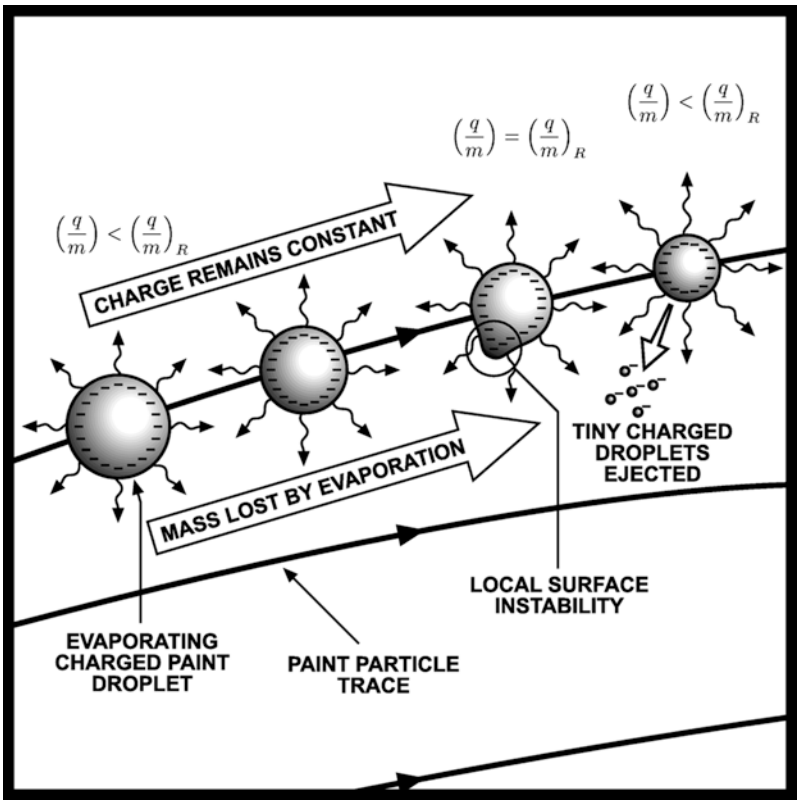

Fig. 3.8 Schematic view of the charged droplet evaporation process

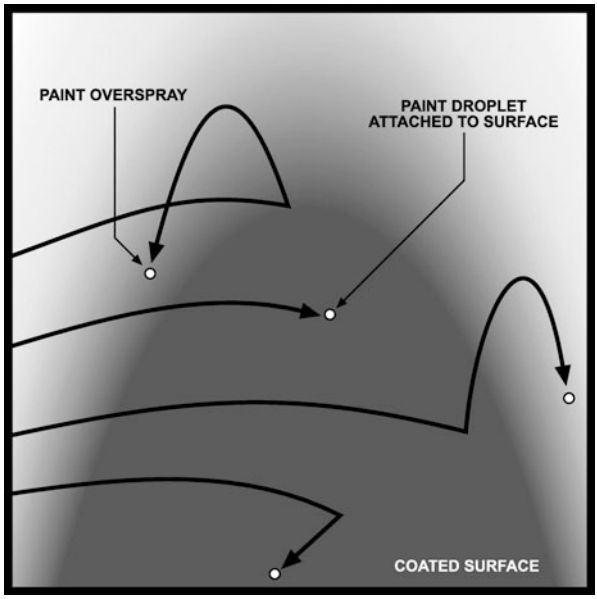

Fig. 3.9 Schematic view of the droplet surface attachment (deposition) process

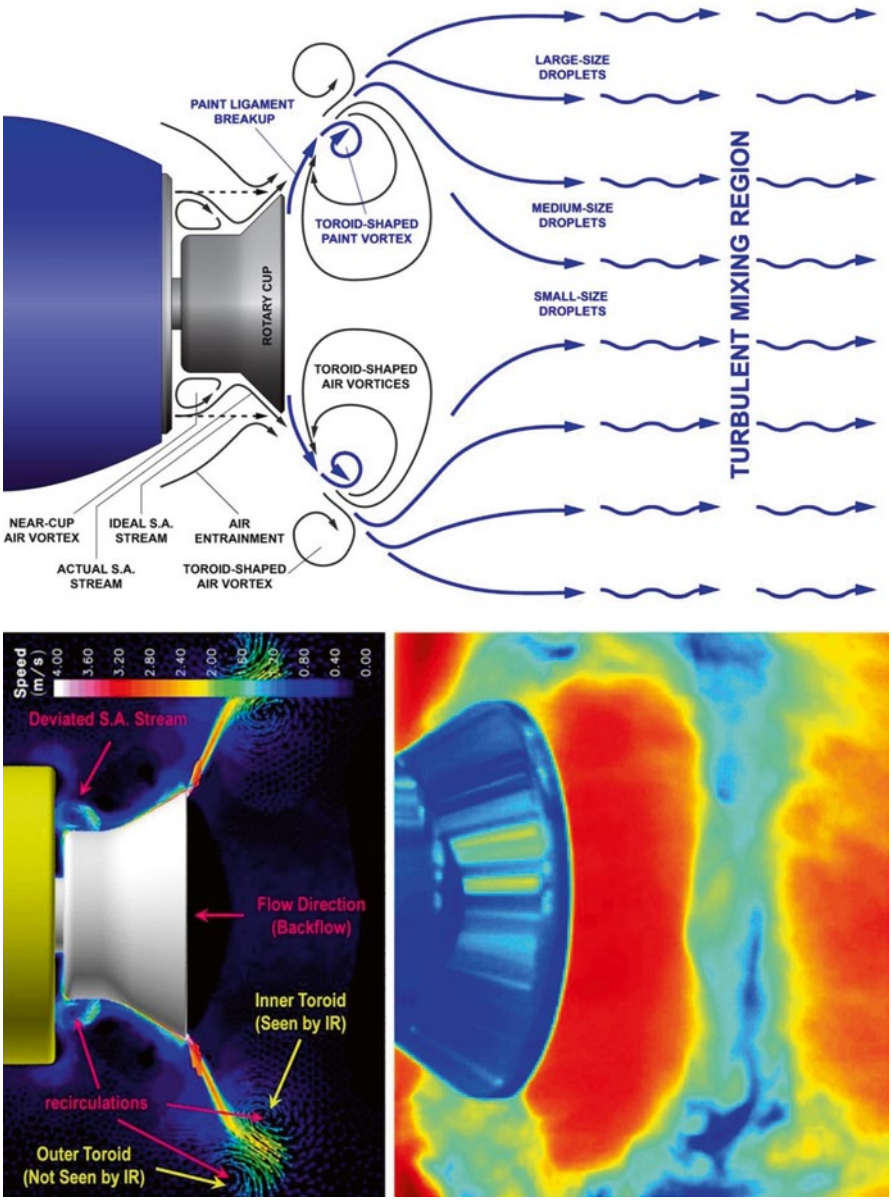

Fig. 3.10 *Top*: Cross-sectional view of the flow around a rotary bell cup atomizer. *Bottom*: Structure of the airflow around a automotive rotary bell atomizer (*left*) depicting inner toroid (wet) and outer toroid (dry). IR thermography image of an operating rotary T/R bell atomizer [4] (*right*) showing the same inner toroid predicted computationally

3.2.1.1 Atomization Mechanisms

It has been established that the drops are produced from rotary atomizers by one of three mechanisms [13, 18]. To explain them, assume that all operational conditions but liquid flow rate are kept constant and that the shaping airflow is not present.

In the first mechanism, at very low flow rates, the liquid spreads outwardly towards the cup's edge, where it forms a small liquid ring or toroid. As liquid continues flowing into the ring, its diameter grows and inertia increases until the restraining surface tension force is overcome. Small disturbances or surface instabilities appear on the outer edge of the ring. These disturbances which initially form like small fingers around the ring, continue to grow in size until spherical globules are formed. As the liquid continues to flow, the spherical globules remain attached to the ring by a stretched thread of liquid called a neck. As the neck thins and the globules grow, they are thrown off as discrete drops by centrifugal forces. Often, when the drop is finally detached, the retaining liquid thread breaks down into a chain of small satellite drops. Since the satellite drops constitute only a small proportion of the total liquid flow rate, a cup operating under these conditions produces a nearly homogeneous spray. This first mechanism is known as the *discrete-drop* or *single-drop* mechanism.

When the liquid flow is increased, the retaining threads grow in thickness and form long jet-like structures. Under the effect of the centrifugal force and the drag generated by the surrounding air, these jet-like liquid threads stretch to form long curved ligaments of uniform diameter that resemble sections of a spiral. As they are stretched further, small perturbations or instabilities appear on their surface. These instabilities continue growing until the curved ligaments break down into drops at some distance from the cup. Since the diameter of the droplets is related to the diameter of the ligament, this atomization mechanism generates droplets of relatively uniform size. The diameters of these drops are smaller than those formed by the discrete-drop mechanism. This second drop formation mechanism is known as the *ligament* mechanism. Ligament formation can be made to produce much finer drops if an electrostatic field is applied between the rotating cup and the grounded target [27]. Most automotive sprayer cups are designed to operate in this regime.

Since the torus diameter is much smaller than that of the cup, the torus may be considered as a linear cylinder of liquid which may be perturbed by standing waves. For the spinning torus of liquid the centrifugal force acts transversely to its axis. Standing waves develop and grow in amplitude and the wave with the greatest growth rate (dominant wave) becomes established. Ligaments of liquid develop from the wave peaks and are projected radially from the cup edge (centrifugated) and then dragged azimuthally under the effect of the surrounding air. Ligament spacing depends on the wavelength that becomes dominant around the circumference of the cup lip. A determination of this wavelength is mathematically complex. For cups with smooth (i.e. non-grooved or non-serrated) edge, it has been found that this wavelength depends on the cup diameter D_c, the cup's rotational speed w_c, the charging electric field E_t at the liquid torus surface, the liquid film thickness h, the liquid kinematic viscosity v, the liquid density ρ and the liquid temperature T [5].

Recent evidence for serrated-edge cups suggests that the number of holes in the liquid supply manifold may also have great influence in the dominant wavelength [23].

With further increase of liquid flow rate, the jets diameter increases but they are unable to remove all the incoming liquid, the ring is forced away and a thin sheet extends around the cup's edge. The liquid leaves the cup in the form of an attenuating sheet which may disintegrate in a number of ways depending on the operating conditions, including rotational speed and viscosity. Disintegration is caused by the effect of aerodynamic waves that grow in amplitude until fragments of the sheet are detached. These fragments contract under the action of surface tension into ligaments of liquid with characteristic cylindrical shape that subsequently break down into drops. The drop size spectrum under this mechanism of formation is wide due to the varied behavior at the region of disintegration. This third mechanism is known as the *sheet* mechanism of drop formation.

Hinze and Milborn [21] and Fraser et al. [18] using smooth lip cups found that the transitions from sheet to ligament formation and ligament to sigle-drop formation are promoted by a decrease of liquid flow rate, rotational speed, density and viscosity, or an increase of cup diameter and liquid surface tension. According to Hinze and Milborn [21], the transition from *single-drop* to *ligament* formation occurs when

$$\left(\frac{Q}{D}\right)\sqrt{\frac{\rho}{\sigma D}}\left(wD\sqrt{\frac{\rho D}{\sigma}}\right)^{0.25}\left(\frac{\mu}{\sqrt{\rho\sigma D}}\right)^{0.167} \geq 2.88\times 10^{-3}, \tag{3.1}$$

where, Q is the total volumetric flow rate injected into the spinning cup, D is the peripheral diameter of the cup edge, ρ is the liquid density, μ is the liquid viscosity, σ is the liquid surface tension, and w is the rotational speed of the cup in rev/s. The transition from *ligament* to *sheet* formation occurs when

$$\left(\frac{Q}{D}\right)\sqrt{\frac{\rho}{\sigma D}}\left(wD\sqrt{\frac{\rho D}{\sigma}}\right)^{0.6}\left(\frac{\mu}{\sqrt{\rho\sigma D}}\right)^{0.167} \geq 0.442. \tag{3.2}$$

When grooves (serrations) are machined on the lip of the cup the transition from ligament formation to sheet formation is delayed. Grooves create disturbances of a fixed frequency on the film at a very influential location, the cup's edge. Under favorable conditions, this frequency gets established and dominates the atomization process. Therefore, for optimum spraying performance the groove's design parameters (shape, size, number, etc.) have to be tuned with the cup's design parameters.

After detaching from the cup's edge, the paint is impinged by high speed air jets (shaping air jets). In addition to diverting the radially ejected droplets toward the target surface forming a spray cone, shaping airflow can play a role in the atomization.

The breakup of liquid drops suddenly exposed to high speed air jets has been studied by Joseph et al. [22] and Lane [26]. As found by the authors, a key element in all cases for liquids such as water is the correlation of breakup parameters with the Weber number, *We*. As categorized by Pilch and Erdman [33], no breakup is observed for $We<12$. For $12<We<18$, vibrational behavior dominates and the flow enhances the amplitude of drop oscillation to produce a few large fragments.

Bag-type fragmentation is observed for $12 < We \leq 50$ and the droplet is blown out into a thin hollow bag attached to a toroidal rim. As the Weber number is increased, more catastrophic modes of breakup are observed and the time to onset of breakup decreases [33].

The aerodynamic breakup of liquid ligaments has been studied by Thomas [49]. This author performed an experimental study of the aerodynamic breakup of viscous Newtonian and non-Newtonian ligaments by shock waves in the Mach number range 1.3–1.67. Thomas [49] confirmed previous findings that the breakup process differs between Newtonian and non-Newtonian fluids. Catastrophic breakup of ligaments in the transverse impulsive flows was observed to develop by the growth of longitudinal surface instabilities along the length of the ligament, normal to the flow. For low-viscosity Newtonian fluids these very rapidly formed a fine delay in the onset of catastrophic breakup. As the viscosity was increased, longitudinal instabilities developed which then formed into discrete droplets, which were subsequently stripped to a fine mist. The wavelength of the instability was seen to be function of the fluid viscosity and appears to have its origin in the Rayleigh Taylor instability. A modified Rayleigh-Taylor theory reported by Joseph et al. [22] exists which correctly predicts the order of magnitude of the initial instabilities observed in Thomas' experiments [49].

The disintegration of liquid sheets produced by spinning atomizer cups subjected to impingement by high velocity air streams have been studied by Fraser et al. [17]. The author found that the liquid sheet does not break down upon immediate impact with the air stream but is deflected away from it. Waves are initiated at the point of impact and the sheet breaks down into drops through the formation of unstable ligaments. The resulting drop size was found to be a function of the sheet thickness. Thus the production of thin uniform liquid sheets is an essential pre-requisite to fine atomization. The uniformity of the thin liquid film reaching the edge of the cup, which is determined by the cup's design and the operating conditions, has a critical influence on the uniformity of the sheet formation and hence the drop formation and size distribution. The presence of grooves at the edge of the cup has to be tuned with an uniform thin film and sprayer operating conditions for optimum spraying performance.

With the introduction of paints high in solids, rotary atomizers have required higher speeds. Current units use air-driven turbines suspended by air-bearing to rotate the cup. The overall mechanism remains the same: (a) use the cup's centrifugal force to atomize the paint, (b) use carefully directed compressed air jets to give the paint drops forward velocity and direction toward the target, (c) use electrostatic charge to attract the droplets toward the target and increase transfer efficiency.

Despite the substantial experimental effort and some limited analytical studies to systematically understand the operation of high speed rotary atomizer cups, i.e. how the main atomizing mechanisms interact with each other and contribute to generate a spray with certain predictable characteristics, rotary spray atomization still remains obscure. The problem is exaggerated because each manufacturer uses different cup designs with potentially questionable understanding of the underlying physical principles of operation. In some cases, these designs show contradictory features (see Fig. 3.11). Since geometrical shape plays an important role in the performance of rotary atomizers, it is expected that cups of different shapes would

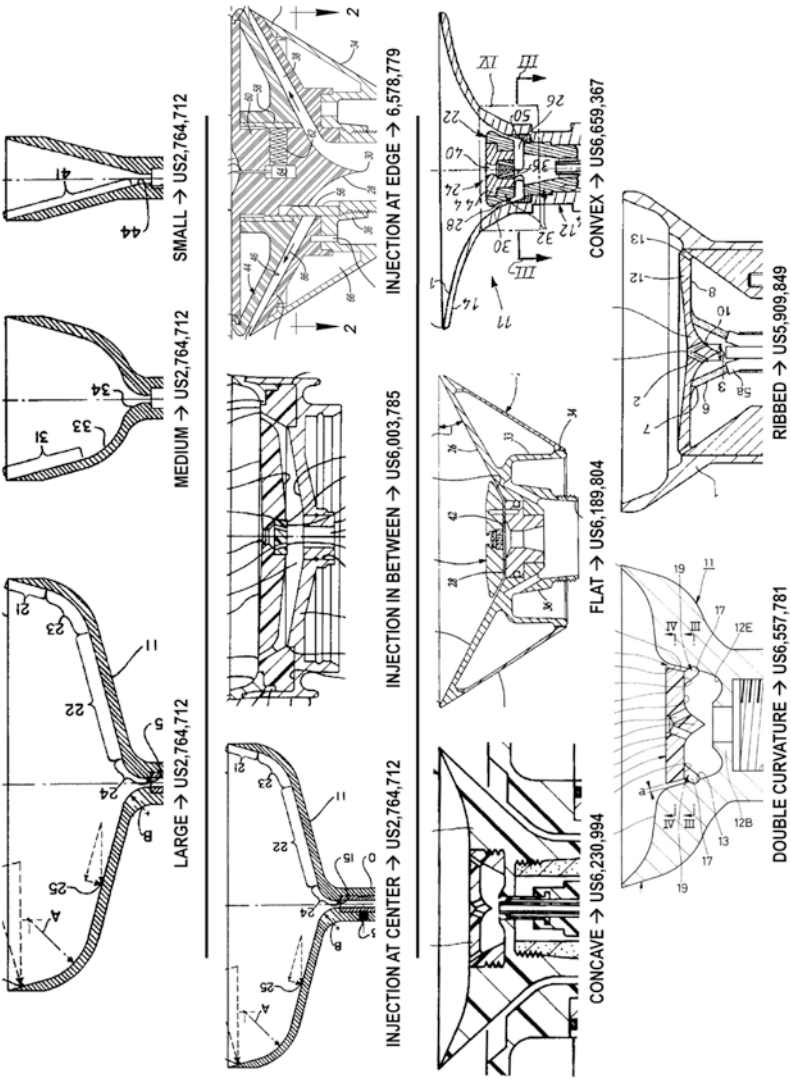

Fig. 3.11 Rotary atomizer cup designs taken from different US Patents (Patent numbers noted) displaying contradictory features

respond differently to adjustments in the operational conditions. As a consequence, it is difficult to establish universal optimal conditions of operation. It is not surprising that high quality automotive spray painting has been regarded as an art rather than a science. In most cases, paint engineers have no choice but to use experience to adjust operational conditions to obtain the desired quality without thoroughly understanding the phenomena taking place, without knowing what to expect and without having means to demand more from the manufacturers.

Electrostatic charging is an important mechanism to enhance paint droplet transfer efficiency by an estimate of about 10 % [9]. Two main charging mechanisms have been used for automotive applications: induction charging and corona charging. In the present investigation, the effect of electrostatic charging on the film flow on the face of the cup has been considered negligible. For details about the influence of electrostatic on droplet atomization, deposition and transport to the surface, please consult Bailey [5].

3.3 Numerical Model for Unsteady Liquid Flow During Rotary Atomization

This section presents the computational model employed to simulate the unsteady liquid flow in rotary atomizer bell cups. First, the basic assumptions necessary to simplify the formulation and to allow computing meaninful results in a timely fashion are presented. Second, the model formulation, consisting of the governing equations and suitable numerical multiphase models to be employed in the calculation, is presented. Finally, the commercial computational software employed in the study is discussed.

3.3.1 Basic Modeling Assumptions

Assumptions that retain only the essential control mechanisms and neglect less influencial ones were needed to make the following Computational Fluid Dynamics (CFD) calculations possible. In the following section, main assumptions employed to achieve this goal are discussed. These assumptions are based on theoretical considerations discussed previously and applied to the specific case of automotive electrostatic rotary spray painting. The model predictions computed under these assumptions need to be validated by experiments.

Assumptions 3.1

1. The booth airflow conditions and the spray gun dimensions are known.
2. The rotary atomizer is not translating (static) within the booth.
3. Booth airflow is considered incompressible and turbulent.
4. Paint properties are known. *Baseline approach:* In the present results, the properties of paint are those of water. The influence on Newtonian and non-Newtonian viscosity will be published elsewhere.

5. The influence of the shaping air is purposely reduced (very low pressure shaping air) to provide only a stabilizing momentum to the generated ligaments and liquid droplets but not to propel them to the surface. The influence of the shaping air jets on the break-up of the droplets as they spin off the sprayer cup is neglected.
6. The influence of mass loss due to evaporation from the face of the rotating cup (mass transfer process) is considered negligible when compared to the mass flow rate of the liquid film (fluid dynamics process).
7. The liquid is assumed to be a simple fluid (single phase) with averaged volumetric properties, i.e. the influence of dispersed solids like metallic flakes is not considered.
8. The influence of electrostatic charging on the liquid film flow is regarded negligible.

Assumption 1 must be satisfied to perform any representative study.

Assumption 2 is based on the analysis of the different times scales involved in the process. The time scale for the movement of the car shell trough the spraying section as well as the speed of the transversal movement of the spraying robot arm are much larger than the other relevant time scales in the process.

Assumption 3 is based on the fact that typical values for the Reynolds number in the spraying section are in the range $5 \times 10^4 - 3 \times 10^5$, moderately turbulent. For simplicity, k-ε would be the turbulence model employed for calculating the airflow. This is a very crude turbulence model in which the influence of the turbulent fluctuations are accounted for via some weighted average of the turbulent quantities. However, the influence of this model on the flow of liquid on the face of the rotary cup is regarded minimal.

Assumption 4 is required for any meaningful simulation. In addition, the baseline assumption is a simplification based on the fact that this study is focused on water-borne paints in which the water content is higher than 75 %. However, it should be noted that this assumption may not be accurate for some of the new water-borne dispersion-type paints exhibiting a very complex shear-thinning rheology, which is very distinct from the Newtonian behavior of water. From the hydrodynamic point of view, this assumption can be easily relaxed if viscosity data are available.

With the exception of a small ring-like atomization region surrounding the shaping air nozzles and the rotating sprayer cup, the airflow shear stress forces are mostly insufficient to upset the surface tension forces, i.e. after leaving the atomization region, the droplets are not split further by the shear forces in the airflow. To isolate the influence of the sprayer cup shape and operating conditions on paint atomization, when appropriate, the shaping air effect on the atomization would be minimized (by reducing shaping air pressure to a minimum). This consideration above is the basis of Assumption 5.

Assumptions 6 and 7 allow to simplify the simulation into that of a two-phase flow process (air-liquid without mass transfer).

Finally, assumption 8 is based on current knowledge.

3.3.2 Model Formulation

This section presents the governing equations that describe the phenomena. The flow of liquid in an automotive rotary sprayer can be classified as a multi-phase (solid-liquid-gas) multi-component (resin-pigment-flake-VOC-air) flow in complicated rotating geometries. Under assumptions 1–7, this phenomena is simplified to be a two-phase (liquid-air) flow in complicated rotating geometries.

3.3.2.1 Basic Conservation Equations

The set of equations solved are the unsteady Navier-Stokes equations in their conservation form. The instantaneous equations of mass and momentum conservation can be written as follows in a stationary frame:

$$\frac{\partial \rho}{\partial t} + \nabla \bullet (\rho \mathbf{U}) = 0, \tag{3.3}$$

and

$$\frac{\partial}{\partial t}(\rho \mathbf{U}) + \nabla \bullet (\rho \mathbf{U} \otimes \mathbf{U}) = \nabla \bullet \{-p\delta + \mu[\nabla \mathbf{U} + (\nabla \mathbf{U})^T]\} + \mathbf{S}_M, \tag{3.4}$$

respectively. Here, $\mathbf{U}=(u, v, w)^T$ is the fluid velocity vector, $\mathbf{S}_M$ is a source of momentum, p is pressure, ρ is the fluid's density, μ is the fluid's dynamic viscosity.

3.3.2.2 Initial and Boundary Conditions

The above system of partial differential equations is subjected to an initial condition, i.e. $\mathbf{U}=\mathbf{U}_0(\mathbf{x})$, where $\mathbf{x}=(x, y, z)^T$, with $\nabla \bullet \mathrm{U}_0(\mathbf{x}) = 0$ (divergence-free mass-conserving field).

Additionally, the above system is subjected to non-slip boundary conditions in all solid boundaries and open boundary conditions at the airflow inlets and outlets. For a non-slip non-rotating non-translating wall, e.g. shaping air cup walls, the velocity of the fluid (air) at the wall boundary is set to zero, so the boundary condition for the velocity becomes: $\mathbf{U}_{\text{wall}}=0$. For a non-slip rotating non-translating wall, e.g. the rotary cup walls, the fluid at the wall boundary moves at the same velocity as the wall. The boundary conditions at the walls of the rotating cup were specified using a rotating frame of reference with a rotating axis located at the cup center. This way the non-slip rotating non-translating wall boundary condition becomes: $\mathbf{U}_{\text{wall}}=\pm\omega\mathbf{R}$, with the sign adjusted according to the direction of rotation (+ for clockwise, − for counter clockwise). Here $\mathbf{R}$ is the radial position vector from the domain axis of rotation to the wall and ω is the domain angular velocity.

There were two types of open boundary conditions used: an inflow-type boundary condition, and an opening-type boundary condition. During the simulation, an

inflow boundary condition allows fluid to cross the boundary only toward inside the domain. With this type of boundary condition, e.g. shaping air inflow or booth inflow, the normal component of the velocity is prescribed. The opening boundary condition allows fluid to cross the boundary surface in either direction.

In the present study, an opening-type boundary condition was used wherever it was known that the fluid could flow in both directions across the boundary, e.g. in the periphery of the domain. For these boundaries, relative pressure values were specified, which is interpreted as "relative total pressure" for regions of inflow within the boundary, and "relative static pressure" for regions of outflow within the boundary. The direction component was specified as normal to the boundary. With this approach, the magnitude of the velocity at open boundaries could be computed as part of the solution.

3.3.2.3 Multi-phase Flow Equations

The Eulerian–Eulerian inhomogeneous multi-phase model was used in the present investigation. Although this model is slightly more computational intensive than the homogeneous case, it was preferred due to its intrinsic flexibility and recommendation by the commercial software developers [30] (Zwart P.: CFX-5 software developer. Personal Communication (2005)). The generalities of this model are as follows.

Let the different phases of fluids be denoted by using lowercase Greek letters $\alpha, \beta, \ldots$, etc. In general, a quantity subscribed with $\alpha, \beta, \ldots$, etc., refers to the value of the quantity for that particular phase, e.g. volume fraction of α is denoted r_α. Thus, the volume V_α occupied by phase α in a small volume V around a point of volume fraction r_α is given by:

$$V_\alpha = r_\alpha V \tag{3.5}$$

The total number of phases is N_P and the volume fraction of each phase is denoted r_α, ($\alpha = 1, \ldots, N_P$). The material density, ρ_α, is the density of the fluid if it is the only phase present, i.e. the mass of α per unit volume of α, while the effective density is defined as:

$$\tilde{\rho}_\alpha = r_\alpha \rho_\alpha \tag{3.6}$$

This equation specifies the actual mass per unit volume of phase α, given that phase α only occupies a fraction of the volume, i.e. the mass of α per unit volume of the bulk fluid. The mixture density is given by:

$$\rho_m = \sum_\alpha \rho_\alpha r_\alpha \tag{3.7}$$

whereas the total pressure in a multi-phase simulation is defined as:

$$p_{tot} = p_{stat} + \frac{1}{2} \sum_\alpha r_\alpha \rho_\alpha U_\alpha^2. \tag{3.8}$$

3.3.2.4 Inhomogeneous Multi-phase Model

Interfacial transfer of momentum is directly dependent on the contact surface area between the two phases. This transfer is characterized by the interfacial area per unit volume between phase α and phase β, and is known as the interfacial area density, $A_{\alpha\beta}$. Note that it has dimensions of one over length. Interfacial transfer can be modeled by using one of the several typical models present in the literature, with each using different algebraic prescriptions for the interfacial area density.

Within the inhomogeneous model three different models for interfacial transfer are available: (1) the particle model (which assumes that one of the phases is continuous and the other is dispersed), (2) the mixture model (which treats both phases symmetrically), and, (3) the free surface model (which attempts to resolve the interface between the fluids). In the present study the free surface model was used.

3.3.2.5 Free Surface Model

The free surface model attempts to resolve the interface between the fluids. If there are just two phases in the simulation (like in the present simulation), the following equation is used for interfacial area density:

$$A_{\alpha\beta} = |\nabla r_\alpha| \tag{3.9}$$

When more than two phases are present, this equation could be generalized as follows:

$$A_{\alpha\beta} = \frac{2|\nabla r_\alpha||\nabla r_\beta|}{|\nabla r_\alpha| + |\nabla r_\beta|}. \tag{3.10}$$

3.3.2.6 Inhomogeneous Multi-phase Conservation Equations

Based on the above definitions, the set of momentum and mass conservation equations that are solved take the form:

$$\begin{aligned}\frac{\partial}{\partial t}(r_\alpha \rho_\alpha \mathbf{U}_\alpha) + \nabla \bullet [r_\alpha(\rho_\alpha \mathbf{U}_\alpha \otimes \mathbf{U}_\alpha)] &= -r_\alpha \nabla p_\alpha \\ &+ \nabla \bullet \{r_\alpha \mu_\alpha [\nabla \mathbf{U}_\alpha + (\nabla \mathbf{U}_\alpha)^T]\} \\ &+ \sum_{\beta=1}^{N_p} (\Gamma^+_{\alpha\beta}\mathbf{U}_\beta - \Gamma^+_{\beta\alpha}\mathbf{U}_\alpha) + \mathbf{S}_{M\alpha} + \mathbf{M}_\alpha,\end{aligned} \tag{3.11}$$

and

$$\frac{\partial}{\partial t}(r_\alpha \rho_\alpha) + \nabla \bullet (r_\alpha \rho_\alpha \mathbf{U}_\alpha) = \mathbf{S}_{MS\alpha} + \sum_{\beta=1}^{N_p} \Gamma_{\alpha\beta}, \tag{3.12}$$

respectively. Here, $\mathbf{S}_{M\alpha}$ describes momentum sources due to external body forces and user defined momentum sources. $\mathbf{M}_{\alpha}$ describes the interfacial forces acting on phase α due to the presence of other phases.

The term $(\Gamma^{+}_{\alpha\beta}\mathbf{U}_{\beta} - \Gamma^{+}_{\beta\alpha}\mathbf{U}_{\alpha})$ represents momentum transfer induced by inter-phase mass transfer.

$S_{MS\alpha}$ describes user specified mass sources, and $\Gamma_{\alpha\beta}$ is the mass flow rate per unit volume from phase β to phase α. This term only occurs if inter-phase mass transfer takes place. In the present investigation, inter-phase mass transfer is neglected.

In addition, a volume conservation equation closure is needed. This equation constraints the volume fractions sum to unity, i.e.

$$\sum_{\alpha=1}^{N_p} r_{\alpha} = 1 \tag{3.13}$$

This equation may also be combined with the continuity equations for each phase to obtain a transported volume conservation equation, which yields,

$$\sum_{\alpha} \frac{1}{\rho_{\alpha}} \left[\frac{\partial \rho_{\alpha}}{\partial t} + \nabla \bullet (r_{\alpha}\rho_{\alpha}\mathbf{U}_{\alpha}) \right] = \sum_{\alpha} \frac{1}{\rho_{\alpha}} \left(S_{SM\alpha} + \sum_{\beta=1}^{N_p} \Gamma_{\alpha\beta} \right) \tag{3.14}$$

In the present case, in which we consider incompressible phases with no sources, this equation simplifies to:

$$\sum_{\alpha} \nabla \bullet (r_{\alpha}\mathbf{U}_{\alpha}) = 0, \tag{3.15}$$

which requires the volume flows to be divergence-free.

The complete set of hydrodynamic equations represent $4N_p+1$ equations in the $5N_p$ unknowns: $\mathbf{U}_{\alpha}=(u_{\alpha}, v_{\alpha}, w_{\alpha})^{T}, r_{\alpha}, p_{\alpha}$. We need N_p-1 more equations to close the system. These are given by constraints on the pressure, namely that all phases share the same pressure field:

$$p_{\alpha} = p, \quad \forall \alpha \in [1, N_p]. \tag{3.16}$$

3.3.2.7 Inter-phase Momentum Transfer Model: Phase Drag

Inter-phase momentum transfer, $\mathbf{M}_{\alpha\beta}$, occurs due to interfacial forces acting on each phase α due to interaction with another phase β. The total force on phase α due to interaction with other phases is denoted $\mathbf{M}_{\alpha}$, and is given by:

$$\mathbf{M}_{\alpha} = \sum_{\beta \neq \alpha} \mathbf{M}_{\alpha\beta} \tag{3.17}$$

Note that interfacial forces between two phases are equal and opposite, so the net interfacial forces sum to zero:

$$\mathbf{M}_{\alpha\beta} = -\mathbf{M}_{\beta\alpha} \Rightarrow \sum_{\alpha} \mathbf{M}_{\alpha} = 0 \tag{3.18}$$

The total interfacial force acting between two phases may arise from several independent physical effects:

$$\mathbf{M}_{\alpha\beta} = \mathbf{M}^{D}_{\alpha\beta} + \mathbf{M}^{L}_{\alpha\beta} + \mathbf{M}^{LUB}_{\alpha\beta} + \mathbf{M}^{VM}_{\alpha\beta} + \mathbf{M}^{TD}_{\alpha\beta} + \mathbf{M}_{S} + \cdots \tag{3.19}$$

The forces indicated above represent the inter-phase drag force (D), lift force (L), wall lubrication force (LUB), virtual mass force (VM), turbulence dispersion force (TD) and solids pressure force (S), respectively, and are valid only for dense solid particle phases. Based on the discussion presented by Salazar [37], of these forces, the only one considered relevant in the present investigation is the inter-phase drag force.

The general form used to model the inter-phase drag force acting on phase α due to phase β is

$$\mathbf{M}_{\alpha} = C^{(d)}_{\alpha\beta}(\mathbf{U}_{\beta} - \mathbf{U}_{\alpha}) \tag{3.20}$$

Note that $C_{\alpha\alpha}=0$ and $C_{\alpha\beta}=C_{\beta\alpha}$. Hence, the sum over all phases of all inter-phase transfer terms is zero.

In the above equation, $c^{(d)}_{\alpha\beta}$ can be written as

$$C^{(d)}_{\alpha\beta} = \frac{C_D}{8} A_{\alpha\beta}\rho_{\alpha}|\mathbf{U}_{\beta} - \mathbf{U}_{\alpha}| \tag{3.21}$$

where C_D is the drag coefficient of the liquid film.

3.3.2.8 Free Surface Flow Model

The implementation of free surface flow is similar to inhomogeneous multi-phase flow along with some special discretization options to keep the interface sharp. These include:

1. A compressive differencing scheme for the advection of volume fractions in the volume fraction equations.
2. A compressive transient scheme for the volume fraction equations.
3. Special treatment of the pressure gradient and gravity terms to ensure that the flow remain well behaved at the interface.

The surface tension model typically used is based on the Continuum Surface Force model introduced by Brackbill et al. [7]. In the current study the surface tension force was modeled as a volume force concentrated at the interface, rather than a

surface force. This approach is particularly useful in discrete control-volume numerical methods.

Considering a primary fluid α (the liquid phase) and a secondary fluid β (the gas phase), the expression for the surface tension force given by the Continuum Surface Force model takes the form:

$$\mathbf{F}_{\alpha\beta} = \mathbf{f}_{\alpha\beta}\delta_{\alpha\beta} \tag{3.22}$$

where,

$$\mathbf{f}_{\alpha\beta} = -\sigma_{\alpha\beta}k_{\alpha\beta}\mathbf{n}_{\alpha\beta} + \nabla_s\sigma, \tag{3.23}$$

and

$$\delta_{\alpha\beta} = |\nabla r_{\alpha\beta}|. \tag{3.24}$$

Here, σ is the surface tension coefficient, $\mathbf{n}_{\alpha\beta}$ is the interface normal vector pointing from the primary fluid to the secondary fluid (calculated from the gradient of a smoothed volume fraction), ∇_S is the gradient operator on the interface and k is the surface curvature defined by:

$$k_{\alpha\beta} = \nabla \bullet \mathbf{n}_{\alpha\beta} \tag{3.25}$$

The two terms summed on the equation for $\mathbf{f}_{\alpha\beta}$ represent the normal and tangential components of the surface tension force, respectively. The normal component arises from the interface curvature and the tangential component from variations in the surface tension coefficient (the Marangoni effect).

The $\delta_{\alpha\beta}$ term is often called the interface delta function; its value is zero away from the interface, thereby ensuring that surface tension forces are active only near to the interface. Furthermore, when the interface between the two fluids intersects a wall, it is possible to account for wall adhesion by specifying the contact angle between the interface and the wall through the primary fluid. The interface normal vector used for the calculations of both curvature and the surface tension force must satisfy the wall contact angle.

3.3.3 Typical Variables Controlled in the Simulations

In this section we discuss briefly the variables typically controlled during the rotary spray painting simulation. Throughout this discussion we assume that the spray gun geometry is well defined and fixed for a particular set of simulation runs. Additionally, we consider that assumptions 1–8 hold.

In the following a list of the variables to be controlled in the CFD simulation is presented: (1) booth airflow conditions, (2) paint properties, if known, (3) gun cup rotational speed, (4) paint flow rate, and (5) shaping air velocity.

The last variable, the shaping air velocity, can be related to the plant-site technique of specifying the shaping air pressure by designing a local nozzle microscale computational model. Finally, note that other transient behavior like film

evaporation has not been implemented in the model. In addition, the baseline study employes a boxy section of the booth around the spray gun. All these simplifications reduce model size which directly influences computational time, and allows meaningful results to be obtained in a timely manner.

3.3.4 Commercial Software Employed in the Simulations

Two commercial software codes (i.e. Fluent-6 and CFX-5) were found to be capable, in principle, of simulating the type of high-speed rotary two-phase flow occurring in the sprayer cup. Details about Fluent-6 and CFX-5 software can be found in [1, 2]. Both software were tested during the feasibility study and re-tested later in the investigation. CFX-5 showed an advantage by allowing to compute meaningful results in a reasonable time. We infer the reason for this difference between these two popular CFD codes is that Fluent-6 seemed to be more sensitive to local grid quality. As a result, CFX-5 was the code selected for the simulations presented in this chapter. Typical time steps for CFX-5 were of the order of 10^{-5} s and a typical run consisted of 10^{-1} s, i.e. requiring in the order of 10^4 time steps. A typical CFX-5 run would take 2 weeks of CPU time in a 32-way Linux cluster. Each node in the cluster consists of two 2.8 GHz Pentium Xeon processors, 4 GB of RAM, and dual 74 GB Ultra320 SCSI HDs under RAID 1 for fault tolerance, featuring both fast GigE over copper and Myrinet interconnect.

3.4 Simulation of Rotary Cup Behavior

The overall aim of this work was to evaluate computationally the performance of the current cup technology by means of the T/R sprayer cup, to diagnose possible atomization problems and, if possible, propose improvements to the current cup design.

3.4.1 Simulation Plan

In the following, a simulation plan consisting of a diagnosis and a parametric study is presented. Specific tasks for each study are also presented.

3.4.1.1 CFD Diagnosis of Current T/R Cup's Performance

Based on the T/R cup geometrical configuration, the feasibility of simulating the sprayer cup operation was to be determined. CFD was to be used for diagnosing its performance, finding the influence of operational parameters, and proposing modification or improvement strategies.

Due to computational power limitations, the analysis was carried out for a rotational speed of 1,000 rpm and liquid flow rates of 400, 800 and 1,000 cc/min. The reason for this somewhat unrealistic limitation is that simulating typical plant site rotational speeds (e.g. 50,000 rpm) and flow rates (e.g. 250 cc/min) requires grid sizes of the order of few microns at the surface of the cup and time steps of the order of 10^{-9} s, which would overwhelm the available computer resources and would significantly increase the time required to obtain meaningful results. Despite these limitations, it will be shown later that comparison with experiments indicate the essential film flow transport mechanisms were preserved.

The specific tasks for this study are as follows:

1. *Feasibility:* Evaluate the feasibility of simulating the operation of the sprayer cup via CFD. Keep only relevant features of T/R cup and simulate performance.
2. *Effect of Liquid Flow:* The effect of the liquid flow injected into the sprayer cup plenum was investigated, including three liquid flow rates: 400 cc/min, 800 cc/min and 1,000 cc/min.

3.4.1.2 CFD on the Effect of Geometrical Parameters on Basic Cup's Performance

Several geometrical parameters would be changed to evaluate their effect on the sprayer cup's performance, and included the conditions of 1,000 rpm and 500 cc/min case.

In the following the specific tasks for this analysis are presented:

1. *Effect of the Surface Angle* (α)*:* The effect of the surface angle (α) on the film stability was investigated. According to the preliminary stability analysis of Srinivasan et al. [44] and the results of Benjamin [6] and Liu et al. [28], the surface angle may have an interesting effect on film stability.
2. *Effect of Delivery Holes Diameter and Number:* The effect of some of the geometrical characteristics of the delivery manifold was studied by changing n_h and D_h while maintaining same liquid flow rate.

3.4.2 Computational Results

Results of the current study are presented in the following with only the most relevant data discussed.

3.4.2.1 Feasibility and Diagnosis of Current T/R Sprayer Cup's Performance

A CFD diagnosis of the current T/R cup's performance as well as the feasibility of using state-of-the-art CFD modeling was attempted. A computational model

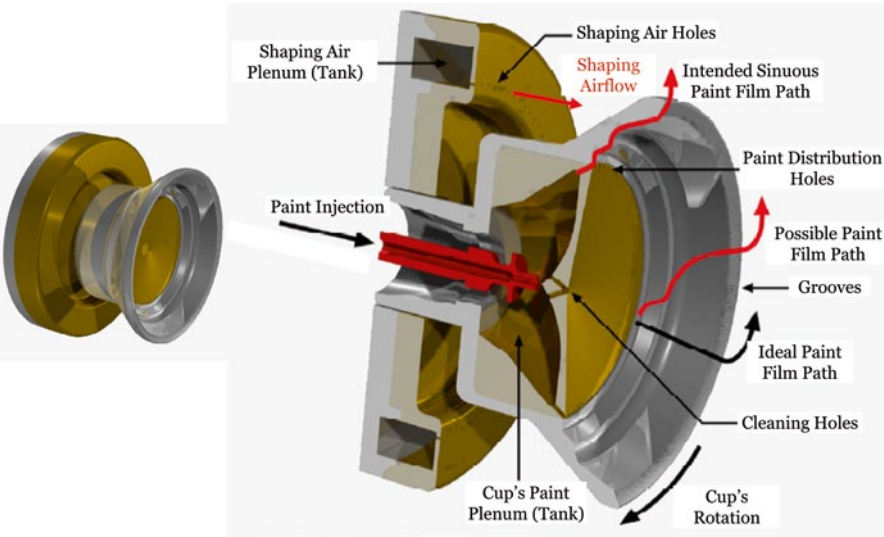

Fig. 3.12 Geometrical model of the T/R bell sprayer and the shaping air cup employed in the simulation. *Left*: External view. *Right*: Cut view showing the different parts of the model as well as the basic operational conditions used

geometry consisting of the T/R sprayer cup (bell) and the corresponding shaping air cup was created, with overall and cut views presented in Fig. 3.12. The geometrical model follows very closely the T/R cup blueprints and is accurate to 1×10^{-6} mm. However, only the portion of the domain out from the inlet of the delivery holes was considered, i.e. the flow in the paint injection pipe and the internal cup plenum was not included.

A computational grid was constructed for a periodic slice of the model corresponding to 4° of angular span, i.e. 90 periodic slices would compose a complete 360° span (full model) of the cup assembly. This model included one paint delivery hole, one shaping air hole and five grooves. After several attempts with different degrees of accuracy, it was determined that a grid of 1.4 million cells with a minimum cell size of 50 μm was suitable for simulating the process. Two frames of reference (static and rotating) were used in the simulation. A view of the composite computational surface grid and a close-up view of the grid around the cup edge displaying the grooves, the middle rib and the liquid supply manifold holes are presented in Fig. 3.13. Notice that the grid has been purposely refined in areas of the cup surface with greater curvature to increase accuracy.

It is important to mention that, although the grid looks fine enough to resolve the geometrical features of the cup, a grid with a minimum cell thickness of 50 μm at the cup surface was not sufficient to accurately compute the film flow under typical plant operational conditions. In fact, based on an analytical prediction of the steady state film thickness on the cup [40], it was found that at typical operating conditions (i.e. liquid flow rates of 250 cc/min and rotary speeds of 30,000–50,000 rpm) the film could be as thin as 4 μm in areas of the cup surface with high acceleration. To resolve such a thin film, a grid with cells of 1 μm in thickness would be needed.

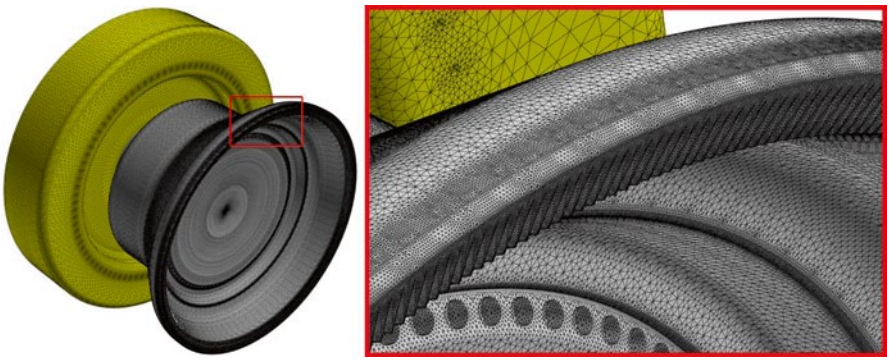

Fig. 3.13 *Left*: Overall view of the computational grid employed in the investigation of the T/R sprayer cup. *Right*: Detail close-up view displaying the grooves, the middle rib and the liquid supply holes

During early stages of the project, an attempt was made to generate a smoothly growing grid of high-accuracy with cells of 5 μm in thickness in the vicinity of the cup's surface. Although this fineness was not small enough to resolve a 4 μm film, the resulting grid was in excess of 30 million cells per 4° slice. Unfortunately, at the time of creation, both the computer system and the software were unable to operate with it due to memory address limitations. It was then decided to reduce the cup's rotary speed to 1,000 rpm and to increase the liquid flow rate to 1,000 cc/min, which generated thicker liquid films possible to be seen in the current grid. This set of operating conditions generated films with thickness between 100–150 μm [40], which would be detectable using the 1.4-million grid.

A direct consequence of this limitation for thin films simulation was that wherever in the surface of the cup the film was thinner than the local resolution (precision) of the model grid, the film may not be displayed appropriately or may look broken. Aside from this limitation, fully stable converged solutions obtained using the present computational model and algorithms rendered accurate predictions.

Feasibility Results

The first step in the simulation consisted in computing the airflow field. A cross sectional view of the airflow field and velocity vectors in the vicinity of the T/R cup operating at 1,000 rpm is presented in Fig. 3.14 in which the booth airflow was blowing downward. As a result of the rotation of the cup, air was thrown off radially and generated a steady region of low pressure at the interior (concave) face of the cup. Air was then sucked into this low pressure region, generating in turn a steady toroidal recirculation around the edge of the cup. A counter rotating toroidal vortex was also generated at some distance from the edge of the cup due to the interaction of the booth airflow and the higher speed shaping airflow.

An unexpected feature was found as a result of the interaction between the shaping airflow and the rotating cup. By design, shaping air jets were aimed at a point

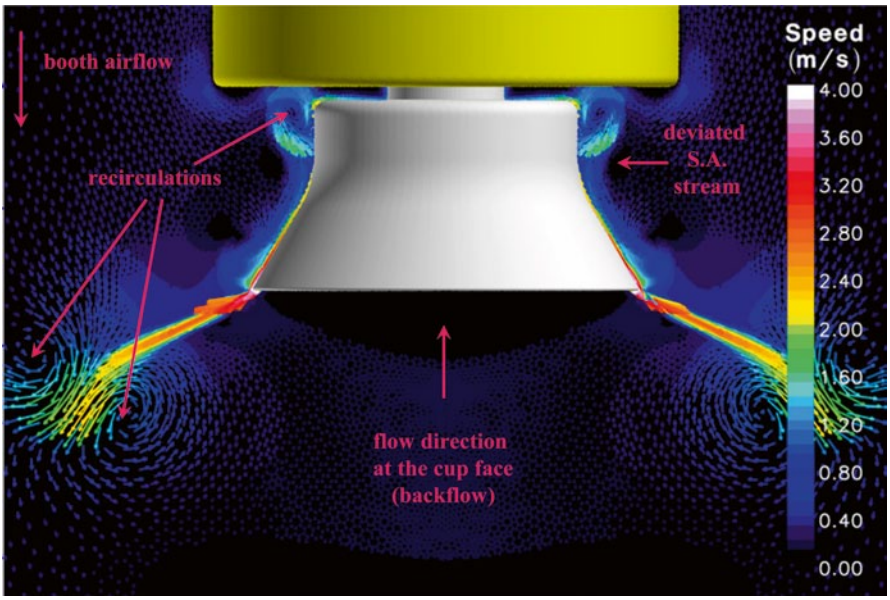

Fig. 3.14 Airflow field and velocity vectors around the T/R sprayer cup operating at 1,000 rpm

near the edge of the cup with the intention of aiding atomization of the paint ligaments and directing the generated droplets toward the surface being painted (e.g. for the T/R bell, the 90 straight holes of the shaping air cup are located at radius 35 mm while the cup edge radius is radius 38.5 mm). However, due to the rotation of the cup and the vacuum generated around the surface, the shaping air jets were diverted toward the external surface of the cup. This effect has several implications: (1) it generates a recirculation zone next to the shaping air cup between the shaping air holes and the cup which may suck overspray and push it into the back of the cup near the cup axis; (2) it slows down the shaping air jets and diffuses them reducing their effectiveness; and (3) it changes the orientation of the shaping air jets such that they do not act on the cup's edge but at a distance from it, favoring overspray formation.

A summary of the simulation results for the case 1,000 rpm and 1,000 cc/min (baseline) that substantiates the feasibility of performing these type of simulations is presented in Fig. 3.15; for brevity, only four relevant frames of the transient simulation are shown. The film is displayed as an iso-surface of volume fraction in which the color legend indicates film speed on a reference system rotating with the cup (relative velocity with respect to the cup). Observe that, after detaching from the cup, the liquid's relative velocity increases as a result of the deceleration in the air of the shed droplets. Also note that the simulation shows areas on the cup's surface that appear without film coverage, which does not mean the film has broken up but rather the film is too thin in these locations (i.e. thinner than the thickness of the computational cell, currently 50 μm) to be resolved by the visualization process.

In addition to demonstrating the feasibility of these calculations, the simulation has shown several interesting unknown features of the transient flow in rotary cups,

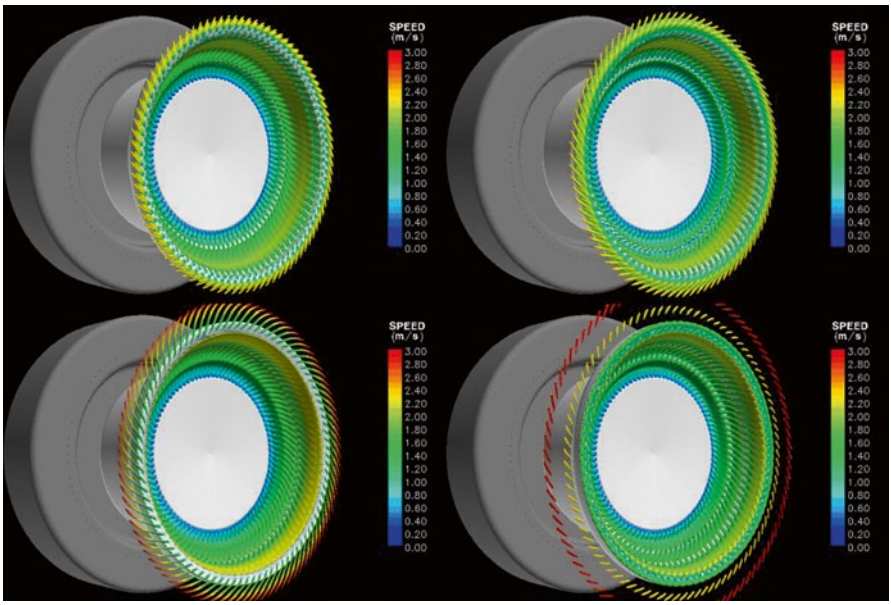

Fig. 3.15 *Top*: Four instances of the simulated atomization process (rotational speed: 1,000 rpm; liquid flow rate: 1,000 cc/min), showing the formation of ligaments that subsequently break into droplets. The color represents the relative velocity of the liquid with respect to the cup

summarized as follows: (1) the rotary droplet generation appears to be a pulsating-like phenomenon; (2) the current cup's design allows two distinct types of detrimental waves to travel along cup's surface (radial and azimuthal); (3) the waves seem to be supported by vortices generated when the paint delivery jets impinge on the cup's surface; and (4) since the groove channels are radial, it is apparent that under certain operating conditions they may interfere with the local liquid flow direction at the edge of the cup.

The existence of the traveling waves was not anticipated: they are a new feature discovered by the CFD simulation. Recently, Kazama [23] in an experimental work inferred about the possibility of unevenness in the film thickness but was not able to prove it experimentally, perhaps because of the inability to record information at the high frame rates necessary for the detection of the film waves. However, recent empirical tests performed by TMC/Trinity Japan under similar operating conditions than those employed in the simulation, provided evidence of the presence of these waves (see Fig. 3.16). The TMC/Trinity experimental results were obtained at a rotational speed of 1,000 rpm and a liquid flow rate of 800 cc/min, for three different values of shaping airflow (0 l/min, 270 l/min and 400 l/min). Note that the traveling waves observed in the CFD simulation can be also observed in the experiments performed with the TR-SM and the 530-33-BMK cups (this provides an additional corroboration of the present CFD results).

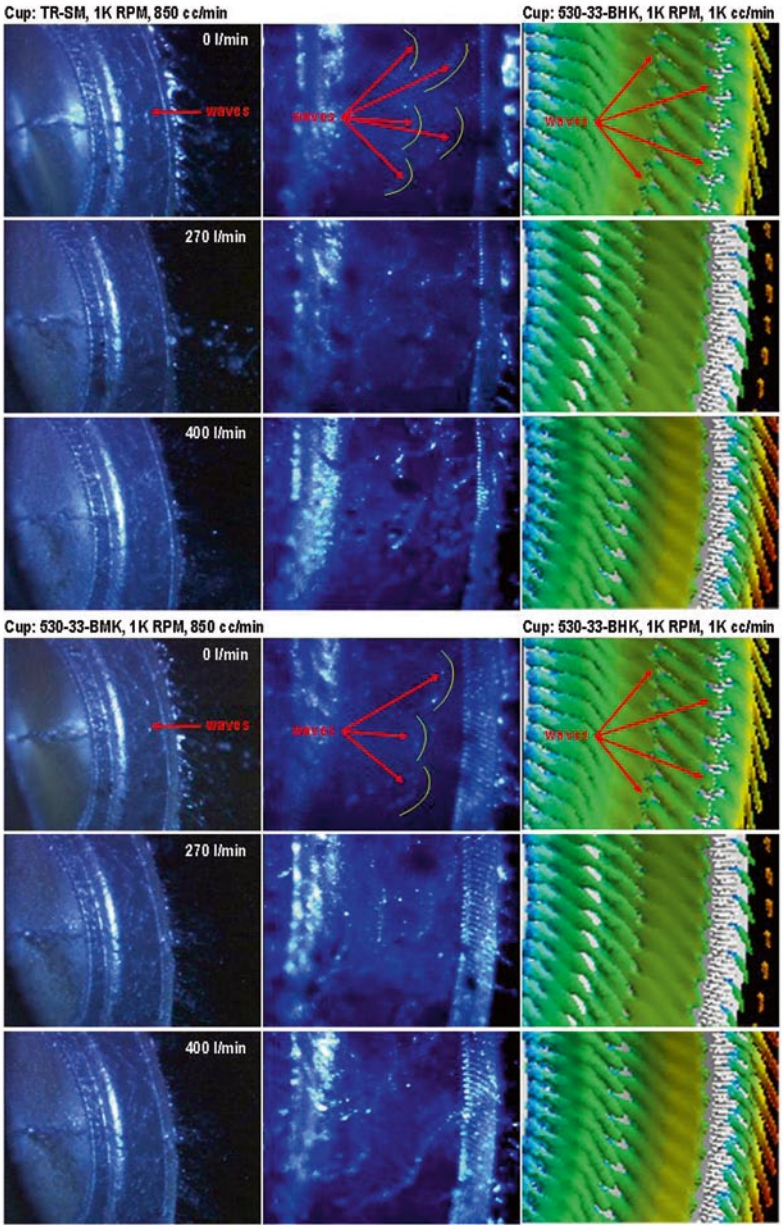

Fig. 3.16 *Top*: Comparison of the experimental observations (cup: TR-SM; rotational speed: 1,000 rpm; liquid flow rate: 850 cc/min) with the results of the CFD simulation (cup: 530-33-BHK; rotational speed: 1,000 rpm; liquid flow rate: 1,000 cc/min). *Bottom*: Comparison of the experimental observations (cup: 530-33-BMK; speed: 1,000 rpm; liquid flow rate: 850 cc/min) with the results of the CFD simulation (cup: 530-33-BHK; rotational speed: 1,000 rpm; liquid flow rate: 1,000 cc/min)

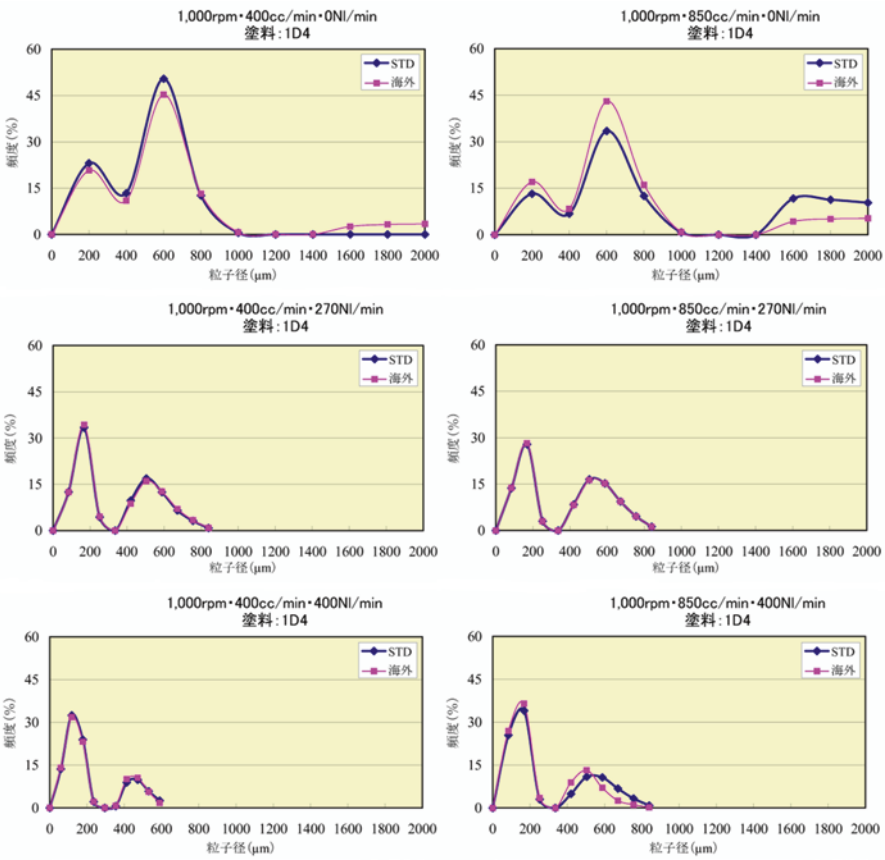

Fig. 3.17 Plots showing the experimental "dual-mode" particle size distribution obtained at 1,000 rpm. Note that this dual-mode is practically insensitive to the liquid flow rate in the range 400–850 cc/min. The bigger particle size mode is damped as the shaping airflow (S/A) pressure (and hence its jet speed) increases, which indicates that S/A is enhancing the atomization of the bigger droplets by facilitating their break-up into smaller ones. S/A is not enhancing atomization of the smaller droplets. In addition to being harder to break (due to the stronger influence of surface tension), smaller droplets follow different trajectories (see figure): they tend to stay at the center of the spray. These "dual-mode" distributions constitute additional corroborations of our CFD findings

The corresponding experimental droplet size distribution obtained at 1,000 rpm is presented in Fig. 3.17. Although the diameters are too large for typical automotive paint applications, the droplet size distribution displays a dual mode shape that appears to be independent of the flow rate and occurring practically at the same droplet size (200 and 600 μm) for both 400 cc/min and 850 cc/min. In both cases, as the shaping air increases, the curves shift to the lower droplet diameter side generating a narrower distribution. This indicates that the shaping airflow enhances atomization. The bigger droplet size mode, which is predominant for the no shaping

airflow case, reduces dramatically as the shaping airflow increases. Note that the change in the smaller droplet size mode seems to be less pronounced for shaping airflow rates higher than 270 Nl/min because smaller droplets (which have smaller *We* numbers) are harder to break (by secondary atomization).

Since current state-of-the-art computational resources (CFD codes and hardware) do not allow simulation of rotary cup operation with films of only few micrometers in thickness, it is not straight forward to extrapolate the current observations to typical plant conditions and to conclude that the same waves are preserved at higher rotational speeds. However, the fact that evidence of these waves have been seen at higher rotational speeds [23], and that earlier investigations [19] indicated waves generated in the liquid film of rotary cups were not mitigated by increasing rotational speed (and hence, centrifugal acceleration), points to the possibility these waves are indeed preserved at higher rotational speeds.

To investigate this possibility, an experiment was conducted by TMC/Trinity, results of which are displayed in Fig. 3.18. The experimental conditions employed were: 25,000 rpm, standard shaping airflow, and three different values of paint flow rate (e.g. 200 cc/min, 300 cc/min and 400 cc/min) within the typical range used in plant-site spray painting applications. To visualize the waves, a camera combined with high-speed stroboscopic light was used. In the figure, back face and front face views are presented with the front face views depicting aspects of the morphology of the paint film on the cup. As inferred, the flowing waves were preserved at higher rotational speeds and occurred at the three liquid flow rates tested. It is apparent that their wave length increased as the liquid flow rate increased from 200 to 300 cc/min, however, no noticeable change is observed as liquid flow rate increased from 300 to 400 cc/min, indicating a weak dependency of these wave characteristics with liquid flow rate within the tested range. The back face views display the ligaments formed as the paint is thrown away from the edge of the cup, and as predicted by the CFD simulation, the ligaments oscillate after forming and became unstable to the point of breaking into droplets (atomization). Also observe that the length of the ligaments increased as the liquid flow rate increased. Since thicker ligaments can extend longer without breaking due aerodynamic instabilities, the achievable ligament length can be used as an indirect indication of the ligament thickness. Therefore, ligament thickness increases with the liquid flow rate. Additionally, notice that for each flow rate case, the ligaments did not have the same length and areas in the cup periphery existed where the ligaments were longer than in others in a cyclical way. This indicated that the film reaching the grooves had periodic non-uniform thickness.

Using the curvature of cup's edge to determine and consolidate the scale of the pictures, it is possible to realize that the cyclical long-short ligament pattern seems to correlate with the number of paint supply holes in the cup. This indicates that the effect generated by the liquid delivery onto the face of the cup is not completely diffused by viscosity (diffusivity) and cup face geometry, even under the effect of such high centrifugal forces. This interesting feature was also present in the baseline simulation in which the number of ligaments generated at the edge of the cup was predominantly the same as the number of paint delivery holes. Evidence of this

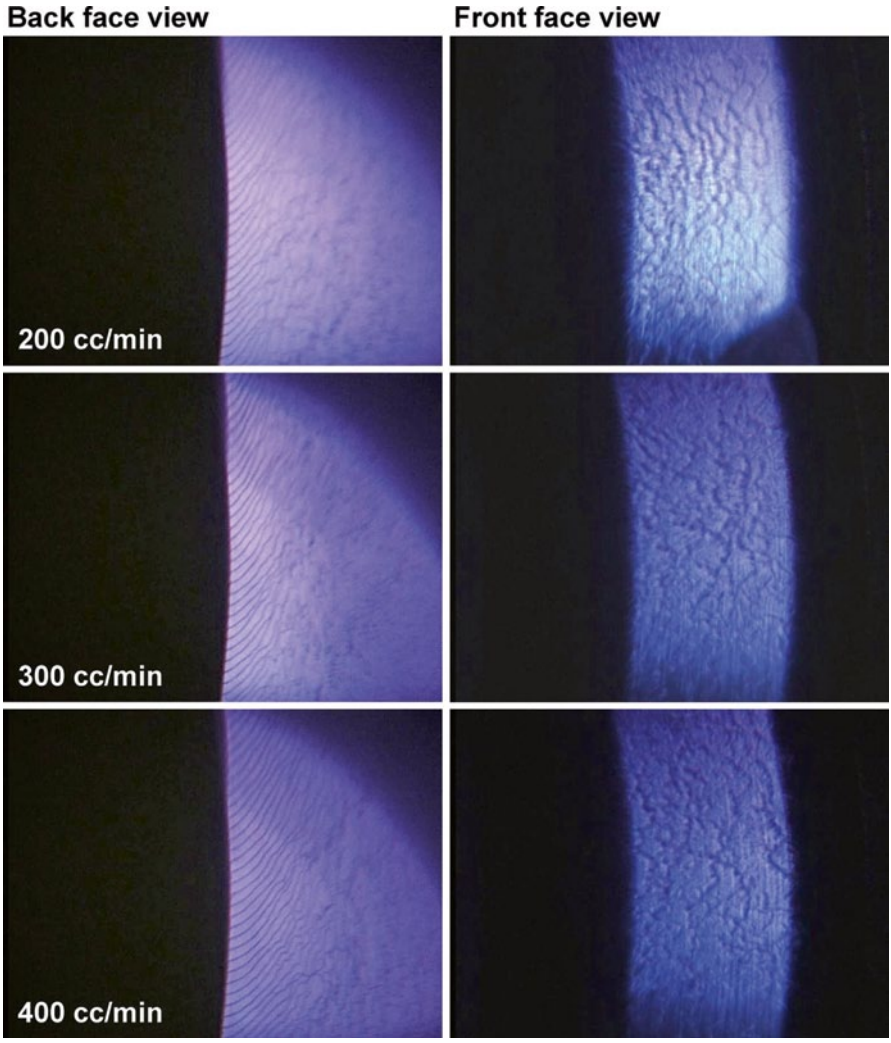

Fig. 3.18 TMC/Trinity experiment at 25,000 rpm for different liquid flow rates. *Left*: View of the back face of the cup showing the formation of ligaments at the edge of the cup. Notice that ligaments become longer as flow increases. Also, observe the cyclical long-short ligament pattern along the edge of the cup. *Right*: Frontal face of the cup displaying waves on the liquid film. Based on the pictures it is apparent that their wave length increases as the liquid flow rate increases from 200 to 300 cc/min. There is noticeable change in the wave length when the liquid flow rate increases from 300 to 400 cc/min

feature was also observed by Kazama [23]. Figure 3.19, reproduced from Ref. [23], presents a high-speed photo of the ligaments generated by a clear-coat paint. As expressed by this author: "*Paint threads of varying lengths are seen extending from the bell edge in a cyclical pattern. It is thought that the difference in length reflects the difference in the thickness of the paint threads. This cyclical pattern coincides*

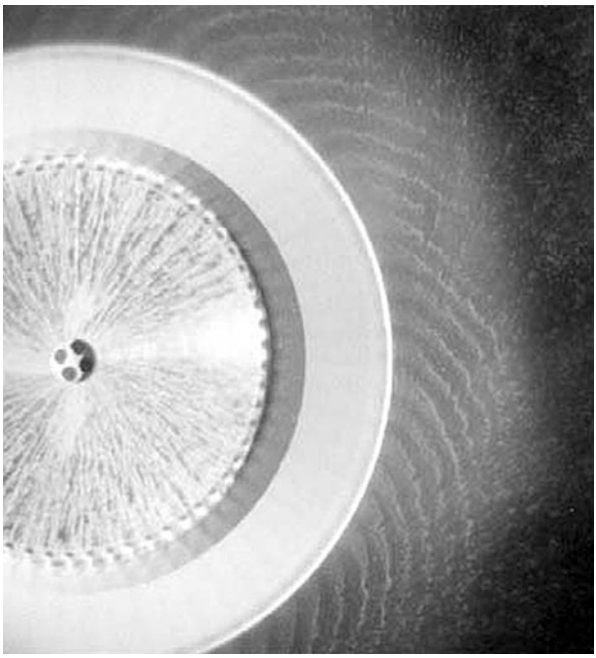

Fig. 3.19 High speed photo of the paint threads generated by a white paint clear coat. (Picture reproduced from [21])

with the number of holes supplying paint to the bell cup surface. It is inferred that a liquid film of uneven thickness formed on the bell cup."

This result obtained with a geometrically different cup that examined herein, indicates that this problem may be occurring in many sprayer cups regardless of the design. It also provides additional corroboration that the current CFD model is able to predict correctly the main flow features occurring during rotary spray painting.

The pictures obtained by TMC/Trinity (Fig. 3.18) and by Kazama [23] (Fig. 3.19), were snap-shots of a transient process. The current simulation results show that, at liquid flow rates of 1,000 cc/min, the film overflowed the grooves in a pulsating way and an overflowed groove was ineffective in breaking the film into ligaments. Strong pulsating flows will generate unsteady values of the liquid flow rate at the cup's edge and, as a result, the effective atomization mechanism may shift frequently from *single-drop* to *ligament* to *sheet*, and back. Every time the film would flood the grooves, the ligaments would grow in diameter resulting in the production of bigger droplets. When the film thickness at the edge would decrease, the diameter of the ligaments would also decrease and would produce smaller droplets. Since the frequency of this pulsation and the overflow-underflow process occurs many times per second, the overall measured result would be a spray with a wide droplet size distribution.

Figure 3.20 presents a summary of the simulated results in which overflowed grooves are depicted and serve also to illustrate the mechanism of formation of ligaments due to instabilities of the liquid toroid accumulated at the cup's edge. Notice that different small protrusions with different sizes and frequencies appeared and

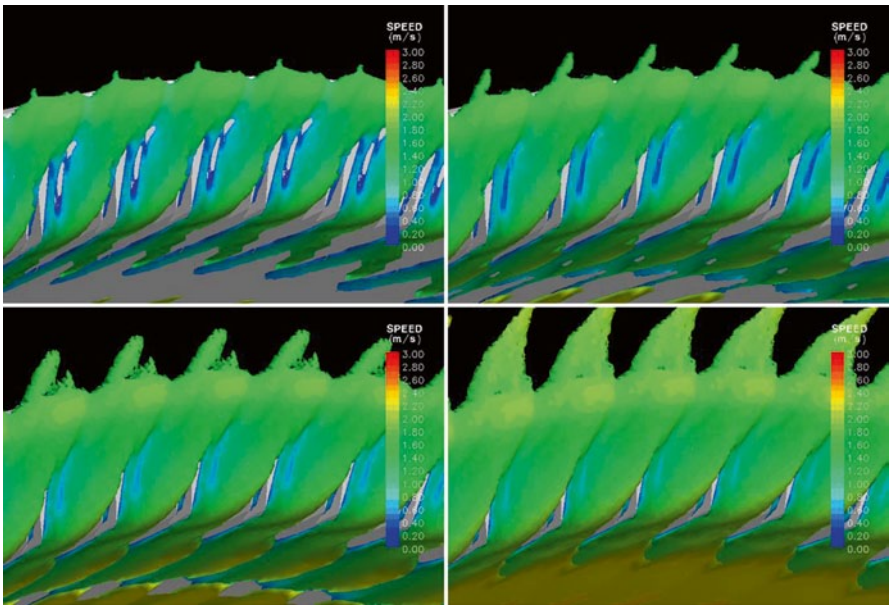

Fig. 3.20 Four frames of the CFD simulation showing how the ligaments form from film instabilities at the cup's edge. Notice that the different small protrusions (with different sizes and frequencies) that appear in the film try to grow simultaneously, but only the one which instability frequency is dominant prevails. This prevailing instability then grows to form the ligament

grew simultaneously, but only the one instability frequency was dominant. This prevailing instability then grew to form the ligaments.

In summary, a combination of effects could be responsible for the generation of sprays with a wide range of droplet sizes. Without considering any possible variation due to the rheology of the paint, the CFD simulation has identified several possible causes. In particular: (1) the unevenness of the liquid film on the cup's surface; (2) the instability generated by the liquid injection holes; (3) the possibility of overflowing the grooves; and, (4) the interference generated by the grooves not aligned with the liquid flow at the cup's edge. A diagram displaying these identified issues with the current cup technology is presented in Fig. 3.21.

To investigate further the nature of these waves as well as to find possible approaches to mitigate them, an analysis was performed of the liquid flow on inclined surfaces, including smooth and patterned surfaces. Scale modeling techniques were used to extrapolate the results to the rotary cup case. A report summarizing the results of this investigation is presented in Srinivasan et al. [45].

Effect of Liquid Flow Rate

The effect of the liquid flow rate injected into the sprayer cup plenum on film formation and droplet generation mechanism was investigated. Three cases were eval-

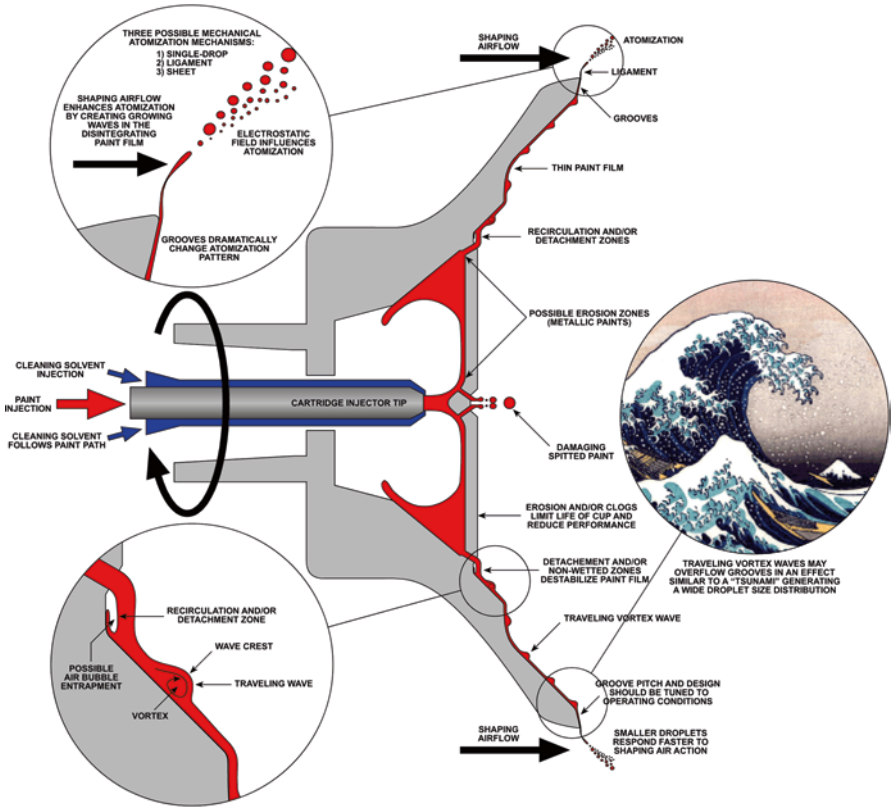

Fig. 3.21 Technical issues with the current T/R sprayer cup technology

uated: 400 cc/min, 800 cc/min and 1,000 cc/min (baseline). During the test, all other parameters, including the grid, numerical solver parameters and time steps were kept unchanged. A summary of the computational results is presented in Fig. 3.22.

Four distinct frames of the transient simulation are presented for each of the cases. Unfortunately, despite repeated efforts, the case 1,000 rpm and 800 cc/min did not converge accurately. Regardless, the results are presented for completeness. It is estimated that comparing the 1,000 cc/min data (baseline) with 400 cc/min data could provide enough information to enable an analysis of the effects of liquid flow rates.

It is apparent that, as Q decreased from 1,000 cc/min to 400 cc/min, the droplet formation regime changed from *ligament* to *single-drop*. Therefore, the droplets are formed via a different atomization mechanism. In the 1,000 cc/min case, long ligaments formed at the edge of the cup. These ligaments extended, oscillated and became unstable due to hydrodynamic forces and, finally, broke into droplets. For the 400 cc/min case, the droplets were formed directly from a toroidal fluid structure formed at the cup's lip. In addition, from Eq. (3.1) it is apparent that for a specified ρ, D and ω, the functional relationship for transition from *single-drop* to *ligament* should take the form:

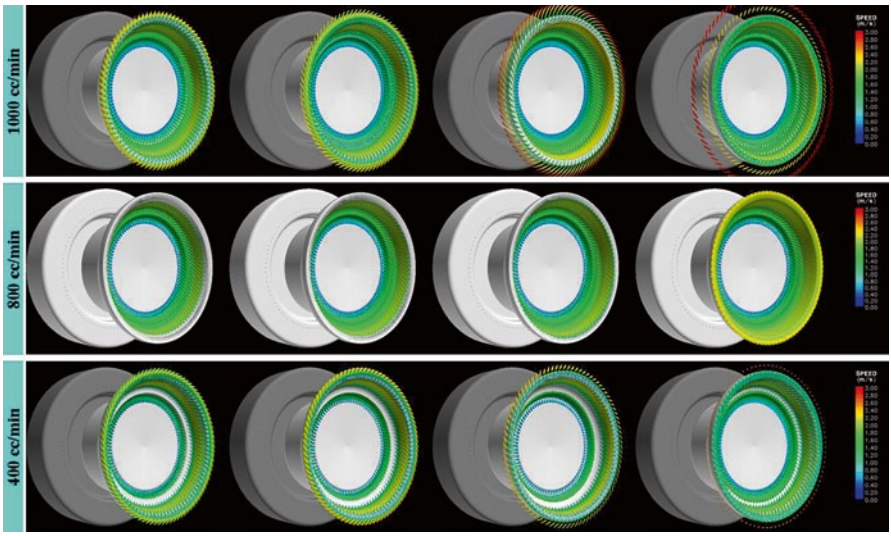

Fig. 3.22 Effect of liquid flow rate on the film and droplet formation mechanism

$$Q\mu^{0.167}\sigma^{-0.708} \geq C_l. \tag{3.26}$$

Similarly, transition from ligament to sheet atomization regime occurred when the following relationship was satisfied:

$$Q\mu^{0.167}\sigma^{-0.708} \geq C_s, \tag{3.27}$$

where both C_l and C_s, $C_s > C_l$, are constants to be determined. Based on Eq. (3.26) it is concluded that increasing liquid flow rate and liquid viscosity while decreasing surface tension should favor ligament formation. However, the value of the left hand side of Eq. (3.26) should not increase so much that it would satisfy Eq. (3.27), indicating transition to the *sheet* atomization regime.

Although not clear in the frames presented in Fig. 3.22, the animations showed it was easy to depict azimuthal film flow oscillations. It is also apparent that the angle of deviation of the flowing film from the radial direction decreased slightly as the liquid flow rate decreased. Keeping the other parameters constant, it seems intuitive that for smaller liquid flow rates the film would be thinner and the angular lag of the upper film layers would reduce, resulting in a more radial flow (less deviation angle). This last result is in agreement with the analytical prediction for the behavior of steady liquid films in rotary cups [40]. However, it does not take into account film instabilities and is incapable of evaluating their influence on the deviation angle. If the instabilities were assumed to be in the form of oscillations about a mean, the average deviation angle could be close to the one determined analytically.

According to the analytical prediction [40], the film flow trajectory at 1,000 rpm, which deviated approximately 23° from the radial direction at the cup's edge for the 1,000 cc/min case, reduced to 13° for the 400 cc/min case. Similarly, at the same radius, the film thickness changed from 99 μm at 1,000 cc/min to 73 μm at 400 cc/min. At this low rotational speed (1,000 rpm), the upper layers of the film reached the grooves at great enough angle to cause detrimental film separation. Based on the same analytical prediction [40] at rotary speed near 30,000 rpm, the deviation angle should have reduced to about 8°. It is clear that the numerical calculations were, at least, qualitatively in agreement with the analytical model and with the TMC/Trinity experiments.

3.4.2.2 Effect of Geometrical Parameters on Basic Cup's Performance

It is important to understand how different geometrical features of the cup influence the overall performance of a sprayer. Judging by the different cup configurations commercially available, it can be understood that the number of parameters involved in their geometrical description may be too great to accommodate them all.

To investigate this issue, it is advisable to use a simplified cup design, namely a Basic Cup. This cup design presents several simplifications in the geometry when compared to the T/R cup, and may allow better control, definition and specificity of the geometrical parameters involved during operation. An effort was made to preserve in the Basic Cup design features shared by most of the commercial sprayer cups available. Only those features expected to be influential were incorporated; in all cases simulated, the fluid injected had the physical properties of water.

An overall aim was to develop a basic understanding of the influence of several of the cup's geometrical design parameters on film stability. A sketch of the geometrical parameters defining the Basic Cup model is presented in Fig. 3.23. Notice that by defining a limited set of parameters, it was possible to generate a large family of cups. It is equally important to mention that, for each simulation with a different value of any of these parameters, new 3-D geometry and computational grids needed to be generated. Since high-quality grid generation is very time consuming, a limit was reached in the number of cases simulated.

Effect of the Surface Angle (α)

The angle (or slope) of the cup's surface is related to the local component of the centrifugal force acting perpendicularly to the film with respect to that acting along the film. Only the component acting along the film generates acceleration and increases local film speed [40], which results in film flow. According to the results of Benjamin [6] and Liu et al. [28], the surface angle may have an interesting effect on film stability in which higher surface angles would be expected to promote liquid film instability.

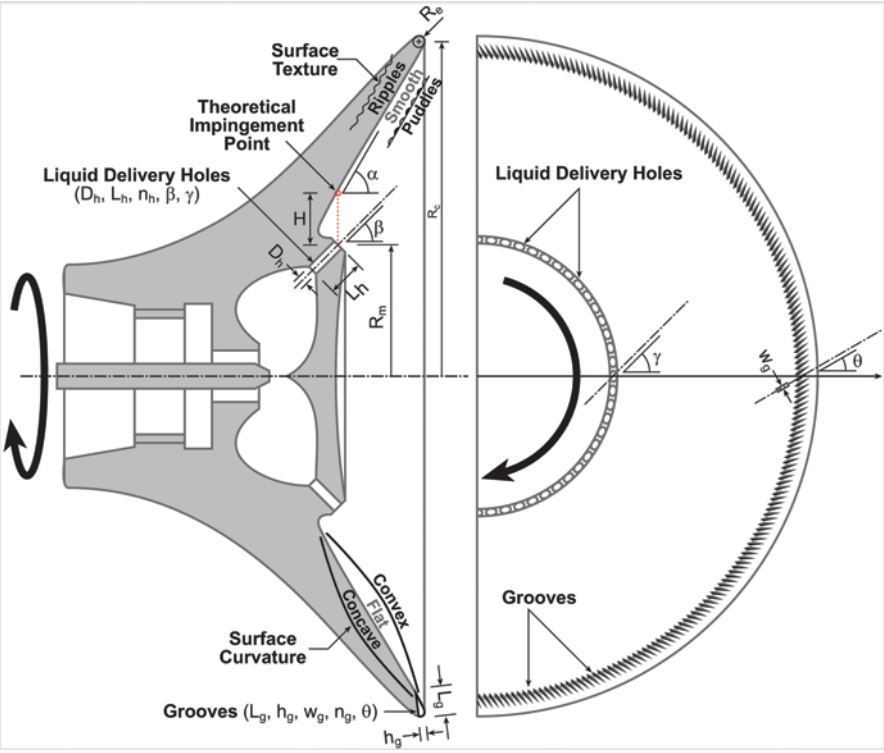

Fig. 3.23 Sketch of the proposed basic cup model

During a numerical analysis of the effect of surface angle, all other geometrical parameters were kept constant (in most cases, the values chosen were as close as possible to those of the T/R cup). Two different surface angles ($\alpha = 45°$ and 60°) were tested for the case $H = 0$ (see Fig. 3.23). A smooth surface, with no edge grooves, was also used. The diameter of the liquid delivery holes and the diameter of the cup were the same as those of the T/R cup. For comparison purposes, 3-D views of the geometric configuration of the cups tested is presented in Fig. 3.24.

Assuming the current model was simulated at 500 cc/min and 1,000 rpm, films of 75–100 μm thick would be generated [40]. This fact required a mesh with smaller cell size at the cup surface. To perform the simulations, two computational grids of 3.4 million cells mesh were created, each of which represented a periodic slice of the model corresponding to 4° of angular span of the cup assembly. This model included one paint delivery hole, one shaping air hole and no grooves. Figure 3.25 presents overall and detailed views of the composite surface grid on the sprayer cup and shaping air tank. Table 3.1 compares the typical mesh features with those of the 1.4 million cell feasibility mesh employed previously.

Notice that for this application, the minimum cell thickness at the cup surface was halved and the volume of the cells in the region of ligament/droplet detection was reduced to 1/8 of the previous value, resulting in an increased accuracy. In addition, it is important to mention that reducing the liquid (water) flow rate to 50 %

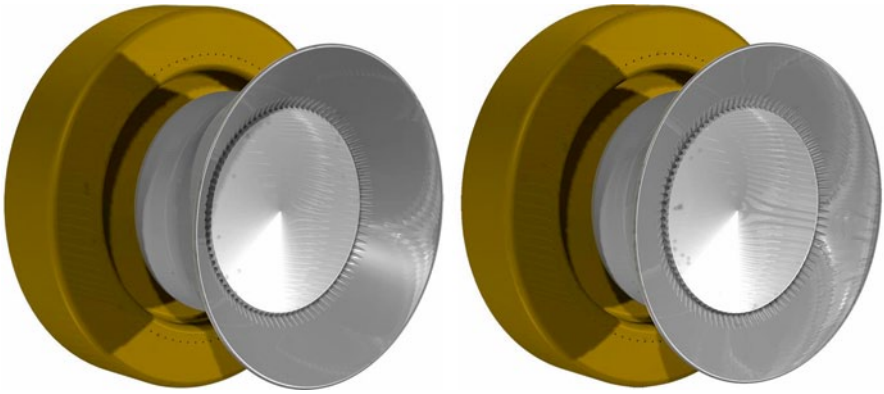

Fig. 3.24 3-D geometrical models for the Simple Cup model with $H=0$ and smooth surface. *Left*: $\alpha=45°$ (baseline). *Right*: $\alpha=60°$. The number of injection holes in both cups is 90. All other geometrical parameters are kept constant

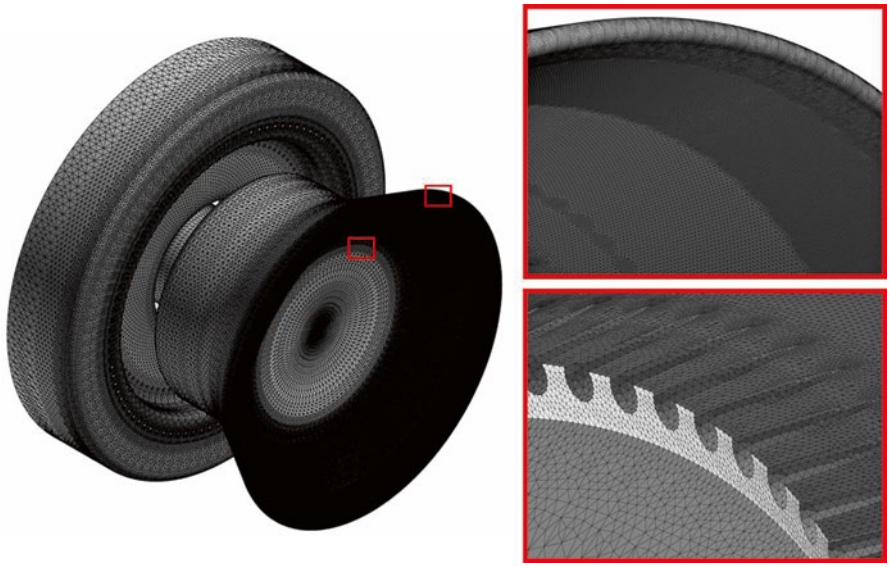

Fig. 3.25 *Left*: Overall view of the computational grid generated on the surface of the sprayer cup and shaping air cup assembly for the case $\alpha=45°$. *Right*: Close-up views of the non-grooved edge and the holes of the paint supply manifold

(from 1,000 cc/min to 500 cc/min) resulted in increasing the number of cells by 240 % to visualize the film.

A summary of the simulation results for the case 1,000 rpm, 500 cc/min, $H=0$, $n_h=90$, $D_h=1$ mm, smooth surface and $\alpha=45°$ and 60°, is presented in Fig. 3.26. For brevity, only four relevant frames of the transient simulation are presented for each case. The case with $\alpha=45°$ will be used as the baseline for all the tests performed.

Table 3.1 Comparison of computational grids employed during simulation

	Current grid	Feasibility grid
Number of grid cells (in millions)	3.4	1.4
Number of grid nodes (in thousands)	6.4	2.8
Minimum cell thickness at cup surface (μm)	25 (uniform)	50–75 (non-uniform)
Minimum detectable film thickness (μm)	50–100	100–200
Cell side for ligament/droplet detection (μm)	100	200
Minimum detectable ligament/droplet (μm)	200–400	400–800

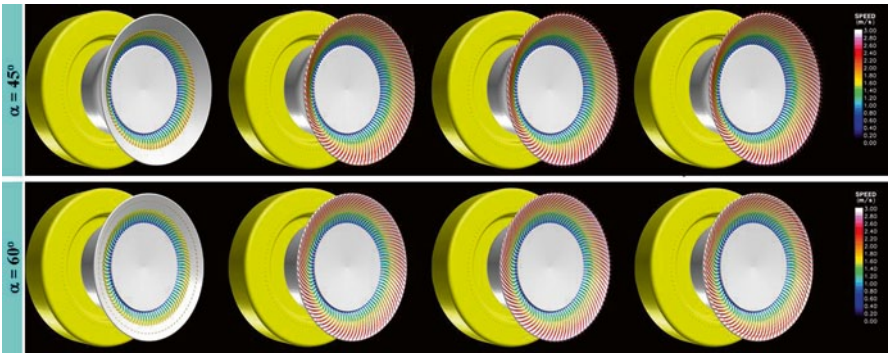

Fig. 3.26 Effect of surface angle (α) on the film stability and droplet generation. As the surface angle increases, the film becomes more unstable. However, the instabilities are felt at a distance from the injection holes, where the film speed is higher

The film is displayed as an iso-surface of volume fraction: the color legend indicates film relative speed with respect to the cup and the places in the face of the cup where the film is not displayed indicate very thin films that were not resolved by the simulation. The film perturbations (jet-like perturbations) generated by the carved-in liquid injection holes (obtained for $H=0$) were hardly damped by the cup surface. Without the effect of the grooves at the edge, the film perturbations reached the cup's edge and generated large, thick ligaments that disintegrated into large droplets. Observe that the larger cup angle tested ($\alpha=60°$) generated additional instabilities in the film. These perturbations became influential at a distance from the injection hole, where the film achieved enough relative speed with respect to the cup surface (see bottom right frame in Fig. 3.26: film perturbation noticeable near the cup's edge).

Effect of Delivery Holes Diameter and Number

Since liquid injection has a strong effect on the growth of the film perturbations, the effects of delivery hole diameters (D_h) and numbers (n_h) were studied by increasing the number of holes while maintaining the same injection flow rate (i.e. reducing D_h accordingly).

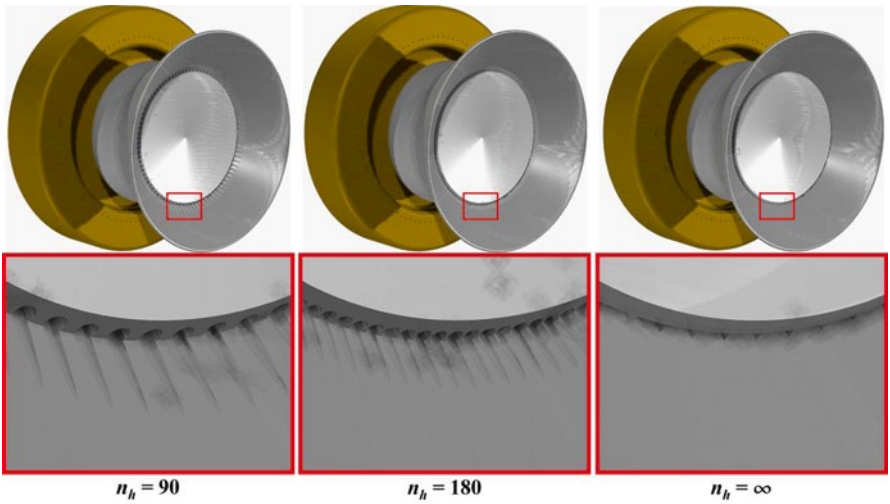

Fig. 3.27 3-D geometrical models employed in the analysis of the effect of delivery holes diameter and number. The three cases studied are $n_h = 90$ (baseline), 180 and ∞. All other geometrical parameters are kept constant

To perform the simulation, two additional 3-D geometries and computational grids were created. Figure 3.27 displays overall and detailed views of the 3-D geometries for the cases studied ($n_h = 90$, 180 and ∞). Notice that as the number of delivery holes increased, the diameter and depth of the carved-in holes decreased to maintain the same liquid injection flow rate. Again, the case $n_h = 90$ and $D_h = 1$ mm, smooth surface, $H = 0$, and $\alpha = 45°$ was used as baseline. Computational grids of similar size as the ones employed in §8.2.1 were employed. For brevity, pictures of these grids are not presented here.

Figure 3.28 shows that, as the number of holes increased, the jet-like perturbations in the film were damped by inter-jet collision and diffusion. However, increasing n_h also produced big ring-like waves traveling in accelerated motion through the cup's surface. The frequency of these waves tended to increase with the number of holes, and these big ring-like waves generated large size droplets. Finally, it is interesting to note that the fingering observed for the case with $n_h = \infty$ did not correspond to a particular number of holes, rather they appeared to be due to inherent instabilities in the system.

3.5 Conclusions

This chapter has presented the potential of using computational fluid dynamics (CFD) modeling as a tool to complement experimental and theoretical analysis in the task of enhancing the current level of understanding of the phenomena taking

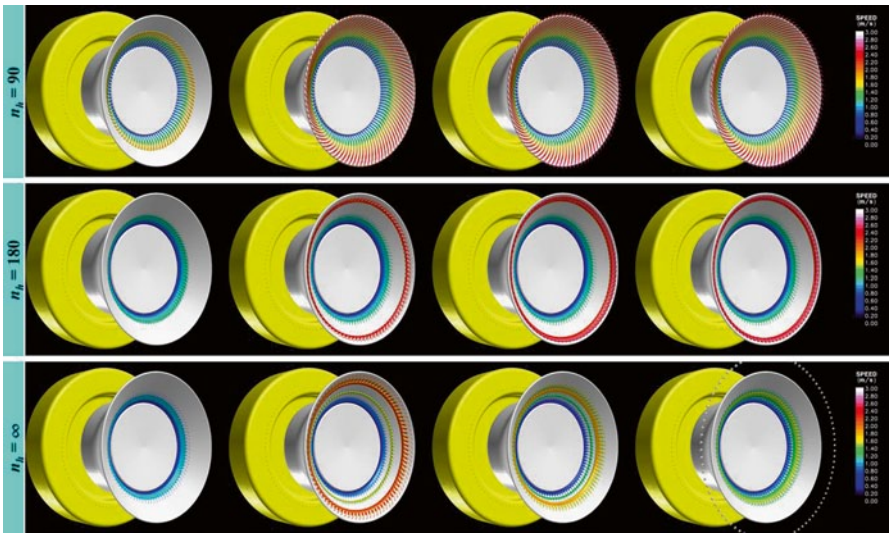

Fig. 3.28 Effect of the paint delivery holes diameter (D_h) and number (n_h). When n_h is changed, D_h is adjusted to maintain the same injection velocity. As n_h is increased, the jet-like perturbations in the film are replaced by large wave-like disruptions that generate droplets of large diameter

place during the fascinating process of automotive rotary paint atomization. The methodology and summarized results presented here are intended to serve just as a guide for future investigations in the field.

Despite the limitations of the models employed in the present investigation, limitations due mainly to computer hardware and numerical algorithms, the results obtained have been capable of bringing insight into relevant mechanisms of atomization as well as different film flow instabilities occurring during the process. These results highlight the realization that much more knowledge and understanding about paint rotary atomization may be still hidden, just waiting to be discovered by those willing to properly use the powerful tool of CFD. The potential impact of this understanding in the automobile manufacturing industry, the environment, and people's life is enormous.

To conclude, it is pertinent to cite a paragraph from Professor Chigier' website [9]:

> The automobile industry needs a solution to the spray problem. They are spending a great deal of money on painting, much of which is wasted. The industry must increase the percentage of paint that is deposited on the target and correspondingly, reduce the percentage of offspray. If the automotive industry used instrumentation and computation for controlling drop size, trajectories and deposition, they would see large scale increases in efficiency, reduced failure to meet painting requirements and reduced generation of toxic pollutants. Use of this advanced spray technology would provide very large financial benefits to the automobile industry.

As shown in this chapter, CFD simulations may be the additional tool needed to help the automobile industry finally solve their rotary spray painting problems.

References

1. ANSYS Fluent User Guide.
2. ANSYS CFX User Guide.
3. Abelson P.H.: Constraints on greenhouse gas emissions. Science. **278,** 783 (1997)
4. Akafuah N.K., Salazar A.J., Saito K.: Paint droplet transport visualization using infrared thermographic technique. In: Proceedings 2010 Painting Technology Workshop, Lexington, Kentucky (2010)
5. Bailey A.G.: Electrostatic spraying of liquids. Wiley, New York (1988)
6. Benjamin T.B.: Wave formation in laminar flow down an inclined plane. J. Fluid. Mech. **107**, 554 (1957)
7. Brackbill J.U., Kothe D.B., Zemach C.: A continuum method for modeling surface tension. J. Computat. Phys. **100**, 335 (1992)
8. Chen M., Kontomaris K., McLaughlin J.B.: Direct numerical simulation of droplet collisions in a turbulent channel flow. Part I: collision algorithm. Int. J. Multiph. Flow. **24**(7), 1079–1103 (1998)
9. Chigier N.: Spray painting of automobiles—problems and solutions, in official Norman Chigier web site http://www.normanchigier.com/DepositionofPaintonCarsAutomobiles-AtomizationandSprayTechnology.html
10. Colbert H., Salazar A.J., Saito K.: Simulation of the effect of evaporation on the trajectory of charged particles. In: Proceedings 2003 Painting Technology Workshop, Lexington, Kentucky (2003)
11. Colbert H., Salazar A.J., Saito K.: Computational parametric study of transfer efficiency in spray painting process. In: Proceedings of the 2004 Painting Technology Workshop, Lexington, Kentucky (2004)
12. Dombrowski N., Lloyd T.L.: Aerodynamic instability and disintegration of viscous liquid sheets. Chem. Eng. Sci. **18**(3), 203–214 (1963)
13. Dombrowski N., Lloyd T.L.: Atomization of liquids by spinning cups. Chemical Engineering J. **8**(1), 63–81 (1974)
14. Domnick J., Scheibe A., Ye Q.: The simulation of the electrostatic spray painting process with high-speed rotary bell atomizers. Part 1: Direct charging, Part. Part. Syst. Charact. **22**, 141 (2005)
15. Domnick J., Scheibe A., Ye Q.: The simulation of the electrostatic spray painting process with high-speed rotary bell atomizers. Part 2: External charging, Part. Part. Syst. Charact. **23**, 408 (2006)
16. Ellwood K.R.J., Braslaw J.: A finite-element model for an electrostatic bell sprayer. J. Electrost. **45**, 1 (1998)
17. Fraser R.P., Dombrowski N., Routley J.H.: The atomization of a liquid sheet by an impinging air stream. Chem. Eng. Sci. **18**(6), 339–353 (1963)
18. Fraser R.P., Dombrowski N., Routley J.H.: The filming of liquids by spinning cups. Chem. Eng. Sci. **18**(6), 323–337 (1963)
19. Fraser R.P., Dombrowski N., Routley J.H.: The production of uniform liquid sheets from spinning cups. Chem. Eng. Sci. **18**(6), 315–321 (1963)
20. Heitbrink W.A., Verb R.H., Fischbach T.J., Wallace M.E.: A comparison of conventional and high volume-low pressure spray-painting guns. Am. Ind. Hyg. Assoc. J. **57**, 304–310 (1996)
21. Hinze J.O., Milborn H.: Atomization of liquids by means of a rotating cup. J. Appl. Mech. **17**, 145–158 (1950)
22. Joseph D.D., Belanger J., Beavers G.S.: Break-up of a liquid drop suddenly exposed to a high speed airstream. Int. J. Multiph. Flow. **25**, 1263 (1999)
23. Kazama S.: Steady-state flow under high centrifugal force: atomization in spray painting. JSAE Rev. **24**, 489 (2003)
24. Klobucar J.: Recent developments in automotive bake oven simulation and testing. In: Proceedings 2005 Painting Technology Workshop, Lexington, Kentucky (2005)

25. Kosusko M., Fisher R.J.: Verification of improved paint transfer efficiency through the use of high volume, low pressure (HVLP) spray guns. In: Proceedings 2002 Painting Technology Workshop, Lexington, Kentucky (2002)
26. Lane W.R.: Shatter of drops in stream of air. Ind. Eng. Chem. **43**, 1312 (1951)
27. Lefebvre A.H.: Atomization and sprays. Taylor and Francis, New York (1989)
28. Liu J., Paul J.D., Gollub J.P.: Measurements of the primary instabilities of film flows. J. Fluid. Mech. **250**, 69 (1993)
29. Misev T.A., van der Linde R.: Powder coatings technology: new developments at the turn of the century. Prog. Org. Coat. **34**, 160–168 (1998)
30. Morales J.C.: CFX-5 software developer. Personal Communication (2003)
31. Occupational Safety and Health Administration: *OSHA Regulations (Standards – 29 CFR), Ventilation: 1910.94 (c)(6)(i) and 1926.57 (h)(6)(i)*
32. Pearce F.: Global warming brings early spring. New. Sci. **2038**, 7 (1996)
33. Pilch M., Erdman C.A.: Use of break-up time data to predict the maximum size of stable fragment for acceleration induced breakup of a liquid drop. Int. J. Multiph. Flow. **13**, 741 (1987)
34. Post S.L., Abraham J.: Modeling the outcome of drop-drop collisions in Diesel sprays. Int. J. Multiph. Flow. **28**(6), 997–1019 (2002)
35. Rieber M., Frohn A.: Three-dimensional Navier-Stokes simulation of binary collisions between droplets of equal size. J. Aerosol Sci. **26**, S929–S930 (1995)
36. Rieber M., Frohn A.: A numerical study on the mechanism of splashing. Int. J. Heat Fluid Flow. **20**, 455–461 (1999)
37. Salazar A.J.: Computational Fluid Dynamics Study of Automobile Assembly Plant Painting Systems. PhD thesis, University of Kentucky, Lexington, Kentucky, U.S.A. (1998)
38. Salazar A.J., Saito K., Bhattacharya S.: Performance evaluation of automotive downdraft booth scrubbers through the use of computational fluid dynamics. In: Proceedings 22nd International Conference on Automobile Body Finishing (SURCAR), Cannes, France (2005)
39. Salazar A.J., Saito K.: Computational analysis of unsteady liquid flow in rotary bell sprayers. In: Proceedings 2005 Painting Technology Workshop, Lexington, Kentucky (2005)
40. Salazar A.J.: An analytical model for film flow characteristics in typical automotive rotary sprayer cups. IAES Internal Report, University of Kentucky, Lexington, Kentucky (2006)
41. Salazar A.J., Vytla S.K., Ando Y.: Modeling the effect of paint emissivity and multi-body reflections on automotive radiation paint curing. In: Proceedings 2010 Painting Technology Workshop, Lexington, Kentucky (2010)
42. Schmidt D.P., Rutland C.J.: A new droplet collision algorithm. J. Comp. Phys. **164**(1), 62–80 (2000)
43. Sharara F.I., Seifer D.B., Flaws J.A.: Environmental toxicants and female reproduction. Fertil. Steril. **70**, 613–622 (1998)
44. Srinivasan V., Salazar A.J., Saito K., Review: on the parameters for stable laminar flow over inclined plane. IAES Internal Report, University of Kentucky, Lexington, KY, U.S.A. (2003)
45. Srinivasan V., Salazar A.J., Saito K.: On the stability of flow over an inclined flat plate. IAES Internal Report, University of Kentucky, Lexington, KY, USA (2003)
46. Srinivasan V., Salazar A.J., Saito K.: Numerical investigation of the impingement of coating droplets onto flat surfaces. In: Proceedings 2005 Painting Technology Workshop, Lexington, Kentucky (2005)
47. Tachi K., Yamada K., Okuda C., Suzuki S.: Study on paint coating by electrostatic rotary atomizer (ii). effects of particle diameter and specific charge on transfer efficiency. Color. Mater. (Japanese). 265–271 (1986)
48. Tachi K., Yamada K., Okuda C., Suzuki S.: Study on paint coating by electrostatic rotary atomizer (iii). effects of rotating cup shape and spray conditions on specific charge. Color Mater. (Japanese). 197–204 (1987)
49. Thomas G.O.: The aerodynamic breakup of ligaments. At. Spray. **13**, 117 (2003)
50. Viti V., Salazar A.J., Saito K.: Investigation of the effect of the electrostatic field on the transfer efficiency of automotive spray guns: a CFD approach. In: Proceedings 2004 Painting Technology Workshop, Lexington, Kentucky (2004)

51. Viti V., Salazar A.J., Saito K.: A numerical study of the coupling between the flow field and the electrostatic field inside an automotive spray paint booth. In: Proceedings 2005 World Science and Engineering Academy and Society, Udine, Italy, WSEAS Paper 491–223 (2005)
52. Viti V., Salazar A.J., Saito K.: Numerical study of the evaporation and break-up of charged droplets in an automotive paint booth. In: Proceedings 2005 Painting Technology Workshop, Lexington, Kentucky (2005)
53. Viti V., Salazar A.J., Saito K.: CFD study of the airflow and VOCs concentration in automotive paint booths. In: Proceedings 2006 Painting Technology Workshop, Lexington, Kentucky (2006)
54. Viti V., Kulkami J., Watve A.: Computational fluid dynamics analysis of the electrostatic spray painting process with a rotating bell cup. At. Sprays. **20**, 1 (2010)
55. Vytla S.K., Ando Y., Salazar A.J.: Computational prediction of body surface temperature during automotive radiation-forced convection paint curing process. In: Proceedings 2011 Painting Technology Workshop, Lexington, Kentucky (2011)
56. Weiss D.A., Yarin A.L.: Single drop impact onto liquid films: neck distortion, jetting, tiny bubble entrainment, and crown formation. J. Fluid. Mech. **385**, 229–254 (1999)
57. Xiao G., Pan C., Cai Y., Lin H., Fu Z.: Effect of benzene, toluene, xylene on the semen quality of exposed workers. Chin. Med. J. **112**, 709–712 (1999)
58. Yu G., Pakkala J.: Analysis of automobile body heating process within a paint bake oven using Computational Fluid Dynamics. In: Proceedings 2008 Painting Technology Workshop, Lexington, Kentucky (2008)

Chapter 4
The Use of Scale Model to Study Film Flow in a Rotary Atomizer Cup

Vedanth Srinivasan, Abraham J. Salazar and Kozo Saito

Abstract The aim of this chapter is to simulate processes of liquid droplet formation and atomization in a typical automotive paint spray system with scale modeling technique. In a spray painting process, paint is sprayed by a bell sprayer cup rotating at high speed to create fine atomized paint particles. The bell sprayers typically rotate at a speed of 30,000 rpm and have liquid (paint) flowing from the center with a flow rate of 300 cc/min. Due to the centrifugal action of the rotation, the liquid flows to the exterior of the bell, where they pass through grooves leading to the formation of ligaments and henceforth droplets due to shear forces acting against the surface tension forces. We designed different types of scale models to simulate the process.

Keywords Scale model · Bell sprayer · Pi-numbers · Tread surface · Instability analysis

Abbreviation List

Nomenclature

F Force
G Gravitational acceleration
H Height of tread
h Film layer thickness
L Characteristic length

K. Saito (✉)
Institute of Research for Technology Development, College of Engineering,
University of Kentucky, Room: RGAN 179, Lexington, KY 40506-0503, USA
e-mail: saito@engr.uky.edu

A. J. Salazar
Institute of Research for Technology Development, College of Engineering,
University of Kentucky, Lexington, KY 40506-0503, USA
e-mail: ajsala00@uky.edu

V. Srinivasan
ANSYS FLUENT
15915 Katy Freeway, Suite 550 Houston, Texas 77094
e-mail:Vedanth.Srinivasan@ansys.com

K. Toda et al. (eds.), *Automotive Painting Technology,*
DOI 10.1007/978-94-007-5095-1_4,

m Mass
Q Flow rate
r Radius of spray cup
t Time
α Inclination angle
Δ Change
μ Dynamic viscosity
ν Kinematic viscosity
π Pi number
ω Angular velocity
ρ Density
σ Surface Tension

Subscripts

c Centrifugal force
g Gravitational force
I Inertial force
M Model
P Prototype

Superscript

′ Model

4.1 Introduction

Scale modeling permits the study of systems that are not tractable in their original scale and form. It shortens experimentation by reducing the number of variables to only a few primary ones and promotes deeper understanding of the original system [1–4]. Scale modeling technique's two most important roles are: (1) To solve problems by developing scaling laws, designing scale models and conducting scale model experiments. (2) To understand the mechanism of nature by carefully analyzing scale model experimental data. Specifically, scale modeling technique provides the following four specific benefits:

- Imagine the full scale phenomena
- Understand mechanisms which control the full scale
- Validate the numerical model predictions
- Develop new products or improve the performance of existing products.

Figure 4.1 depicts flow-chart of scale modeling technique vs. numerical modeling.

Here we apply scale modeling technique to reveal control mechanisms of a prototype bell-sprayer cup using scale modeling technique. The transfer efficiency of the current painting process with the present design is only about a 50 % meaning that only 50 % of the total paint sprayed can reach the target for coating surface and the rest of paint is an unusable waste for coating. It is essential to understand

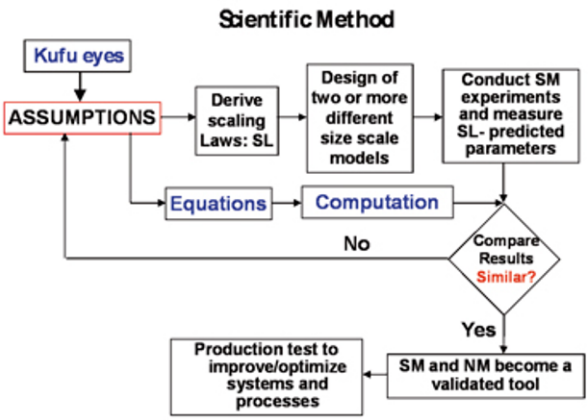

Fig. 4.1 Flow chart of scale modeling technique vs. numerical modeling [1]

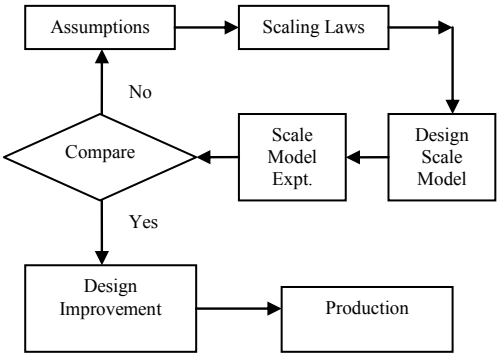

Fig. 4.2 Flow chart representation of scaling process

the mechanism of the current paint transfer process and paint spray atomization for an effective improvement of the current spray paint technology (Toda, see Sect. 1 in this book). Toda mentioned in his chapter that our current understanding of the control mechanism in spray painting technology is far from complete and there is a strong need for basic scientific study on paint atomization and transfer. Scale modeling can be a good engineering approach to identify major parameters that control atomization and transfer processes, and whose result also can help validate numerical model predictions and select input parameters for calculations. Thus the combination of scale modeling and numerical modeling can help effectively achieve a cost-efficient design of paint spray equipment and device (Fig. 4.2).

4.2 Scaling Laws

The centrifugal forces due to the rotation of a bell sprayer are the primary driving forces for the liquid to land in the periphery of the atomizer. Shearing force of the rotation acts on the surface tension forces of the liquid influences atomization process, whose concept is schematically depicted in Fig. 4.3.

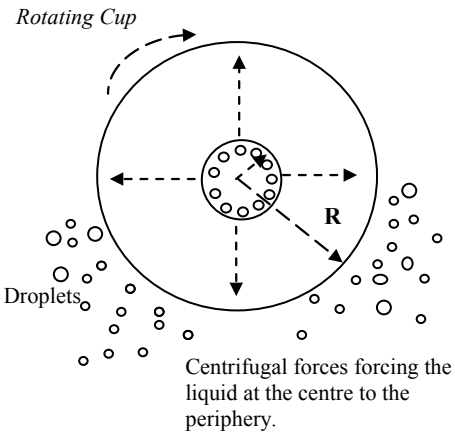

Fig. 4.3 Top view of a bell sprayer with forces

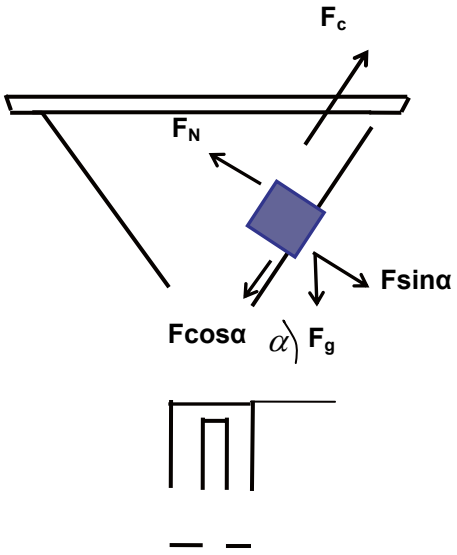

Fig. 4.4 Prototype force diagram

The centrifugal forces acting on the system can be written as (Fig. 4.4),

$$F_c = \frac{mu^2}{r} = m\omega^2 r,$$

Where ω is the angular velocity (in rotations per minute), r is the radius of the rotating bell sprayer and m is the mass of the liquid. This force is considered as the inertia force of the liquid [5] and is rewritten in the characteristic form,

$$F_i = \rho(l^2 h)u^2,$$

where ρ is the fluid density, l is the characteristic length (and can be the length associated with cup surface), h is the film layer thickness, and u is the radial velocity. Gravitational forces may be involved since the cup surface is inclined, but it would be smaller compared to the centrifugal force acting in the opposite direction.

The surface tension force affects propagation of the paint film in the radial direction until it reaches the edge of the cup, where atomization takes place, influencing the size of sprayed paint droplets. The corresponding surface tension forces can be written as,

$$F_\sigma = \sigma l.$$

The viscous force will act on the thin liquid film when it moves on the cup surface. The viscous force can be written as:

$$F_v = \mu l u,$$

where μ is the liquid's kinetic viscosity, l is a characteristic length taken to be the inclined plate length, and u is the fluid velocity as it flows on the inclined surface. As a result, the flowing two independent pi-numbers will be formed.

$$\pi_1 = \frac{F_i}{F_\sigma} = \frac{\rho l^2 h u^2}{\sigma l} = \frac{\rho l h u^2}{\sigma}$$

and

$$\pi_2 = \frac{F_i}{F_v} = \frac{\rho l^2 u^2}{\mu l u} = \frac{\rho l u}{\mu}.$$

The scaling requirement is:

$$\pi_i = \pi_i'$$

Where i = 1, 2,… and prime (′) indicated model from $\pi_1 = \pi_1'$ and $\pi_2 = \pi_2'$.

All models represent the case of an inclined plate [6–8], of certain surface configurations, water was chosen as the working liquid since it has the same kinetic viscosity as the paint sprayed by the cup. Water flows naturally from the top side till the end of the plate, Fig. 4.5, water flows through orifices coming from a stabilizer plenum tank to maintain a constant flow rate as seen in Fig. 4.6. The plate has walls from both sides to maintain the desired channel flow regime which is assumed to simulate the layer formation of liquid in the cup; these walls are transparent such that side observations of the flow are possible. The flat plate is inclined at an angle α, the more inclination the more inertial effect on the flow. Two surface configuration are studied, a flat and treaded surfaces.

Three sets of experiments were conducted to verify the scaling laws for the flat plate models, and to make key observations for the nature of flow observed to help us in predicting the behavior of the liquid layer formation in the cup, the results, as discussed further on, for the three sets of experiments: the first set of experiment

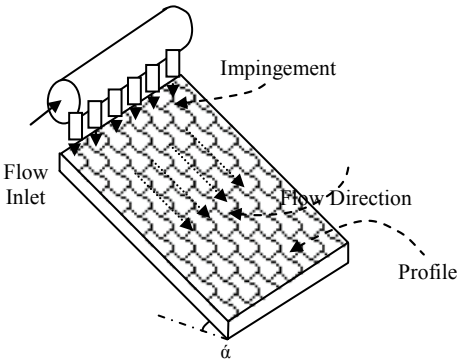

Fig. 4.5 Flow over an inclined surface

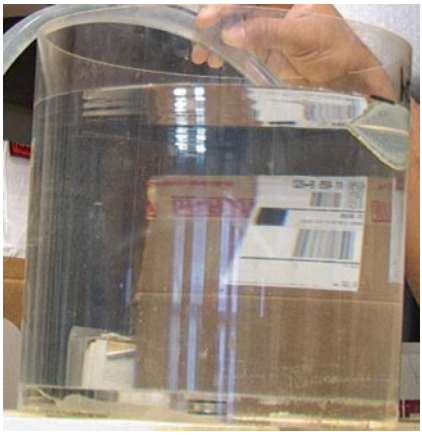

Fig. 4.6 Stabilizer tank maintains a constant flow rate

was a flat plate of aluminum, in flat we mean not having any predefined shapes on the surface and assumed to be smooth hence no considerations are made for the surface roughness in this case. The second set had a surface with a tread configuration of certain size and depth, this experiment is split into two parts since both sides of the plate was made for the same configuration hence a bump and a groove cases were studied. For these two cases the main interest was to validate the scaling laws for the models and to make quantitative results of the flow nature by measuring the frequency and amplitude of the instability waves in the flow. Which was possible my taking video and still images of the side view of the flow. The last set consisted of studying the flow behavior over the lateral sides of the plate to give and idea of how the liquid flow behaves in the transverse directing of the main stream. In order to be able to make these observations, a transparent flat plate was used under certain lighting conditions which enabled us to observe the flow from the bottom side of the plate, hence be able to see the flow in all directions other than the height of the layer formed.

Table 4.1 Analytical and experimental results

Scaling ratio	0.5
Q (l/s)	
Analytical	0.02893
Experimental	0.03342
Error (%)	13.3

4.3 Results

4.3.1 Experimental Verification of Scaling Laws

The method for verifying the scaling laws was made by changing the flow rate while maintaining the same fluid layer thickness, since the flow rate is related to the flow velocity through the flow cross sectional area, which is the width of the plate times the fluid layer.

The scaling law is modified to account for the flow rate measurements.

$$\pi_1 = \pi_1' \Rightarrow \frac{l}{l'} = \left(\frac{u}{u'}\right)^2 = \left(\frac{Q/A}{Q'/A'}\right)^2 = \left(\frac{Q/wh}{Q'/w'h'}\right)^2$$

therefore, the final relation is:

$$\frac{l}{l'} = \left(\frac{Q}{Q'}\right)^{2/3}$$

This final relation is obtained by maintaining the same fluid layer in both prototype and the scale model as the flow rate is changed. The width '*w*' is considered as the characteristic length. *Scaling ratio=0.500*. Dimensions of the model and prototype are as found in Table 4.1. The analytical scaling laws for this scaling factor will conclude the following flow rate.

$$\frac{l}{l'} = \left(\frac{Q}{Q'}\right)^{2/3} \Rightarrow Q' = \frac{Q}{(l/l')^{3/2}} = \frac{Q}{\sqrt{2^3}} = \frac{Q}{2\sqrt{2}}$$

Flow rate for the prototype was measured after the fluid layer flowing on the surface was observed visually to be 2 mm (Fig. 4.7). Then, the flow rate was measured by calculating the fluid volume difference over a measured period of time:

$$Q = \frac{\Delta V}{\Delta t} = \frac{1 \text{ liter}}{12.22 \text{ s}} = 81.83 \times 10^{-3} \frac{\text{liter}}{\text{s}}$$

Hence for a scaling ratio of ½ the model flow rate should be:

$$Q' = \frac{Q}{(l/l')^{3/2}} = \frac{81.83 \times 10^{-3}}{\sqrt{2^3}} \frac{\text{liter}}{\text{s}} = 28.93 \times 10^{-3} \frac{\text{liter}}{\text{s}}$$

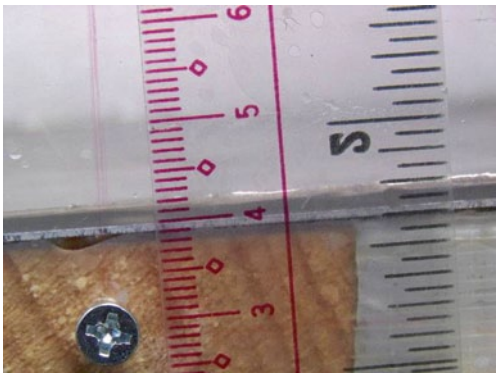

Fig. 4.7 The water layer thickness was approximately 2 mm for both prototype and scaled model

As for the scaled model, the area is reduced by half but instead of cutting the plate to the desired dimensions, we fixed boundaries to the original size such that water will flow only on half of the plate. The flow rate was adjusted until the liquid layer thickness of 2 mm was achieved. Similar measurements were done like the prototype. The resulting flow rate was:

$$Q' = \frac{\Delta V'}{\Delta t'} = \frac{1 \text{ liter}}{29.92 \text{ s}} = 33.42 \times 10^{-3} \frac{\text{liter}}{\text{s}}$$

The result is a close value compared to the one obtained by the scaling similarity.

This error could be due to the following factors:

- Layer thickness measurement. The film shows instability patterns, thus, the layer thickness varies.
- Errors in measurement the actual liquid flow rate.
- Boundary layer interaction due to sidewalls.
- Local instabilities in the flow.
- Variation in the inlet liquid flow rate.

4.3.2 Stability Analysis for Flat and Treaded Plates

Flat surface (prototype) characteristics: 60.96 cm length by 20.32 cm width (24 by 8 in.), Angle of Inclination: 45°:

The liquid flow along the length of a flat plate was observed and investigated for flow instabilities and viscous effects. The observations hint at formation of a variable height liquid layer during the flow. For all the experiments the flow rate was maintained constant by having a fixed level of water in a reservoir and leveling through an orifice opening at its bottom. The instability present spreads over the surface and hence the flow is not uniform. This is the primary cause for creating non-uniform droplets from a bell sprayer. We present the plot of film thickness with time reference (Fig. 4.8). The experiment suggested the existence of surface instabilities and is represented by the crest and trough of the wave persistent in the

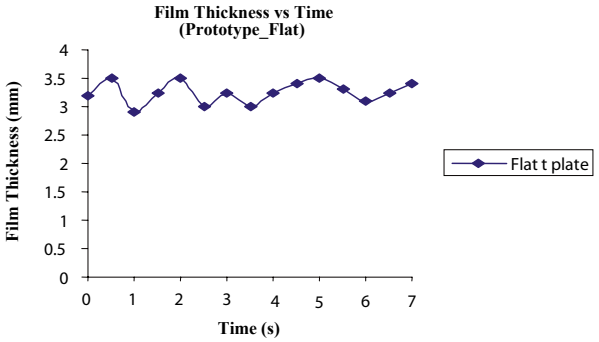

Fig. 4.8 Flow wave nature on a flat plate

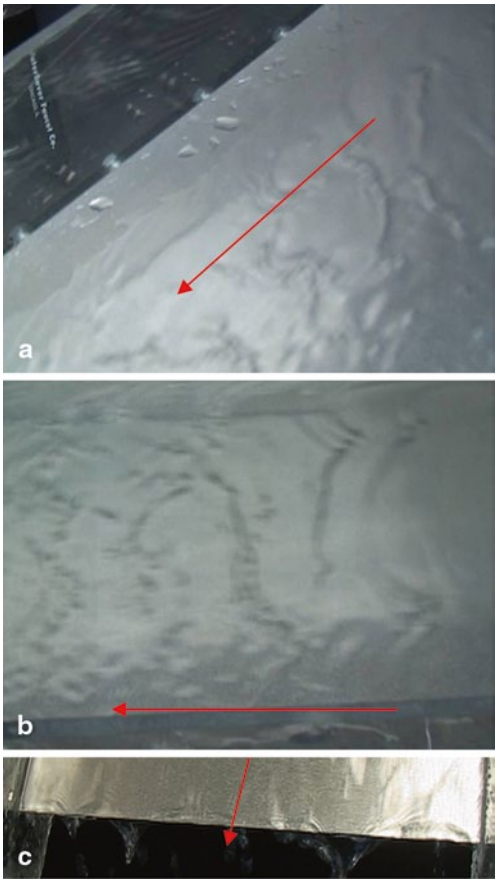

Fig. 4.9 Wave instabilities on the flow over a smooth surface. **a** Lateral view. **b** Top view. **c** Flow at the plate edge

flow (Fig. 4.9). The profile of the surface instability resembles as sine/cosine family of waves and hence we can associate them with a wave number and frequency. The numerics are discussed below. Data taken at different time intervals to obtain film thickness at that instant (Table 4.2):

Table 4.2 Wave amplitude for flat surfaces

Time (s)	Height (mm)	Time (s)	Height (mm)
0.0	3.20	4.0	3.25
0.5	3.50	4.5	3.40
1.0	2.90	5.0	3.50
1.5	3.25	5.5	3.30
2.0	3.50	6.0	3.10
2.5	3.00	6.5	3.25
3.0	3.25	7.0	3.40
3.5	3.00		

Fig. 4.10 Wave flow nature for tread surface

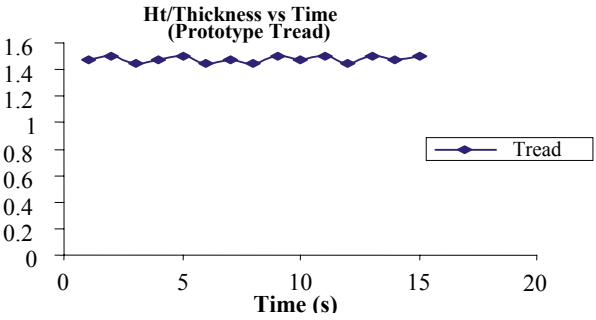

Table 4.3 Wave heights of a treaded surface (prototype)

Time (s)	H/Thickness	Time (s)	H/Thickness
1.00	1.475	9.00	1.500
2.00	1.500	10.0	1.475
3.00	1.450	11.0	1.500
4.00	1.475	12.0	1.450
5.00	1.500	13.0	1.500
6.00	1.450	14.0	1.475
7.00	1.475	15.0	1.500
8.00	1.450		

Treaded surface (Prototype) characteristics: 30.48 cm length by 20.32 cm width (12 by 8 in.), Angle of Inclination: 45°.

The experiment was conducted in the similar way as described in the general method above for the treaded surface of given dimensions. This plate was used as the prototype. After the readings of the film thickness were taken at regular intervals, the non-dimensional quantity of the ratio of the film thickness to the height of the bump was calculated. This was then plotted against the time intervals. From the plot we observe a stable top layer of the film flow over the plate. This is reasonable because the effect of the eddies is taken care of by the bumps on the surface which have a leveling effect on the film top layer, when compared to a flat plate. The plot for the treaded prototype plate is shown below (Fig. 4.10). The thickness of the tread on the plate is about 2 mm approximately. The height represents the height of the water film on the plate (Table 4.3).

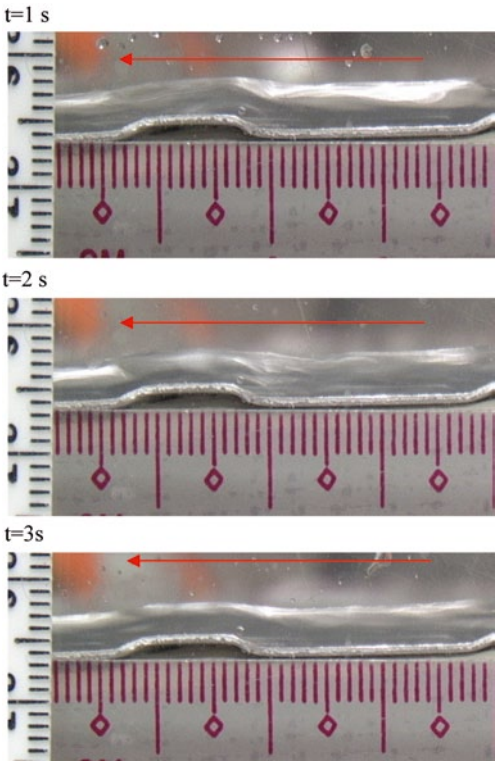

Fig. 4.11 Flow over tread surface

For the experiment concerning a tread surface model, the dimensions were 22.9 by 15.2 cm (9 by 6), with a plate thickness ~0.5 mm. More on experimentation is discussed.

4.3.3 Flow Over the Tread Surface Model

Experiments were performed on a tread surface inclined at an angle of 45°. The flow was visualized at different time intervals and a history of the flow behavior was created (Fig. 4.11). The data that was obtained from the visualization technique has been shown in the following table (Table 4.4).

$H = 1.5$ mm is the height of the top surface from the cavity bottom.

Plotting the above data, gives us the plot of height of the film against the time scale (Fig. 4.12). Note that the height has been normalized with the bump thickness.

It can be clearly seen that the fluctuations in the film thickness is about 0.3 mm which is clearly less than the fluctuations obtained during the case of flow over the flat plate. It was also observed that, in over all sense the flow on the top layer had its smoothness preserved. A few experimental observations for time $t = 0$–4 s have been shown below:

Table 4.4 Wave heights of a treaded surface (model)

Time (s)	h (mm)	h/H
0.0	3.00	2.000000
0.5	3.20	2.133333
1.0	3.10	2.066667
1.5	3.00	2.000000
2.0	3.10	2.066667
2.5	3.15	2.100000
3.0	3.50	2.333333
3.5	3.20	2.133333
4.0	2.90	1.933333
4.5	3.10	2.066667
5.0	3.00	2.000000
5.5	3.20	2.133333
6.0	3.10	2.066667

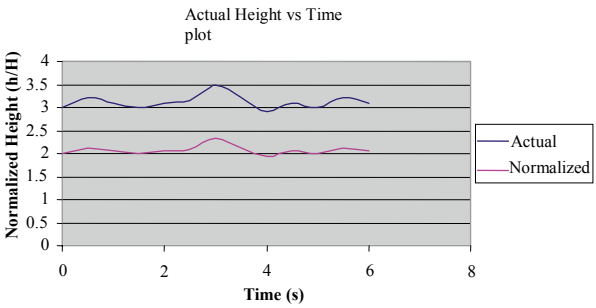

Fig. 4.12 Plot of normalized height vs. time

Considering the fact that the surface of the film had little instabilities, we pursued to conduct a few experiments for lower flow rate of the liquid (water).

It can be clearly seen that as the flow rate is reduced the local turbulence that was previously seen in other configuration seem to have smoothened.

4.3.4 Discussions on Flow over Tread Surface

Clearly notice the little instabilities present in the flow. The flow over the tread is similar to flow in an expanding cross sectional channel and hence creation of local eddies and small vortices in the region close to the bump. A schematic of the film flow over a tread surface is as shown (Fig. 4.13).

The local flow separation due to sudden increase in the channel height causes disruption in the flow. However, by combining the flow with proper height of the bump, these effects could be minimized (Figs. 4.14–4.16).

Region R represents local instabilities present in the flow over the tread surface. These can be attributed to the interaction between the gravitational forces to the inertial forces at higher angle of inclination (Fig. 4.17).

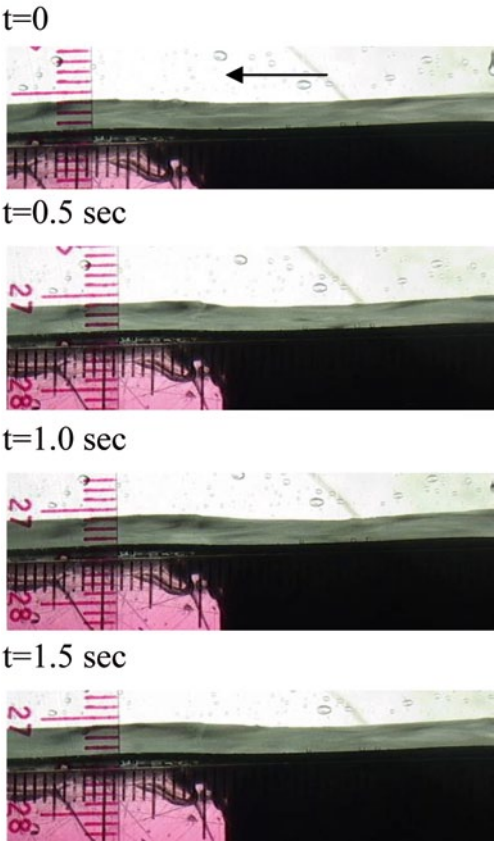

Fig. 4.13 Flow over tread surface

4.3.5 Flow over Inverted Tread Surfaces

The given tread surface was inverted and hence the liquid was made to flow over cavities unlike over bumps in the previous case.

Flow of a fluid over cavities is depicted as below. The cavities in the path of the flow create vortices and dissipate energy within their region. These vortices help in stabilizing the flow on the surface.

Experiments concerning flow over the inverted tread surfaces were carried out and data is shown below (Table 4.5):

Plots were made for normalized height against time intervals. Following observations were made at different time intervals. In addition, a closer view of the flow over the cavities at different time intervals reveal the following (Please see Fig. 4.22).

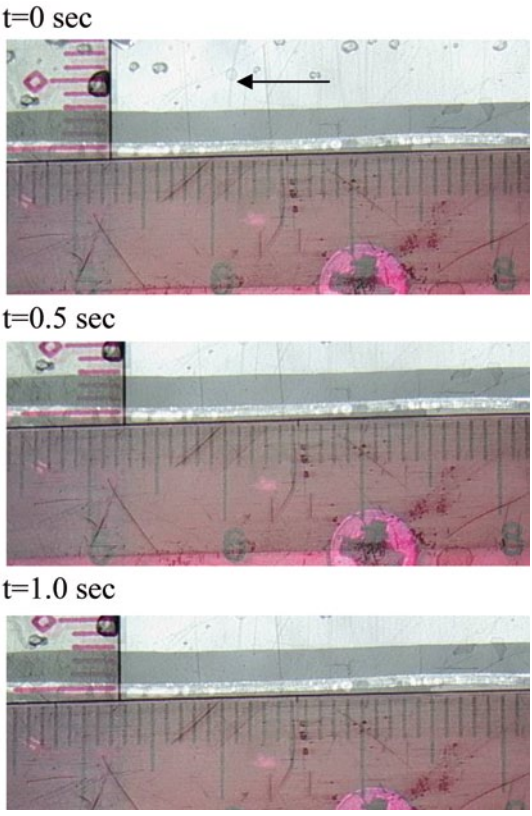

Fig. 4.14 Flow over tread surface at low flow rate, complete laminar flow and observe no disruptions

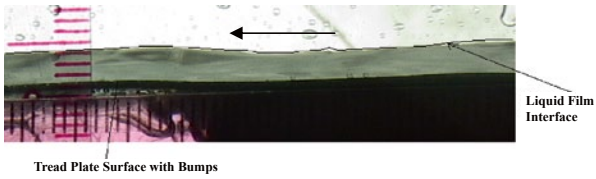

Fig. 4.15 Obtaining profile of the wavy surface

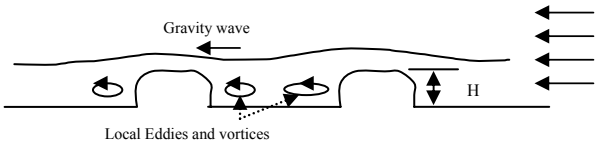

Fig. 4.16 Schematic of flow over bumps

4.3.6 Visualizing the Flow over the Inverted Surfaces

It was observed that the flow over the current configuration was smoother than flow over the bumpy tread surfaces. Selected pictures are shown for observation of the readers.

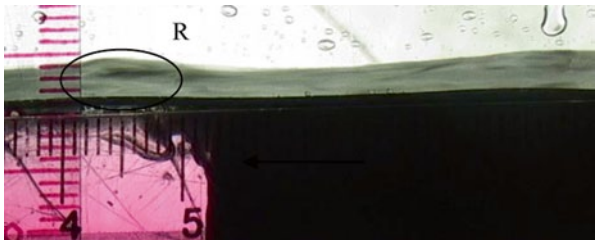

Fig. 4.17 Instabilities present in the flow

Table 4.5 Wave heights of an inverted tread surface

Time (s)	*h* (mm)	*h/H*
0.0	2.500	1.666667
0.5	2.600	1.733333
1.0	2.550	1.700000
1.5	2.650	1.766667
2.0	2.600	1.733333
2.5	2.500	1.666667
3.0	2.550	1.700000
3.5	2.500	1.666667
4.0	2.525	1.683333
4.5	2.550	1.700000
5.0	2.550	1.700000

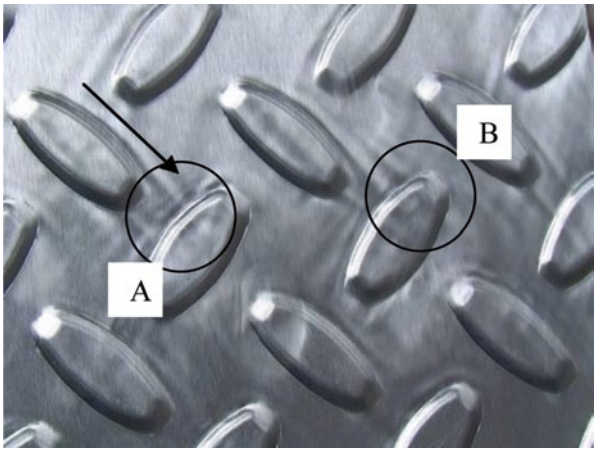

Fig. 4.18 *A* and *B* indicate presence of secondary flow in the transverse direction

Also notice from the top view taken of the flow, the secondary flow pattern that was observed previously in case of the flow over the bumps (Figs. 4.18–4.21, 4.23). The presence of small vortices of low strength is shown in our previous closer observations.

Comparison Between Flat and Treaded Plates The flow profiles over a flat plate and over a treaded surface have been obtained. From the profiles we can clearly

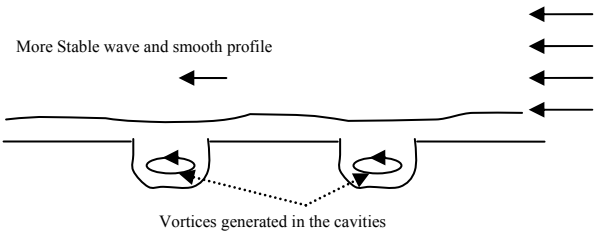

Fig. 4.19 Schematic of flow over puddles

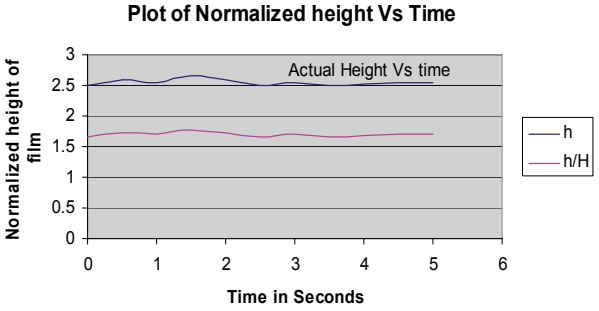

Fig. 4.20 Normalized height as a function of time

observe that the flow over a treaded surface is better than the flow over the flat surface. This, as discussed above is due to the leveling effect the bumps have on the fluid flow over the treaded surface. But the flow over the treaded surface too has some instability present which do not make it the perfect choice for the profile of a bell-sprayer. Thus, the flow over the flip side of the treaded surface is considered. We observe that the flow over the flip side has less instability when compared to the flow over the bump side.

Observations for a Transparent Plate The third experiment with a transparent plate was made to get qualitative measurements of the flow of all direction except for the height of the layer formed on the inclined surface. Figure 4.24 shows a model made of plexi-glass, dimension of the plate are of 30.5 cm length by 20.3 cm length (12 by 8 inch) and inclination of 28°. The water flows along its length through the pipe holes on the top edge of the plate.

In order to be able to visualize the flow, lighting should be fixed in a suitable manner to show the flow details. Having the light in the way shown in Fig. 4.25 will make the light rays pass through the transparent plate where the flow is taking place. If the flow is flowing smoothly in the main flow along the inclination, light will be transmitted without making any shadows. The shadows appears as flow is changing direction as seen in Fig. 4.26 and denoted as secondary flow.

Discussions on Flow over Transparent Plate Figure 4.26 shows two flow patterns: main flow in the direction of flow from top to bottom along the inclined surface, and a secondary flow in the lateral direction. As was explained in the pervious experiments made on both flat and tread surfaces, the water flow in a wavy motion along

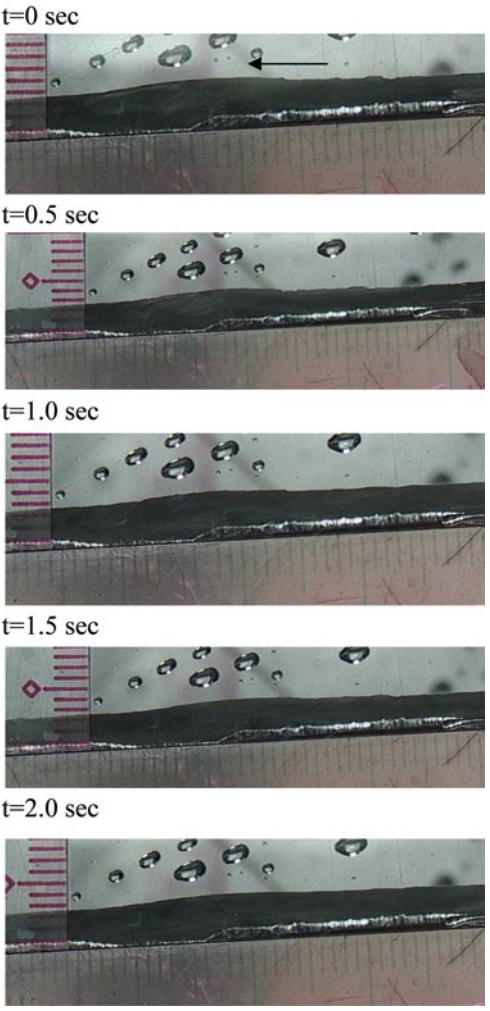

Fig. 4.21 Flow over the cavities at different time intervals

the surface causing the instability of flow, which is seen in the attached video file (transparent_plate_video) (Fig. 4.27). The secondary flow happens as a result of the inlet flow pattern; the water leaving the orifice openings on the tube tend to form another profile as they leave the orifice and hit the surface, as these profiles merge together to form the main flow they interfere causing the secondary flow in the lateral direction which is observed in the upstream flow as the flow is being developed. As flow gets more developed, the secondary flow is minimal. However, the flow is observed to have a wavy motion along the lateral direction which coincides with the side view observations conducted for the other type of surfaces. This wavy pattern makes the flow highly irregular, turbulent flow. Since the surface is smooth and water layers tend to ride each other like ocean waves due to the inertia force.

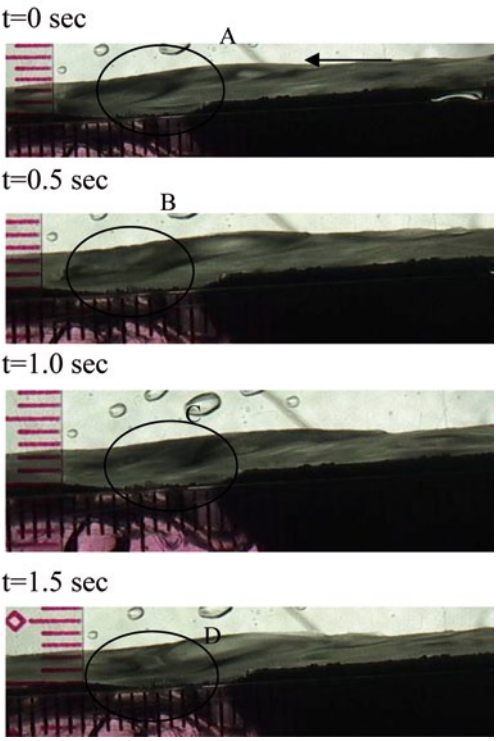

Fig. 4.22 Regions *A, B, C* and *D* show the moving local instabilities produced due to sudden increase in the channel height in the flow

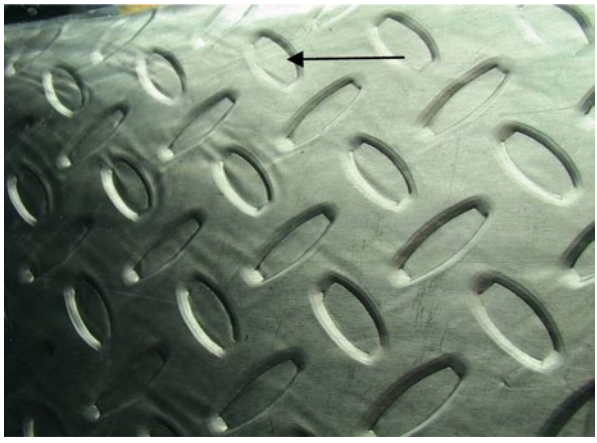

Fig. 4.23 Top view of flow over the inverted model

4.4 Conclusions

Numerous experiments were conducted on the flat plate and over bumped surfaces and the flow behavior was analyzed in depth. It was observed that flow over flat plate is inherently unstable due to interaction between the surface tension forces and

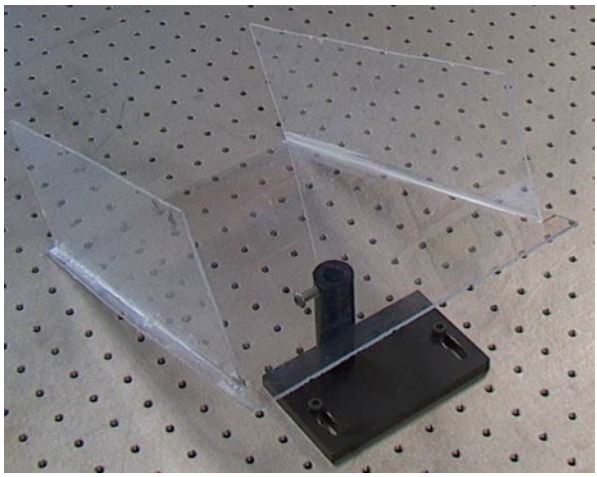

Fig. 4.24 Transparent plate

Fig. 4.25 Lighting fixture for a bottom view of a transparent plate

gravity counterparts. The presence of bumps produced smooth surface in the flowing liquid. But it was discussed that, presence of an obstacle in the flow path creates local eddies and vortices which could potentially interact with the flow obstructing the smooth profile of the flow. However, an inverted bump or presence of a cavity in the flow seems to reduce the instability present in the flow. The dimensions of the cavities however can be decided based on the flow requirement. The cavity depths could increase based on the type of flow, laminar or turbulent or a transition from one to another. The presence of cavities would not increase the film depth rather, maintain a constant thickness. The flow over the cavities create eddies, but unlike

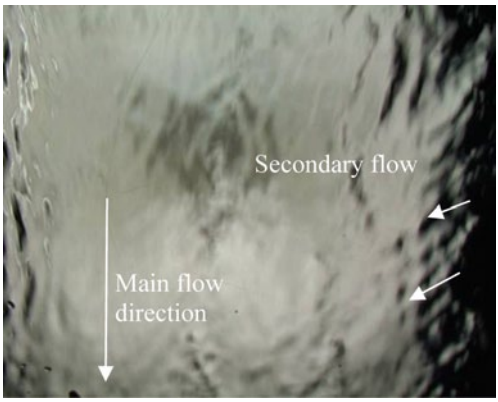

Fig. 4.26 Flow visualization as seen from the bottom of the transparent plate

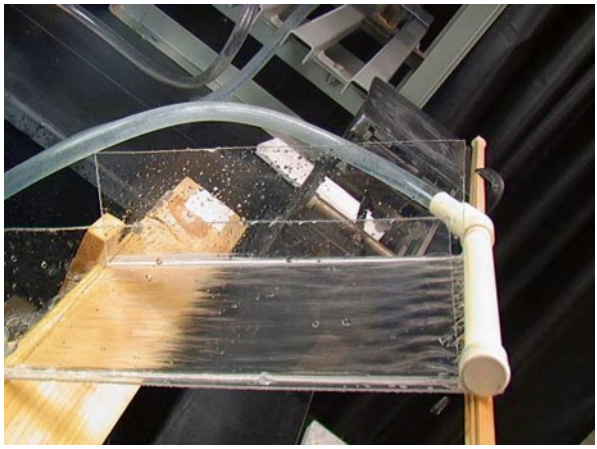

Fig. 4.27 Perspective side view of the liquid flow over a transparent plate

the bump nature, these cavities do not hinder the main flow by the eddy generation inside them. It would hence be appropriate to model the flow based on flow over cavities placed in a pattern, so that the flow smoothening takes place and the vortices do not hinder with the main course of the flow.

References

1. Emori R.I., Saito K., Sekimoto K.: Scale models in engineering (Mokei Jikken no Riron to Ohyou), 3rd ed. Gihodo, Tokyo (2000). ISBN:4-7655-3252-6 C3053 (second print in 2008 in Japanese)
2. Saito K. (ed.), Progress in scale modeling: Summary of the First International Symposium on Scale Modeling (ISSM in 1988) and Selected Papers from subsequent Symposia (ISSM II in 1997 through ISSM V in 2006), Springer, Berlin (2008)
3. Tanigawa Y., Alloo R., Tanaka N., Yamazaki M., Ohmori T., Yano H., Salazar A.J., Saito K.: Development of a new paint over-spray eliminator. Prog. Scale Model. 3, 325–342 (2008)

4. Kuwana K., Hassan M.I., Singh P.K., Saito K., Nakagawa J.: Scale-model experiment and numerical simulation of steel teeming processes. SME J. Mater. Manuf. Process. **23**, 1–6 (2008)
5. Batchelor G.K.: An introduction to fluid dynamics. Cambridge, London (1967)
6. Kondic L., Diez J.: Flow of thin films on patterned surfaces: controlling the instability. Phys. Rev. **E 65**, 045301~R (2002)
7. Abd-El-Malek M.B., Tewfick A.H.: Internal gravity waves with free upper surface over an obstacle. Nonlinear Math. Phys. **2**(N 2), 158–171 (1995)
8. Thiele U., Knobloch E. Front and back instability of a liquid film on a slightly inclined plate. Phys. Fluid. **15**(4), 892–907 (2003)

Part III
Painting Technology—Visualization and Characterization

Chapter 5
Automotive Paint Spray Characterization and Visualization

Nelson K. Akafuah

Abstract Understanding the automotive paint atomization and how the atomized paint droplets are transferred from the atomizer to the target surface is a necessary step in the continuous improvement of the paint application process. Ensuring increased transfer efficiency and improvement in coated surface quality require continuous improvement in the application process and reformulation of the paint, especially for metallic paints to satisfy consumer demands. The solutions for these problems require multiple approaches—such as new paint formulation, operation optimization, new paint applicator designs, and improved understanding of the paint droplet transfer process. The ability to visualize the internal structures of the paint spray transfer process is vital to understanding the role that the atomization mechanisms have on the evolution of the paint droplets as they travel from the paint applicator to the target surface. This chapter, therefore, seeks to address some of these issues by focusing on the visualization and characterization of the paint spray transfer process.

This chapter discusses existing and new technologies for paint spray visualization and characterization, with particular emphasis on a new technique that uses infrared thermography based approach. This technique allows the visualization of the internal structures and the macroscopic features of the paint spray transfer process. In addition, the paint droplet volume fraction and the paint droplet number density inside the spray are computed by the new technique. This provides quantitative information about the droplet distribution inside the continuous gas phase.

Keywords Atomization · Cavitation · Infrared thermography · Volume fraction · Number density

N. K. Akafuah (✉)
Institute of Research for Technology Development, College of Engineering,
University of Kentucky, KY 40506-0503, Lexington, USA
e-mail: nkakaf0@engr.uky.edu

K. Toda et al. (eds.), *Automotive Painting Technology,*
DOI 10.1007/978-94-007-5095-1_5,

5.1 Introduction to Automotive Painting

Painting a car is one of the most expensive operations in automotive manufacturing. It is more involved than most people think. The painting operation typically comprises 30–50 % of an automotive assembly plant's cost. This high cost is as a result of two factors—the desire to have high quality coatings and the necessity of meeting strict environmental requirements. The coated surface must be finished in a manner that provides an outstanding coating surface quality. Reduction in volatile organic compound (VOC) emission is also required to meet strict environmental protection laws. The application of automotive paint is a field of concern because of the amount of air pollution it creates. A large amount of expense is incurred in mitigating the pollution effects. Improvements and indeed, dramatic changes in automotive painting operations will continue to be propelled by the increasing global awareness about protecting the environment.

Automotive paint has two purposes—to make the car look good and to protect the underlying metal or synthetic body panels from the harsh environment to which they are exposed. A typical automotive painting process will include the following steps: galvanizing, pretreatment, E-coat, anti-chip coatings, primer-surfacers, base coats, and clear coats.

Galvanizing This process refers to the coating of galvanized steel parts with thin layers of zinc. Zinc is chemically more active than steel, thus the corrosive element tend to feed upon the zinc preventing rusting of the underlying steel parts.

Pretreatment This procedure involves sequences such as degreasing, rinsing, air or temperature drying, phosphate treatment, and again rinsing and drying. Pretreatment is used to help the primer bond to the metal.

E-Coat This step requires the electro-coating of primer, which involves dipping the metal parts in a tank and passing an electric current through the body part and the liquid paint solution. The electro-coating enables the primer to get into places a spray gun wouldn't reach; it also helps the primer to bond with the metal substrates and to produce a uniform coating thickness.

Anti-Chip Coating This is sometimes applied to lower body panel areas and the under parts of the automobile body.

Primer-Surfacer This is a second stage of primer applied on top of the E-coat primer. It helps make the paint resistant to stone chips and promotes adhesion of the top coat to the E-coat, thus preventing delamination.

Base Coats The base coat is the color coat. Some colors must be applied in a greater film thicker than others for good coverage. Solvent-borne coats are applied to a slightly greater film thickness than waterborne coats.

Clear Coats The clear coat is mainly a protective coating—protecting the base coat from UV damage.

The anti-chip coating, primer-surfacer, base coat, and clear coat are normally applied by spraying. Spray painting requires the use of atomizers. The quality of the atomization influences the quality of the coating. In addition to the atomization of the paint during the paint application process, other factors such as the chemistry and material composition of the paint influence the quality of the coating. The appearance (color, gloss, and texture) of a coated surface greatly affects a customer's perception of product quality [1]. The paint job is the first thing a shopper notices on a car, and the paint color quality can make or break a sale. Appearance is very important in judging the quality of a car, and color is one of the most important considerations in determining appearance. The latter makes constant improvements in quality and color crucial. As automotive makers strive to make better looking, longer lasting finishes, the cost associated with painting continues to increase. Moreover, customer expectations for the attributes given by the appearance of coatings increase continually as manufacturers compete to provide those surfaces that offer enhanced surface characteristics. Coating composition, together with application procedures, paint film formation processes, and coated surface characteristics determine the appearance of a coating film [2].

Automotive coatings are generally applied in the form of liquid or powder, using spray atomizers. Paint sprays are droplet/particle systems which consist of a large number of paint droplets/particle dispersed in a gaseous medium, often air or a mixture of air and the vapor of the volatile components of the paint. The liquid paint droplet/particle distribution in the gas phase during transfer from the atomizer to the target surface influences film-build consistency. This needs to be maintained to minimize paint applicator-related coating defects. The distribution of the liquid and gas phases in the time-spaced domain is described by the liquid volume fraction (f_v) [3]—defined as the ratio of equivalent volume of the liquid to a given volume of the gas and liquid mixture [4]. The droplet number density is defined as the number of liquid droplets per unit volume.

Understanding the atomization process and how the paint droplets are transferred from the atomizer to the target surface helps in the improvement of the paint application process with the prevention and reduction in paint application-related defect. Ensuring increased transfer efficiency and improvement in coated surface quality require continuous improvement in the application process and reformulation of the paint, especially for metallic paints to satisfy consumer demands. The solutions for these problems require multiple approaches—such as new paint formulation, operation optimization, new paint applicator designs, and improved understanding of the paint droplet transfer process. The ability to visualize the internal structures within the paint spray envelope during the paint spray transfer from atomizer to the target surface is vital to understanding the role that the atomization mechanisms have on the evolution of the paint droplets as they travel from the paint atomizer to the target surface. This chapter, therefore, seeks to address some of these issues by focusing on the visualization and characterization of the paint spray envelope.

5.2 Spray Atomization

A spray is generally considered as a system of droplets immersed in a continuous gaseous phase [5]. There are many occurrences of spray phenomena in power and propulsion applications, industrial applications, and nature [6]. Sprays are produced as a result of atomization, which is defined as the disintegration of liquid into droplets [5, 7]. Atomization of a liquid into discrete droplets can be brought about by the use of diverse mechanism like aerodynamic, mechanical, ultrasonic, or electrostatic forces. For example, the breakup of a liquid into droplets can be achieved with the impingement of a gas in two-fluid atomization, with centrifugal forces in rotary atomization, with ultrasonic vibration utilizing a piezoelectric transducer in ultrasonic atomization, or with electrostatic/electromagnetic fields in electrostatic/electromagnetic atomization.

Atomization processes may also be classified according to the energy used to produce the instability on the liquid element. For example, pressure atomizers use pressure energy, rotary atomizers use centrifugal energy, two fluid atomizers use gaseous/fluid energy, and ultrasonic or acoustic atomizers use vibratory energy [5, 7].

When a liquid is sprayed, it forms ligaments due to the interaction of the surface tension and the air resistance [5]. The surface tension breaks the liquid jet into individual droplets that are capable of holding themselves together at their velocities. Very large droplets once formed will split further if the surrounding ambient resistance overcomes the surface tension. In the vast majority of industrial processes air-assisted atomizers are used where compressed air supplies the required energy for atomizing the liquid.

5.3 Paint Atomizers

The two common paint atomizers utilized in the automotive industry are high-speed rotary bell atomizer and air spray guys. These two types of atomizers are described briefly in this section.

5.3.1 High-Speed Rotary Bell Atomizer

A high-speed rotary bell atomizer (Fig. 5.1) is generally a device in which liquid is supplied to the center of the rotating bell cup. The rotating bell cup is designed in a way that it widens toward the rim. The friction between the liquid and the bell cup wall causes the liquid to rotate at roughly the same speed as the bell cup. This rotary motion creates centrifugal forces within the liquid that induces it to flow radially outward toward the rim of the bell cup. If the rotational speed of the bell cup is sufficiently high, the liquid will arrive at the rim in a thin continuous film.

PPH 308 high speed rotary atomizer
(*courtesy KREMLIN REXSON & SAMES*)

PPH 701-FP5 high speed rotary atomizer
(*courtesy KREMLIN REXSON & SAMES*)

Fig. 5.1 High speed rotary bell atomizer

The mechanism of disintegration of the film into droplets is affected by the size and geometry of the bell cup, its rotational speed, the liquid flow rate, and the physical properties of the liquid [5, 8, 9].

5.3.2 Air Spray Gun

Air spray guns are twin fluid atomizers which use the kinetic energy of the flowing air stream to shatter the paint into ligaments and then into droplets. They are mostly external mixing, that is, a paint nozzle opening and an atomizing air dispensing annulus release outwardly from the atomizing head. The liquid paint flow dispensed through the paint dispensing nozzle is dispersed and atomized by the airflow which is diffused and blown around the paint flow. The paint nozzle opening is located at the center facing to the outside of the atomizing head. An annular air hole is provided around the nozzle hole, and compressed air is blown as it surrounds the paint flow from the nozzle hole. The paint and the compressed air are dispensed separately and are mixed and atomized in front of and outside the atomizing head (Fig. 5.2).

Most spray guns have lateral air holes provided on both sides, and compressed air is supplied from both sides to the spray flow in order to adjust the shape of the spray pattern. Consequently, a spray flow sprayed in a circular pattern at the center may be flattened by changing the airflow pressure and quantity from the lateral air holes. In the case of this spray gun, better atomization is achieved when compressed air quantity (or pressure) is increased, such that the painted surface is provided with a higher quality finish as a consequence of the spraying of finer particles.

Graco Finex HVLP Air-Spray Gun
Courtesy Graco

Dux pressure feed spray gun
Courtesy Dux Area

Fig. 5.2 Air spray gun

5.4 Electrostatic Spray (E-Spraying)

Electrostatic spraying is a widely used technique for coating a conductive substrate. Both the high-speed rotary bell atomizer and the air spray gun can be used for e-spraying. E-spraying refers to spray coating process that utilizes an electric field to increase the overall transfer efficiency. E-spray can be categorized based on three specific criteria: method of charging (direct conduction, corona, induction, or turboelectric); method of atomization (stationary low-flow nozzle, high velocity jet, or rotating disc or bell); and the material nature of the bulk material (liquid or powder). There are three primary ways in which liquids can be electrostatically charged: direct conduction, corona, and induction; whereas for powders, either triboelectric or corona charging are the most practical.

In *triboelectric charging*, the impact of the powder with the tubing walls produces an electrostatic charge, the polarity and to some degree the magnitude of which is based on the triboelectric series. The material is carried pneumatically through a long and sometimes tortuous path prior to release from the nozzle. The nozzles for triboelectric E-spray are in most cases made of the same plastic material as the tubing and are therefore limited to low-flow applications; otherwise, nozzle erosion could become a factor. However, the magnitude of the charge is also a very strong function of the number of impacts. A common application of triboelectric charging E-spray application would be ink-jet toner cartridges.

In *direct conduction*, the spray material has a relatively high conductivity (e.g. an aqueous solution), and the voltage is applied to the source of the sprayed material. For this technique, the liquid is emitted from the nozzle already charged and instantly atomized. Atomization in sprays using direct conduction is often achieved by utilizing a stationary, low-flow nozzle. For example, the flow from a charged syringe will produce Taylor cones—a phenomenon in which the meniscus of the liquid in a capillary which produces a cone that ejects fine droplets.

In *a corona charging system*, the sprayed droplets are charged after atomization by passing through a corona field. This is an effective technique, but it poses safety

hazards due to a high probability of arcs in the presence of flammable materials like solvent-borne paints. Also, from a practical standpoint, liquid can land on the corona-producing electrode prior to charging causing a decrease in performance. However, for dry powders, corona charging can be very efficient. Because the nozzle can be made of wear-resistant metals to act as the ground for the corona, high velocity jets can be used such as those of the powder-coat spray industry.

In *induction charging*, the voltage is applied in proximity to the nozzle so that the liquid travels near the source and picks up some of the electric charge. To avoid current flowing back to the feed tank, the material has to have a high bulk resistivity. Due to its comparatively low charging efficiencies, mechanical assistance is required to atomize the spray. For this reason, the preferred methods for atomization for inductively charged systems are rotary atomization, air assisted atomization, or a combination of both.

5.5 Spray Characterization

Practical atomizers do not generally produce sprays of uniform droplet size at any given operating condition; instead the spray can be regarded as a spectrum of droplet sizes distributed about some arbitrary defined mean value [10]. In order to accurately assess and understand droplet size data, all of the key variables such as nozzle type, pressure, capacity, liquid properties, and spray angle have to be taken into consideration [5]. The droplet size testing method should also be fully understood. The measurement techniques, the type of droplet size analysis technique, the data analysis, and the reporting methods all have a strong influence on the results [10].

5.5.1 Droplet Size Distribution in Sprays

Accurate knowledge of droplet size distribution as a function of the conditions of the spray system is a prerequisite for the fundamental analysis on the transport of mass, heat, and phase separation in dispersed systems [11]. Detailed characterization of sprays is critical in optimizing atomizer design and validating mathematical modeling predictions. Spray characteristics include the droplet size and velocity distribution, spray pattern, spray coverage, and spray angle. Sprays are multiphase flows which are generally a complex system commonly consisting of droplets which have a range of properties. This property range almost always includes droplet diameter, velocity, and concentration, which usually includes non-sphericity, mass/heat transfer, and temperature variations. In addition, other properties that are commonly present in some regions of the spray include droplet break-up, physical property variations, and coalescence. At the most basic level, multiphase flows may be characterized by an average spray length scale. However, there are a number of definitions, and this is a source of much confusion. Standard texts [5, 7] offer definitions, and the two most commonly used are D_{10} and D_{32}.

The linear average diameter (D_{10}) is defined as the diameter of a uniform droplet set with the same number and sum of diameters as the real set, providing a simple "average" measure with which to compare different sprays. However, most multiphase processes involve heat and/or mass transfer, and the representative length scale used here is the Sauter Mean Diameter, expressed as SMD or D_{32}, which is the diameter of a uniform droplet set with the same total volume to total surface area ratio as the real set.

Spray characterization techniques normally record data that are typically in the form of number count per class size. The data are arranged into a mathematical representation referred to as a droplet size distribution. The mathematical representation is most often dependent on the characterization techniques used. Some of the most common droplet size distribution functions used in industry include normal, log-normal, root normal, Nukiyama-Tanasawa, Rosin-Rammler, and upper-limit distribution function [5, 7, 12]. It should be noted that no single distribution function can characterize all experimental measurement data of droplets sizes, and none of these functions is universally superior to any other for representing droplet size distribution [7].

In many applications, a mean droplet size is a factor of foremost concern. Mean droplet size can be taken as a measure of the quality of an atomization process. It is also convenient to use only mean droplet size in calculations involving discrete droplets, such as multiphase flow and mass transfer processes [5]. Various definitions of mean droplet size have been employed in different applications; a summary is provided by Liu [7].

The expressions for the mean droplet diameters take the form of a generalized equation as follows:

$$D_{ab} = \left[\frac{\int_{D\min}^{D\max} D^a (dN/dD) dD}{\int_{D\min}^{D\max} D^b (dN/dD) dD} \right]^{1/(a-b)}, \quad \text{or} \quad D_{ab} = \left[\frac{\sum N_i D_i^a}{\sum N_i D_i^b} \right]^{1/(a-b)} \tag{5.1}$$

Where $D_{\min}$ and $D_{\max}$ are the minimum and maximum droplet diameters respectively, and a and b take any value according to the definition. For example for the Sauter Mean Diameter (D_{32}); a is 3 and b is 2. The D_{32} is perhaps the most widely used. It represents the diameter whose ratio of volume to surface area is the same as that of the entire droplet sample.

In characterizing the droplet size distribution, at least two parameters are typically necessary, i.e., a representative droplet diameter, (e.g. mean droplet size) and a measure of droplet size range (e.g. standard deviation or q). Many representative droplet diameters have been used in specifying distribution functions. The definitions of these diameters and the relevant relationships are summarized by Liu [7].

Many authors [13–18] have used maximum entropy formulations to derive probability density function for the prediction of droplet size distribution. Liu [7] provided a detailed summary of empirical and analytical correlations for droplet size distribution.

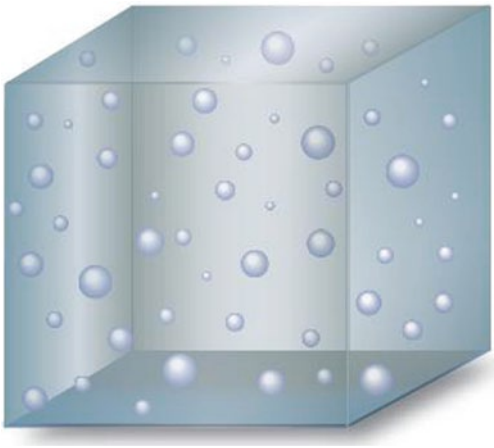

Fig. 5.3 The measurement volume for the spatial distribution [10]

5.5.2 Droplet Sampling Techniques

There are two different types of droplet size sampling techniques: spatial and flux also called temporal [10]. The spatial technique is implied when a collection of droplets occupying a given volume is sampled instantaneously. Generally, spatial measurements are collected with the aid of holographic means such as high-speed photography or light scattering instruments. This type of measurement is sensitive to the number density in each class size and the number of particles per unit volume. The spatial sampling technique is depicted in Fig. 5.3.

The flux technique occurs when individual droplets pass through the cross section of a sampling region and are examined during an interval of time. Flux measurements are generally collected by optical instruments that are capable of sensing individual droplets. This type of measurement is sensitive to the particle flux. The sampling technique is critical for understanding droplet size data. Typically, nozzles measured using the spatial technique will report droplets smaller on average than nozzles measured using the flux technique. When comparing data from different sources, it is important to identify the differences in sampling techniques. This should help resolve many data discrepancies. The flux sampling technique is depicted in Fig. 5.4.

The sampling technique used can also be application-driven. For example, gas conditioning, cooling, or similar processes would be better served with a spatial sampling technique. According to Schick [10], in applications requiring accurate spray deposition such as painting and agricultural spraying, a flux sampling technique would be more appropriate. Flux methods are more sensitive to individual droplet sizes and velocity and provide the additional detail required by some applications.

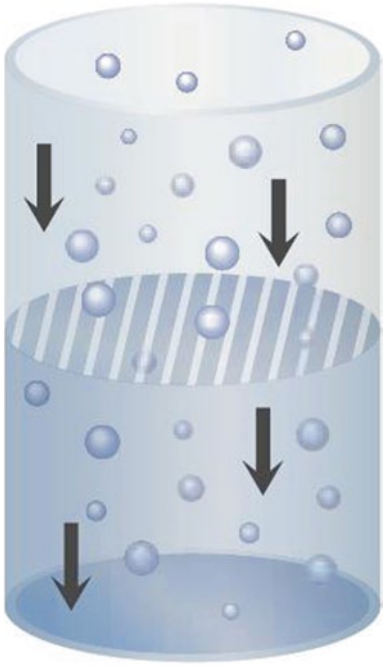

Fig. 5.4 The measurement cross-section for the flux distribution [10]

5.5.3 Droplet Size Measurement Techniques

Various measurement techniques have been developed and applied with different degrees of success. For the measurement of droplet properties in sprays, non-intrusive techniques are often desired [7]. The measurement should not create a disturbance in the spray pattern. An ideal measurement technique should have large range of capability to measure both the spatial and temporal distribution. Such a technique should tolerate wide variations in droplet properties at some extreme conditions present in sprays in various engineering applications. An appropriate technique should also be able to acquire sufficient representative samples to ensure reasonable measurement accuracy. Rapid sampling and data processing means are hence needed for the analysis of measurement results. The sampling, data acquisition, and processing system must be fast enough to record every droplet passing through the measurement volume when measuring the number density of the spray [7].

The measurement techniques for droplet sizing may be grouped conveniently into four primary categories: (a) mechanical methods, (b) electrical methods, (c) optical methods, and (d) acoustical methods. Mechanical methods are relatively simple and low cost. Droplets are collected in either liquid or frozen state, followed by microscopic or sieving analysis. Electrical methods involve the detection and analysis of electronic pulses generated by droplets in a measurement volume or on a wire. The electronic signals are then converted into digital data and calibrated to produce information on droplet size distribution. Optical methods have been

developed in recent years and are finding an increasing range of applications. Some of the optical methods are capable of simultaneously measuring droplet size and velocity, as well as velocity and number density [5]. An acoustical method has been evaluated for the measurements of fine droplets.

5.5.3.1 Optically-Based Droplet Size Measurement Techniques

In this section we focus our attention on optically-based droplet size measurement techniques and provide a brief review of three of the most widely used. A wide range of optically-based droplet size measurement techniques have been developed and are in use. Although each measurement technique has its own advantages and limitations, most optical methods have an important, common attribute of allowing droplet size measurements to be made without disturbing the flow field being measured. The optical methods generally fall into one of two categories: Imaging or Non-Imaging. The most important sub-class is the single droplet counting method of which Black et al. [19, 20] provides an extensive review. Other methods include ensemble light scattering methods of droplet sizing, which integrates in one dimension [21], and Domann and Hardalupas [22] which focuses upon planar methods.

Phase Doppler Anemometry (PDA) [23–26] is generally considered the most accurate method for spray characterization despite its high capital cost and the requirement for skilled operation in order to optimize the system set-up and subsequent data interpretation. PDA is a Laser-Doppler Velocimeter (LDV) based method for non-intrusive, simultaneous measurements of the diameter and velocity of spherical particles [24, 25]. The technique relies on measuring the time delay that occurs when the light scattered by a droplet traversing the intersection of two coherent laser beams arrives at two spatially separated photo detectors. Through good design and proper set-up, the method has the potential to gather accurate data at extremely high data rates with good statistical certainty. However, measurement accuracy is dependent upon a number of factors including laser power, optical configuration, droplet homogeneity, sphericity, and concentration. It also requires a skilled set-up and operation to obtain accurate results.

One of the fundamental limitations of PDA is the inability to accurately measure non-spherical droplets [27]. Such conditions are observed at the interface where an initial liquid sheet breaks up into ligaments subsequently forming initially large and often non-spherical droplets; therefore, PDA is an inherently unsuitable instrument to characterize near-orifice flows. This is an unfortunate limitation since the near-orifice region is where the spray is defined, and the process of atomization is occurring. This creates particular problems for data certainty since only a small fraction of the spray mass is spherical in the near-orifice region. In addition, the best optical geometry is specific and may not be available in the experiment. Curved window surfaces need complex optical corrections to be employed which, while valid for LDA work, are difficult to extend to PDA [28, 29].

The Malvern Particle Analyzer is another widely used particle analyzer. It is based on the Fraunhofer diffraction of a parallel beam of monochromatic light by a

moving droplet. When a droplet interacts with a parallel beam of light, a diffraction pattern is formed. For monodisperse spray, the diffraction pattern is of the Fraunhofer form. It comprises a series of alternate light and dark concentric rings whose spacing is related to the droplet size. For a polydisperse spray, the diffraction pattern comprises a number of the Fraunhofer pattern with series of overlapping diffraction rings, each of which is produced by a different group of droplets sizes [30]. The Fourier transform receiver lens focuses the diffraction patterns onto a multi-element photo detector that measures the light energy distribution. The photo detector consists of 31 semicircular photosensitive rings surrounding a central circle. Each ring is most sensitive to a particular small range of droplet sizes. The output of the photo detector is multiplexed through an analog-digital converter. The measured light energy distribution is then converted to the droplet size distribution. The measured data may be either analyzed in terms of a histogram with 15 size classes or presented in the format of normal, log-normal, Rosin-Rammler, or other modes that are independent of the known models.

Imaging is probably one of the most accurate and least expensive techniques for measuring droplet size and velocity. It has the potential of measuring droplets in dense, fast-moving sprays that are of particular interest in power generation [7]. In the imaging method, an image of the droplets is taken with a light pulse of sufficient intensity and sufficient short duration to yield a sharp image of the droplets. The major advantage is that a visual record of the spray under investigation provides a simple means to check what is and (more importantly) is not being measured and the ability to quantify arbitrarily shaped objects. Until recently, the error and time required for manual analysis of the images [31] has been the reason why imaging methods have not been more prevalent.

One of the most common image analysis methods available in the market is the Particle/Droplet Image Analysis (PDIA) technique by Oxford Lasers Inc. In the PDIA technique the object diameter is based upon the measured area/perimeter rather than local object curvatures as is the case of PDA. The PDIA technique, as reported by Whybrew et al. [32], uses an automated segmentation thresholding algorithm for the quantitative analysis of droplet or particle images. This method is based upon the original approach adopted by Yule et al. [33], in terms of determining the degree of image focus from the edge gradient intensity of a droplet image. In a preliminary study, Kashdan et al. [34] examined probability density function correction schemes to account for edge contact correction and depth of field (DOF) biasing effects which are diameter dependent.

5.6 Spray Visualization

Spray visualization is generally carried out to give qualitative information of the spray flow field. It also provides information of the geometric features of the spray which includes spray pattern, spray cone angle, and spray coverage. Traditionally, spray visualization has been achieved by several optical methods, including but not

limited to, high speed photography, Schlieren technique, shadowgraph technique, and holography.

High speed photography is the most common spray visualization technique. This imaging technique requires two main components: a light source to illuminate the spray and an imaging device. The illumination for high speed photography can roughly be divided into three modes namely: Laser Light Sheet (LLS), stroboscopic lighting, and backlighting or front lighting. For laser light sheet illumination of the spray for imaging, the laser light is passed through a cylindrical lens to create the laser sheet which is expanded to penetrate the entire spray vertically to illuminate the center vertical plane. The imaging device or camera is positioned normal to the plane of the laser light sheet to acquire images of the spray structure.

For stroboscopic lighting, the stroboscope must be synchronized with the imaging device or camera for recording. The system consists of a flashing strobe light and an imaging device or camera with an open shutter. Stroboscopic images must be taken in darkness so that every time the strobe flashes, a still image is taken of a moving object at that instant. Another illumination method is backlighting, where the light source and the imaging device are placed at opposite sides of the object to be imaged while facing each other. There are several combinations of the above three illumination methods in high speed photography.

Im et al. [8] used high speed photography for spray visualization in which laser light sheet generated by a copper-vapor laser was used to illuminate the spray. Domnick and Thieme [9] used stroboscopic lighting with a nanolight of 18 ns flash to captured images of liquid disintegration process at the bell cup edge of a high speed rotary bell atomizer using a video camera. The flash is synchronized with the video camera yielding a frame rate of 25 frames per second. Settles [35] used two visualization approaches; one is stroboscopic lighting with a xenon flash of about 1 μs duration for illumination and Super Video Home System (S-VHS) videotape at standard 30 Hz frame rate. The second is a Continuous Wave (CW) Argon-ion laser beam which was spread into a sheet by a glass rod for illumination.

To investigate spray propagation in a gas turbine combustor, Schober et al. [36] used the LLS technique for detail and effective two-dimensional characterization of liquid fuel spray. Lee et al. [37] used backlight scattering to capture spray images which were analyzed by measuring spray penetration, spray angle, and total spray volume of dimethyl ether fuel spray. A strobe light was used as the backlight in this case. Versteeg et al. [38] used a copper-vapor laser as the illumination source in conjunction with a Kodak HS4540 high speed digital camera for image recording. The laser provided a pulsed light source with a frequency of 9 kHz. Fiber-optic light delivery was used to provide front and backlighting.

A second method commonly used for spray visualization is the Schlieren technique. The Schlieren technique is based on the deflection of a collimated light beam crossing gradients of the index of reflection in a transparent medium (i.e., it provides images of the refractive-index-gradient fields). It is, therefore, suited for applications in which deviations of light are intended to be visualized as they appear, e.g., at the refraction-gradient due to density-discontinuities in a fluid [39]. Settles [40] and Settles et al. [41] used the Schlieren technique in the visualization of a

combustion driven High-Velocity Oxy-Fuel (HVOF) thermal spray torch utilized to apply metallic coatings to surfaces. The hot supersonic jet produced by this equipment spreads rapidly and vigorously entrains the surrounding air. This visualization is critical to understand the process since direct visual observation belies its true character.

The Shadowgraph technique is a companion of Schlieren, and is also based on light refractions. While the Schlieren image displays the deflection angle, shadowgraph displays the ray displacement resulting from the deflection. There are three main differences between the Schlieren and shadowgraph techniques. First the shadowgram is not a focused optical image; it is a mere shadow. The Schlieren image, however, is what it purports to be: an optical image formed by a lens, and thus it is bearing a conjugate optical relationship to the Schlieren object. Second, Schlieren methods require a knife-edge or some other cutoff from the refracted light, where no such cutoff is needed or allowed in shadowgraphy. Finally, the luminance level in a Schlieren image responds to the first spatial derivative of the refractive index in the Schlieren, e.g. $\partial n/\partial x$. However, the shadowgram response is the second spatial derivative, or Laplacian, e.g. $\partial^2 n/\partial x^2$ [40]. Bellofiore et al. [42] used a flash shadowgraph technique for the visualization of a dense spray of water and kerosene. Bae et al. [43] utilized shadowgraph, and Mie Scattering observed the spray from a Valve-Covered-Orifice (VCO) nozzle and a Start-On-Injection (SOI) nozzle. In their setup for shadowgraph visualization, Bellofiore et al. [42] used a Xenon flash lamp with 15 μs pulse length, a Pulnix TM-6710 digital camera (to acquire 8-bit 640×200 pixel frames at 240 Hz), and a BNC delay generator for time-based generation synchronization.

A fourth visualization technique is holography. It is a technique that allows the light scattered from an object to be recorded and later reconstructed so that it appears as if the object is in the same position relative to the recording medium as it was when originally recorded. The image changes as the position and orientation of the viewing system changes in exactly the same way as if the object were still present, thus making the recorded image (hologram) appear three-dimensional [39]. Feldmann et al. [44] used short time holography for the visualization of both subcooled and superheated sprays generated in a flat spray nozzle.

5.7 Infrared Thermography Application in Paint Spray Visualization and Characterization

An infrared thermography-based paint spray visualization and characterization technique recently presented by Akafuah [45], is covered here in some detail. The technique allows the visualization of the internal structures and the macroscopic features of the paint spray transfer process. In addition, the paint droplet volume fraction and the paint droplet number density inside the spray are computed by the new technique. This provides quantitative information about the droplet distribution inside the continuous gaseous phase.

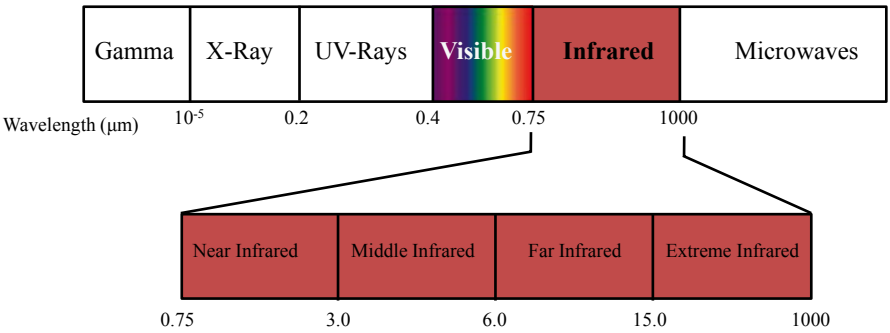

Fig. 5.5 The electromagnetic spectrum showing the subdivision of the infrared spectral band [45]

The technique utilizes a thermal radiation source in the form of a uniformly heated blackbody background as the emitter and an infrared camera as the receiver. As a result of the presence of the spray, the infrared energy emitted by the source is attenuated as it passes through the spray before reaching the receiver. The infrared detector, therefore, receives a damped signal as a result of the attenuation of the emitted intensity. This damped image is recorded to provide an attenuation map of the spray, which is post-processed using theoretical and empirical equations to extract information about the liquid volume fraction and droplet number density.

5.7.1 Infrared Thermography

Infrared thermography transforms the thermal energy emitted by an object in the infrared spectral band of the electromagnetic spectrum into a visible image. It is known that any object at a temperature above absolute zero, that is 0 °K (−273.16 °C) emits electromagnetic radiation in the form of rays which fall in the infrared spectral band of the electromagnetic spectrum. Within the infrared spectral band of the electromagnetic spectrum at the short-wavelength end, the boundary of the limit of visual perception lies in the deep red. At the long-wavelength end, it merges with the microwave radio wavelength in the millimeter range. The infrared spectral band of the electromagnetic spectrum ranges from 1–1000 μm. This band is further subdivided into four smaller bands, the boundaries of which are arbitrarily chosen. They include: the near infrared (0.75–3 μm), the middle infrared (3–6 μm), the far infrared (6–15 μm), and the extreme infrared (15–1000 μm). You will find this illustrated in Fig. 5.5.

Infrared thermography is a non-contact, non-intrusive technique, which enables us to see thermal energy. The energy emitted by a body is mainly a function of its surface temperature, and consequently, infrared thermography may be considered a two-dimensional technique of temperature measurement. Thus infrared thermography is the science of detecting and measuring variations in heat emitted by an object and transforming them into visible images.

5.7.2 Mathematical Treatment of Infrared Spray Visualization and Characterization

The Infrared thermography-based visualization and characterization technique introduced in this book is an optical method which uses infrared imaging to characterize and visualize the entire flow field of a liquid spray. The technique employs an emitter which is a uniformly heated blackbody background as a thermal radiation source, and a receiver which is an infrared detector. The method provides a two-dimensional image in which the value is associated to each pixel on an intensity scale. This value accounts for the amount of infrared energy emitted by the source which then travels through the spray. As a result of the presence of the spray, the infrared energy emitted by the source is attenuated.

For a given fluid, this attenuation is a function of droplet size, spray density, and the complex refractive index ($m = n - ik$) of the material being sprayed. The infrared detector, therefore, receives a damped signal as a result of the attenuation of the emitter intensity. This damped image is recorded to provide an attenuation image of the spray. This image is post-processed using theoretical and empirical equations to extract information about the spray volume fraction, number density, and macroscopic information.

5.7.2.1 The Radiation Model

In this section, consider a spray visualization system consisting of a radiative source of uniform or known intensity distribution and a camera or similar device capable of detecting the attenuation of the radiative intensity caused by the presence of any obstacle within a certain wavelength range. Radiative intensity is defined as radiative energy transferred per unit time, solid angle, spectral variable, and area normal to the pencil of rays. This radiative energy travels in the form of electromagnetic waves with a certain wavelength. The camera detects the attenuation of the radiative energy as it travels through a participating media consisting of a liquid spray made up of droplets with a certain size distribution. The spray is generated by a nozzle or similar atomization device. A schematic of the concept is shown in Fig. 5.6.

The scattering and absorption coefficients of a group of droplets are directly related to the droplet number density and their effective cross-sectional areas. These effective areas are called the scattering and absorption cross-sections, $C_{sca\lambda}$ and $C_{abs\lambda}$ [46]. Generally $C_{sca\lambda}$ and $C_{abs\lambda}$ are a function of the particle orientation, the complex refractive index ($m = n - ik$), the particle size relative to the wavelength, and the polarization of the incoming radiative beam. It is assumed that the bulk of the spray is made up of spherical droplets, and orientation is of no concern. Likewise, only unpolarized light is considered since this is a good approximation for most heat transfer processes [46].

Considering the microscopic view of the spray, an electromagnetic wave or photon passing through the immediate vicinity of spherical particles or droplets will be absorbed, scattered, or both. The scattering is attributable to three separate phenom-

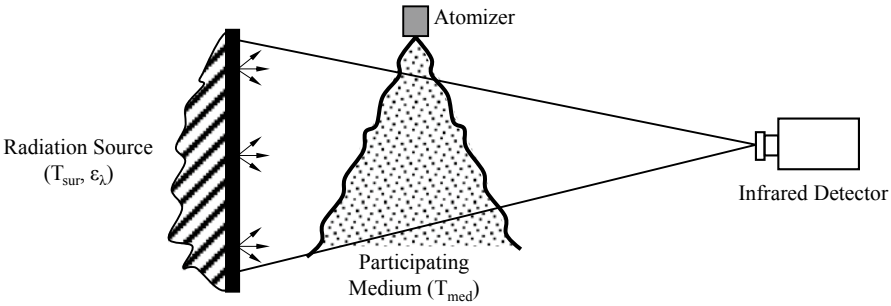

Fig. 5.6 A schematic of the infrared visualization model

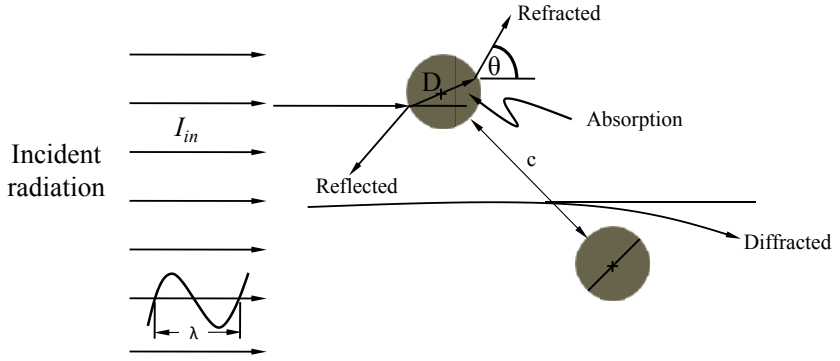

Fig. 5.7 The interaction between electromagnetic waves and spherical particles [47]

ena namely diffraction, reflection at the particle surface, and refraction in a particle. Figure 5.7 illustrates the interaction between electromagnetic waves and spherical particles [47].

5.7.2.2 Infrared Radiation Formulation

It is now appropriate to focus attention upon the incoming radiant beam with intensity $I_{in\lambda}$ impinging upon an absorbing, emitting, and scattering particulate medium. As the beam traverses the medium, its intensity is attenuated by absorption and by out-scattering of energy into other directions. The intensity of the beam is enhanced by the in-scattering of radiation from other directions into the direction of propagation or by emitted energy from the particles. The variation of intensity in the medium is described by the equation of transfer [48],

$$\frac{dI_{\omega\lambda}(s)}{ds} = -a_\lambda I_{\omega\lambda}(s) + a_\lambda I_{\omega\lambda b}[s, T(s)] - \sigma_\lambda I_{\omega\lambda}(s) + \frac{\sigma_\lambda}{4\pi}\int_{4\pi} I_{\omega\lambda}(s)\Phi_\lambda(\omega_i \rightarrow \omega)d\omega_i \tag{5.2}$$

where $I_{\omega\lambda}$ is the directional spectral intensity; s is the distance traveled in the medium, and a_λ and σ_λ are the absorption and scattering coefficients, respectively. Equation (5.2) also includes the emitted energy of the particles $I_{\omega\lambda b}$ from the Planck's Distribution evaluated at the particle temperature T, and the scattering phase function from direction ω_i into the direction ω, $\Phi_\lambda(\omega_i - \omega)$. By introducing the definitions of the optical thickness τ_λ and the scattering albedo Ω_λ the following expressions are obtained

$$\tau_\lambda = \int_0^s (\sigma_\lambda + a_\lambda) ds, \quad \Omega_\lambda = \frac{\sigma_\lambda}{\sigma_\lambda + a_\lambda}. \tag{5.3}$$

The equation of radiative transfer, Eq. (5.2) can be rewritten as:

$$\frac{dI_{\omega\lambda}(\tau_\lambda)}{d\tau_\lambda} = -I_{\omega\lambda}(\tau_\lambda) + (1 - \Omega_\lambda) I_{\omega\lambda b}[\tau_\lambda, T(\tau_\lambda)] + \frac{\Omega}{4\pi} \int_{4\pi} I_{\omega\lambda}(\tau_\lambda) \Phi_\lambda(\omega_i \to \omega) d\omega_i. \tag{5.4}$$

Appropriate boundary conditions have to be introduced in order to make the formulation complete and well posed. Transparent boundaries are assumed at all sides of the problem. On the face radiated by the main source, a known diffuse irradiation may be taken into account [49]:

$$I_{\omega\lambda}(\tau_\lambda = 0) = I_{0\lambda}(o). \tag{5.5}$$

Throughout the rest of the analysis we make the simplifying assumptions that the local emission of and the scattering of the electromagnetic waves into the direction of propagation is negligible. We also assume that there is no evaporation of the liquid droplets. The vapor phase attenuation is neglected in our analysis. Under these assumptions, the source term in Eq. (5.4) is negligible. Thus, the equation of transfer reduces to:

$$\frac{dI_{\omega\lambda}(\tau_\lambda)}{d\tau_\lambda} = -I_{\omega\lambda}(\tau_\lambda). \tag{5.6}$$

The solution of Eq. (5.6) with boundary condition Eq. (5.5) becomes

$$I_\lambda(\tau_\lambda) = I_{0\lambda}(0) \exp(-\tau_\lambda). \tag{5.7}$$

This indicates that the intensity of the propagating beam simply decays exponentially with optical distance travelled. Solving for the optical thickness from Eq. (5.7) yields

$$\tau_\lambda = -\ln\left(\frac{I_\lambda(\tau_\lambda)}{I_{O\lambda}(0)}\right). \tag{5.8}$$

Thus, the optical thickness in the direction of propagation can be computed based upon the attenuation of the radiative intensity acquired by the detector.

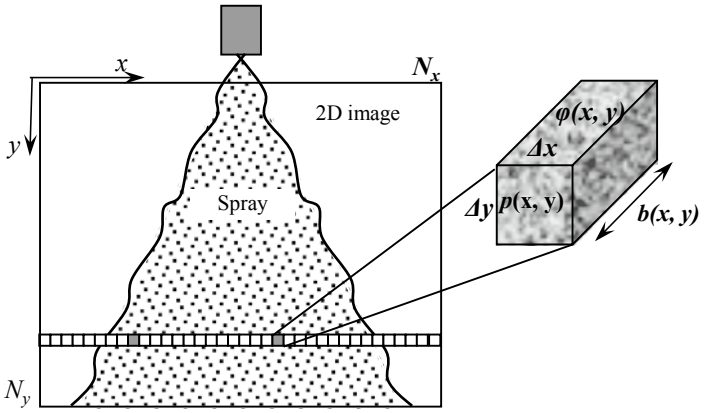

Fig. 5.8 A schematic of the attenuation map of the spray

5.7.2.3 Two-Dimensional Infrared Image Analysis

When a captured two-dimensional digital image of a spray showing the attenuation of the radiant intensity is examined as a result of the presence of the spray droplets, the image contains a finite sequence of pixels $p(x, y)$, for $1 \leq x \leq N_x$ and $1 \leq y \leq N_y$, where N_x and N_y are the number of pixels in the x- and y- directions, respectively. The pixel size is $\Delta x \Delta y$, where Δx and Δy are usually constant throughout the image and may be equal (i.e., $\Delta x = \Delta y$). Each pixel $p(x, y)$ is a two-dimensional view of an attenuation volume $\varphi(x, y)$ with an effective attenuation depth $b(x, y)$, corresponding to the depth of the spray in a direction normal to the image at the location of the pixel $p(x, y)$. Therefore, the dimensions of each attenuation volume or voxel can be expressed as $\Delta x \Delta y b(x, y)$ (Fig. 5.8). Within each attenuation volume, there exists a finite number of droplets $n(x, y)$ with a corresponding droplet size distribution.

It is assumed that the attenuation of the infrared energy in the air surrounding the spray is negligible. That is, the attenuation of the rays occurs only within the attenuation volume $\varphi(x, y)$. The optical thickness defined in Eq. (5.3) is rewritten in terms of the extinction coefficient $\kappa_\lambda(x, y)$ as:

$$\tau_\lambda(x, y) = \int_0^{b(x,y)} (\sigma_\lambda(x, y) + a_\lambda(x, y))ds = \int_0^{b(x,y)} \kappa_\lambda(x, y)ds. \tag{5.9}$$

Equation (5.9) can be integrated to yield the optical thickness expressed in terms of the effective extinction coefficient $\bar{\kappa}_\lambda(x, y)$ and the physical path length $b(x, y)$ as follows:

$$\tau_\lambda(x, y) = \int_0^{b(x,y)} \kappa_\lambda(x, y)ds = \bar{\kappa}_\lambda(x, y)b(x, y). \tag{5.10}$$

Despite the fact that the droplets in the integration path $b(x, y)$ exhibit a size distribution and can be concentrated unevenly along it, the effective extinction coefficient $\bar{\kappa}_\lambda(x, y)$ is considered independent on both the droplet size distribution and the droplet concentration. Therefore, the extinction coefficient can be expressed as:

$$\bar{\kappa}_\lambda(x, y) = \begin{cases} \frac{\tau_\lambda(x,y)}{b(x,y)} & \text{for} \quad b(x, y) \neq 0 \\ 0 & \text{for} \quad b(x, y) = 0 \end{cases}. \tag{5.11}$$

The scattering and absorption coefficients are defined as the fraction of the total propagating energy which is scattered out of, or absorbed from, a radiant beam per length of travel, respectively. The scattering and absorption coefficients of a group of particles (or droplets) as presented by Tien and Drolen [46] are directly related to the number density of these particles (or droplets) and their effective cross-sectional areas. These effective areas are called the scattering and absorption cross-sections, $C_{sca\lambda}(x, y)$ and $C_{abs\lambda}(x, y)$.

The size parameter χ, is defined as the ratio between the droplet circumference and the light wavelength, i.e., $\chi = \pi D_m/\lambda$. The geometric cross section of the droplet m is given by $G_m(x, y) = \pi D_m^2(x, y)/4$. For $\chi > 10$, light scattering can be approximated by geometric optics [48], the extinction cross-section, which is the sum of $C_{sca\lambda}(x, y)$ and $C_{abs\lambda}(x, y)$, that would equal the physical cross-section $G_m(x, y)$ evaluated using the surface-based average droplet size $D_{20}(x, y)$ of the spray. Therefore, for each pixel in the image we obtain a value of $G_m(x, y)$ that contains information relevant to the integration path $b(x, y)$ along the attenuation volume $\varphi(x, y)$. This gives us

$$G(x, y) = \pi D_{20}^2(x, y)/4 \tag{5.12}$$

Where $D_{20}(x, y)$ is defined as,

$$D_{20}(x, y) = \left(\frac{\sum_{m=1}^{n} n_m(x, y) D_m^2(x, y)}{\sum_{m=1}^{n} n_m(x, y)} \right)^{1/2} \tag{5.13}$$

which means that the scattering and absorption of all droplets contained within the attenuation volume $\varphi(x, y)$ are equivalent to those of $n(x, y)$ droplets of an equivalent diameter $D_{20}(x, y)$.

The absorption and extinction cross-section can be non-dimensionalized using the physical cross-section of the droplets. The resulting parameters presented by Tien and Drolen [46] are called scattering, absorption, and extinction efficiencies,

$$Q_{sca\lambda}(x, y) = \frac{C_{sca\lambda}(x, y)}{G(x, y)};\ Q_{abs\lambda}(x, y) = \frac{C_{abs\lambda}(x, y)}{G(x, y)};\ Q_{ext\lambda}(x, y) = \frac{C_{ext\lambda}(x, y)}{G(x, y)}. \tag{5.14}$$

With this notation, the scattering and absorption coefficients are given by:

$$\begin{aligned}\sigma_\lambda(x,y) &= n(x,y)C_{sca\lambda}(x,y) = G(x,y)n(x,y)Q_{sca\lambda}(x,y)\\ a_\lambda(x,y) &= n(x,y)C_{abs\lambda}(x,y) = G(x,y)n(x,y)Q_{abs\lambda}(x,y)\\ \bar{\kappa}_\lambda(x,y) &= n(x,y)C_{ext\lambda}(x,y) = G(x,y)n(x,y)\,Q_{ext\lambda}(x,y).\end{aligned} \tag{5.15}$$

Within each pixel [or attenuation volume $\varphi(x,y)$], there are $n(x,y)$ droplets having a droplet size distribution with diameters varying from $D_{min}(x,y)$ to $D_{max}(x,y)$. Define an effective diameter based on the total volume occupied by the droplets within the attenuation volume $\varphi(x,y)$ as:

$$D_{30}(x,y) = \left(\frac{\sum_{m=1}^{n} n_m(x,y)D_m^3(x,y)}{\sum_{m=1}^{n} n_m(x,y)}\right)^{1/3}. \tag{5.16}$$

This equation signifies that the volume of droplets within each control volume can be represented by $n(x,y)$ droplets of equivalent diameter $D_{30}(x,y)$. These are related to the liquid volume fraction $f_v(x,y)$ of the droplets within the attenuation volume $\varphi(x,y)$. Using Eq. (5.16), the volume fraction $f_v(x,y)$ is defined as:

$$f_v(x,y) = \frac{\pi n(x,y)\,D_{30}^3(x,y)}{6} \tag{5.17}$$

Where $n(x,y)$ is the number of droplets per unit volume expressed as:

$$n(x,y) = \frac{6f_v(x,y)}{\pi D_{30}^3(x,y)}. \tag{5.18}$$

Substituting for of $G(x,y)$ (Eq. 5.12) and $n(x,y)$ (Eq. 5.17) into Eq. (5.14) yields:

$$\bar{\kappa}_\lambda(x,y) = \left(\frac{\pi D_{20}^2(x,y)}{4}\right)\left(\frac{6f_v(x,y)}{\pi D_{30}^3(x,y)}\right)Q_{ext\lambda}(x,y) = \left(\frac{3}{2}\right)\frac{f_v(x,y)Q_{ext\lambda}(x,y)}{D_{32}(x,y)} \tag{5.19}$$

where $D_{32}(x,y) = D_{30}^3(x,y)/D_{20}^2(x,y)$ is commonly known as the surface area moment mean or the Sauter Mean Diameter (SMD), and represents the diameter of a droplet that has the same ratio of area to volume as that of the droplets contained within the attenuation volume $\varphi(x,y)$. Substituting Eq. (5.13) into Eq. (5.19), the liquid volume fraction can be defined in terms of Sauter Mean Diameter as:

$$f_v(x,y) = \begin{cases} \left(\dfrac{2\tau_\lambda(x,y)}{3Q_{ext\lambda}(x,y)\,b(x,y)}\right) D_{32}(x,y), & \text{for } b(x,y) \neq 0 \\ 0, & \text{for } b(x,y) = 0 \end{cases} . \quad (5.20)$$

An expression for the droplet number density per unit volume can be obtained by introducing the formulas for $D_{30}(x, y)$ (Eq. 5.31) and $D_{20}(x, y)$ (Eq. 5.13) into Eq. (5.20), which yields:

$$n(x,y) = \begin{cases} \dfrac{4\tau_\lambda(x,y)}{\pi\, Q_{ext\lambda}(x,y) b(x,y) D_{20}^2(x,y)}, & b(x,y) \neq 0 \\ 0, & b(x,y) = 0 \end{cases} . \quad (5.21)$$

For the droplet number density and the liquid volume fraction to be computed, the depth $b(x, y)$ of the spray at each pixel location and the extinction efficiency $Q_{ext\lambda}(x, y)$ needs to be known. To compute the droplet number density, the values of D_{30} and D_{20} need to be estimated.

5.7.2.4 Estimation of the Spray Depth at Each Pixel Location

The infrared visualization and characterization technique was applied to two automotive paint applicators—a high-speed rotary bell atomizer and a High Volume Low Pressure (HVLP) air-assisted atomizer. The high-speed rotary bell atomizer produces axisymmetric sprays. The HVLP air-assisted atomizer, however, produces a fan-shaped spray. Centrifugal forces are the main atomization mechanism of the high-speed rotary bell atomizer. The HVLP air-assisted atomizer utilizes air pressure forces to achieve atomization.

The value of $b(x, y)$**,** which is the depth of the spray in a direction normal to the image at each pixel $p(x, y)$ location, is computed as illustrated in Fig. 5.9. The high-speed rotary bell atomizer and the UCA sprays have circular cross-sectional areas as illustrated in Fig. 5.9a. The HVLP air-assisted atomizer has an elliptical cross-sectional area as shown in Fig. 5.9b. For the high-speed rotary bell and the UCA sprays using edge detection methods, the radius **R** at each cross-sectional location along the image of the spray are estimated from which the values of $b(x, y)$ are computed using Eq. (5.22). Note that the spray produced by the high-speed rotary bell atomizer starts-off as a hollow spray with an annular cross-sectional area. But, the spray becomes a solid spray with a circular cross-sectional area as it approaches the target surface. Consequently, a circular cross-sectional area is assumed for simplicity.

$$b(x,y) = 2[R(y)^2 - \{x - R(y)\}^2]^{1/2} \quad (5.22)$$

For the HVLP air-assisted atomizer, the major axes of the spray are estimated at each cross-sectional location along the image of the spray using edge detection methods. Thus for the HVLP air-assisted atomizer, two images are captured for each condition tested. An image is captured for the long axis and a second image

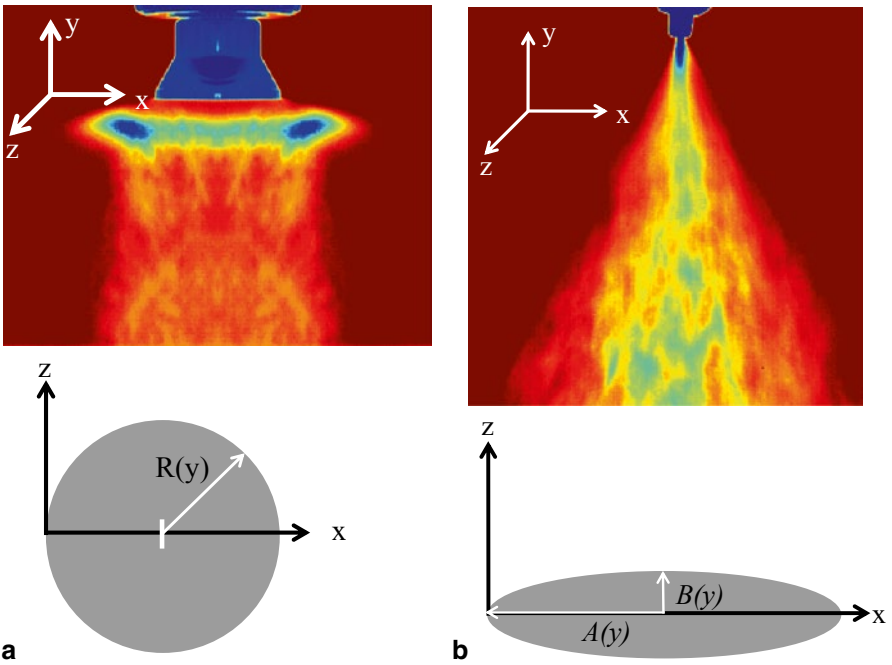

Fig. 5.9 Computation of the spray depth $b(x, y)$: **a** the cross-section of the high-speed rotary bell atomizer and the UCA Spray, **b** the cross-section of the HVLP air-assisted atomizer spray

is captured for the short axis. From the captured images, the values of $b(x, y)$ are computed using Eq. (5.23).

$$b(x, y) = 2\frac{B(y)}{A(y)}[A(y)^2 - \{x - A(y)\}^2]^{1/2} \tag{5.23}$$

5.7.2.5 Extinction Efficiency

To solve for the extinction efficiency, the numerical solution of Matzler [49] was followed. The extinction efficiency Q_{ext_λ} is given by the following expression:

$$Q_{ext\lambda} = \frac{2}{\chi^2}\sum_{n=1}^{N_{\max}}(2n+1)\cdot \mathrm{Re}[a_n + b_n] \tag{5.24}$$

Where a_n and b_n are Mie coefficients defined as:

$$a_n = \frac{[D_n(m\chi)/m + n/\chi]\psi_n(\chi) - \psi_{n-1}(\chi)}{[D_n(m\chi)/m + n/\chi]\zeta_n(\chi) - \zeta_{n-1}(\chi)} \tag{5.25}$$

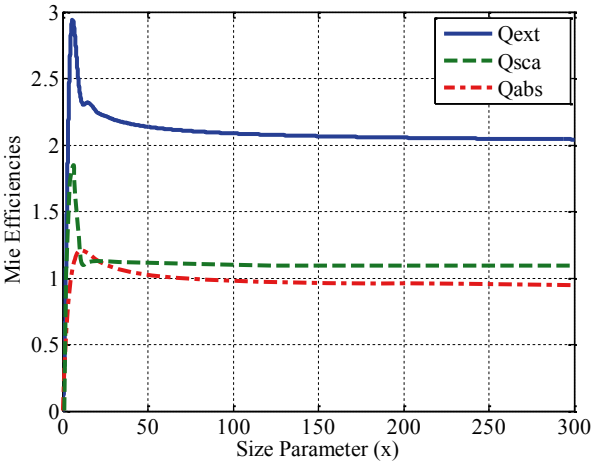

Fig. 5.10 The Mie efficiencies for water

$$b_n = \frac{[mD_n(m\chi) + n/\chi]\psi_n(\chi) - \psi_{n-1}(\chi)}{[mD_n(m\chi) + n/\chi]\zeta_n(\chi) - \zeta_{n-1}(\chi)} \tag{5.26}$$

Where ψ_n and ξ_n are the Ricatti-Bessel functions, and

$$N_{\max} = \max(\chi + 4\chi^{1/3} + 2). \tag{5.27}$$

The scattering efficiency is similarly defined as:

$$Q_{sca\lambda} = \frac{2}{\chi^2} \sum_{n=1}^{N_{\max}} (2n+1) \cdot [|a_n|^2 + |b_n|^2] \tag{5.28}$$

and the absorption efficiency is obtained by satisfying the energy conservation as:

$$Q_{abs\lambda} = Q_{ext\lambda} - Q_{sca\lambda}. \tag{5.29}$$

Following the numerical solution by Matzler [49] using MATLAB, the Mie efficiencies are obtained for water, using a complex refractive index of 1.33 + 0.00001i. A plot of the Mie efficiency values is shown in Fig. 5.10 for water. The value for the extinction efficiency (Q_{ext}) from the numerical solution asymptotically approaches 2.1. Thus, the constant value of 2.1 is assumed for the extinction efficiency in our analysis.

With the Mie extinction efficiency obtained, the droplet volume fraction can be computed once the SMD (D32) is known. The D32 values are obtained from experimental measurements using the Malvern Spraytec Particle Analyzer.

5.7.2.6 Estimation of D_{30} and D_{20} using Empirical Formulation

To compute the droplet number density using Eq. (5.21), we compute D_{30} and D_{20} by employing the Nukiyama-Tanasawa Distribution Function [12].

$$\frac{dN}{dD} = BD^2 \exp -(CD^q) \tag{5.30}$$

where N is the normalized number distribution of droplets; B is a constant; C is the size parameter; q is a distribution parameter; and D is the droplet diameter. In effect B, C, and q are constants that are adjusted to best fit the experimental data [13–18]. When Li and Tankin [13] took the limits of the droplet size to be zero and infinity, by using information entropy, they subsequently found the distribution function to be:

$$\frac{dN}{dD} = \frac{\pi}{2}\frac{\rho_l \dot{n}}{\dot{m}_l} D^2 \exp - \left(\frac{\pi}{6}\frac{\rho_l \dot{n}}{\dot{m}_l} D^3\right) \tag{5.31}$$

Where ρ_l is the liquid density, $\dot{m}_l$ the liquid mass flow rate, and $\dot{n}$ the droplet number density per unit time. This is a form of the Nukiyama-Tanasawa Distribution Function where distribution parameter (q) is no longer a free variable but equal to 3.

From the definition of SMD given by the following expression

$$D_{32} = \frac{\int_0^\infty \left(D^3 \frac{dN}{dD}\right) dD}{\int_0^\infty \left(D^2 \frac{dN}{dD}\right) dD} \tag{5.32}$$

and substituting Eq. (5.31) into Eq. (5.32) we have an expression of the SMD in terms of the liquid density, the liquid mass flow rate, and the droplet number density per unit time as follows:

$$D_{32} = \frac{1}{\Gamma(\frac{5}{3})}\left(\frac{6}{\pi}\frac{\dot{m}_l}{\rho_l \dot{n}}\right)^{1/3}. \tag{5.33}$$

Similarly from the definition of D30 (Eq. 5.16), we obtain the expression of D30 in terms of the liquid density, the liquid mass flow rate, and the droplet number density per unit time as follow:

$$D_{30} = \left(\frac{6}{\pi}\frac{\dot{m}_l}{\rho_l \dot{n}}\right)^{1/3}. \tag{5.34}$$

From Eq. (5.34) and (5.33), we obtain an expression of D_{30} in terms of D_{32}, from which the value for D_{30} can be obtained once D_{32} is measured from the experiment.

$$D_{30}(x, y) = \Gamma(\tfrac{5}{3}) D_{32}(x, y). \tag{5.35}$$

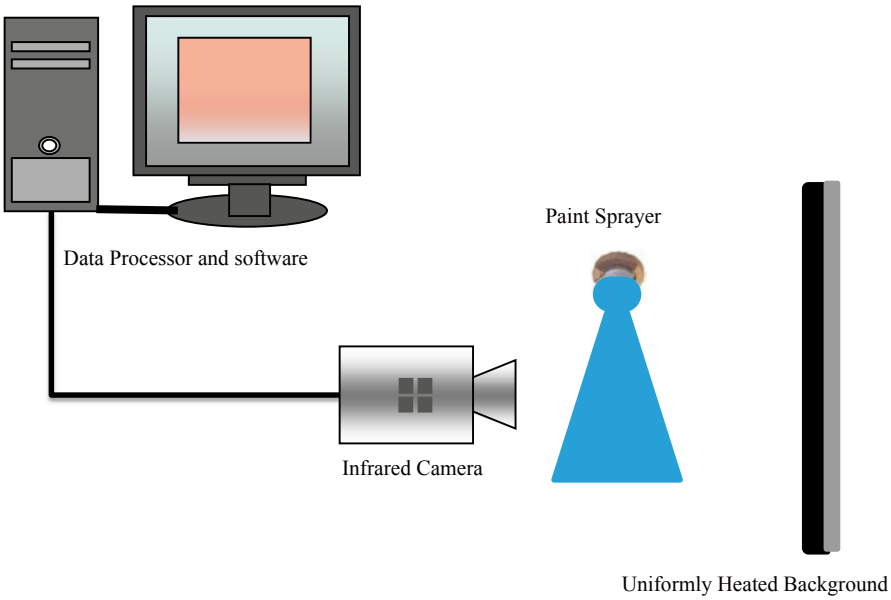

Fig. 5.11 A schematic of the experimental setup for the infrared visualization and characterization technique

Similarly D_{20} is solved from its definition (Eq. (5.13)), yielding:

$$D_{20}(x,y) = [\Gamma(\tfrac{5}{3})]^{1/2} D_{30}(x,y) = [\Gamma(\tfrac{5}{3})]^{1/2}\Gamma(\tfrac{5}{3}) D_{32}(x,y). \tag{5.36}$$

With an expression obtained for D_{20} and D_{30} in terms of D_{32}, one only needs to know D_{32} from which the values of D_{20} and D_{30} can be estimated using these mathematical relationships. The droplet number density can then be obtained using Eq. 5.21.

5.7.3 Practical Application of Infrared Thermography to Paint Spray Visualization and Characterization

A schematic of the experimental setup of the infrared thermography-based visualization and characterization technique is illustrated in Fig. 5.11. The setup includes the paint applicator, the infrared camera, the radiation source, and a data processor. The infrared energy radiated by the background is attenuated by the spray, and the attenuated image is captured by the infrared camera.

To acquire high quality infrared images of the spray flow field, the blackbody background temperature was set at 30 °C. This temperature setting was to allow for a temperature difference between the coldest sections of the spray and the background not to exceed 10 °C. This is necessary for excellent temperature contrast

needed to view details of the spray flow field using infrared imaging. The working fluid was generally at room temperature, with the average temperature measured at 22 °C. The background temperature was allowed to stabilize at the required temperature setting of 30 °C before measurements are made. Once the background temperature stabilizes at 30 °C, the atomizer was started, and the required operational conditions for which the measurements to be acquired are set. The spray was allowed to stabilize under these conditions before images are captured using the infrared camera.

The captured infrared images are later post-processed using the MATLAB image processing toolbox. The temperature map of the spray flow field is expressed as a map of radiant flux per unit surface area (W/m^2), using the following equation:

$$E = \varepsilon \sigma T^4 \tag{5.37}$$

Where ε is the emissivity of the blackbody background given as 0.96, σ is the Stefan-Boltzmann constant, given as $5.670 \times 10^{-8}\ W/m^2 \cdot K^4$, and T the temperature measured by the infrared camera is express in Kelvin.

5.7.4 Infrared Visualization Results

This section presents the visualization results for two atomizers—high speed rotary bell atomizer and high volume low pressure (HVLP) atomizer. Note that the infrared wavelengths are attenuated less than the visible wavelengths by the spray [50, 51]. This is attributable to the fact that the attenuation of the electromagnetic wave within a scattering and an absorbing medium like a liquid spray with the same size distribution will decrease with increasing wavelength within the electromagnetic spectrum.

5.7.4.1 High-Speed Rotary Bell Atomizer Visualization Results

The infrared thermography-based visualization results for the high-speed rotary bell atomizer for a liquid flow rate of 100 cc/min at bell cup rotational speeds of 20,000, 30,000, 40,000, and 50,000 rpm are shown in Fig. 5.12a. Similar plots are repeated for a liquid flow rate of 200 cc/min in Fig. 5.12b, a liquid flow rate of 300 cc/min in Fig. 5.12c, and a liquid flow rate of 400 cc/min in Fig. 5.12d.

The infrared images are captured at 300 frames/s for each bell cup rotational speed. It can be observed from Figs. 5.12a–d that at 20,000 rpm the liquid droplets in the spray travels farther in the radial direction than the other rotational speeds. This behavior is explained in Fig. 5.13. The shaping air, whose primary purpose are to support the transport of the paint droplets, stabilize the flow conditions around the atomizer, and permit a precise alignment of the spray pattern by limiting the atomizing cone which is supplied at a direction perpendicular to the trajectory of the liquid droplets.

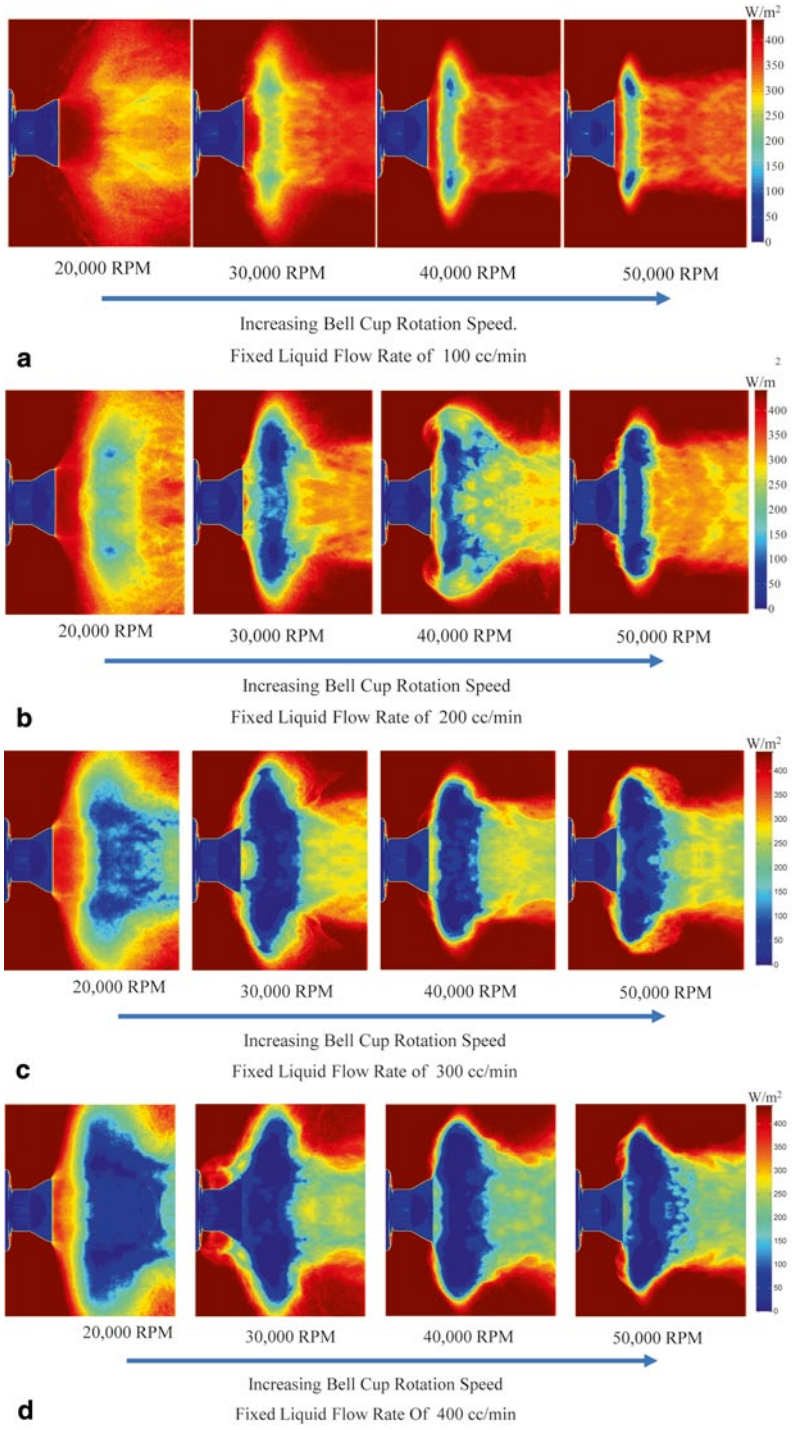

Fig. 5.12 **a** Infrared visualization of the high-speed rotary bell atomizer showing increasing bell cup rotational speed for a liquid flow rate of 100 cc/min. **b** Liquid flow rate 200 cc/min. **c** Liquid flow rate 300 cc/min. **d** Liquid flow rate 400 cc/min

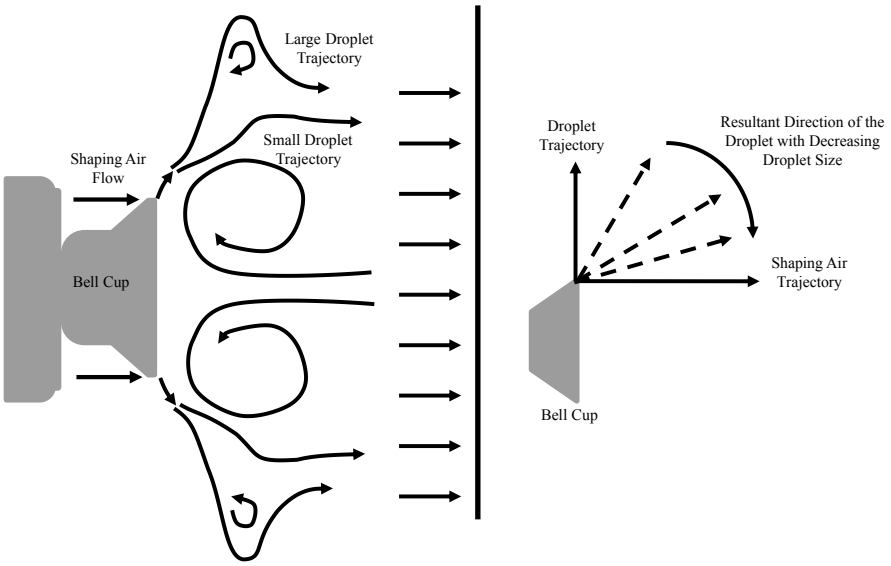

Fig. 5.13 A schematic of the droplet trajectory in the high-speed rotary bell atomizer

The droplets follow a radial trajectory because of the centrifugal force used in generating them. As a result of the presence of the shaping air, the resultant trajectory of the droplets then becomes a function of the inertia of the droplets and the force of the shaping air. The radial travel distance of the droplets reduces with increasing bell cup rotational speed, because the larger droplets have more inertia which resist the momentum force of the shaping airflow. As droplet size reduces with increasing bell cup rotational speed, the droplets become more affected by the shaping airflow, and thus their radial travel is curtailed. Note that the shaping airflow pressure was maintained constant, at 0.4 MPa, for all the conditions tested to simulate a practical operational condition.

Figure 5.14 shows the SMD of the high-speed rotary bell atomizer for a liquid flow rate of 100 cc/min as a function of bell cup rotational speed demonstrating that the SMD values decreases with increasing bell cup rotational speed. Figure 5.15 illustrates the plot of the droplet size distribution for a liquid flow rate of 100 cc/min at various bell cup rotational speeds. A leftward shift of the droplet size distribution is observed with increasing bell cup rotational speed because the droplet size decreases with increasing bell cup rotational speed.

The SMD and the droplet size distribution plots are not repeated here for the other liquid flow rate condition tested because the trend is similar. Figures 5.12a–d shows that under each bell cup rotational speed, the attenuation of the infrared energy increases with increasing liquid flow rates. Figure 5.16 shows the infrared thermographic image of the high-speed rotary bell atomizer with a fixed bell cup rotational speed of 40,000 rpm for increasing liquid flow rate.

The infrared thermographic image obtained is a function of the extinction of the infrared energy radiated by the source as it passes through the spray. The extinction

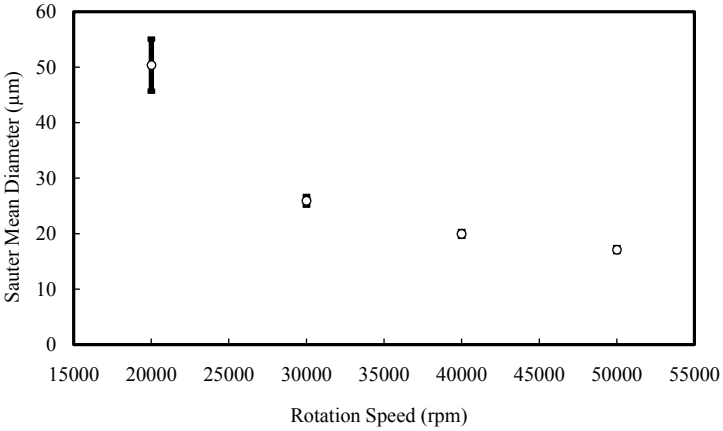

Fig. 5.14 The Sauter mean diameter of the high-speed rotary bell atomizer for a liquid flow rate of 100 cc/min at various bell cup rotational speeds

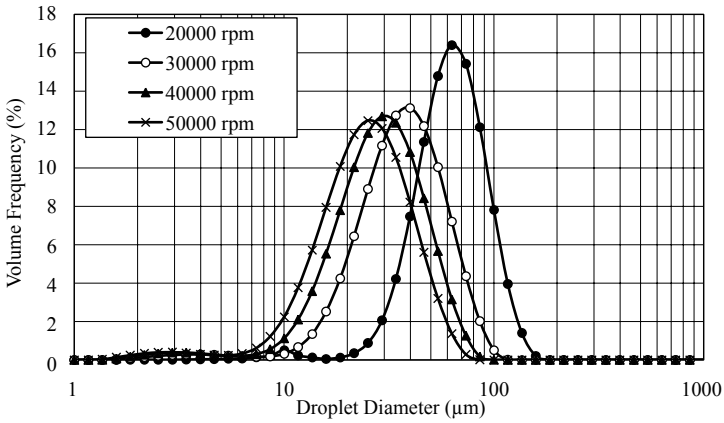

Fig. 5.15 Droplet size distribution of the high-speed rotary bell atomizer for a liquid flow rate of 100 cc/min at various bell cup rotational speeds

is a function of the density of the participating medium (the spray). As the density of the portion of the spray increases, so does the attenuation of the infrared energy. Clearly shown in Fig. 5.16, increase in liquid flow rate increases the density of the spray. The corresponding plot of the SMD is shown in Fig. 5.17 where the SMD increases with increasing liquid flow rate at a constant bell cup rotational speed. To maintain the same SMD at increasing liquid flow rate, the bell cup rotational speed must be increased accordingly.

The high-speed rotary bell atomizer produces axisymmetric sprays, a cross section of which is illustrated in Fig. 5.18. The cross-section at location *a* in Fig. 5.18 has the appearance of a hollow spray; a closer look reveals a toroid shape ring, the

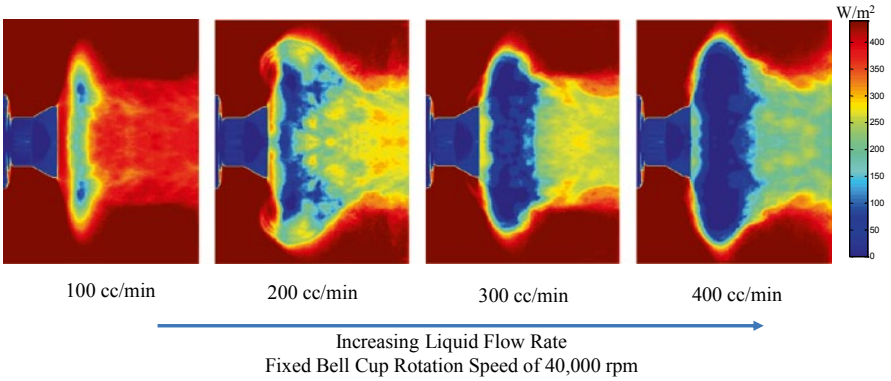

Fig. 5.16 Infrared visualization of the high-speed rotary bell atomizer spray at a bell cup rotational speed of 40,000 rpm, showing increasing liquid flow rate

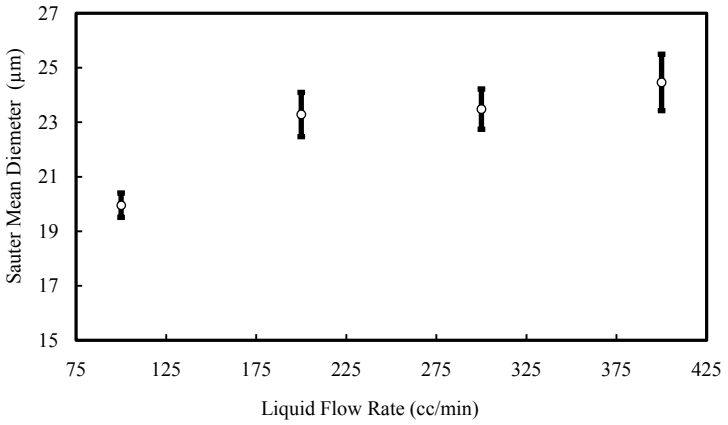

Fig. 5.17 The Sauter mean diameter of the high-speed rotary bell atomizer spray at a bell cup rotational speed of 40,000 rpm, showing increasing liquid flow rate

detail of which is shown in Fig. 5.19, where the infrared images are taken at an angle. The interaction between the liquid droplets and the shaping airflow generate vortices which form a toroid-shaped ring. The illustration of the toroid vortex tube generated as a result of this interaction is shown in Fig. 5.13. Figure 5.18 shows that the toroid shape collapses into a full spray in the cross-section at location *b* further downstream from location *a*.

The toroid-shaped vortex ring observed in the high-speed rotary bell atomizer spray is formed as a result of the interactions between the shaping airflow and the liquid droplets. The interaction between these two high speed flows impinging perpendicularly on each other creates a vortex motion. This vortex motion forms the toroid-shaped vortex ring which exhibits periodic vortex shedding illustrated

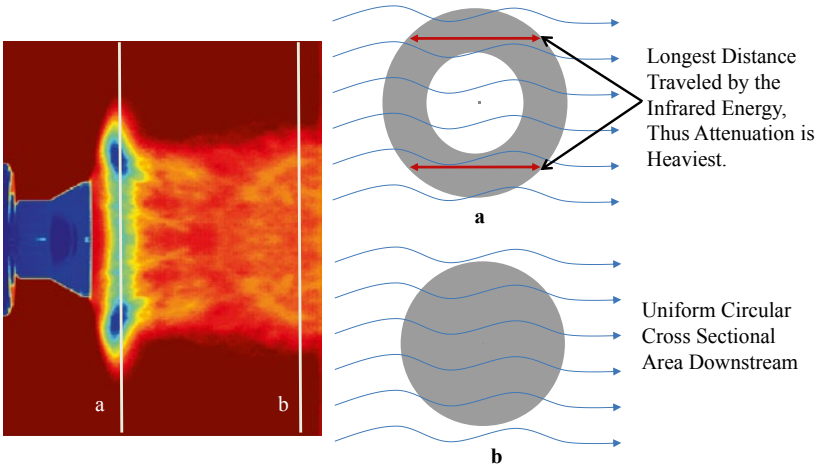

Fig. 5.18 The cross-sectional area of the high-speed rotary bell atomizer spray

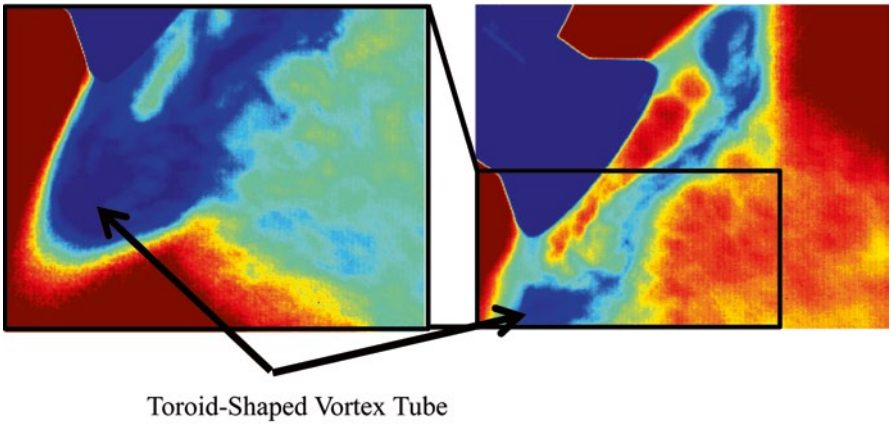

Fig. 5.19 A detailed structure of the toroid-shape inside the high speed rotary bell atomizer spray

in Fig. 5.20. Vortex shedding is an unsteady flow that takes place in special flow velocities. In this flow, vortices develop around the toroid-shaped vortex tube, created as a result of the interaction between the shaping airflow and the liquid droplets which detach periodically from either side of the main vortex tube.

5.7.4.2 High Volume Low Pressure Air-Assisted Atomizer Visualization Results

For the infrared visualization of the HVLP air-assisted atomizer, two measurement orientations are considered to fully describe the spray pattern: the orientation of the

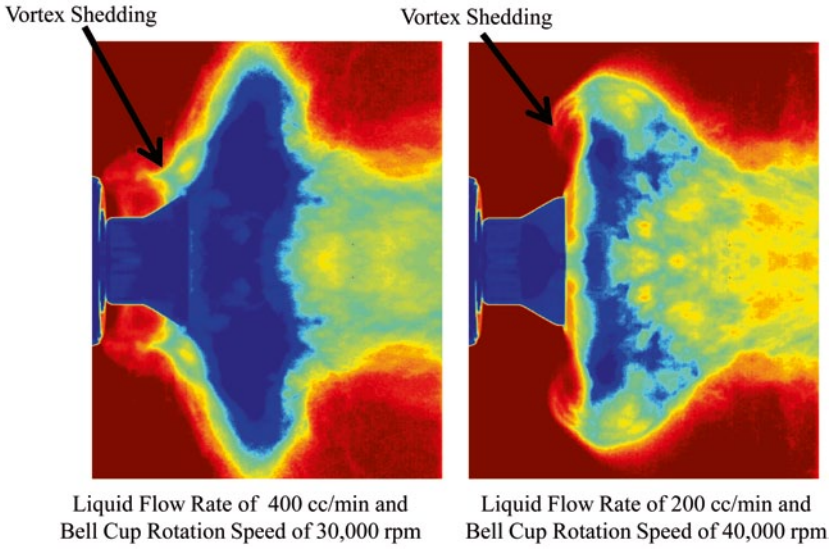

Fig. 5.20 The infrared image showing vortex shedding from the toroid shaped vortex tube

measurement taken along the long axis of the fan-shaped spray (Fig. 5.21a) and the orientation of the measurement taken along the short axis of the fan-shaped spray (Fig. 5.21b).

Unlike the high-speed rotary bell atomizer which produces axisymmetric spray patterns, the HVLP air-assisted atomizer generates a fan-shaped spray. By taking measurements of both orientations and using an edge detection technique, the values of the major axis of the assumed elliptical cross-sectional area of the fan-shaped spray are estimated along the spray axis. With the major axis obtained, the depth of the spray, b, can be computed along the spray axis. The value of b is needed to compute the liquid volume fraction and the droplet number density (Eqs. 5.20 and 5.21).

The infrared visualizations of the long axis of the spray generated by the HVLP air-assisted atomizer are shown in Fig. 5.22 for the increasing liquid flow rate with all other parameters remaining constant. The corresponding infrared visualizations of the short axis of the spray from the HVLP air-assisted atomizer are shown in Fig. 5.23. The SMD and droplet size distribution for these conditions are respectively presented in Figs. 5.24 and 5.25. Figure 5.22 shows that the spray angle opens up with an increase in the liquid flow rate while keeping all other operational parameters constant. Correspondingly, in Fig. 5.23 the SMD increases almost linearly with an increase in the liquid flow rate. Figure 5.25 shows a rightward shift of the droplet size distribution with an increase in the liquid flow rate.

The infrared signal attenuation gets stronger as the droplet sizes and concentrations increase (Fig. 5.22), as demonstrated in the image of the short axis showing a much denser spray because the optical path length is longer. The increasing liquid flow rate shows a progressively denser core from a liquid flow rate of 100 cc/min

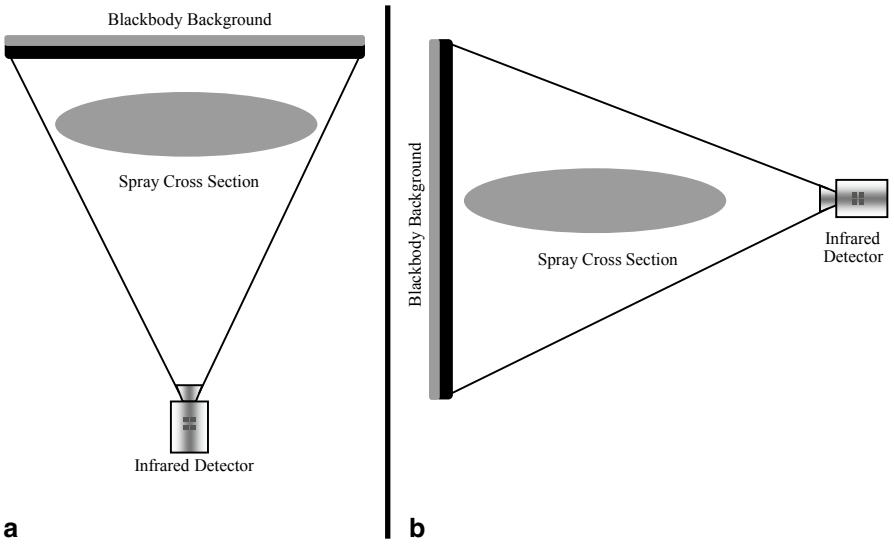

Fig. 5.21 A schematic of the cross section of the flat spray and the measurement orientation. **a** Orientation for the long axis. **b** Orientation for the short axis

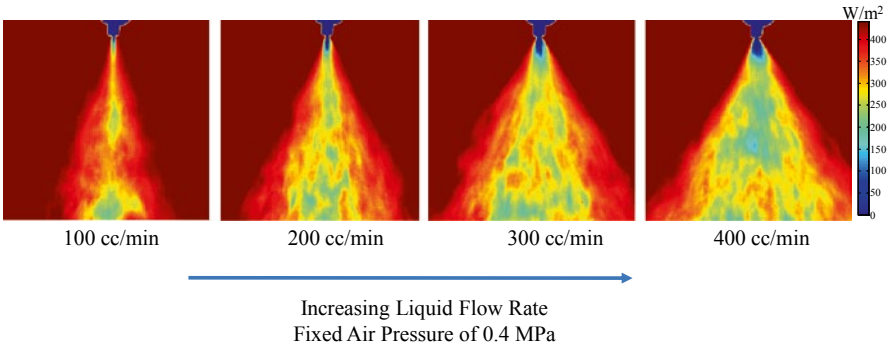

Fig. 5.22 Infrared themographic images of the long axis of the HVLP air-assisted atomizer, with increasing liquid flow rate at a fixed air pressure of 0.4 MPa

to 400 cc/min, with the less dense core observed at a liquid flow rate of 100 cc/min, and the densest core observed at 400 cc/min.

Figure 5.26 shows the infrared images for the HVLP air-assisted atomizer illustrating the increasing spray angle as a result of increasing liquid flow rates while maintaining all other operational parameters. The spray angle at a liquid flow rate of 100 cc/min was measured to be about 40°. For a liquid flow rate of 200 cc/min, the spray angle was determined to be about 50° and about 65° for a liquid flow rate of 300 cc/min. For a liquid flow rate of 400 cc/min, the spray angle was assessed to be about 70°.

A careful observation of the infrared thermographic images obtained for the HVLP air-assisted atomizer measured along the short axis (Fig. 5.23), reveals an ex-

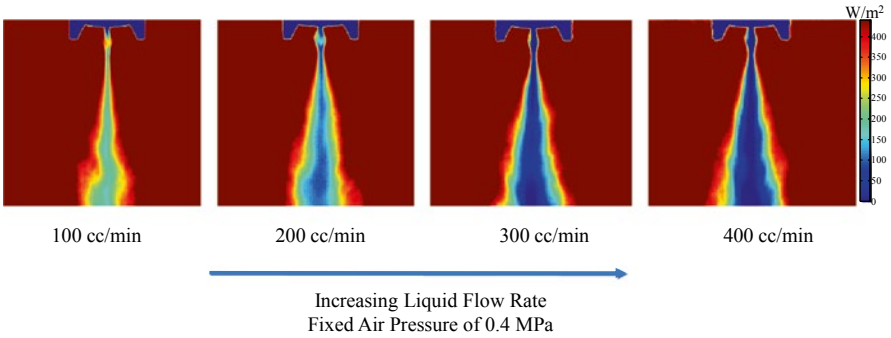

Fig. 5.23 Infrared themographic images of the short axis of the HVLP air-assisted atomizer, with increasing liquid flow rate at a fixed air pressure of 0.4 MPa

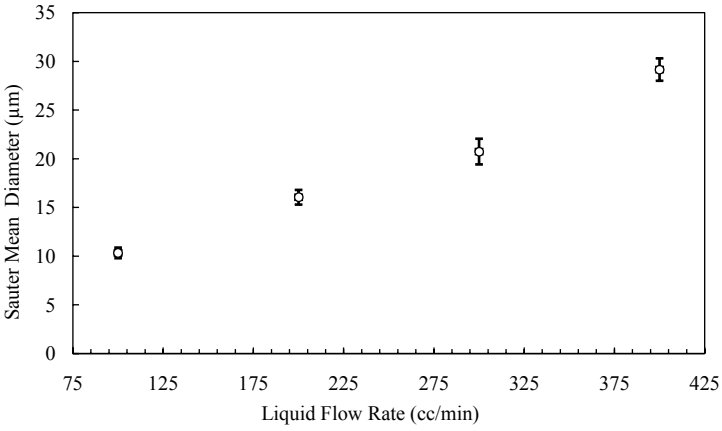

Fig. 5.24 The Sauter mean diameter of the HVLP air-assisted atomizer with increasing liquid flow rate

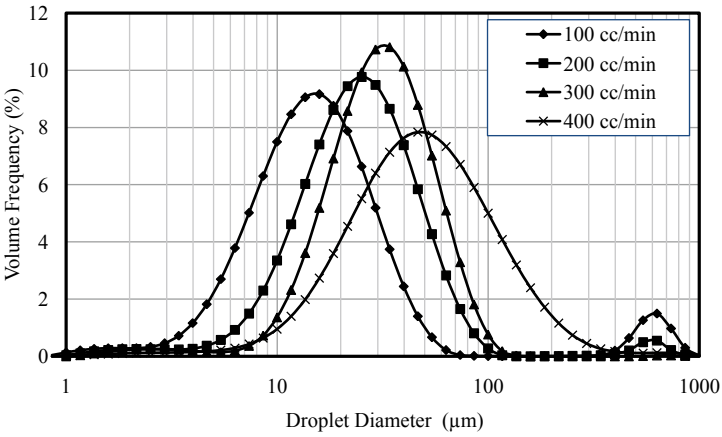

Fig. 5.25 Droplet size distribution of HVLP air-assisted atomizer at various flow rates

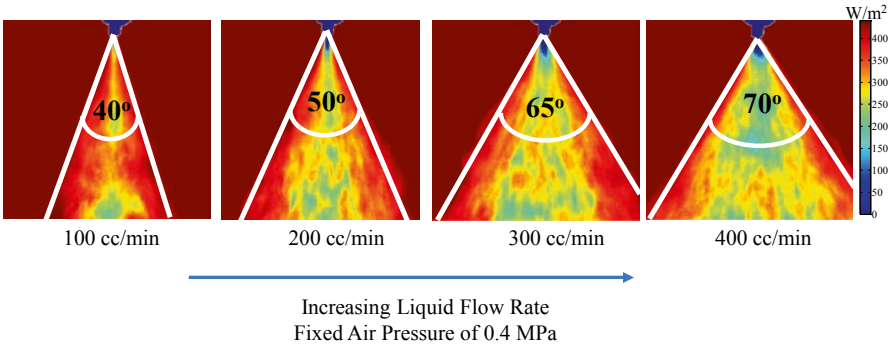

Fig. 5.26 Infrared themographic images of the long axis of the HVLP air-assisted atomizer, with increasing liquid flow rate at a fixed air pressure of 0.4 MPa showing increasing spray angle

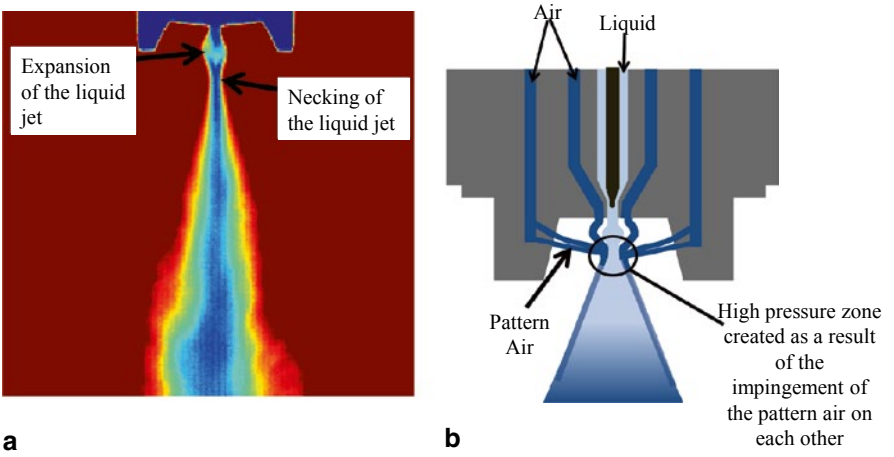

Fig. 5.27 A schematic explaination of the expansion and necking in the infrared images along the short axis of the HVLP air-assisted atomizer. **a** The infrared image showing the bottleneck. **b** schematics explaining the phenomenon

pansion region just outside of the nozzle exit. The liquid jet emerging from the liquid nozzle opening comes into contact with the annulus atomizing air. Figure 5.27 show that the two-fluid mixture appears to expand just outside the nozzle exit, and then necking is observed before the spray begins to open up.

The lateral air supplied from both sides of the spray impinges on each other and is used to adjust the shape of the spray pattern. The impingement of the lateral pattern air creates a high pressure zone which forces the twin fluid mixture emerging from the nozzle to form a bottleneck at the region of the impingement. This constriction, as a result of an increased pressure zone, causes the jet upstream to expand creating the blob that is observed in Fig. 5.26 and is explained by the illustration in Fig. 5.27b.

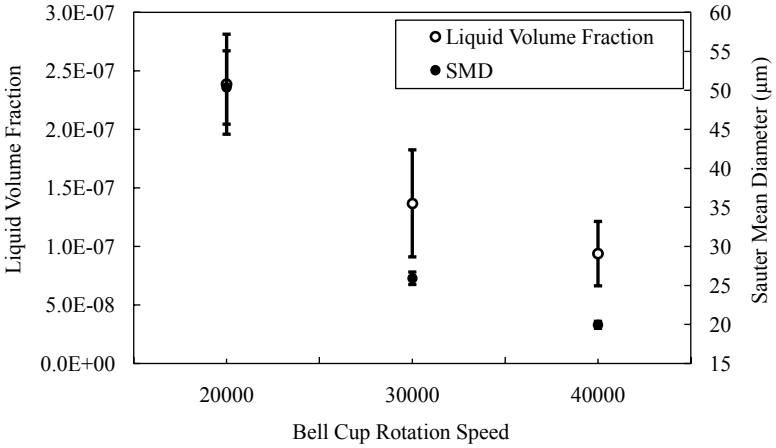

Fig. 5.28 A comparison of the liquid volume fraction and the Sauter mean diameter for the high-speed rotary bell atomizer showing increasing bell cup rotational speed for a liquid flow rate of 100 cc/min

5.7.4.3 The Volume Fraction and the Number Density Results for High-Speed Rotary Bell Atomizer

The droplet size measurements are made along the spray center line 150 mm downstream from the rotary bell cup exit, using the Malvern Spraytec system. The images are analyzed at a pixel location corresponding to the measurement volume of the Malvern Spraytec system. With the SMD (D_{32}) obtained, the liquid volume fraction f_v, is calculated at the chosen pixel location using Eq. (5.20). The corresponding droplet number density is obtained from Eq. (5.21). The data were processed and averaged in time over 900 frames obtained at 300 frames/s.

Figure 5.28 compares the liquid volume fraction and the SMD as a function of bell cup rotational speed at a pixel location on the spray centerline 150 mm from the rotating bell cup tip for a fixed liquid flow rate of 100 cc/min. Figure 5.29 compares the droplet number density and the SMD as a function of bell cup rotational speed at a pixel location on the spray centerline 150 mm from the rotating bell cup tip for a fixed liquid flow rate of 100 cc/min. Similar results for a liquid flow rate of 400 cc/min are shown in Figs. 5.30 and 5.31 for the liquid volume fraction and the droplet number density, respectively. The trend for both liquid flow rates was similar, with both the liquid volume fraction and the SMD decreasing while the bell cup rotational speed was increasing. On the other hand, the droplet number density increased with decreasing SMD and increasing bell cup rotational speed.

As the droplet size reduced, the liquid volume fraction f_v, which is defined as the ratio of equivalent volume of the liquid to a given volume of the gas and liquid mixture, decreased accordingly. This occurred because as the spray mixture became finer, air (which is the continuous medium) fills in between the droplets,

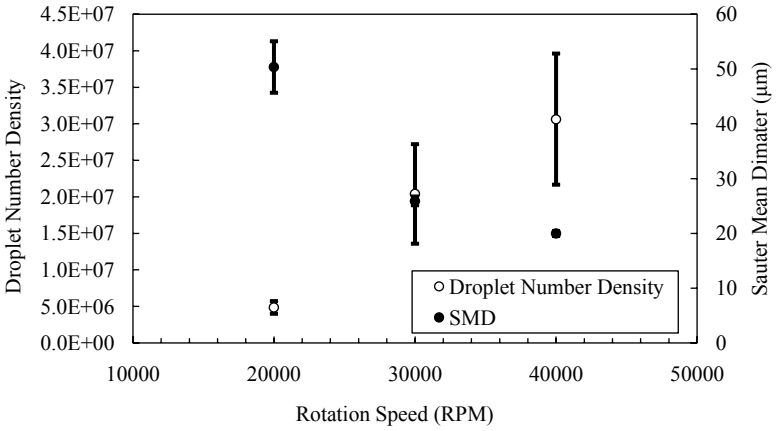

Fig. 5.29 A comparison of the droplet number density and the Sauter mean diameter for the high-speed rotary bell atomizer showing increasing bell cup rotational speed for a liquid flow rate of 100 cc/min

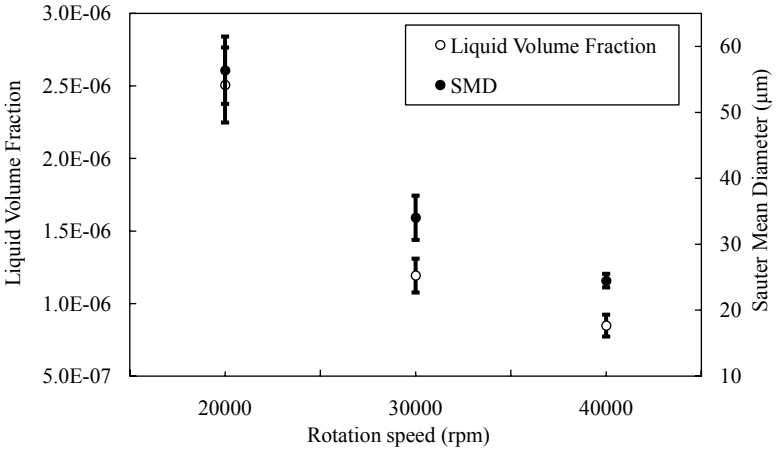

Fig. 5.30 A comparison of the liquid volume fraction and the Sauter mean diameter for the high-speed rotary bell atomizer showing increasing bell cup rotational speed for a liquid flow rate of 400 cc/min

consequently causing the volume fraction to reduce. Similarly, the droplet number density, which is defined as the number of liquid droplets per unit volume, increases with decreasing droplet size. This is attributable to the fact that as the spray becomes finer, the number of liquid droplets occupying a given volume in the spray increases as bigger droplets breakdown to form smaller droplets, the number count per unit area increases.

Figure 5.32, compares the liquid volume fraction and the SMD as a function of liquid flow rate at a pixel location on the spray centerline 150 mm from the rotat-

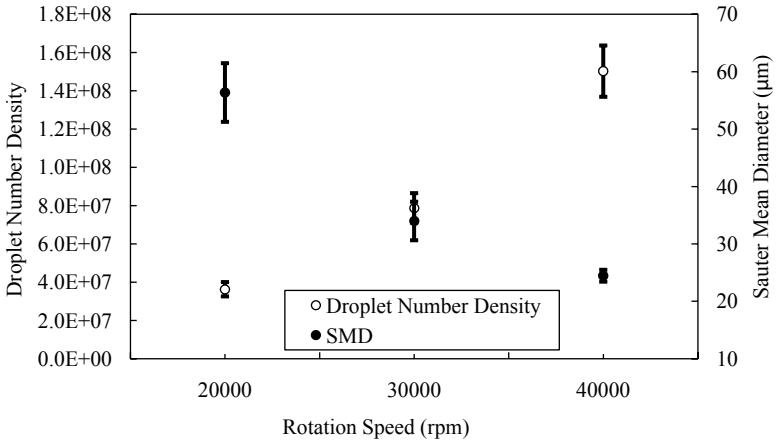

Fig. 5.31 A comparison of the droplet number density and the Sauter mean diameter for the high-speed rotary bell atomizer showing increasing bell cup rotational speed for a liquid flow rate of 400 cc/min

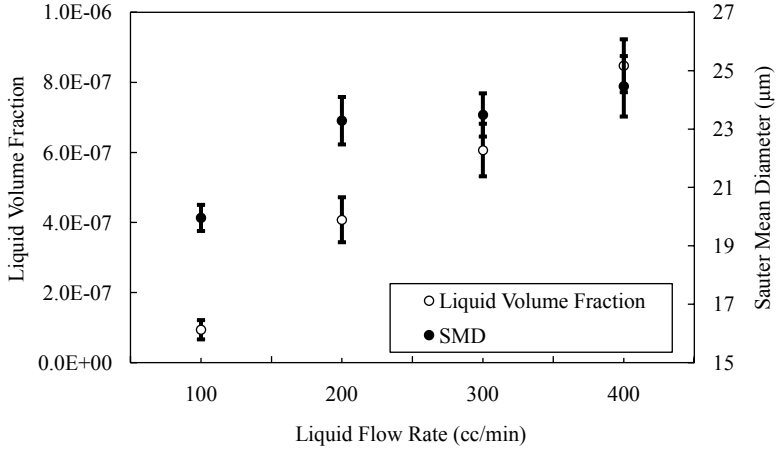

Fig. 32 A comparison of the liquid volume fraction and the Sauter mean diameter for the high-speed rotary bell atomizer showing increasing liquid flow rate for a fixed bell cup rotational speed of 40,000 rpm

ing cup tip for a fixed bell cup rotational speed of 40,000 rpm. Similarly, Fig. 5.33 compares the droplet number density and the SMD as a function of liquid flow rate at a pixel location on the spray centerline at 150 mm from the rotating bell cup tip for a fixed bell cup rotational speed of 40,000 rpm. The SMD, the liquid volume fraction, and the droplet number density all increase with increasing liquid flow rate at a fixed bell cup rotational speed of 40,000 rpm.

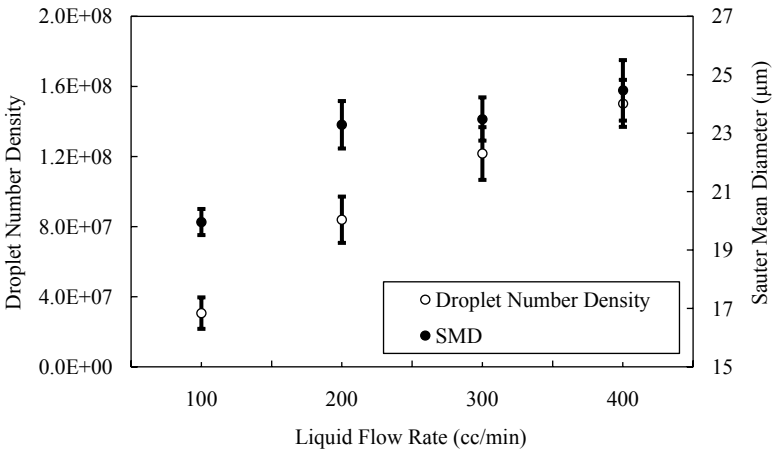

Fig. 33 A comparison of droplet number density and the Sauter mean diameter for the high-speed rotary bell atomizer showing increasing liquid flow rate for a fixed bell cup rotational speed of 40,000 rpm

5.7.4.4 Volume Fraction and Number Density Results for High Volume Low Pressure Air-Assisted Atomizer

As was in the case of the high-speed rotary bell atomizer, the droplet size measurements for the HVLP air-assisted atomizer are made along the spray center line of the longer cross sectional axis at 100 mm downstream from the nozzle exit using the Malvern Spraytec system. The infrared images are analyzed at a pixel location corresponding to the measurement volume of the Malvern Spraytec system. With the SMD obtained, the liquid volume fraction f_v is calculated at the chosen pixel location using Eq. (5.20). The corresponding droplet number density is obtained from Eq. (5.21). The data were processed and averaged in time over 900 frames obtained at 300 frames/s. The standard deviations for the measurement are shown as error in the plot.

Figure 5.34 compares the average liquid volume fraction and the average SMD as a function of liquid flow rate at a pixel location on the spray centerline 100 mm from the nozzle exit for a fixed air pressure of 0.4 MPa. Similarly, Fig. 5.35 compares the average droplet number density and the SMD as a function of liquid flow rate at a pixel location on the spray centerline at 100 mm from the nozzle exit for an air pressure of 0.4 MPa. The SMD and the liquid volume fraction increases with increasing liquid flow rate. The droplet number density, on the other hand, decreases with increasing liquid flow rate.

5.7.5 Comparison between the High-Speed Rotary Bell Atomizer and the HVLP Air-Assisted Atomizer

Figure 5.33 shows the average droplet number density and the average SMD as a function of liquid flow rate for the high-speed rotary bell atomizer and Fig. 5.35 for

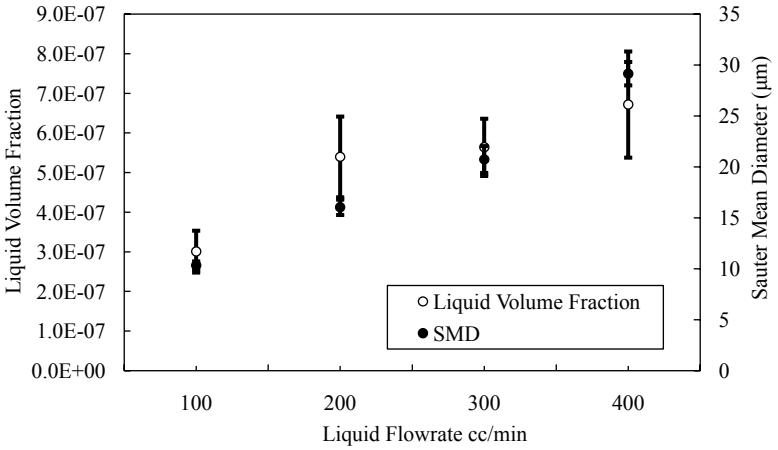

Fig. 34 A comparison of the liquid volume fraction and the Sauter mean diameter for HVLP air-assisted atomizer showing increasing liquid flow rate at a fixed air pressure of 0.4 MPa

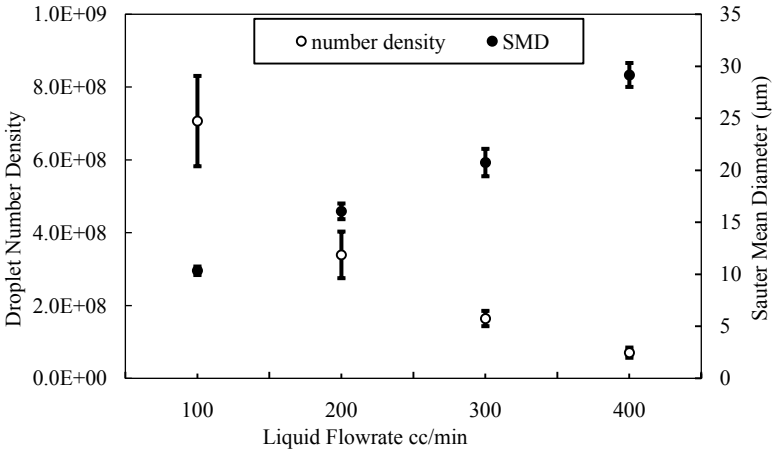

Fig. 35 A comparison of the droplet number density and the Sauter mean diameter for HVLP air-assisted atomizer showing increasing liquid flow rate at a fixed air pressure of 0.4 MPa

the HVLP air-assisted atomizer. Comparison of these two-figure results indicates that the droplet number density and SMD increases with increasing flow rate in Fig. 5.33 for the high-speed rotary bell atomizer, while the droplet number density decreases with increasing SMD and liquid flow rate for the HVLP air-assisted atomizer (Fig. 5.35).

The explanation of the difference in the variation of droplet number densities with increasing liquid flow rates lies in the atomization mechanism resulting in the shape of the spray produced by both atomizers. Infrared visualization of the spray from both atomizers with increasing liquid flow rate is shown in Fig. 5.15 and for the high-speed rotary bell atomizer and in Fig. 5.22 for the HVLP air-assisted atom-

izer. Figure 5.15 illustrates that with increasing liquid flow rate, the spray generated by the high-speed rotary bell atomizer occupies the same space while maintaining its shape. This implies that the spray becomes denser and increases in droplet number densities with increasing flow rates. As the spray generated by the HVLP air-assisted atomizer opens up in Fig. 5.22, the spray pattern becomes larger, and the spray angle grows from 40° at the liquid flow rate of 100 cc/min to 70° at a liquid flow rate of 400 cc/min. As a result, the area of the spray envelope becomes larger with the increasing liquid flow rates. With the enlarging spray envelope, the increasing droplet sizes, and liquid flow rates the spray becomes less dense and decreases in droplet number density.

5.8 Conclusion

Automotive coating is an expensive operation compounded by increasing global awareness about protecting our environment. This chapter provided a general overview of automotive coating, and presents a novel method for visualizing and characterizing paint spray. The method uses an infrared camera as a receiver and a uniformly heated background as a thermal radiation source. The technique provides images in which the value associated with each pixel accounts for the amount of infrared energy emitted by the source and attenuated by the spray. As a consequence of the scattering and absorption taking place, the attenuation of the infrared energy occurs, and the infrared detector receives a reduced signal.

The performance of the method was tested using two different types of atomizers: the high-speed rotary bell atomizer and the low pressure air atomizer. Macroscopic features like spray pattern and angle, together with the flow structure in the entire spray flow field, were obtained and presented. Several theoretical and empirical correlations were derived from which the liquid droplet volume fraction and the liquid droplet number density of the spray were estimated from the visualization data with the SMD acquired via the Malvern Spraytec system.

The visualization method presented here has an advantage over visual photography in the sense that, radiation with wavelength in the visible band of the electromagnetic spectrum is attenuated more than radiation with wavelength in the infrared band. As a result, the method presented in this chapter has the potential to reveal detailed structure inside a medium than visible photography. The new technique offers a unique application of the infrared transmission mode widely used in nondestructive testing to view a multiphase medium.

In summary, the results presented herein demonstrate that this new technique has great promise in the qualitative characterization of sprays. As compared to other optical methods available, this new technique is easy to setup and takes very little time to acquire a high quality image of the spray. It can be applied in environments where current laser-based illumination photographic methods cannot be used, making a real-time and in-process imaging of spray transfer processes possible.

References

1. McKnight, M.E., Martin, J.W.: Advanced methods and models for describing coating appearance. In: Proceedings of organic coatings—waterborne; high solids; powder coatings, 23rd International Conference, Athens, Greece, pp. 307–319, 7–11 July 1997
2. Bruan, J.H., Fields, D.P.: Gloss of paint films: effects of pigment size. J. Coat. Technol. **66**, 93–98 (1994)
3. Frohn, A., Roth, N.: Dynamics of droplet. Springer, New York (2000)
4. Sirignano, W.A.: Fluid dynamics and transport of droplets and sprays. Cambridge University Press, New York (1999)
5. Lefebvre, H.: Atomization and sprays. Hemisphere Pub. Corp, New York (1989)
6. Sirignano, W.A.: Fluid dynamics of sprays—1992 freeman scholar lecture. J. Fluid Eng. **115**, 345–378 (1993)
7. Liu, H.: Science and engineering of droplets: fundamentals and applications. Noyes Publications, New York (2000)
8. Im, K.-S., Lai, M.-C., Liu, Y., Sankagiri, N., Loch, T., Nivi, H.: Visualization and measurement of automotive electrostatic rotary-bell paint spray transfer processes. J. Fluid Mech. **123**, 237–245 (2001)
9. Dominick, J., Thieme, M.: Atomization characteristics of high-speed rotary bell atomizers. Atomization and Sprays **16**, 857–874 (2006)
10. Schick, R.J.: An engineer's practical guide to drop size. Spraying Systems Co, Wheaton (1997)
11. Mugele, R.A., Evans, H.D.: Droplet size distribution in sprays. Ind. Chem. **43**, 1317–1324 (1951)
12. Nukiyama, S., Tanasawa, Y.: Experiments of the atomization of liquids in an airstream. Trans. Soc. Mech. Eng. Japan **5**, 62–75 (1939)
13. Li, X., Tankin, R.S.: Droplet size distribution: a derivative of a Nukiyama-Tanasawa type distribution function. Combust. Sci. Technol. **56**, 65–76 (1987)
14. Li, X., Tankin, R.S.: Droplet size distribution in sprays by using information theory. Combust. Sci. Technol. **60**, 345–357 (1988)
15. Semio V., Andare, P., Carvalho, M.: Spray characterization: numerical prediction of Sauter mean diameter and droplet size distribution. Fuel **75**, 1707–1714 (1996)
16. Dumouchel, C., Boyaval, S.: Use of the maximum entropy formalism to determine drop size distribution characteristics. Part. Part. Sys. Charact. **16**, 177–184 (1999)
17. Ayres, D., Caldas, M., Semiao, V., Da GracaCarvalho, M.: Prediction of the droplet size and velocity joint distribution for sprays. Fuel **80**, 383–394 (2001)
18. Cao, J.: On the theoretical prediction of fuel droplet size distribution in nonreactive diesel sprays. J. Fluids Eng. **124**,182–185 (2002)
19. Black, D.L., McQuay, M.Q.: Laser-based particle measurements of spherical and on spherical particles. Int. J. Multiph. Flow **27**, 1333–1362 (2001)
20. Black, D.L., McQuay, M.Q., Bonin, M.P.: Laser-based techniques for particle size measurement: a review of sizing methods and their industrial applications. Prog. Energy Combust. Sci. **22**, 267–306 (1996)
21. Swithenbank, J., Beer, J.M., Taylor, D.S., Abbot, D., McCreath, C.G.: A laser diagnostic for the measurement of droplet and particle size distribution. In: 14th American Institute of Aeronautics and Astronautics, Aerospace Sciences Meeting, Washington, D.C: AIAA Paper; pp. 76–99, 26–28 Jan 1976
22. Domann, R., Hardalupas, Y.: Evaluation of the planar drop sizing technique. In: Proceedings of ICLASS, Pasadena, California, 16–20 July 2000
23. Durst, F., Zare, M.: Laser doppler measurements in two phase flows. In: Proceedings of the LDA-Symposium, Copenhagen, Denmark, pp. 403–429, 25–28 Aug 1975

24. Manasse, U., Wriedt, T., Bauckhage, K.: Phase-doppler sizing of optically absorbing liquid droplets: comparison between mie theory and experiment. Part. Part. Sys. Charact. **9**, 176–185 (1992)
25. Manasse, U., Wriedt, T., Bauckhage, K.: Phase doppler sizing of optically absorbent single and multicomponent liquid droplet using semiconductor devices. Meas. Sci. Technol. **4**(3), 369–377 (1993)
26. Bachalo, W.D.: The phase doppler method: analysis, performance evaluations, and applications. Part. Part. Sys. Charact. **11**, 73–83 (1994)
27. Damaschke, N., Gouesbet, G., Grehan, G., Mignon, H., Tropea, C.: Response of PDA systems to non-spherical droplets. In: Proceedings of ILASS-Europe, Florence, Italy, pp. 382–388 (1997)
28. Pitcher, G., Wigley, G.: A study of the break-up and atomisation of a combusting diesel spray by phase doppler anemometry. In: Proceedings of the 6th International Symposium on Application of Laser Techniques to Fluid Mechanics, Lisbon, Portugal (1992)
29. Pitcher, G., Wigley, G.: Simultaneous two-component velocity and drop-size measurements in a combusting diesel spray. In: Proceedings of the 7th International Symposium on Application of Laser Techniques to Fluid Mechanics, Lisbon, Portugal (1994)
30. Hirleman, E. D.: Modeling of multiple scattering effects in Fraunhofer diffraction particle size analysis. Part. Part. Sys. Charact. **5**(2), 57–65 (1988)
31. Herbst, A.: Droplet sizing on agricultural sprays—a comparison of measurement systems using a standard droplet sizing classification scheme. In: Conference on liquid atomization and spray systems, Zurich, Switzerland, Sept 2001
32. Whybrew, A., Nicholls, T.R., Boaler, J.J., Booth, H.J.: Diode lasers—a cost effective tool for simultaneous visualization, sizing and velocity measurements of sprays. In: Proceedings of ILASS-Europe, Toulouse, France, 5–7 July 1999
33. Yule, A.J., Chigier, N.A., Cox, N.W.: Measurement of particle sizes in sprays by the automated analysis of spark photographs. Particle size analysis. In: Proceedings of a conference organized by the Analytical Division of the Chemical Society and held at the University of Salford, 12–15 Sept 1977, pp. 61–73, Heyden Press, Salford (1978)
34. Kashdan, J.T., Shrimpton, J.S., Booth, H.J., Whybrew, A.: Assessment of particle characterization via phase doppler anemometry and automated particle image analysis techniques. In: Proceedings of the 10th International Symposium on Application of Laser Techniques to Fluid Mechanics; Lisbon, Portugal, 10–13 July 2000
35. Settles, G.S.: A flow visualization study of airless spray painting. In: Proceedings of the 10th Annual Conference on Liquid Atomization and Spray Systems. Ottawa, Canada, pp. 145–149, 18–21 May 1997
36. Schober, P., Meier, R., Schafer, O., Wittig, S.: Visualization and phase doppler particle analysis measurement of oscillating spray propagation of an airblast atomizer under typical engine conditions. Annals N Y Acad. Sci. **972**, 277–281 (2002)
37. Lee, S-W., Murata, Y., Daisho, Y.: Spray and combustion characteristics of dimethyl ether fuel. Proceedings of Institute of Mechanical Engineers Part D. J. Automob. Eng. **219**, 97–102 (2005)
38. Versteeg, H.K., Hargrave, G.K., Kirby, M.: Internal flow and near-orifice spray visualization of a model pharmaceutical pressurized metered dose inhaler. J. Phy. Conference Series, **45**, 207–213 (2006)
39. Mayinger, F., Feldmann, O.: Optical measurements, techniques and applications. Springer, New York (2001)
40. Settles, G.S.: Schlieren and shawdograph techniques, visualizing phenomena in transparent media. Springer, New York (2001)
41. Settles, G.S., Hackett, B.H., Miller, J.D., Weinstein, L.M.: Full-scale Schlieren flow visualization. In: Crowder, J.P. (ed.) Flow Visualization VII. Begell House, New York (1995)
42. Bellofiore, A., Ragucci, R., Di Martino, P., Cavaliere, A.: Taylored binarization of spray shadowgrams for morphhology investigation. In: 2007 Annual Meeting of the Italian Section of the Combustion Institute, Napoli, Italy, 20–22 June 2007

43. Bae, C., Yu, J., Kang, J., Kong, J.: Effect of nozzle geometry on the common-rail diesel spray. Society of Automotive Engineers, Technical Paper Series 2002–01–1625 (2002)
44. Feldmann, O., Mayinger, E.H.F., Gebhard, P.: Evaluation of pulsed laser holograms of flashing sprays by digital image processing and holographic particle image velocimetry. Nucl. Eng. Des. **184**, 239–252 (1998)
45. Akafuah, N.K.: Visualization and characterization of ultrasonic cavitating atomizer and other automotive paint sprayers using infrared thermography. PhD Thesis, University of Kentucky (2009)
46. Tien, C.L., Drolen, B.L.: Thermal radiation in particulate media with dependent and independent scattering. Annu. Rev. Numer. Fluid Mech. Heat Transfer **1**, 1–32 (1987)
47. Modest, M.F.: Radiative heat transfer. McGraw-Hill, New York (1993)
48. Van de Hulst, H.C.: Light Scattering by Small Particles. Wiley, New York (1981)
49. Matzler, C.: MATLAB Functions for Mie Scattering and Absorption, Research Report No. 2002–08, Institut fur Angewandte Physik (2002)
50. Labs, J., Parker, T.: Diesel fuel spray droplet sizes and volume fractions from the region 25 mm below the orifice. Atomization and Sprays **13**(5–6), 425–442 (2003)
51. Labs, J., Parker, T.: Two-dimensional droplet size and volume fraction distribution from the near-injector region of high-pressure diesel sprays. Atomization and Sprays **16**(7), 425–442 (2006)

Part IV
Painting Technology—Research and Education—An Integrative Approach

Chapter 6
Hitozukuri and Monozukuri in Relation to Research and Development in Surface Coating

K. Saito, A. J. Salazar, K. Kreafle and E. Grulke

Abstract This chapter addresses the rich set of meanings evoked by the terms *monozukuri* and *hitozukuri*, which refer to a centuries-old philosophy deeply rooted in Japanese culture. The former refers to the art of making things with excellence, skill, spirit, zeal, pride, and more. The latter refers to the need to educate and train a person to become expert in *monozukuri*. Together, *monozukuri* and *hitozukuri* can provide the basis for a balanced approach to using technology and enhancing human capacities, one where integration and synthesis play a more important role than specialization and analytical skills. This chapter is intended to address how *monozukuri* and *hitozukuri* can be applied to benefit twenty-first century advanced manufacturing, using automobile painting technology research and development as an example.

Keywords *Monozukuri* · *Hitozukuri* · Globalization · Win-win partnership · Spray painting technology · Painted surface inspection · A new generation painting system

K. Saito (✉) · A. J. Salazar · K. Kreafle · E. Grulke
Institute of Research for Technology Development, College of Engineering,
University of Kentucky, 40506-0503, Lexington, KY, USA
e-mail: saito@engr.uky.edu

A. J. Salazar
e-mail: ajsala00@uky.edu

K. Kreafle
e-mail: ken.kreafle@tema.toyota.com

E. Grulke
e-mail: egrulke@engr.uky.edu

K. Toda et al. (eds.), *Automotive Painting Technology,*
DOI 10.1007/978-94-007-5095-1_6,

6.1 Introduction

The University of Kentucky's Institute of Research for Technology Development (IR4TD) operates through interdependent and sustainable partnership with industry. This unique institute is a good example of University of Kentucky's (UK) effort to seek a new and better way of doing research, education, and service.

It is sometimes claimed that industry and academia are two very different cultures, with the former concerned with how to deliver reasonably-priced high quality products to customers in a timely fashion [1], while the latter academic institutions, focus on education, research, and service. Yet this difference does not mean there is no common ground. Toyota's Chairman, Fujio Cho stressed the importance of "hitozukuri and monozukuri" in his anniversary lecture at Toyota Motor Vietnam [2]. A common mission does exist between companies that value "hitozukuri and monozukuri" and academic institutions that focus on education and research. This chapter discusses IR4TD's win-win strategy in R&D based on principles of hitozukuri and monozukuri, and our recent progress in surface coating and inspection technology.

Hitozukuri and monozukuri (both are Japanese words) may require some explanation for non-Japanese audiences. Monozukuri consists of "mono" which means "products," and "zukuri" which means "process of making or creation". But the word means more than simply making something; it has overtones of excellence, skill, spirit, zest, and pride in the ability to make things, good things, very well. Monozukuri is not mindless repetition; it requires creative minds and is often related to craftsmanship which can be learned through lengthy apprenticeship practice rather than the structured curricula taught at traditional schools. Monozukuri represents the maker's philosophy of how to make things—the philosophy deeply rooted to Japanese tradition in Zen [3], and Confucius's teaching [4], two important pillars to support the centuries-old, Japanese culture. Monozukuri is therefore a philosophy rather than technique or method.

If "mono" is replaced with "hito" which means human, monozukuri becomes hitozukuri, education the closest English word. But hitozukuri contains a much broader meaning and stresses a life-long process of learning. Hitozukuri emphasizes several different steps of human development, whose original form was emphasized by Confucius in his famous six different human development stages. It goes: "when I (Confucius) was fifteen years old, I decided to study; at thirty I became independent; at forty I focused; at fifty I realized my mission in my life; at sixty I became able to listen to people without bias and prejudice; finally at seventy I attained the stage that my thinking and action are harmonized with nature" [4]. Hitozukuri is a continuous life-long process of human development.

Looking at education and research on the other side of world, America, the National Science Foundation which provides funding for American universities and government laboratories to study broader aspects of science and engineering, assesses the effectiveness of academic institutions based on productive faculty, quality students, and a strong support system. Productive faculty and quality students require a special academic environment that supports the current education and

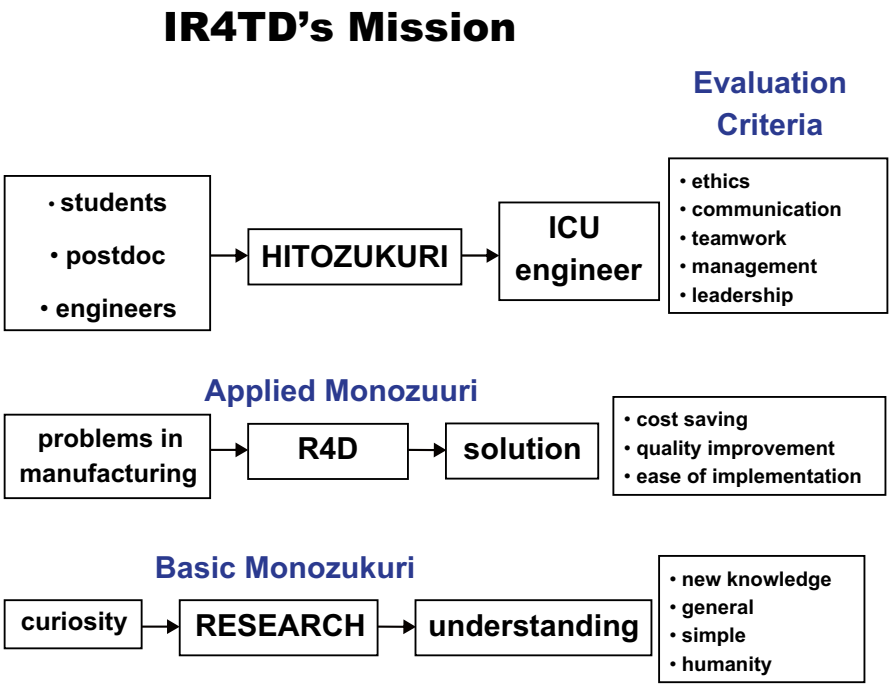

Fig. 6.1 Schematic diagram of IR4TD's mission in hitozukuri and monozukuri

research and stimulates their future learning and research. Creating a supportive and stimulating environment for all the members of IR4TD research team to function best is important but challenging, since all individuals think and act differently. Therefore, IR4TD encourages each individual to go through a particular training to find each individual's strengths and utilize his or her strengths to achieve the status of ICU (innovative, creative and unique) engineer. ICU engineer is a product of past, present and future—the current stage of the researcher's innovative mind comes from his or her unique past history which will help his or her creativity now and in future activities. Figure 6.1 describes a schematic of hitozukuri, applied and basic research (here applied research is called applied monozukuri and basic research is called basic monozukuri).

There are two different types of University research: curiosity-driven basic research (basic monozukuri) and purpose-driven applied research (applied monozukuri). R4D is a good example of applied research. IR4TD believes that it is important to keep both applied and basic research, because if university researchers only conduct R4D research by staying inside the boundary determined by a well focused R4D plan, ignoring curiosity-driven basic research, we will lose our ability to see the entire forest, a vision so important to help us look at the same problem from different points of view [5, 6].

6.2 Painting Technology Consortium

Toyota's Kentucky plant was opened in 1986. This was also the same year that I (Kozo Saito) joined UK. This fortunate coincidence gave me a new opportunity to study the automobile manufacturing process [7]. Toyota's managers and engineers and UK faculty members soon started discussing collaboration in research. Toyota's Japanese executives were instrumental in starting this joint partnership. In 1993, UK's College of Engineering received the project to study the automobile coating process. For the next four years, our focus was mostly learning the automobile coating system and processes by visiting Toyota plants, paint booth manufacturers, and paint companies both in the US and Japan. During this learning period, Toyota provided continuous and steady funding without asking for short term results related to immediate practical applications.

We started to conduct a series of scientific studies on automobile coating technology. We found that some automobile coating processes were largely experience-based, and required scientific analysis for effective improvements. We often asked questions: What are the scientific principles to support this process, that equipment, and that system? After collecting data at various plant sites and in discussions with engineers and operators, we then conducted laboratory experiments and CFD (Computational Fluid Dynamics) model calculations.

Abraham Salazar who joined our group in 1996 as a doctoral student (research faculty at UK) had a strong background in CFD. He analyzed the airflow pattern containing paint particles and the capturing mechanism of typical conventional wet scrubbers used by automobile manufacturers to capture over-sprayed paint. His CFD analysis, based on fluid dynamics, helped us to scientifically estimate waste in energy use and relative efficiency in particle capturing of existing wet scrubbers.

Our next task was focused on how to improve the performance of wet scrubbers. This task required new ideas through thinking outside-the-box and a paradigm shift. We learned from nature that sand dune structure in a desert can be the most efficient way to capture paint particles with minimum energy consumption. This approach led our team to invent Vortecone in collaboration with Toyota and Trinity engineers. Vortecone wet scrubber is 30–50 % energy efficient and has a higher capturing capability than other similar products available on the market [8]. Our team's success lies in the combination of the following factors: Basic research to understand the capturing mechanisms, thinking outside-the-box, paradigm shift, and Toyota' continuous and steady funding support. Without any of the above elements, I doubt this invention would have been possible. In this case, the box was technology, that is, the outcome if human thought combined with engineering principles. We shifted our focus to nature, another source for models of how to make things efficiently.

This initial success attracted other companies to pay attention to the University of Kentucky's automobile coating research, leading to the establishment of UK's Painting Technology Consortium (PTC) in 1999. In the following year, we initiated the annual Painting Technology Workshop [9] with the following aims: (1) to provide a place where industry engineers, government agency regulatory personnel,

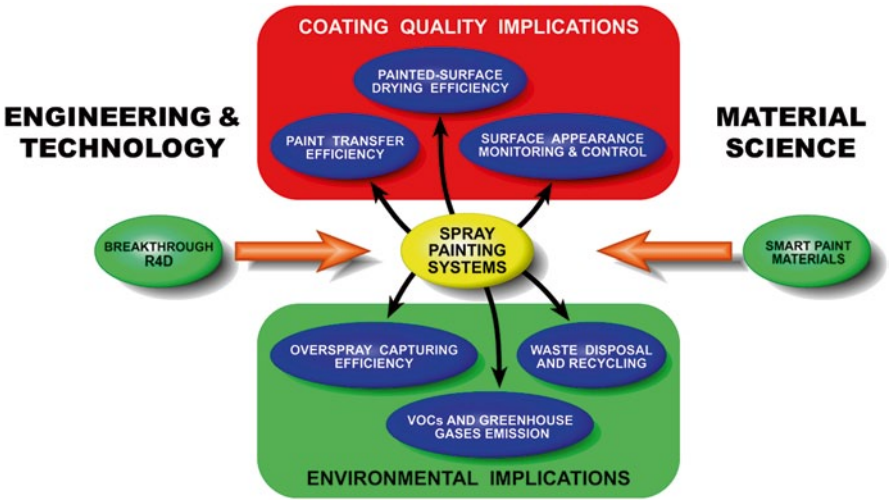

Fig. 6.2 Six different coating research areas of UK's PTC

and academic researchers meet and discuss coating research and technology development, (2) to share common problems in coating technology and seek win-win solutions, and (3) to provide educational and training opportunity. Figure 6.2 shows six different areas of UK's PTC coating research.

In the meantime, UK's PTC received ever-increasing requests from industry for immediate and long-term solutions to process problems and challenges beyond automobile coating technology. This led to the creation of Institute of Research for Technology Development (IR4TD), a stepped-up version of the Painting Technology Consortium (PTC), with broader aims to cover almost all types of engineering problems related to manufacturing industries. The following summarizes IR4TD's mission and operational principles.

6.3 IR4TD

The Institute of Research for Technology Development (IR4TD) was proposed in 2006 and approved in 2007. To stress the way research and development are integrated in our work, we call our approach R4D—research *for* development. We chose the number 4 instead of the word to suggest our difference from engineering as usual. The new institute's purpose is to directly and effectively respond to requests from industries. R4D is a demand-pull rather than a supply-push approach; we respond to the needs of clients who approach us rather than approach companies with our research interests. This partnership development approach is based on the win-win buffer theory proposed by Cho et al. [10], who promotes the importance of

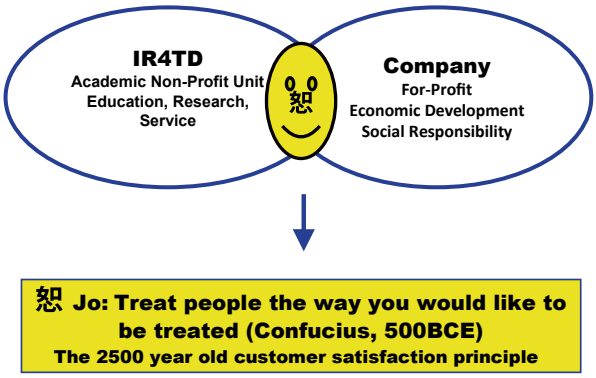

Fig. 6.3 The win-win buffer theory

creating common interests among different parties and different individuals when they work together. The common interest will emerge when each individual or each party is willing to seek an interdependent relationship where push-principle is replaced with pull-principle. Cho's buffer theory is based on Confucius's teaching where compassion "Jo" is the foundation for human relationship building [4]. Figure 6.3 shows a schematic of Cho's buffer theory.

IR4TD's mission is aligned with the University of Kentucky's strategic plan. It states: "The University will accelerate industry-funded research and partnerships, technology transfer, and business development to advance Kentucky's economy… we must seize opportunities to develop further our intellectual property, corporate relationships, and business ventures, and we must enhance our efforts to fulfill the vision and promise of UK's Research Campus."

Our R4D approach has worked to help us build industry relationships that continue to grow and to offer us more challenging and complex problems. The approach also provides an excellent education for our graduate students in tackling pressing industry problems, working as a team, accepting responsibility, coping with real budgets and real deadlines, communicating effectively with clients, and understanding their point of view. A client may see a problem with the current process; we can see in fact that they have come to the limits of a current technology so that a new generation technology or even a radical new approach to the whole question is needed. The "R" of our work is not simply paired with the "D" but tied directly to needed innovations.

Overall, this approach leads to:

- High probability of immediate in-plant benefit to the company;
- High likelihood that new technology needs will be accurately identified
- Thus, new generation technologies that fit efficiently into the company's manufacturing systems, and the potential for discovering "quantum leap" (revolutionary) solutions that can be transferred to other industries; and
- A higher percentage of successful proposals (>60 %).

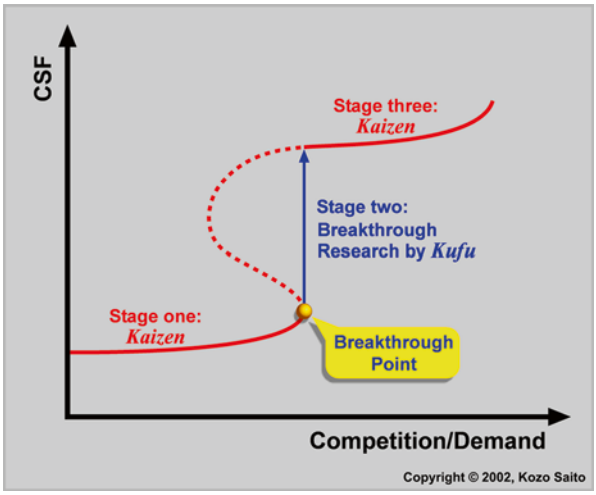

Fig. 6.4 Research for development function theory. (CSF stands for customer satisfaction factor)

6.4 Two Kinds of Innovation in Research and Development: Incremental and Major

6.4.1 In-Plant Improvements

A corporate client identifies manufacturing issues that have significant impact on its costs structure. IR4TD research team proposes concepts for in-plant improvements that could be integrated into the company's manufacturing systems; it could be encoded in hardware or software products meeting improved efficiency and production targets while remaining within the cost basis of the plant. Prototyping is essential for the overall solution to fit into existing manufacturing systems. Projects may be completed within 3–12 months, depending on the urgency of the manufacturing issue.

This part of our research is what the recent Department of Commerce report *Manufacturing in America* calls "incremental innovation." Where the first kind of innovation is major and dramatic, this second type of innovation is "the steady improvement in products and manufacturing processes within major technology lifecycles. Such improvement involves much less dramatic improvements, but collectively these innovations have a significant effect." Figure 6.4 illustrates typical progress in technology development in a customer satisfaction (CSF)-competition/demand diagram, where evolutionary progress is made by the continuous improvement through Kaizen and revolutionary progress is made by major breakthroughs in research. It is important to see that both incremental and major innovations are necessary to form the entire innovation process. As can be seen in Fig. 6.4, stage–one Kaizen (incremental innovation) is leading to the breakthrough (unsteady) point providing the condition for the major innovation to occur; therefore, the ma-

jor innovation is not a stand-alone activity. After the technology jump created by breakthrough technology, stage-three Kaizen will start to provide small incremental improvements to the new technology, leading eventually to another breakthrough point. This is a typical Kaizen cycle in R&D. Interestingly, the Fig. 6.4 diagram is similar to a well-known S-curve of ignition theory in combustion. In the ignition theory, the vertical line is temperature and the horizontal line is Damkoler number (non-dimensional time: flow time divided by chemical reaction time) [11]. The breakthrough point is the ignition point; after that point, suddenly flaming occurs, pushing the pre-ignition temperature (350 °C) to the post-ignition temperature (1,500 °C). Note: here again, thinking by analogy as a way to shift a point of view.

6.4.2 New Generation Technology Development: Is the Current Spray Painting Technology Able to Achieve 100 % Transfer Efficiency by Kaizen?

An important question related to current spray cup technology: Is it possible to achieve 100 % transfer efficiency by improving the current spray cup design? This question needs to be answered before any effort toward 100 % transfer efficiency takes place. The IR4TD team discussed how to obtain this answer, and identified the need for basic study that can reveal the mechanism of the current rotary spray cup: how does it work and what is the limitation of the current design. Careful inspection of the current spray cup design and review of a high speed video of atomized paint mist behavior revealed that the paint film thickness on the cup surface can be on the order of 10 μm; on the ejection velocity of paint from the cup's edge it is a few meters per second. The atomization process includes interaction between liquid, gas and a geometrically complex solid surface.This highly transient phenomenon requires an instrument capable of measuring three-D velocity vector components with a micro-meter level spatial resolution and sub-micron second time resolution in approximately 10 cm×10 cm area. This is simply not achievable within the current timeline and budget. Computational fluid dynamic (CFD) modeling has a better chance to achieve this goal, if we can simplify the atomization process capturing only the essential mechanisms, ignoring the secondary effects to the degree that we can manage our CFD calculations with UK's supercomputers.

This study has been one of the most challenging and difficult tasks since the initiation of our group. Abraham Salazar (CFD expert and lead of this project) coordinated this project with three other members. This project required at least the following knowledge: (1) phase transition between liquid and gas, (2) surface instability of liquid film, (3) liquid-surface wetability, (4) molecular level Rheology on non-Newtonian fluid, (5) liquid atomization, (6) ligament formation and breakdown, (7) computer code making and modification, and (8) advanced CFD methods.

As a result, we eventually identified the limitation of the current spray cup design, due to the inherent instability of thin liquid film on the rotating cup surface.

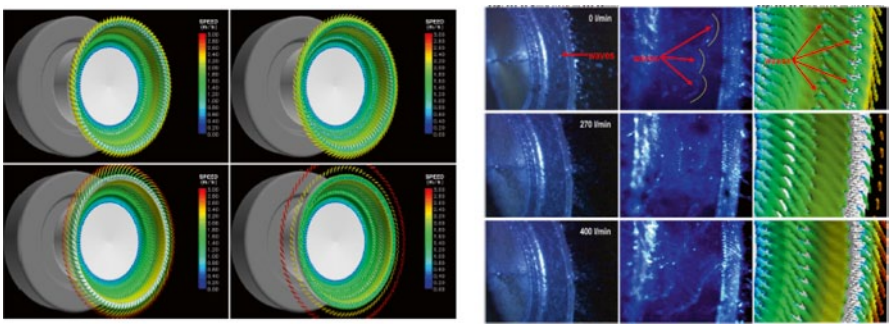

Fig. 6.5 CFD simulation of trajectory of water ligaments and droplets ejected from a rotating spray cup (*left*), and the measured and calculated liquid surface structure (*right*)

Due to this instability of liquid (paint) film, the current spray cup design is not able to eject the same diameter size droplets all the time. Figure 6.5 shows our CFD simulation of ejected water droplet trajectory which shows periodic motion associated with the surface wave, and shows experimentally measured and CFD calculated surface wave structure. Our CFD calculation images (left) are similar to the high speed photography images obtained by Nissan's laboratory [12].

After this basic research was done, the next step was the generation of ideas to create new types of paint applicators. Here again, outside-the-box thinking and paradigm shift will help in this idea generation process. This research is still on-going; we created several new ideas, tested concepts, prototyping is half-way completed and planning for eventual commercialization has began.

6.5 Opportunity for Start Ups and Commercialization

IR4TD activities will create new technologies, some of which will be commercialized by starting small high technology businesses. Others will be licensing technology to IR4TD industrial collaborators, spin-offs from IR4TD sponsors, and technology transfer to companies that are not sponsors of IR4TD projects. The preferred route will depend on the technology, the potential markets, and selecting commercialization methods that have a high probability of success. To commercialize research results created by IR4TD, recently Synova R&D LLC was formed. Synova will closely work with IR4TD researchers to assess application of their research results. This new collaboration cycle is shown in Fig. 6.6 whose aim is to create a self-supporting Institute, where research begins with ideas followed by proof of concept and prototyping. Commercialization is the fourth and the final step which transforms research results into commercial products to create a revenue stream. Table 6.1 lists six different projects recently identified for commercialization.

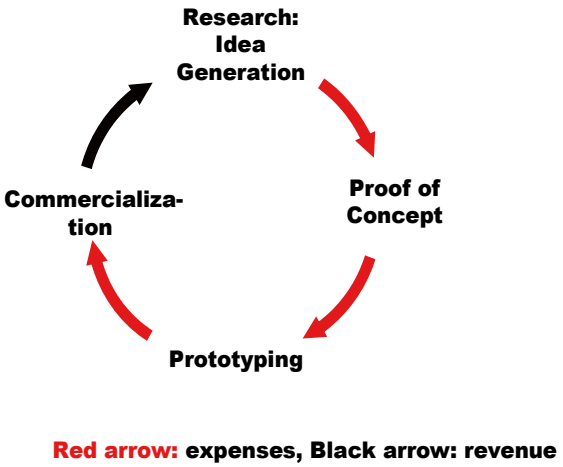

Fig. 6.6 Research-commercialization cycle

Table 6.1 List of potential commercialization projects

Project	Description
1	Vortecone over-spray capturing device for coal ash capturing
2	Infrared thermography inspection of the condition of bridge coating
3	Infrared thermography inspection of bacteria and infectious disease
4	Digital paint applicator
5	Quick curing paint
6	Bio-diesel from waste vegetable oils and biomass from agricultural waste

6.6 Lean Manufacturing and Engineering Problem Solving

The current IR4TD structure includes hitozukuri and monozukuri which includes Lean Manufacturing. Lean Manufacturing is a philosophy or a way of thinking to improve efficiency and effectiveness of any system by continuously applying a small incremental step of improvement, known as Kaizen. For the benefit of readers, therefore, only the problem solving process practiced in Lean Manufacturing is schematically shown in Fig. 6.7 in comparison with scientific method and making assumption cycles of Fig. 6.8.

The late Professor Emori who was famous for his engineering spirit and a strong advocate for the engineer as problem solver for industry problems, once said: "Engineers need to learn two distinctly different methods: science as a tool to understand things, and engineering as a tool to create things" [13, 14]. His belief in engineering problem solving resonates well with the founder of arerothermochemistry, von Karman, who once declared, "Scientists see things that exist and ask why. Engineers

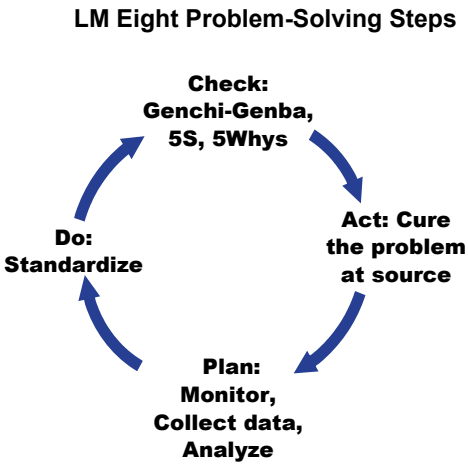

Fig. 6.7 LM problem solving cycle consisting of eight different steps of problem solving

dream things that do not exist and ask why not" [15]. The engineer's role to create new products, invent things, and find solutions for industry's problems is clear. Professor Emori claimed: "Engineering problem solving is an art but not a science." He believed that ultimately engineering problem solving is deeply related to an engineer's psychological state of mind and on how the engineer sees the world, rather than what kind of technical skills and scientific knowledge the engineer has. This means that learning engineering and science is not enough. There is a third element: professional intuition, probably the most important, yet most difficult to master, but required for the engineering problem solving process. Taiichi Ohno, one of the pioneers who developed Toyota Production System, once declared that the essence of TPS is to develop the well trained "eyes" that can see waste which is invisible to the untrained [1, 2].

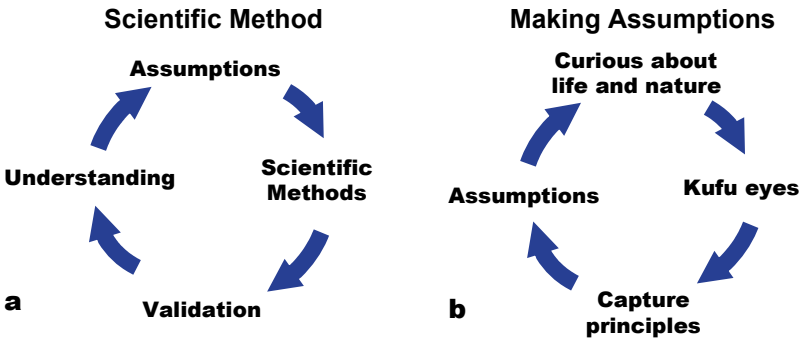

Fig. 6.8 How we make assumptions in scientific method

6.7 Kufu and Monozukuri

To effectively conduct research and technology development, we conduct experiments (both full scale and scale model), evolve theory, perform computations, and use professional intuition. My readers may be familiar with the first three traditional tools [5], but not the fourth one, which may require some explanation.

The fourth tool is not discussed very much in scientific and engineering communities, although it has been used for years by scientists, engineers and skilled craftsmen. I call it Kufu, the term that was used by Suzuki in his book: *Zen and Japanese Culture* [3]. The following provides some background information on how Kufu plays an important role in the breakthrough and discovery processes of scientific research and technology development.

> The term Kufu is the most significant word used in connection with Zen and also in the fields of mental and spiritual discipline. Generally, it means 'to seek the way out of a dilemma' or 'to struggle to pass through a blind alley.'
> A dilemma or a blind alley may sound somewhat intellectual, but the fact is that this is where the intellect can go no further, having come to its limit, but an inner urge still pushes one somehow to go beyond. As the intellect is powerless, we may enlist the aid of the will; but mere will, however pressing, is unable to break through the impasse. The will is closer to fundamentals than the intellect, but it is still on the surface of consciousness. One must go deeper yet, but how? This how is Kufu. No teaching, no help from the outside is of any use. The solution must come from the most inner part of oneself. One must keep knocking at the door until all that makes one feel an individual being crumbles away.
> That is, when the ego finally surrenders itself, it finds itself. Here is a newborn baby. Kufu is a sort of spiritual birth pang. The whole being is involved. There are physicians and psychologists who offer a synthetic medicinal substance to relieve one of this pang. But we must remember that, while man is partially mechanistic or biochemical, this does not by any means exhaust his being; he still retains something that can never be reached by medicine. This is where his spirituality lies, and it is Kufu that finally wakes us to our spirituality.

Kufu plays a significant role in monozukuri, as explained by Professor Emori in his famous book in Scale Modeling [14], "professional intuition leads to Kufu, the best tool in engineering problem solving." Taiichi Ohno, one of the fathers of the Toyota Production System, reminds us that "If you look up the word 'engineer' in an English dictionary, you might find 'technologist,' while in Japanese, its meaning uses the character for 'art'" [1]. A schematic showing characteristics of Eastern culture on which professional intuition is based, is shown in Fig. 6.9, in comparison to characteristics of Western culture on which scientific methods are based.

A skilled craftsman can design parts or fix problems based mainly on his/her experience and professional intuition and not on scientific reasoning and understanding. His/her experience and know-how can help solve industry problems. Three scientific methods—theory, experiment and computation—can help us to understand why the craftsman's solution worked for a particular problem, but may not work for different types of problems. Here again, the craftsman's role is the same as the engineer's role in creation and problem solving, while a scientist's role is needed here to understand why the solution worked.

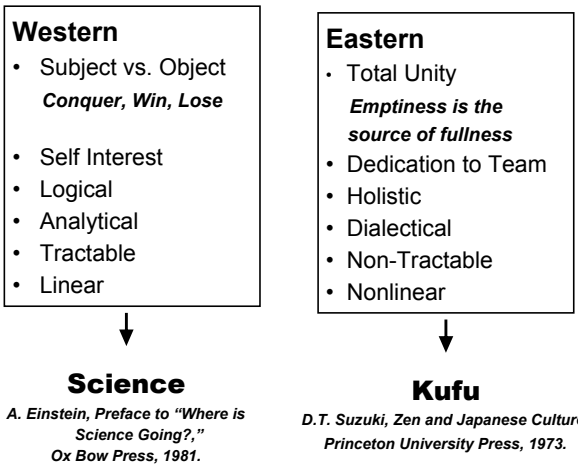

Fig. 6.9 Comparison between Western mode of logical thinking vs. Eastern mode of holistic approach: Kufu. ([3])

Both engineering and scientific functions are required when industry wants to develop an effective continuous improvement system in its operation [18]. It would be nice for industry to have these two functions in its organization. However, the scientific function often finds difficulty in justifying its accountability on company costs. On the other hand, the University can be an excellent source for the company's scientific function.

There are two different types of University research: curiosity-driven basic research and purpose-driven applied research. R4D is a good example of applied research, as we discussed earlier. It would be harmful, however, if University researchers only conducted R4D research, staying inside the boundary determined by a well focused R4D plan and ignored curiosity-driven basic research. History has proven that many technology inventions were made by looking at the same problem from a different point of view [18, 19].

A good balance between basic research and applied research, therefore, is clearly needed for a university researcher to effectively solve industry problems [7, 15]. Successful university-industry collaboration on research is like growing a fruit tree; basic research is its roots, R4D is the branch to bear fruit, and an interdependent team is the trunk. Figure 6.10 depicts this win-win concept of university-industry partnership.

6.8 Some Recent Research Progress on Coating Technology

6.8.1 Surface Inspection by Infrared Thermography

The quality of painted surface can be inspected either by human eyes or machines. Human inspection may be convenient but requires training and may be inconsistent.

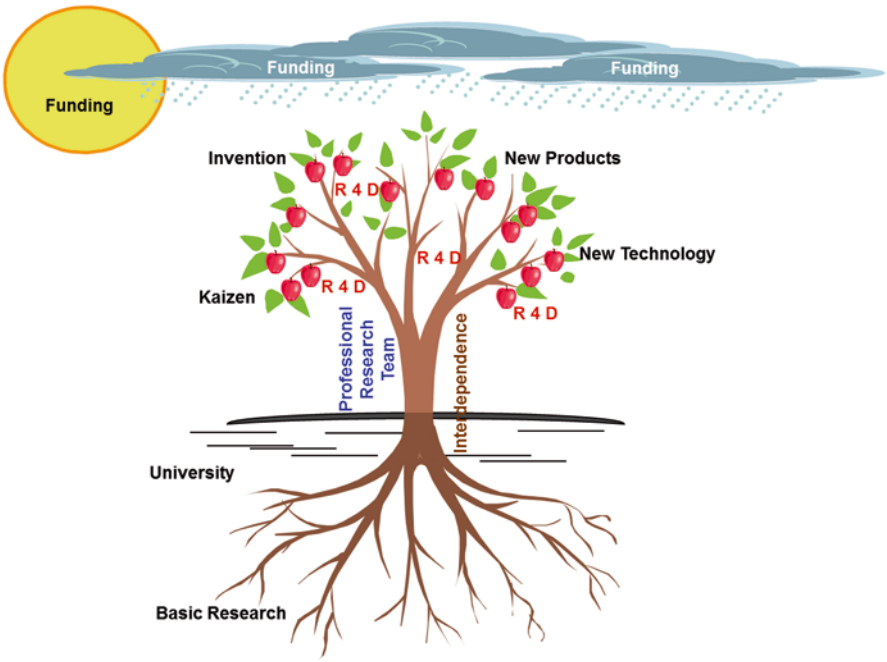

Fig. 6.10 Schematic of university-industry partnership to achieve the win-win results

Machine inspection can be superior to human inspection, once reliability, consistency and accuracy are assured.

To replace human inspection by machine inspection, we normally choose CCD camera or anything similar to human inspection. Humans are flexible enough to identify the curved surface, the difference in color, shade, and dust on the surface. However, a CCD camera and other similar visual inspection systems are not flexible enough or accurate enough.

We applied an infrared thermography technique to identify both surface and in-depth defects. IR thermography can detect surface defects based on difference either in emissivity or thermal diffusivity. If the defective part has different thermal property, then it creates different temperature structure from the normal area when a thermal wave passes through that defective part. The different thermal structure can be seen as a temperature difference in the IR image captured by an IR camera. Figure 6.11 shows a emission mode of IR thermography system applied to identify both surface and sub-surface defects on a moving surface [19, 20].

There are two ways to apply a stimulant (either heat pulse or continuous heat) to the surface. Detection can be made by transmission mode or reflection model. The transmission mode can monitor at the back surface of the media how heat wave passes through the media from the surface to back. The emission mode detects the change of temperature or emissivity at the same surface as the heat (stimulant) input is given. Detailed information about this patented technology is available [19, 20].

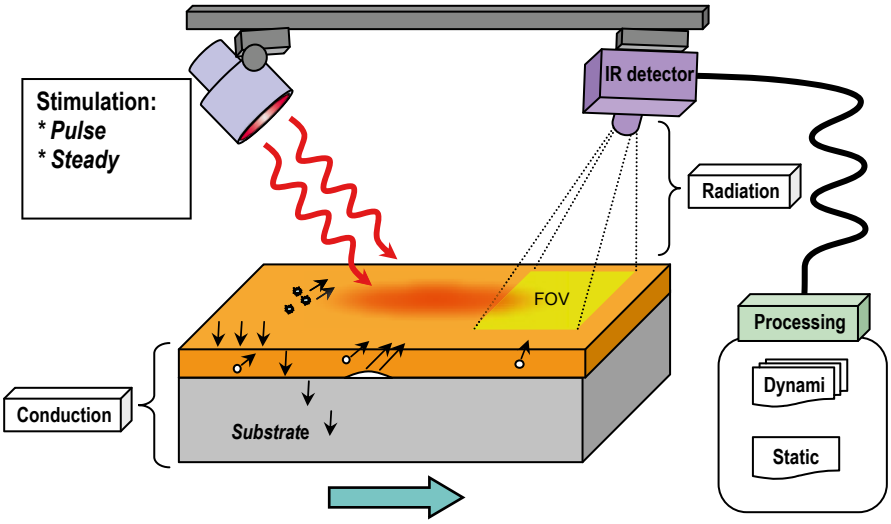

Fig. 6.11 An emission mode IR thermography system to identify both surface and sub-surface defects in a moving surface. [19, 20]

6.9 Summary

The principles of our coating research are in line with the University of Kentucky's three mission components—education, research and service—goal is to improve the quality of our life, make our society safer, environment cleaner, and provide opportunity for everyone to become better persons. IR4TD plays a part in this larger mission of academic institutions articulated by Boyer: "The aim of education is not only to prepare students for a productive career, but also to enable them to live lives of dignity and purpose; not only to generate knowledge, but to channel that knowledge to human ends; not merely to study government, but to help shape a citizenry that can promote the public good. Thus, higher education's vision must be widened if the nation is to be rescued from problems that threaten to diminish permanently the quality of life" [16].

Let me close by quoting Albert Einstein's message on the role of science in human affairs and education

> There are two ways in which science affects human affairs. The first is familiar to everyone: Directly, and to an even greater extent indirectly, science produces aids that have completely transformed human existence. The second way is educational in character—it works on the mind. Although it may appear less obvious to cursory examination, it is no less incisive than the first. [17]

Acknowledgements This section was developed by the sponsorships from KY EPSCoR: Funding to Support Proposing a Kentucky-Based NSF Engineering Research Center in Surface Coatings Research and Applications, and the IR4TD general fund. Kozo Saito acknowledges Professor Forman Williams for his invaluable comments on the entire course of this lecture material, and Dr. Bob Gregory for comments on Mingei in relation to monozukuri.

References

1. Ohno, T.: Toyota Production System: Beyond Large-Scale Production. Productivity Press, Cambridge, MA (1988)
2. Cho, F.: Toyota production system. In: Saito, K. (ed.) Principles of Continuous Learning Systems. McGraw-Hill, New York (1995)
3. Suzuki, D.T.: Zen and Japanese Culture. Princeton University Press, Princeton (1973)
4. Kanaya, O.: Confucius. Iwanami Bunko 33-2002-1, Iwanami, Tokyo (1982) (in Japanese)
5. Wilson, E.B. Jr.: An Introduction to Scientific Research. McGraw-Hill, NY, (1954)
6. Ferguson, E.S.: Engineering and the Mind's Eye. The MIT Press, Cambridge (1992)
7. Saito, K.: Development of the University of Kentucky—Toyota Research Partnership: Monozukuri. The lecture note for the Toyota Motor Vietnam 10th Anniversary lecture, Hanoi University of Technology, Hanoi, Oct 2005. http://www.caer.uky.edu/energeia/volumes17.shtml; http://www.rgs.uky.edu/odyssey/spring05/contents.html
8. Salazar, A.J., Saito, K., Alloo, R.P., Tanaka, N.: Wet scrubber paint spray booth including the wet scrubber US Patent 6,024,796, Feb 2000 and US Patent 6,093,250, July 2000
9. Toda, K.: Wet scrubber and paint spray booth including the wet scrubber. Coating Technology: Japanese Coating Technology Association, vol. 39, pp. 101–105 (2004)
10. Cho, F., Todd, L., Grulke, E., Kreafle, K., Pittman, M., Saito, K.: Group discussion on TPS principles, Toyota Headquarter Office, Nagoya, 23 Oct 2007
11. Williams, F.A.: Combustion Theory, 2nd ed. Benjamin Cummings, San Francisco (1985)
12. Salazar, A.J. and Saito, K.: Computational Analysis of Unsteady Liquid Flow in Rotary Bell Sprayer UK Painting Technology Workshop, Lexington, KY (2005)
13. Emori, R.I.: Toys and scale models. Progress in Scale Modelling, K. Saito Ed, Springer 2008
14. Emori, R.I., Saito, K., Sekimoto, K.: Scale Models in Engineering: Its Theory and Applications, 3rd ed. Giho-do, Tokyo (2000)
15. Williams, F.A.: Significance of scale modeling in engineering science. Progress in Scale Modelling, K. Saito Ed, Springer 2008
16. Boyer, E.L.: Scholarship Reconsidered: Priorities of the Professoriate. The Carnegie Foundation for the Advancement of Princeton, Princeton (1990)
17. Einstein, A.: Out of My Later Years. The Albert Einstein Memorial, National Academy of Sciences, Washington, DC 1950
18. Hall, A.: Introduction to Lean Sustainable Quality Systems Design. Arlie Hall, Lexington (2006)
19. Omar, M.: Department of Mechanical Engineering, University of Kentucky, Lexington (2005)
20. Saito, K., Ali, H., Numasato, A., Omar, M., Sakakibara, M., Suzuki, T., Tanigawa, Y.: System and methods for inspecting coatings. US Patent 7,129,492 B2, Oct 2006